ISSN 0711-6659

canadian acoustics
acoustique canadienne

SEPTEMBER 1999
Volume 27 -- Number 3

SEPTEMBER 1999
Volume 27 -- Numéro 3

PROCEEDINGS

SEMAINE CANADIENNE D'ACOUSTIQUE
ACOUSTICS WEEK IN CANADA

1999

CAHIERS DES ACTES

canadian acoustics

acoustique canadienne

THE CANADIAN ACOUSTICAL ASSOCIATION
P.O. BOX 1351, STATION "F"
TORONTO, ONTARIO M4Y 2V9

L'ASSOCIATION CANADIENNE D'ACOUSTIQUE
C.P. 1351, SUCCURSALE "F"
TORONTO, ONTARIO M4Y 2V9

CANADIAN ACOUSTICS publishes refereed articles and news items on all aspects of acoustics and vibration. Articles reporting new research or applications, as well as review or tutorial papers and shorter technical notes are welcomed, in English or in French. Submissions should be sent directly to the Editor-in-Chief. Complete instructions to authors concerning the required camera-ready copy are presented at the end of this issue.

ACOUSTIQUE CANADIENNE publie des articles arbitrés et des informations sur tous les domaines de l'acoustique et des vibrations. On invite les auteurs à soumettre des manuscrits, rédigés en français ou en anglais, concernant des travaux inédits, des états de question ou des notes techniques. Les soumissions doivent être envoyées au rédacteur en chef. Les instructions pour la présentation des textes sont exposées à la fin de cette publication.

CANADIAN ACOUSTICS is published four times a year - in March, June, September and December. The deadline for submission of material is the first day of the month preceeding the issue month. Copyright on articles is held by the author(s), who should be contacted regarding reproduction. Annual subscription: $10 (student); $50 (individual, institution); $150 (sustaining - see back cover). Back issues (when available) may be obtained from the CAA Secretary - price $10 including postage. Advertisement prices: $400 (centre spread); $200 (full page); $120 (half page); $80 (quarter page). Contact the Associate Editor (advertising) to place advertisements. Canadian Publication Mail Product Sales Agreement No. 0557188.

ACOUSTIQUE CANADIENNE est publiée quatre fois par année - en mars, juin, septembre et décembre. La date de tombée pour la soumission de matériel est fixée au premier jour du mois précédant la publication d'un numéro donné. Les droits d'auteur d'un article appartiennent à (aux) auteur(s). Toute demande de reproduction doit leur être acheminée. Abonnement annuel: $10 (étudiant); $50 (individuel, société); $150 (soutien - voir la couverture arrière). D'anciens numéros (non-épuisés) peuvent être obtenus du Secrétaire de l'ACA - prix: $10 (affranchissement inclus). Prix d'annonces publicitaires: $400 (page double); $200 (page pleine); $120 (demi page); $80 (quart de page). Contacter le rédacteur associé (publicité) afin de placer des annonces. Société canadienne des postes - Envois de publications canadiennes - Numéro de convention 0557188.

EDITORIAL / ÉDITORIAL

Welcome to the 1999 Proceedings Issue of Canadian Acoustics. It contains details of the final programme and two page summaries of the Technical Symposium of Acoustics Week in Canada 1999 to be held in picturesque Victoria in October. Keeping with the usual trend, the Victoria conference also is promising to contain an impressive collection of papers in acoustics. The meeting will clearly be very interesting. See you there!

Many initiatives were proposed during the last executive meeting of the association. One of the initiatives has to do with the contents of the journal. We have taken the proposal seriously and have started implementing a few of the suggestions. We have a long way to go! We have included in the June 1999 issue abstracts of graduate degrees. We therefore request the academic supervisors to submit theses abstracts (both MS and Ph. D) to the journal after the defense of the research work so that we can publish them periodically. We are also planning to include two-to-three page summaries of institutions that conduct acoustical research. For instance, we hope to publish a description of the Institute of Research in Construction of the National Research Council in the December 1999 issue of the journal. Once again, we request all the research labs and university institutes that conduct acoustical work to submit brief descriptions of their facility. These initiatives, we hope, will make the journal more interesting to the readers and will also highlight the diverse work undertaken across Canada.

Bienvenue à l'édition 1999 du journal l'Acoustique Canadienne. Cette "edition contient des détails du programme final et deux pages de résumés du Colloque Technique de la semaine d'Acoustique au Canada 1999 qui se tiendra dans la ville pittoresque de Victoria en Octobre. Conservant la tendance habituelle, la conférence de Victoria promet de contenir une collection impressionnante d'articles sur l'acoustique. La conférence sera certainement très intéressante. Je vous donc rendez-vous là-bas!

Beaucoup d'initiatives ont été proposées au cours de la dernière réunion exécutive de l'association. L'une d'entreselles concerne le contenu du journal. Nous avons pris la proposition sérieusement et avons commencé à mettre en application quelques unes des suggestions. Nous avons beaucoup de chemin à faire! Nous avons inclus dans le numéro de juin 1999 les sommaires de thèse de graduation. Nous invitons donc les tuteurs à soumettre au journal les sommaires de thèse (MS et Ph. D) après soutenance afin que nous puissions les publier périodiquement. Nous envisageons également inclure deux à trois pages sommaire des établissements qui font de la recherche en acoustique. Par exemple, nous espérons éditer une description de l'Institut de Recherche dans la Construction du Conseil National de la Recherche dans l'édition du journal de Décembre 1999. Une fois de plus, nous demandons à tous les laboratoires de recherche et instituts universitaires qui conduisent des recherches en acoustique à soumettre de courtes description de leur moyens. Ces initiatives, nous espérons, rendrons le journal plus intéressant aux lecteurs et mettrons en valeur également les divers travaux entrepris à travers le Canada.

WHAT'S NEW ??

Promotions
Deaths
New jobs
Moves
Retirements
Degrees awarded
Distinctions
Other news

Do you have any news that you would like to share with Canadian Acoustics readers? If so, send it to:

QUOI DE NEUF ?

Promotions
Décès
Offre d'emploi
Déménagements
Retraites
Obtention de diplômes
Distinctions
Autres nouvelles

Avez-vous des nouvelles que vous aimeriez partager avec les lecteurs de l'Acoustique Canadienne? Si oui, écrivez-les et envoyer à:

Francine Desharnais, DREA Ocean Acoustics, P.O. Box 1012, Dartmouth NS, Email: desharnais@drea.dnd.ca

Proceedings of Acoustics Week In Canada 1999
Actes DE LA Semaine Canadienne D'Acoustique 1999

Table of Contents / Tables des matières

DECISIONS, DECISIONS, DECISIONS...

When it comes to choosing a noise measurement device, one decision is easy...**CEL Instruments!**

We offer a full line of quality sound level meters and noise dosimeters to meet every need and budget! And all of CEL Instrument's Meters meet ANSI S1.4 in full.

Discover the many advantages that CEL products have to offer — *all at a price you can afford!*

CALL 800-366-2966
OR WRITE TODAY!

CASELLA INSTRUMENTS

17 Old Nashua Road #15, Amherst, NH 03031
Fax: 603-672-8053

APPELEZ LE 800-366-2966
OU ÉCRIVEZ-NOUS AUJOURD'HUI!

Lorsque vient le temps de choisir un instrument de mesure du bruit, la décision est simple...**les CEL Instruments!**

Nous offrons une gamme complète d'instruments de mesure du niveau sonore et de dosimètres de bruit, afin de satisfaire tous les besoins et budgets! Et tous les instruments offerts par les Instruments CEL rencontrent entièrement la norme ANSI S1.4.

Découvrez tous les avantages que les produits CEL ont à offrir - et ce, à un prix abordable!

DES DÉCISIONS...TOUJOURS DES DÉCISIONS...

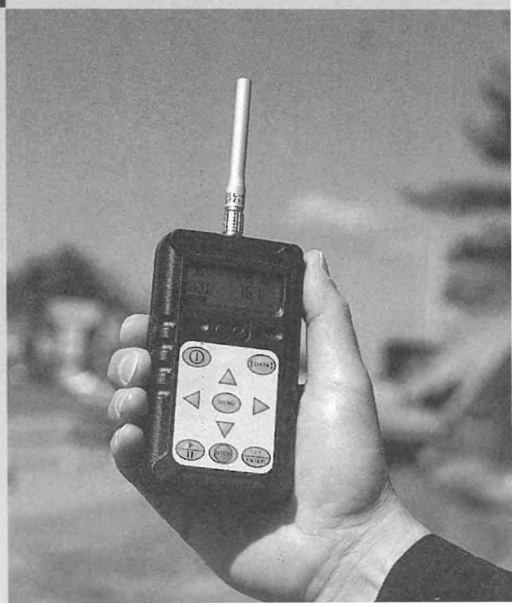

Acoustics Week in Canada 1999, Victoria BC : Preliminary Schedule

Monday, October 18, 1999 : Morning Sessions

	Salon AB	Breakout Room ABC
	Plenary Speaker	
8:30–9:10	*It is about Communication.* Charles A. Laszlo, University of British Columbia	
	Underwater Acoustics: Instruments, Experiments, and Data Processing	**Architectural and Engineering Acoustics I**
9:20–9:40	*Use of the Discrete Wavelet Transform to Enhance Spectral Display Using Noise Reduction Techniques.* Terry Sullivan, Royal Military College of Canada	*Application of Prediction Methods to the Optimal Design of Classrooms.* Murray Hodgson and Nelson Heerema, University of British Columbia
9:40–10:00	*Transmission of Acoustic Cross-spectral Matrices Over Low-bandwidth Communications Channels.* Garry J. Heard, Ron Verrall, David Thomson, and Gordon Ebbeson, Defence Research Establishment Atlantic	*Predicting the Effect of Seat Absorption in Concert Halls.* Murray Hodgson, University of British Columbia; Philippe Jean and Jean-Paul Vian, Centre Scientifique et Technique du Bâtiment, St. Martin d'Hères, France
10:00–10:20	*The Spinnaker Project: An Arctic Acoustics Tale.* Ron Verrall, Defence Research Establishment Atlantic	*Measuring the in situ Airborne Sound Insulation Using the Acoustic Intensity Technique.* T.R.T. Nightingale and R.E. Halliwell, National Research Council
10:20–10:40	*Measurement of Underwater Sound Intensity Vector.* Daniel Hutt, Paul C. Hines and Andrew Hamilton, Defence Research Establishment Atlantic	*Results of a Systematic Study of Airborne Sound Transmission Through a Cavity Wall Assembly.* T.R.T. Nightingale and J.D. Quirt, National Research Council
10:40–11:00	**Coffee**	**Coffee**
	Underwater Acoustics: Sound Propagation	**Architectural and Engineering Acoustics II**
11:00–11:20	*Nonlocal Tops and Equivalent Bottms for Atmospheric Propogation Problems.* David J. Thomson, Defence Research Establishment Atlantic	*Vibration Transmission at Joist/Floor Connections in Wood Frame Buildings.* Ivan Bosmans and T.R.T. Nightingale, National Research Council
11:20–11:40	*A 2-D Description of 3-D Effects in Sound Propogation.* Oleg O. Godin, University of Victoria	*A Review of the Skydome Acoustical Model.* Jeffrey S. Bamford, Engineering Harmonics Inc.
11:40–12:00	*Simulations of Full-field Tomography of Oceanic Currents in Shallow Areas.* Dmitry Yu Mikhin, Atlantic Oceanographic and Meteorological Lab / NOAA	*Localized Sound Reproduction Using a Directional Source Array.* D.I. Havelock and A.J. Brammer, National Research Council
12:00–12:20	*Energy-conserving and Reciprocal Solutions for Higher-order Parabolic Equations.* Dmitry Yu Mikhin, Atlantic Oceanographic and Meteorological Lab / NOAA	*Numerical Modeling of Porous-elastic Materials Using Hierarchical Elements.* S. Rigobert, Laboratoire des Sciences de l'Habitat, France; N. Atalla, Universite de Sherbrooke; F. Sgard, Laboratoire des Sciences de l'Habitat
12:20–1:50	**Lunch**	**Lunch**

Acoustics Week in Canada 1999, Victoria BC : Preliminary Schedule

Monday, October 18, 1999 : Afternoon Sessions

	Salon AB	Breakout Room ABC
	Underwater Acoustics: Oceanography and Noise	**Noise and Noise Control I**
1:50–2:10	*Acoustic Measurements of the Two-layer Exchange Flow in the Bosphorous (Strait of Istanbul).* Frank Gerdes, University of Victoria	*Acoustic Liner Design for a Helicopter Turboshaft Inlet.* Sid-Ali Meslioui, Aiolos Engineering Corp.
2:10–2:30	*Radiated Autospectra from 160 Hz to 2000 Hz of Individual Breaking Ocean Waves.* Rex. K. Andrew	*IBANA—Insulating Buildings Against Noise from Aircraft.* J.S. Bradley, National Research Council
2:30–2:50	*The Underwater Acoustic Noise Field on Sable Bank.* F. Desharnais, G.J. Heard, M.G. Hazen, I.A. Fraser, Defence Research Establishment Atlantic	*Active Noise Control in Enclosed Spaces.* Jingnan Guo and Murray Hodgson, University of British Columbia
2:50–3:10	*Simulation of Underwater Ambient Noise Time Series.* Daniel Hutt, Paul C.Hines and Andrew Rosenfeld, Defence Research Establishment Atlantic	*Preliminary Investigation of Active Control of Airport Run-up Noise.* Pierre Germain, Jingnan Guo, Murray Hodgson and Mark Cheng, University of British Columbia
3:10–3:30	**Coffee**	**Coffee**
	Underwater Acoustics: Localization	**Noise and Noise Control II**
3:30–3:50	*Range Dependent Matched Field Source Localization and Tracking in Shallow Water on a Continental Slope Region of the Northeast Pacific Ocean.* Martin L. Taillefer and N. Ross Chapman, University of Victoria	*The Evolution of Environmental Noise Legislation for Alberta's Energy Industry over Three Decades.* David C. DeGagne, Alberta Energy & Utilities Board
3:50–4:10	*Source Localization Using Regularized Matched-mode Processing.* Nicole E. Collison and Stan Dosso, University of Victoria	*System for Predicting, Visualizing and Auralizing Industrial Noise During Computer "Walk-through."* Murray Hodgson and Nelson Heerema, University of British Columbia
4:10–4:30	*High Resolution Beamforming Techniques Applied to a DIFAR Sonobuoy.* Daniel Desrochers and R.F. Marsden, Royal Military College of Canada	*Broadband Acoustic Absorber Panels.* Sid-Ali Meslioui, Aiolos Engineering Corp.
4:30–4:50	*Regularized Acoustic Inversion for Towed-array Shape Estimation.* Nicole E. Collison and Stan Dosso, University of Victoria	*Railway Right of Way.* Cameron Sherry, Enviro Risque Inc.
4:50–5:10	*Array Element Localization of the Haro Strait Experiment Using a Two-step Inversion Method.* Vanessa Corre, N. Ross Chapman and Mike Wilmut, University of Victoria.	
8:00–10:00	**CAA Annual General Meeting**	

Acoustics Week in Canada 1999, Victoria BC : Preliminary Schedule

Tuesday, October 19, 1999 : Morning Sessions

	Salon AB	Breakout Room ABC
	Plenary Speaker	
8:30–9:10	*The Effects of Anthropogenic Noise on Canadian Marine Mammals.* Christine Erbe, Institute of Ocean Sciences	
	Underwater Acoustics: Seabed Acoustics I	**Speech Production / Perception and Psycho-Acoustics I**
9:20–9:40	*Amplitude vs. Angle Investigations on Shallow Marine Sediments.* M. Riedel, University of Victoria and F. Theilen, University Kiel, Germany	*Description of Speech Produced by Infants with Bronchopulmonary Dysplasia: Methodological Issues and Preliminary Data.* Susan Rvachew, Dianne Creighton, Naida Feldman and Reg Sauve, Alberta Children's Hospital
9:40–10:00	*The Effect of Thin-beds on Attenuation Estimates for Shallow Sub-bottom Classification.* Stephen F. Bloomer, N. Ross Chapman, University of Victoria; William T. Collins, Quester Tangent Corp.	*Acoustic Correlates of Speech Intelligibility in a Child with Progressive Dysarthria.* Megan M. Hodge, University of Alberta
10:00–10:20	*Frequency-dependent Seabed Scattering on Browns Bank.* Y. Jia and R. Courtney, Geological Survey of Canada	*An Acoustic Analysis of Boundary-signalling Differences Between Languages with Contrastive and Non-contrastive Duration.* Zita McRobbie, Simon Fraser University
10:20–10:40	*Acoustic Characterization of a Fishing Bank.* R. Courtenay, B.J. Todd, and V. Kostylev, Geological Survey of Canada	*The Effect of Noise on Foreign-accented Speech: an Acoustic Analysis.* Herman Chi Nin Li, Simon Fraser University
10:40–11:00	**Coffee**	**Coffee**
	Underwater Acoustics: Seabed Acoustics II	**Speech Production / Perception and Psycho-Acoustics II**
11:00–11:20	*A Whole Lotta Shakin' Going On: the Peculiar Seismo-acoustics of Soft Marine Sediments.* David M. F. Chapman, Defence Research Establishment Atlantic, and Oleg A. Godin, University of Victoria	*Acoustic Correlates for Seven Styles of Singing.* Laura Anne Bateman, University of Victoria
11:20–11:40	*Inversion for Geoacoustic and Geometric Parameters Using a Full-wave, Range-dependent Forward Modelling Technique.* J. Viechnicki and N.R. Chapman, University of Victoria	*Relation Between Performance and Confidence Ratings for Sound Localization in Virtual and Free-field Acoustic Space.* G.R. Arrabito, J.R. Mendelson, Defence and Civil Institute of Environmental Medicine; S.L. Van Blyderveen and R.B. Crabtree, University of Toronto
11:40–12:00	*Geoacoustic Inversion of Mediterranean Sea Data.* Mark R. Fallat, MacDonald Dettwiler and Associates, and Stan Dosso, University of Victoria	*A Comparative Study on Cantonese Rising Tones: Native Cantonese Speakers and Canadian Raised Cantonese Speakers.* Connie So, Simon Fraser University
12:00–12:20	*Probability Distributions for Geoacoustic Inversion.* Stan Dosso, University of Victoria	*Word Recognition by Elderly Listeners: Contributions of Gap Detection.* Natalie Haubert, Margaret Kathleen Pichora-Fuller, University of British Colmbia; Bruce Schneider, University of Toronto
12:20–1:50	**Lunch**	**Lunch**

Acoustics Week in Canada 1999, Victoria BC : Preliminary Schedule

Tuesday, October 19, 1999 : Afternoon Sessions

	Salon AB	Breakout Room ABC
	Sound Quality and Standards	**Speech Production / Perception and Psycho-Acoustics III**
1:50–2:10	*Subjective Evaluation of Different Error Correction Schemes for Application with a 900 MHZ Frequency Hopper Communication System.* Kimberly Braaten, University of Regina; Dean Foster, Bruno Korst-Fagundes and Haoye Shen, Acoustics Group-ENC Nortel	*Modality Specific Attentional Mechanisms Govern the Attentional Blink.* Kim Goddard and Elzbieta B. Slawinski, University of Calgary
2:10–2:30	*L'utilisation de plans d'experience afin de choisir la modélisation acoustique d'un téléphone mains-libres.* Joris Brun-Berthet, Frédéric Laville and Stéphane Dedieu, Ecole de Technologie Supérieure, Montreal	*Children's Detection of Tonal Signals in Roving Level Noise Maskers: Frequency and Level Effects.* Prudence Allen and Suzanne Turpin, University of Western Ontario
2:30–2:50	*International Comparisons on Acoustical Calibrations and Measurements.* George S.K. Wong, National Research Council	
2:50–3:10	*Hearing Protectors Standards Activities.* Alberto Behar, C.I.H. Noise Control	
3:10–3:30	**Coffee**	**Coffee**

	Salon A	Salon B	Breakout ABC
SPECIAL SESSIONS	**Occupational Hearing Standards for the Canadian Coast Guard**	**Sound Transmission Classes of Walls and Floors**	**Acoustic Ecology**
3:30–3:50	*Development of Bona Fide Occupational Requirements for Hearing in Canadian Coast Guard Operations.* Laurel Ritmiller, BC Research Inc.; Stan Forshaw; Murray Hodgson, UBC and Chantal Laroche, University of Ottawa	*Control of Low Frequency Sound and Vibration Transmission Through Wood Frame Floors.* Clair W. Wakefield, Wakefield Acoustics Ltd.	*Acoustic Ecology: Concept and Case Study.* Kathleen Pichora-Fuller, University of British Columbia
3:50–4:10	*Characterizating Ship Acoustical Environments for Speech Communication.* Murray Hodgson, UBC	*The Acoustic Significance of the Placement of Shear Walls in Party Wall Construction.* Douglas W. Whicker, BKL Consultants	*Identification of Gated Environmental Sounds.* Christiane Spanik and Kathleen Pichora-Fuller, University of British Columbia
4:10–4:30	*Estimates of Speech Intelligibility Base on Equivalent Speech- and Noise-Spectrum Levels & Hearing Thresholds.* Stanley Forshaw; Laurel Ritmiller, BC Research Inc.; Murray Hodgson, UBC	*Aggregate Subjective Ratings of Airborne Sound Insulation.* J.S. Bradley, National Research Council	*Machine Recognition of Sound Sources.* Carol P. Jaeger and Charles A. Laszlo, University of British Columbia
4:30–4:50	*Audibility of Signals and Alarms in a Coast Guard Environment.* Chantal Laroche, University of Ottawa; Murray Hodgson, UBC; Laurel Ritmiller, BC Research Inc.; Stanley Forshaw	*Discussion*	*Simulation of Contact Sounds in Interactive Virtual Environments.* Dinesh Pai, University of British Columbia
6:30 7:00–9:00	**Cash Bar** **AWC99 Banquet** } *Terrace Room*		

The Effects of Anthropogenic Noise on Canadian Marine Mammals

Christine Erbe
Institute of Ocean Sciences, Sidney BC, V8L 4B2, Canada, erbec@dfo-mpo.gc.ca

Introduction

Canada is very rich in marine mammal diversity including various species of whales, porpoises, dolphins, seals, sea lions, the polar bear and the sea otter. Unfortunately, the population status of many of these is "at risk": The Committee of the Status of Endangered Wildlife in Canada (COSEWIC) of the Canadian Wildlife Service, Environment Canada, currently lists the bowhead whale, the right whale and some populations of beluga whales as endangered; the N Pacific humpback whale, the N Atlantic harbour porpoise, resident BC killer whales and the sea otter as threatened; and the blue whale, fin whale and polar bear as vulnerable.

Threats to these marine mammals include accidental or intended takings (killings); entanglement in debris or fishing gear; habitat destruction; water contamination due to industrial pollution, oil spills, toxic chemicals, waste and sewage; changes in water temperature and salinity; physical alteration of habitat during offshore construction; overfishing of prey; and underwater noise exposure. Since the beginning of the industrial revolution, the world's oceans have become increasingly noise. Ship traffic, hydrocarbon and mineral exploration, offshore construction, all contribute to the noise pollution of marine mammal habitat.

Noise can have a variety of effects on marine mammals: 1) Behavioural disturbance. Particularly if important behaviour such as mating, nursing or feeding is disrupted or if animals are scared away from critical habitat, the impact will be biologically significant (i.e. affecting the long-term survival of the species). 2) Masking. Marine mammals rely primarily on their acoustic sense for communication and orientation. Noise thus has the potential to interfere with the animals' communication sounds, echolocation (odontocete active sonar) signals, environmental sounds (e.g. surf) animals might listen to for orientation, the sound of prey, and the sound of predators. 3) Hearing loss. Sudden bursts of noise or prolonged exposure to loud noise can cause temporary or permanent threshold shifts. 4) Physiological damage to other organs and tissues (brain, heart, lungs, vestibular system etc.).

Canada currently has no regulations for industrial noise emission in marine mammal habitat. In an effort to establish regulations, we need to understand both the propagation of broadband and often intermittent noise through the ocean and the relationship between received sound spectrum levels and impact thresholds.

Impact assessment package

A software package has been developed that combines a sound propagation model and impact threshold models. As input parameters, this software package requires the source level and spectrum of the noise of interest; physical oceanography data about the local ocean environment such as bathymetry, bottom and surface loss data and sound speed profiles; and bioacoustical information about the target species in form of an audiogram (hearing thresholds for single frequencies), critical auditory bands (the width of the ear's auditory filter), spectra of typical animal vocalizations, reported sound levels of disturbance, and criteria for hearing damage. As output, the software produces plots of the zone of audibility, the zone of disturbance, the zone of masking and the zone of hearing damage around a noise source as a function of depth and range.

The sound propagation model is based on ray theory and calculates received noise levels as a function of depth, range and frequency. It is based on Bowlin's RAY code [1] with modifications for eigenray searching, an inclusion of surface loss and frequency-dependent absorption by ocean water.

The audibility model takes the received noise spectra as a function of depth and range from the sound propagation model and compares them to the animal's audiogram and typical natural ambient noise spectra for the receiver location. If at least at some frequencies, the received noise spectrum exceeds both the audiogram and the ambient noise, the noise source is considered audible.

The disturbance model is based on observed disturbance reactions to anthropogenic noise in the wild. For some species, received noise levels causing behavioural disturbance can be found in the literature. This is often around 120 dB re 1mPa [2].

The masking model calculates received noise levels in the critical auditory bandwidths of the animal's ear and compares them to bandlevels of typical vocalizations of the target species. If the noise is louder than the signal in all bands, masking occurs. Alternatively, the masking model can be linked to more complex software simulations of masking involving neural networks [3] which are based on masking experiments with captive marine mammals [4].

The hearing damage model is based on threshold criteria for human workplace noise exposure. If continuous noise exceeds the audiogram by 80dB repeatedly over a couple of hours, a threshold shift might occur at the corresponding frequencies [2].

Icebreaker Noise affecting Beluga Whales in the Beaufort Sea

The impact assessment package is applied to the case of propeller cavitation noise emitted by an actively icebreaking

icebreaker in beluga habitat in the Beaufort Sea. The noise is broadband consisting of sharp pulses occurring 11 times per second and has a source level of 203 dB re 1mPa @ 1m [4].

This noise is audible to belugas at all depths out to ranges of 35km. Closer to the surface, the low-frequency part of the noise spectrum is audible within 70km.

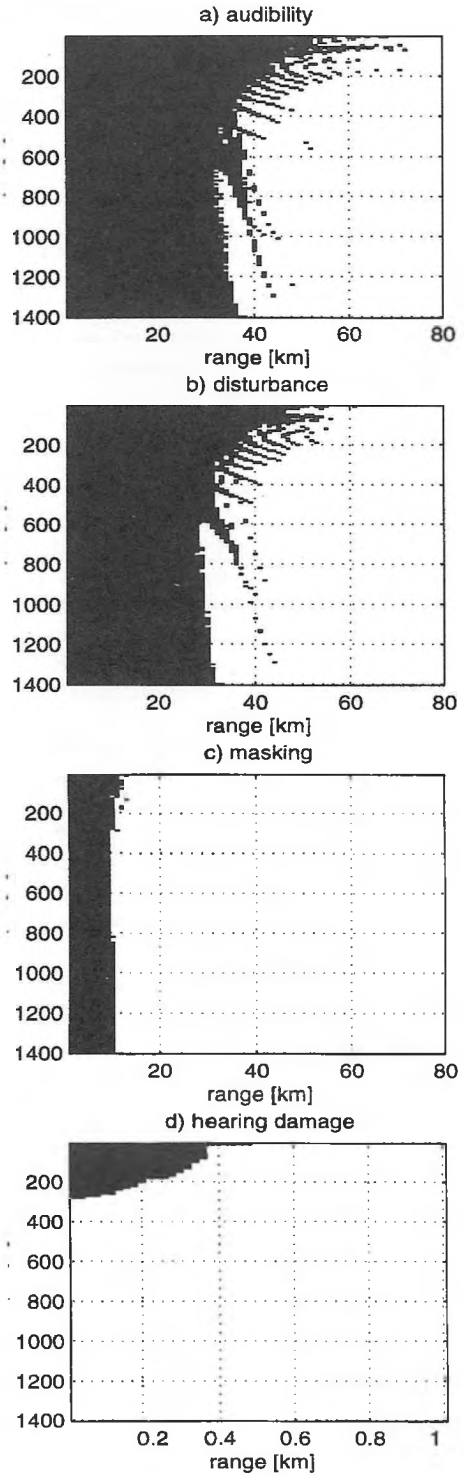

Fig.1: Zones of impact on beluga whales around an icebreaker located in the top left corner at (0,0).

Disturbance thresholds are based on field experiments [5]. The zone of behavioural disturbance is only slightly smaller than the zone of audibility.

Masking of beluga communication signals to the point of non-detectability occurs at all depths out to a range of about 10km. Hearing damage could occur if animals stayed within 300m depth and 500m range repeatedly for many hours.

Conclusion

Icebreaker cavitation noise is audible to beluga whales over long ranges. The animals tend to avoid icebreakers almost as soon as they detect them. Therefore, belugas do not get close enough for potentially harmful effects to occur such as masking or even auditory damage. However, problems can arise in heavily industrialized areas where underwater noise emitted by various sources adds up and is omnipresent for long durations. Here, animals might either be permanently scared away from critical habitat or be adversely affected because they have nowhere to flee to.

Case studies for threatened Canadian marine mammal species and industrialized areas are currently being undertaken. In summary, this software package finds its application in environmental assessments of man-made noise with respect to its impact on marine mammals. Noise sources of concern to the Department of Fisheries and Oceans Canada include offshore hydrocarbon exploration (drill ships, oil rigs, tankers, trenchers, pipeline lay barges), seismic exploration, mineral mining, ocean dredging, fishing vessels, cargo vessels, ocean acoustic research, military activities, ocean liners, ferries, pleasure boats, private boats and the whale watching fleet.

References

1. Bowlin, J., Spiesberger, J., Duda, T., and Freitag, L. (1992). "Ocean acoustical ray-tracing software RAY," Tech. Rep. WHOI-93-10, Woods Hole Oceanographic Institution, Woods Hole.

2. Richardson, W.J., Greene, C.R., Jr., Malme, C.I., and Thomson, D.H. (1995). Marine Mammals and Noise (Academic Press, San Diego).

3. Erbe, C., King, A.R., Yedlin, M., and Farmer, D.M. (1999). "Computer models for masked hearing experiments with beluga whales (Delphinapterus leucas)," J. Acoust. Soc. Am. 105(5),2967-2978.

4. Erbe, C., and Farmer, D.M. (1998). "Masked hearing thresholds of a beluga whale (Delphinapterus leucas) in icebreaker noise," Deep-Sea Res. II 45,1373-1388.

5. LGL and Greeneridge (1995). "Acoustic effects of oil production activities on bowhead and white whales visible during spring migration near Pt. Barrow, Alaska -1991 and 1994 phases: Sound propagation and whale responses to playbacks of icebreaker noise," OCS Study MMS 95-0051. Rep. for U.S. Minerals Management Service, Herndon VA.

Transmission of Acoustic Cross-spectral Matrices Over Low-bandwidth Communications Channels

Garry J. Heard, David J. Thomson, Gordon R. Ebbeson, and Ronald I.Verrall
Defence Research Establishment Atlantic
P.O. Box 1012 Dartmouth, Nova Scotia, CANADA B2Y 3Z7

INTRODUCTION

This paper is concerned with an initial look at how to transmit spectral information from a remote underwater acoustic array to a receiver that may be located anywhere on earth. This goal is a common desire in the fields of underwater acoustics, bio-acoustics, and oceanography.

The only viable way to succeed at this goal is to make use of satellite telemetry. Unfortunately, restrictions imposed by the necessary satellite coverage (open oceans and polar regions), the costs, and the need for relatively simple, small devices at the remote array location strongly restrict the bandwidth of the communications channel.

Previous remote systems have made use of the relatively inexpensive ARGOS satellite system, but these applications are limited to those with extremely low data rates on the order of 0.5-3.5 kBytes/day[1]. The Naval Research Laboratory (NRL) has investigated the other end of the spectrum by employing an 8.5 m-high surface buoy supporting a 1.5 m-diameter, stabilized, satellite transmitting-receiving dish antenna [2]. Neither of these systems are suitable for the majority of remote acoustic array applications: one because the data rate is far too low and the other because of the cost and sheer size of the equipment in addition to the high cost of the satellite time.

At present, and in the near future, it does not appear that there are any satellite systems that could be considered ideal for the majority of remote-array applications, at least for the marine field where the antenna can be expected to be constantly moving. There are two low-bandwidth, relatively low-cost satellite options that offer at least a partial solution: ORBCOMM and IRIDIUM [1]. These systems employ relatively simple antennae that should be adaptable for marine buoy use. Both of these systems have limitations related to availability, data packet lengths, and number of messages. Neither system would be capable of continuous operation and in both cases the inbound (remote location to fixed receiver) data rate is 2400 baud. Further investigation and experiments will be required to determine the applicability of these communication systems to marine remote-array applications.

Having established the motivation for this paper and discussed the options for actual implementation of remote satellite-linked arrays, we now turn our attention to the problem of reducing the array data to a volume manageable over a low-bandwidth communications link. Our particular interest is in transmitting information from a remote array that would allow us to locate and track a source of noise. Our preferred method of acoustic noise location in the ocean is known as matched field processing (MFP) [3].

In its simplest form, MFP consists of correlating spatially-distributed spectral information, often appearing as a cross-spectral matrix, with field replicas generated from an acoustic propagation model. The replicas are generated for hypothetical source locations (e.g., different ranges and depths) spread over a search grid. The correlations produce an ambiguity surface whose maximum value is interpreted as the true location of the acoustic source. Usually, the problem is complicated by the fact that the acoustic environment is not well known and global optimization over a multi-dimensional state-space is required to produce useful results. Such processing is quite demanding and not currently feasible to locate in a small remote array; hence, it is necessary to return array data to a location where it can be processed.

In the next section we consider the transmission rates necessary to return raw acoustic data, spectral data, and finally selected cross-spectral matrices to a laboratory location. In the third section we illustrate two methods for reducing cross-spectral matrices based on observed properties of such matrices and show the effect of the compression on the MFP results for synthetic test data. We do not consider the use of established compression algorithms which would be applied as a matter of course.

DATA RATES

In order to gain a perspective on the scope of the problem, consider a hypothetical array with 20 hydrophones, each sampled at 2500 Hz in order to provide a useful array bandwidth of 1000 Hz. Consider also that each sample is composed of 16 bits or two bytes. This example array would result in a raw data rate of 105 Bytes/sec. In addition to the raw acoustic data it is also necessary to establish a data protocol to allow for error detection and subsidiary information such as array identification, frequency, sample time, control commands, and averaging time. An additional physical layer protocol may be imposed by the communication system and this protocol may or may not be included in the published data transmission rates of the satellite system. Both protocols essentially act as an overhead on the raw acoustic data. Each data packet could easily require 24-48 Bytes of non-acoustic information. If data messages of 1 kByte are possible, then the overhead would be approximately 5%; however, it is not clear that packet lengths of 1 kByte will be possible and overhead could exceed 40%.

Recall that the existing satellite systems have inbound data rates of 2400 baud corresponding to approximately 240 Bytes/sec. Transmitting raw data from an array is clearly impossible, as together with protocol overhead, a compression ratio of about 700 would be required.

Another possibility is to transmit beam spectra from the array. With 1-Hz resolution, the 1000-Hz acoustic bandwidth would require 1000 numbers for each spectrum. Eight-bit (1 Byte) representation would be sufficient, implying that at least 5 seconds would be required to transmit each spectrum. Since a 20-element array would be easily capable of providing 10 independent beams it would require about 1 minute to transmit a snapshot. This situation would have limited use as spectra would be required more frequently for many applications. The high degree of order and similarity in the spectra would allow for reasonable compression ratios using any number of standard techniques. It is conceivable that data compression techniques would allow enough spectra to be transmitted for the majority of applications.

Cross-spectral matrices comprise other data types that could be

transmitted and have the advantage of allowing MFP and other advanced signal processing techniques to be carried out at the receiver location.

In the case of our hypothetical 20-element array, a cross-spectral matrix (CSM) is composed of 400 complex numbers. This array would require 3200 Bytes with single-precision representation. Transmitting an entire matrix would take about 16 seconds. Tracking and localization applications would require numerous CSM's at different times and frequencies. Since applications would employ averaging times of between 0.5 to 25 seconds, it is clear that we would soon fall behind and the result would be snapshot acoustic information with relatively low duty-cycles.

Fortunately, CSM's are Hermitian and therefore we can immediately save channel bandwidth by sending only the diagonal and upper-triangular part of the matrix. Although this symmetry reduces the data to be transmitted by almost half, even this data reduction is not sufficient and further compression is desired.

CSM COMPRESSION

Two relatively simple schemes for reducing the amount of data in a CSM are discussed in this section. The first scheme consists of a threshold operation on the CSM and a subsequent sparse matrix representation of the thresholded matrix. The second method consists of an eigenvalue/eigenvector decomposition of the CSM followed by elimination of eigenvalue/eigenvector pairs based on the magnitude of the eigenvalues. The CSM matrices are reconstructed from the reduced data sets and MFP is applied. The effects of successive increases in the level of compression are observed on the peak ambiguity value and the determined location (range, depth) of the acoustic source.

Two synthetic data sets are included in the current work. These data sets are COLNOISE A (40 dB SNR, source at 9.1 km, 66 m depth) and B (-5 dB SNR, source at 9.7 km, 58 m depth) taken from the matched field processing benchmark problems [4]. The COLNOISE data include a coloured spectral background due to breaking waves at the ocean surface. The test environment consists of a shallow water region of 100-m uniform depth. A weakly downward refracting sound-speed profile exists in the water column and the bottom is consistent with a clay sediment overlying a homogeneous half-space.

CSM's generally contain a few dominant values and many smaller values. It was expected that the small values could be eliminated. Indeed, this seems to be true, as the MFP results (Fig. 1) show that for both high and low SNR test cases a significant portion of the CSM could be set to zero without affecting the localization result. For the high SNR case, we were able to lower the threshold to 65% of the modulus of the largest element without disturbing the localization result. For the low SNR case, we were able to lower the threshold to about 30% of the maximum modulus value. In both cases the sparse matrix representation resulted in over 80% compression without including the additional 50% compression available due to the symmetry of the CSM. Thresholding provides a data compression rate that may be independent of the SNR, clearly many applications could obtain a potential 10:1 reduction in the data rate.

Eigenvector based MFP has been successfully carried out by others [5] in the past. It has long been known that a few eigenvalues are generally much larger than the rest and that MFP can be successful with just one or a few of the largest eigenvalue/eigenvector pairs. The use of eigenvalue/eigenvector decomposition appears attractive for compressing the CSM data since each CSM can be reduced to RE(N+1) Bytes, where R is the number of bytes in the floating point representation, N is the number of hydrophones, and E is the number of eigenvalues retained. For our example array with single-precision representation this works out to 168 Bytes/eigenvalue, or only 5.25% of the original matrix size. In both the COLNOISE A and B test cases, using only the largest eigenvalue/eigenvector pair proved to be sufficient, providing an almost 20:1 reduction in the data rate.

SUMMARY

This paper has discussed the potential for transmitting spectral data from a remote array via existing low-bandwidth satellite communication channels. Two methods of reducing the necessary data have been presented and illustrated with synthetic test cases. It is apparent that the existing satellite channels are insufficient for continuous operation, but should meet the requirements of some applications where periodic snapshots of data will suffice.

REFERENCES

1 Mah, K. Satellite data telemetry. Seimac Ltd. Dartmouth, NS, TR-421-99-002, 1999.

2 Rupar, M.A., Goldstein, J.A., Krout, T.L. Data telemetry and acquisition system for acoustic signal processing investigations. NRL Report NRL/MR/5550-96-7820, Naval Research Laboratory, Washington, DC, 1996.

3 Tolstoy, A. Matched field processing for underwater acoustics. World Scientific, Singapore, 1993.

4 Porter, M.B., Tolstoy, A. The matched field processing benchmark problems. J. Computat. Acoust. 2(3), 161-185, September 1994.

5 Ozard, J.M. Matched field processing in shallow water for range, depth, and bearing estimation: results of experiment and simulation. J. Acoust. Soc. Am., 86(2), 744-753, August 1989.

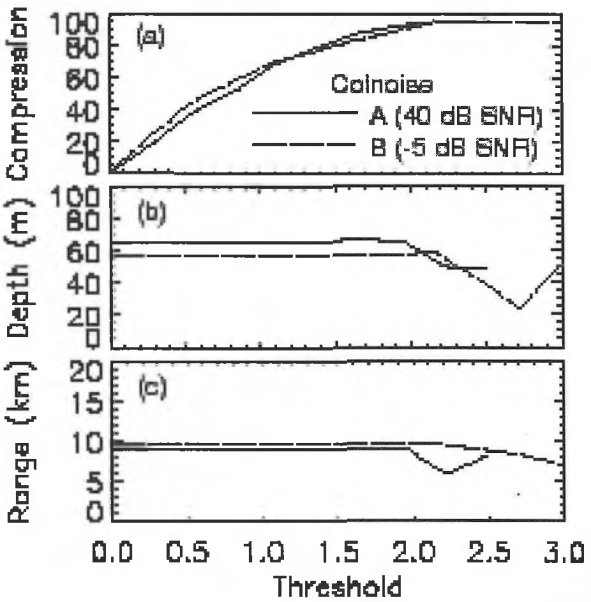

Figure 1. Matched field localization results using CSM with elements smaller than threshold set to zero. (a) sparse matrix compression percentage exclusive of additional reductions available from symmetry, (b) depth estimate, (c) range estimate.

THE SPINNAKER PROJECT: AN ARCTIC ACOUSTICS TALE

Ronald I. Verrall
Defence Research Establishment Atlantic
P.O. Box 1012 Dartmouth, Nova Scotia, CANADA B2Y 3Z7

INTRODUCTION

During the late 1980's, a joint Canadian-American project was initiated to install a hydrophone array on the bottom of the Arctic Ocean and to telemeter the data back to shore over a fiber-optic cable. The array was to be placed near the edge of the continental shelf north of Ellesmere Island, N.W.T., and the fiber-optic cable was to be brought ashore near Canadian Forces Alert, which is on the north coast of the Island (Figure 1).

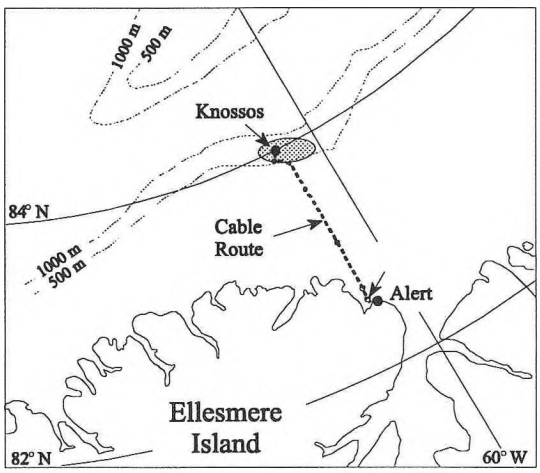

Figure 1: Map showing array site and cable route.

There were three main purposes for this installation. The first was to gather ambient noise and other environmental data in that particular part of the Arctic Ocean. The second was to use the array to prove-out new techniques of analyzing the data gathered from large arrays. The term 'matched-field processing' is generally applied to these algorithms. The third purpose was to develop and demonstrate the technical capability of installing such a complicated system under the heavy continuous ice cover of the Arctic Ocean.

The project was planned and directed by two defence laboratories, the Canadian Defence Research Establishment Pacific (DREP), located in Victoria, BC, and the American Naval Command, Control and Ocean Surveillance Center, Research, Development, Test and Evaluation Division (NRaD), located in San Diego, CA. The work very conveniently separated into two main parts. The Americans built the low-powered hydrophone array and installed it on the ocean bottom. They also designed and installed the hardware to transmit the data along the fiber-optic cable. The Canadians were responsible for laying the fiber-optic cable between the array and the shore, across the shore and into the analysis room in CFS Alert. This involved the design, construction and operation of an autonomous underwater vehicle that laid 180 km of cable under the polar ice. The recording and analysis of the data was a joint responsibility.

Some of the original planning and strategy sessions were held in a well known Victoria pub; consequently the whole scheme became known as 'Project Spinnaker'.

This paper concentrates on the Canadian contribution: the design, testing and operation of the cable-laying AUV, and the installation of the cable in the Arctic Ocean.

THE AUV THESEUS - DESIGN SPECIFICATIONS

Starting in the early 1990's, DREP had a series of contracts with International Submarine Engineering Research (ISER) of Vancouver, BC to design and build a large autonomous underwater vehicle that was capable of laying cable in ice-covered waters. Later, this AUV was known as Theseus - named for the hero of Greek mythology who laid a string behind himself on his way into the labyrinth.

The design constraints on Theseus were severe. The vehicle had to carry (and lay) up to 220 km of fiber-optic cable in an operating area where the ocean is completely ice-covered, mostly by multi-year ice 3.5 to 10-m thick, with ice keels that can dip to a depth of 30 metres or more. Water temperatures are very near freezing, and the currents could be as high as 25 cm/s (0.5 knots).

The navigational ability of the system had to be such that the AUV could pilot itself to a spot 180 km offshore and then 'fly' through a 200-m-wide loop of rope that was suspended from the ice. This ability was achieved by designing the basic navigational system to have an accuracy of about 1% and then updating the vehicle's dead-reckoned position at a series of acoustic beacons that were hung below the ice at known locations. In order to minimize the amount of cable falling through the water column behind the vehicle, Theseus had to follow the bottom (without running into it) at an altitude of about 20 m. Acoustic telemetry was a necessary feature so that communication was possible with the vehicle - especially in emergencies. (Continuous communication with the vehicle was possible as long as Theseus was connected to the shore via the fiber-optic cable.) Since Theseus had to travel both out to the array and then back to shore, it was designed to have an endurance of 450 km. Finally, in order for the AUV to be transportable from the nearest airport (Alert) out onto the ice, it was to be built in modules, each one having a weight less than 1400 kg.

THESEUS - A DESCRIPTION

Figure 2 shows a cut-away view of Theseus, and Table 1 lists the vehicle's principle features.

PROPULSION: The vehicle is propelled by a single 6-hp brushless dc motor and a 61-cm-diameter propeller. Power for this motor (and for all the vehicle's 'hotel' power) is provided by a 360-kWH silver-zinc battery pack, which gives Theseus the capability of a mission at least twice as long as the one described here.

NAVIGATION: Theseus monitors its position by dead reckoning. It uses a Honeywell 726 ring-laser-gyro inertial navigation unit (INU) to provide heading and attitude data. It uses a Doppler sonar to measure the speed over the ground in both the forward and lateral directions. This combination was chosen to provide a position accuracy of 1% of distance travelled, but we found that with careful adjustment the cross-track error could be reduced to about 0.05%. The sonar also measures the altitude above the sea floor,

which is crucial since Theseus is programmed to fly close to the bottom.

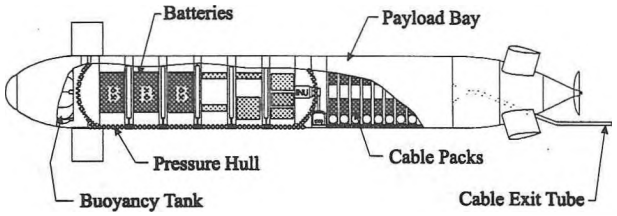

Figure 2: A cut-away schematic showing batteries and electronics in the (dry) pressure hull and the fiber-optic cable packs in the (flooded) payload bay.

Table 1: Theseus's principal features.

Length	10.7 m (35 feet)
Diameter	127 cm (50 inches)
Displacement	8600 kg (19,000 lbs)
Speed	2 m/s (4 knots)
Range	700 km (380 nm)
Maximum operating depth	425 m verified, 1000-m (3280-foot) design depth

CABLE DISPENSING SYSTEM: For 220 km of cable to be stored in a vehicle this size, the cable had to be small - 2 mm in diameter. The cable consisted of a single-mode fiber encased in a steel tube which, in turn, was surrounded by an e-glass wrapping. This was coated with Surlyn plastic. This cable was wound onto eleven spools (of 20 km each) which were stacked longitudinally along the vehicle axis, the appropriate ends being spliced together (Figure 2). The cable, which is pulled from the centre of the spool, is prevented from collapsing into a tangle by gluing the turns together with a special weak adhesive. For simplicity, no active dispensing devices were used; a tension of two to four pounds in the cable was maintained by the glue. The cable leaves the vehicle by way of an exit tube, which keeps the cable away from the screw.

The cable weighs about 2 lb/km (8.9 N/km) in water, and about 200 km of cable were deployed. This loss of 1800 N had to be prevented from affecting Theseus's neutral buoyancy and trim. Surrounding each cable spool is a toroidal ballast tank which is initially empty but which fills with water as the cable is dispensed. This keeps the net buoyancy of each spool/tank assembly near neutral.

ARCTIC CABLE LAYING

Getting Theseus assembled and working in the Arctic involved a lot of very specialized logistics. First, a small village of tents was assembled on the ice of Jolliffe Bay, about 6 km west of Alert. The biggest and most important of these was the tent for Theseus, which was 20 m by 11 m. Inside this tent a hole was made in the 1.7-m-thick ice for Theseus. A hot water drill was used to cut out blocks of ice, each weighing about 4 tonnes. The final hole was 12.2 m by 1.5 m, with extra cut-outs for Theseus's fins - about 70 tonnes of ice.

Two travelling gantry cranes were set up to carry Theseus from its assembly track over to this hole. (Actually, the first job of one of the cranes was to lift the blocks of ice onto the surface.) Next Theseus's assembly track was set up and levelled. Finally, a floor was laid on the ice and two furnaces were installed to heat the tent. Meanwhile, the rest of the camp, which included a mess tent, sleeping tents, a workshop tent and a tent for two Diesel generators was being established.

When all was ready, a Bell 212 helicopter slung the individual vehicle sections from Alert to the ice camp, where they were quickly placed in the warm tent. The next several days were spent loading batteries, electronics and all the fiber-optic cable into Theseus. The cable end was spliced to a pre-laid cable that passed through a hole which had been drilled through the fore-shore in 1994. This hole, which curved upwards, came up into the ocean bottom at a depth of 30 m, deep enough to protect the cable from the largest ice keels. From the beach the cable ran overland to a control centre in Alert. As long as the cable was continuous between Theseus and the shore, the control centre could monitor Theseus's location and health, and, if necessary, take control of the vessel.

Twenty days after it had been slung out to the Jolliffe camp, Theseus was finally ready to carry out its mission. On 17 April, 1996, Theseus left the shore camp, navigated itself through a fairly narrow channel and headed north. At three waypoints Theseus homed-in on acoustic beacons and used their known locations to update its dead-reckoned position. Two more beacons helped Theseus pass through the rope loop that captured the cable. Twenty four hours after departure Theseus successfully completed its first major task by flying through the loop. Once the cable had settled to the bottom of the loop it was pulled to the surface in order to splice it to the cable coming up from the hydrophone array. However, before the cable was cut, Theseus was commanded to return to shore. Note that its return was completely autonomous.

SUBSEQUENT CABLE REPAIRS

The acoustic array worked perfectly for about two months, but on 20 June the data stream suddenly stopped. An Optical Time-Delay Reflectometer (OTDR) at Alert showed no breaks in the shoreward 150 km of cable. Any break would have to be outboard of that. So, in 1997 we returned to Alert prepared both to fix cables and to replace the laser out at the array.

When we arrived we discovered a new cable break 14 km from Alert. Using P-code GPS we set up a camp on the ice over the estimated location of the break and sent down a Phantom ROV to find the cable. It turned out - both here and elsewhere - that the cable was always easy to find because it had been laid with such accuracy by Theseus. The two ends of the break were brought up to two different holes in the ice, and a short piece of connecting cable was slung under the ice between the two holes. Splices were made at the two holes, and the cable was dropped away. A second break was then found at 28 km. It was fixed, and then the laser was replaced at the array. This still left a break, but by this time we had run out of time. More details on this and subsequent repairs can be found in Reference 1.

REFERENCES

1 Verrall, R., Butler, B. 'Testing the Waters: Technologies Converge to Lay Arctic Cable'. GPS World, Vol 10, #5, May '99, pp 23-31.

Measurement of Underwater Sound Intensity Vector

Daniel Hutt, Paul C. Hines and Andrew Rosenfeld
Defence Research Establishment Atlantic
P.O. Box 1012, Dartmouth, Nova Scotia, Canada, B2Y 3Z7

Localization of underwater sound sources and characterization of ambient noise fields can be achieved through measurement of the sound intensity vector. To evaluate this concept, a passive hydrophone array called SIRA (Sound Intensity Receiver Array) has been developed for measurement of underwater sound intensity in the frequency range 100 to 6000 Hz. The array is composed of three pairs of omnidirectional hydrophones with the pairs aligned along orthogonal axes. The intensity is the time average of the product of instantaneous acoustic pressure and particle velocity. The instantaneous pressure is the average of the pressures measured by a hydrophone pair and the velocity is derived from the pressure gradient. Each hydrophone pair provides one of the components of the three dimensional intensity vector.

1. Description of instrument

SIRA was developed under contract for DREA by Guigné International Ltd. (GIL), Paradise, Nfld., Canada. To achieve the full frequency range of 100 to 6000 Hz, the mounting structure can be configured for two different hydrophone spacings, 8 cm or 19 cm. The 19 cm spacing is used to make measurements at frequencies down to 100 Hz while the 8 cm spacing allows measurements to be made up to 6000 Hz. Neither spacing can provide measurements over the entire frequency range as a result of the trade-off between errors in approximating the pressure gradient at high frequencies and susceptibility to noise at low frequencies, where the gradient is small. The hydrophones used in SIRA are model 1042 transducers from International Transducer Corp., Santa Barbara, CA. They are 35 mm-diameter spheres and are omnidirectional to better than 0.5 dB below 25 kHz. The hydrophones have sensitivities of approximately -200 dB//V/μPa in the band 1 kHz to 10 kHz. A photograph of the array with hydrophone spacing of 8 cm is shown in Fig. 1.

The SIRA preamplifiers, custom-built by GIL, have built-in high- and low-pass filters with cutoff frequencies of 100 Hz and 20 kHz, respectively. The preamplifiers have a 12 dB fixed gain at the input stage with 60 dB of additional gain selectable in 12 dB increments. All preamplifiers had 60 dB gain for the measurements presented here. At 1 kHz, the pre-amplifier noise is less than -165 dB//V/Hz$^{1/2}$ at all gain settings. Phase matching between the six preamplifiers is better than ±0.3° across the frequency band. The preamplifiers were paired to minimize the phase mismatch along each SIRA axis. Phase matching between pairs is better than ±0.05° across the frequency band. The inter-channel gain matching between all preamplifiers is better than ±0.3 dB and gain matching between axial pairs is better than ±0.1 dB. Plots of the preamplifier phase and gain can be seen in Ref. 1.

The SIRA mechanical apparatus is made up of a tubular pressure vessel 20 cm in diameter by 63.5 cm long which contains the preamplifiers and other electronics. The hydrophones are supported at the end of 1-m long stainless steel tubes which are attached to the bottom of the pressure vessel.

2. Intensity signal processing

The magnitude of the intensity component in direction $\bar{x}$ is the time averaged product of the instantaneous acoustic pressure p(t) and the particle velocity component $u_x(t)$,

$$I_x = \overline{p(t) \cdot u_x(t)} \quad . \tag{1}$$

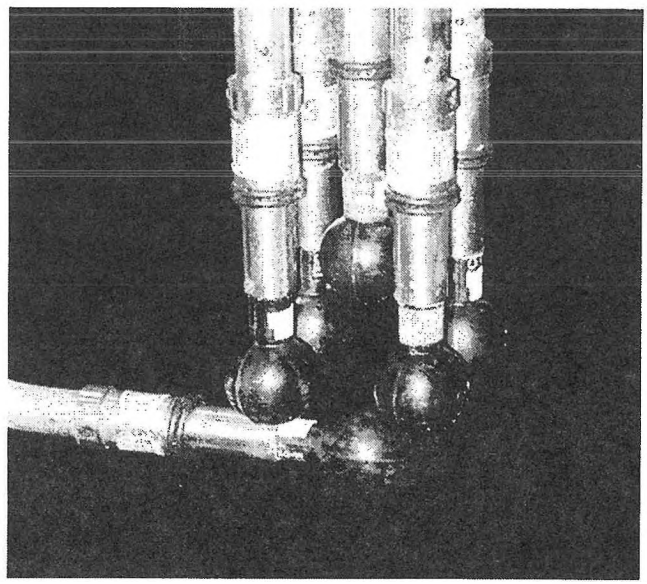

Fig. 1 Close-up of SIRA hydrophones and supporting structure. The hydrophone spacing is 8 cm.

SIRA uses pressure transducers to provide both pressure and particle velocity. This is referred to as the pressure-pressure method. The particle velocity is derived from the pressure gradient using the finite difference approximation,

$$u_x(t) = \frac{1}{\rho} \int_0^t \frac{p_{x2} - p_{x1}}{d} dt \quad , \tag{2}$$

where ρ is the water density and d is the distance between hydrophones x_1 and x_2. Equation 2 yields an exact value for the particle velocity in the limit of vanishingly small kd. In practice, kd must be large enough to give a measurable difference signal. It is easily shown that the error in $u_x(t)$ as calculated with Eq. 2 is only 5% for kd = 1 and 17% for kd = 2. For the 8 cm spacing of the SIRA hydrophones, kd = 1 represents a frequency of 3 kHz and kd = 2 represents a frequency of 6 kHz. The benefits of increased signal to noise ratio justify the measurement of intensity at these relatively high kd values.

The intensity can be calculated more efficiently by expressing Eq. 1 in terms of the Fourier transforms of $p_{x1}(t)$ and $p_{x2}(t)$. The time averaged intensity component I_x is then given by the imaginary part of the cross spectrum of the pressure signals[2],

$$I_x = \frac{\mathrm{Im}\left[S_{x1}(\omega) S_{x2}^*(\omega) \right]}{\rho \omega d} \quad , \tag{3}$$

where $S_{x1}(\omega)$, $S_{x2}(\omega)$ are the Fourier transforms of $p_{x1}(t)$, $p_{x2}(t)$ and ω is the angular frequency, 2πf. If the measurements are made in the far field, then the three components of the intensity vector given by Eq. 3 yield the direction to the source via,

$$\theta = \tan^{-1}(I_y / I_x) \quad \text{and} \quad \phi = \cos^{-1}(I_z / I) \quad , \tag{4}$$

where $I = \sqrt{I_x^2 + I_y^2 + I_z^2}$.

3. Measurement set-up

Preliminary results presented here were obtained at the DREA acoustic calibration barge facility. The barge is 36 m long by 17 m wide and contains a rectangular well, 9 m by 18 m, which is open to the sea. The barge is located in the Bedford Basin near DREA in water of approximately 42 m depth. The array was mounted in the barge well so that its center was at a depth of 10 m. The projector was a type J11 transducer, produced by the US Naval Underwater Sound Reference Laboratory. With both the array and projector at depths of 10 m and separated by 10 m, sound pulses up to 10 ms in length could be received at the array before the arrival of the first reflection. A computer synthesized the transmitted waveforms and handled the digitization and recording of the time series data.

4. Dipole response functions

The performance of the intensity array can be evaluated by measuring the difference signal of hydrophone pairs for a narrowband acoustic wave as a function of array rotation angle. Ideally, when a pair of hydrophones is aligned with their axis perpendicular to the direction to the source, the received signals should cancel. In this orientation, any difference signal is due to imbalance in gain and phase response, scatter from the array components and the presence of system electronic noise and acoustical ambient noise. For kd<<1, and assuming a plane acoustic wave, the measured difference signals can be compared to an ideal dipole. An example is shown in Fig. 2 where measured data are displayed as dots and the curves are those of an ideal dipole given by cos(θ) for the x axis and sin(θ) for the y axis.

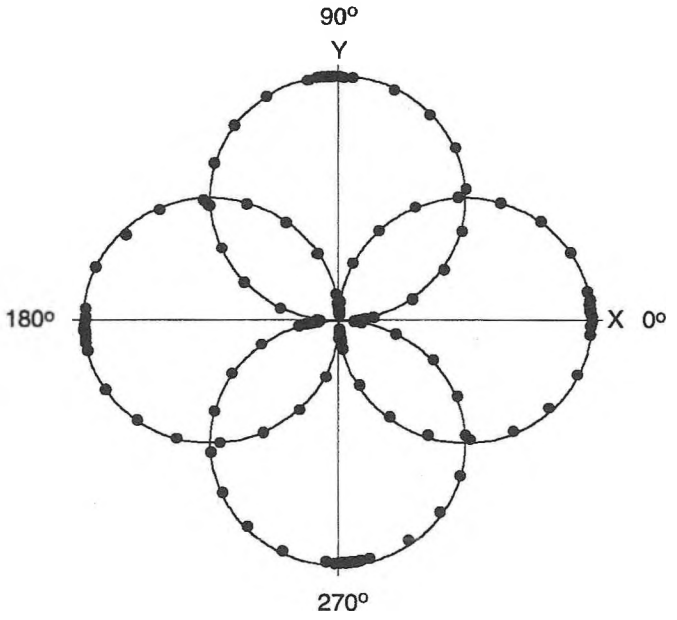

Fig. 2 Measured difference signals (points) and ideal dipole response (curves) for d = 19 cm and f = 500 Hz, plotted on a linear scale.

The measurements shown in Fig. 2 were made at a frequency of 500 Hz with a hydrophone spacing of 19 cm (kd = 0.4). The data points are based on the coherent average of 10 pulses, each of 10 ms duration. Data are normalized by the maximum value at the dipole lobes. The signal to noise ratio was approximately 35 dB during the measurements. The agreement between the measurements and ideal dipole indicates good performance for the horizontal SIRA channels. The symmetry of the dipole plots shows that the inter-channel phase matching is good. This is consistent with the fact that the best phase matching occurs at 500 Hz with an error of approximately 0.2°.

For the data shown in Fig. 2, the average value of the x and y nulls is 4.9% of the lobe maxima. If the data were expressed as intensity, the mean of the nulls would be -26 dB with respect to the lobe maxima. Measurements of the dipole pattern were obtained for frequencies from 500 Hz to 4000 Hz. The deepest set of nulls was obtained at 4000 Hz with a value of -32.5 dB. The presence of unavoidable ambient noise contributes to the residual difference signal at the nulls. Measurements made under quieter conditions and with greater angular resolution near the nulls could reveal that the SIRA nulls are deeper than presented here. Also, it is possible to correct for the measured channel phase and gain imbalances which could result in even better performance.

5. Direction to signal source

Processing the data of Fig. 2 to yield the x and y intensity vector components allows the direction to the source to be calculated via Eq. 4. A comparison of the calculated direction to the source and the measured array orientation angle is shown in Fig. 3. The standard deviation of the difference between measured and calculated angles is 1.4°. Although the width of the array is only 6% of a wavelength at 500 Hz, intensity processing allowed the direction to the source to be determined with an accuracy of 1.4°. Using conventional beamforming methods, an array would have to be several wavelengths in size to measure the direction to the source with the same accuracy.

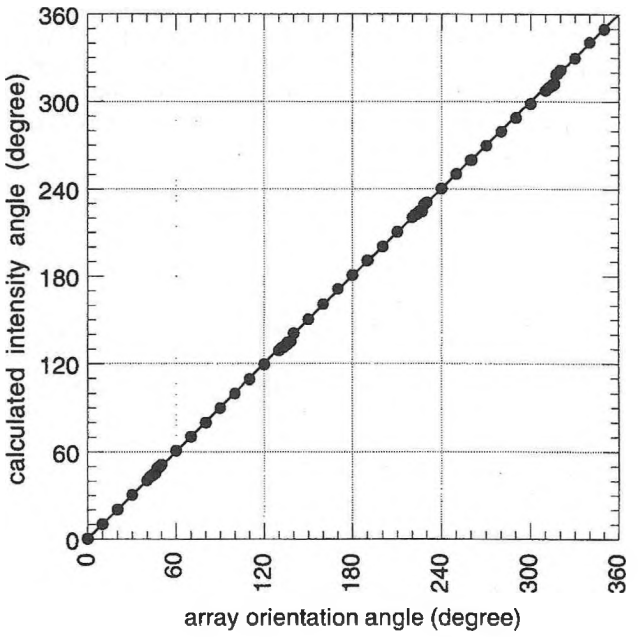

Fig. 3 Direction to acoustic source calculated from intensity vector components using Eq. 4 for f = 500 Hz and d = 19 cm.

6. References

1. Hines. P. C. and D. Hutt, "SIREM: An instrument to evaluate superdirective and intensity receiver arrays", Proc. Oceans'99, Seattle, WA (1999).
2. Fahy, F. J., *Sound Intensity*, Elsevier Applied Science, London (1989).
3. Franklin, J. B., "Intensity measurements and optimum beam forming using a crossed dipoles array", Defence Research Establishment Atlantic, DREA CR/97/443 (1997).
4. Cron, B. F., B. C. Hassell and F. J. Keltonic, "Comparison of theoretical and experimental values of spatial correlation", J. Acoust. Soc. Am. 37(3) 523-529 (1965).

NONLOCAL TOPS AND EQUIVALENT BOTTOMS FOR SOUND PROPAGATION IN AIR PROBLEMS

David J. Thomson
Defence Research Establishment Atlantic
P.O. Box 1012, Dartmouth, Nova Scotia, Canada, B2Y 3Z7

INTRODUCTION

One-way wave equations derived from parabolic equation (PE) approximations are widely used to model underwater and atmospheric sound propagation (see [1, Chap. 6], [2] and the references therein). Finite-difference PE solvers based on Padé series expansions provide accurate and efficient solutions to these one-way fields for range-varying geoacoustic environments [3]. For layered media, alternative approaches based on normal mode, multipath expansion or wavenumber integration representations are available [1], [4]. Since proper analysis of acoustic field behaviour often relies on using more than one propagation model, it is desirable to obtain numerical agreement between models in situations where different models apply.

To solve a PE numerically, the computational grid must be terminated top and bottom. In outdoor sound applications, the acoustic field is usually assumed to satisfy a locally-reacting (constant impedance) boundary condition along the ground plane [2], [4]. This condition is easily incorporated into finite-difference PE models [5]. On the other hand, wavenumber integration codes such as SAFARI, that were developed specifically for underwater sound propagation applications, do not incorporate this locally-reacting condition directly [6], [7]. In the first part of this paper, we design an equivalent fluid whose reflection response is numerically equivalent to that produced by a constant impedance surface.

Wavenumber integration models inherently satisfy a radiation condition as $z \to \infty$. In contrast, PE solvers usually handle upgoing waves by appending an artificial absorbing layer to the computational mesh in order to attenuate the radiated energy. In the second part of this paper, we present a nonlocal boundary condition (NLBC) that exactly transforms the semi-infinite PE problem with a radiation condition at $z \to \infty$ to an equivalent PE problem in a bounded domain [8], [9], [10], [11].

We provide a numerical example that compares SAFARI predictions (obtained with an equivalent bottom) to PE predictions (obtained with an NLBC top) for a problem that typifies outdoor sound propagation.

PE BASICS

For sound propagation in 2D (range r, height z), the outgoing spatial component $p(r,z)$ of the acoustic pressure $p\exp(-i\omega t)$ can be recovered from the reduced field $\psi = p\exp(-ik_0 r)\sqrt{k_0 r}$, where $k_0 = \omega/c_0$, by solving

$$\frac{\partial \psi}{\partial r} = ik_0\left(-1+\sqrt{1+X}\right)\psi. \qquad (1)$$

Here $X = N^2 - 1 + k_0^{-2}\rho\partial_z\left(\rho^{-1}\partial_z\right)$, $N = n(1+i\alpha)$, $n = c_0/c$ and ρ, c and α denote the density, sound speed and absorption, respectively. The field ψ also satisfies a radiation condition as $z \to \infty$. Setting $\delta = k_0\Delta r$, the formal solution to (1) is given by

$$\psi(r+\Delta r, z) = \exp\left(-i\delta + i\delta\sqrt{1+X}\right)\psi(r,z)\ . \qquad (2)$$

One higher-order procedure for solving (2) involves expanding the square-root operator in the Padé series [12]

$$-1+\sqrt{1+X} \approx \sum_{m=1}^{M}\frac{a_m X}{1+b_m X}\ , \qquad (3)$$

so that (2) can be cast in the form

$$\psi(r+\Delta r, z) = \prod_{m=1}^{M}\exp\left(\frac{i\delta a_m X}{1+b_m X}\right)\psi(r,z)\ . \qquad (4)$$

For sufficiently small δ, each propagator can be accurately approximated by its unitary Cayley form and (4) can be solved recursively for $m = 1,\ldots,M$ as

$$\left(1+c_m^- X\right)\psi_m(r,z) = \left(1+c_m^+ X\right)\psi_{m-1}(r,z)\ , \qquad (5)$$

where $c_m^\pm = b_m \pm \frac{1}{2}i\delta a_m$, $\psi_0(r,z) \equiv \psi(r,z)$ and $\psi_M(r,z) \equiv \psi(r+\Delta r, z)$. The operator X is handled numerically using a three-term finite-difference approximation so that each system in (5) is tridiagonal. This procedure advances the PE field one range step. In this paper, we limit our discussion to the single-term PE that results when $M = 1$, $a_1 = \frac{1}{2}$, and $b_1 = \frac{1}{4}$.

EQUIVALENT BOTTOM

The reflection coefficient associated with a locally-reacting boundary is given by (θ is the grazing angle)

$$R'(\theta) = \frac{Z'\sin\theta - 1}{Z'\sin\theta + 1}\ , \qquad (6)$$

where $Z' = X + iY$ is the ground impedance normalized by $Z_a = \rho_a c_a$, the impedance of air. In contrast, the reflection coefficient due to a uniform half-space can be written as

$$R(\theta) = \frac{(Z_g/Z_a)\sin\theta - \sqrt{1-\cos^2\theta/n_g^2}}{(Z_g/Z_a)\sin\theta + \sqrt{1-\cos^2\theta/n_g^2}}, \qquad (7)$$

where $Z_g = \rho_g c_g$ and $n_g = (c_a/c_g)(1+i\alpha_g)$ are the impedance and refractive index of the lossy ground, respectively. The goal is to choose c_g, ρ_g, and α_g to make $R = R'$ for all θ. Although this can't be done exactly, we can satisfy $Z_g/Z_a = Z'$ approximately by choosing c_g so that $n_g^2 \gg 1$ and solving for ρ_g and α_g from

$$\frac{(\rho_g c_g)/(\rho_a c_a)}{1+i\alpha_g} = X + iY\ , \qquad (8)$$

to determine the parameters of the equivalent fluid [10].

NONLOCAL TOP

PE calculations of sound propagation in air usually approximate the radiation condition as $z \to \infty$ by appending an absorbing layer to the top of the computational grid and setting the field to zero at the top of the absorber [1], [2]. Here, we introduce a nonlocal boundary condition (NLBC) that can be applied at a finite height $z = h$ and that does not require an absorbing layer. The medium in $z > h$ is assumed to be uniform. For the first-order PE corresponding to $M = 1$, an NLBC can be derived in the form [11]

$$\left\{ \frac{\partial}{\partial z} + i \left(\rho_a / \rho_g \right) \Gamma_1 \right\} \psi(r + \Delta r, h) = 0, \qquad (9)$$

where Γ_1 is the vertical wavenumber operator defined by

$$\Gamma_1^2 = k_0^2 \left(N_g^2 - 1 + \frac{4i}{\delta} \frac{1 - \mathcal{R}}{1 + \mathcal{R}} \left[1 + \frac{i}{\delta} \frac{1 - \mathcal{R}}{1 + \mathcal{R}} \right]^{-1} \right), \qquad (10)$$

and $\mathcal{R} = \exp(-\Delta r \partial_r)$ is a range translation operator. Noting that $\mathcal{R}^j \psi(r, h) = \psi(r - j\Delta r, h)$, Γ_1 can be expanded in a Taylor series in $\mathcal{R}$ to yield a nonlocal implementation of (9), i.e., the field $\psi(r + \Delta r, h)$ is expressed in terms of the known field along $0 \to r$. Nonlocal boundary conditions derived from spectral formulations are considered elsewhere [8], [9], [10].

EXAMPLE

Consider the sound speed profile $c(z) = 330 + 0.12z$ m s^{-1} for $0 < z < 100$ m capped by a uniform half-space of speed 342 m s^{-1} [5]. The air in $z > 0$ is taken to have uniform density 0.0012 g cm^{-3} and absorption 0 dB λ^{-1}. Calculations are carried out for a 40-Hz source at $z = 2$ m and a receiver along $z = 1$ m above an impedance plane where $Z' = 31.4 - 38.5i$. Choosing $c_g = 33$ m s^{-1} in (8) yields $\rho_g = 0.9422$ g cm^{-3} and $\alpha_g = 66.92$ dB λ^{-1} for the equivalent fluid for use with SAFARI. The NLBC in (9) for use with the PE model was applied along the top of the refracting layer, $z = 100$ m. The PE calculations were carried out using $\Delta r = 1$ m, $\Delta z = 0.25$ m and $c_0 = 330$ m s^{-1}. SAFARI and PE predictions of transmission loss ($-10 \log_{10} |p|^2$) versus range are compared in Fig. (1). The agreement between the two model predictions is observed to be excellent. For this downward refracting profile, several trapped modes are observed to interfere coherently as a function of range.

REFERENCES

[1] F.B. Jensen, W.A. Kuperman, M.B. Porter and H. Schmidt, *Computational Ocean Acoustics*, (AIP Press, New York, 1994).

[2] M. Galindo, M.R. Stinson and G. Daigle, "Comparison of some methods used for prediction of atmospheric sound propagation," Can. Acoust. **25**(4), 3–11 (1997).

[3] M.D. Collins and E.K. Westwood, "A higher-order energy-conserving parabolic equation for range-dependent ocean depth, sound speed, and density," J. Acoust. Soc. Am. **89**, 1068–1075 (1991).

[4] K. Attenborough, S. Taherzadeh, H.E. Bass, X. Di, R. Raspet, G.R. Becker, A. Güdesen, A. Chrestman, G.A. Daigle, A. L'Espérance, Y. Gabillet, K.E. Gilbert, Y.L. Li, M.J. White, P. Naz, J.M. Noble and H.A.J.M. van Hoof, "Benchmark cases for outdoor sound propagation models," J. Acoust. Soc. Am. **97**, 173–191 (1995).

[5] K.E. Gilbert and M.J. White, "Application of the parabolic equation to sound propagation in a refracting atmosphere," J. Acoust. Soc. Am. **85**, 630-637 (1989).

[6] H. Schmidt, "SAFARI Seismo-Acoustic Fast field Algorithm for Range-Independent environments User's Guide," SACLANT Undersea Research Centre, San Bartolomeo, Italy, Rep. SR–113, 1988.

[7] A. Güdesen, "Application of the SAFARI model to sound propagation in the atmosphere," J. Acoust. Soc. Am. **87**, 1968–1974 (1990).

[8] J.S. Papadakis, M.I. Taroudakis, P.J. Papadakis and B. Mayfield, "A new method for a realistic treatment of the sea bottom in the parabolic approximation," J. Acoust. Soc. Am. **92**, 2030–2038 (1992).

[9] J.S. Papadakis, "Exact, nonreflecting boundary conditions for parabolic-type approximations in underwater acoustics," J. Comp. Acoust. **2**, 83–98 (1994).

[10] D.J. Thomson and M.E. Mayfield, "An exact radiation condition for use with the *a posteriori* PE method," J. Comp. Acoust. **2**, 113–132 (1994).

[11] D. Yevick and D.J. Thomson, "Nonlocal boundary conditions for finite-difference parabolic equation solvers," J. Acoust. Soc. Am. **106**, 143–150 (1999).

[12] M.D. Collins, "Benchmark calculation for higher-order parabolic equations," J. Acoust. Soc. Am. **87**, 1535–1538 (1990).

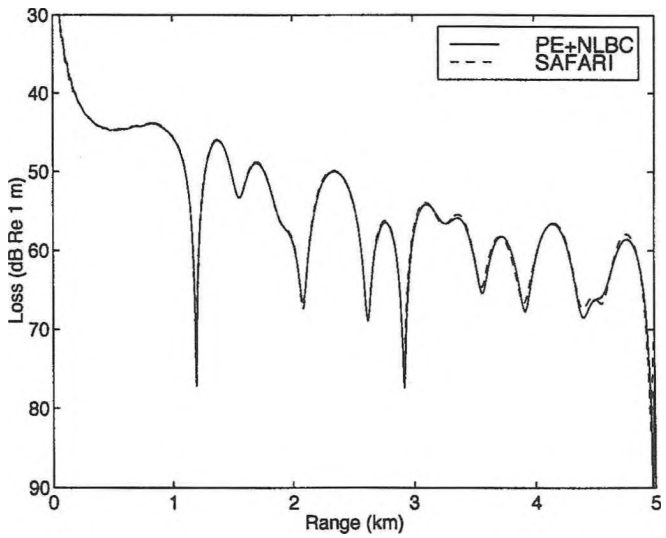

Figure 1: Transmission loss comparison.

A 2-D Description of 3-D Effects in Sound Propagation

Oleg A. Godin

School of Earth and Ocean Sciences, University of Victoria, P.O. Box 3055, Victoria, BC, V8W 3P6 &

Introduction

Mathematical modeling of low-frequency acoustic fields in the three-dimensionally inhomogeneous ocean is a computationally-intensive problem that remains intractable unless certain approximations are made to substitute the wave equation with a parabolic equation or to justify a reduction of the original problem to a sequence of 1-D and/or 2-D problems.

The adiabatic approximation [1, Sect. 7.1.3] is frequently used when modal concepts are applied to modeling and interpretation of the underwater acoustic fields in a range-dependent waveguide. For the 3-D problem of sound propagation in horizontally-inhomogeneous waveguides with gradual variation of the environmental parameters in the horizontal plane, the adiabatic mode method transforms into so-called "vertical modes - horizontal rays" approximation. Within this approximation, individual modes propagate from the CW source, without coupling, along certain curves in the horizontal plane. The curves are known as horizontal (or modal) rays, and their shape depends on sound frequency, mode order, and horizontal gradients of environmental parameters. Modal phase is given by an integral of the mode wavenumber along the horizontal ray, while modal amplitude depends on the variation of the cross section of a ray tube of the horizontal rays [1, Sect. 7.2].

It is typical to make a further approximation and substitute modal rays by radials from the source to receivers. Such an approximation is motivated by two facts. First, environmental parameters are often measured only along a radial. Second, modal ray curvature is normally small compared to the reciprocal of propagation range. The straight-ray approximation makes numerical tracing of modal rays unnecessary. It greatly reduces computational load and is especially important, if not imperative, for modeling broad-band fields and/or solving inverse problems in 3-D.

Although the straight modal ray approximation is implicit in the bulk of applications, its domain of validity has not been established. Moreover, it remains an open question what is the right way to calculate the modal amplitude along the radial. An expression originally proposed by Pierce [2] has been criticized as inconsistent with the reciprocity principle [3, 4]. Other expressions for the amplitude were put forward in [1, Sect. 7.2.2; 3; 4]. In this paper, we apply a perturbational analysis of horizontal ray equations to study accuracy of the straight modal ray approximation and to systematically derive an expression for the adiabatic mode amplitude that is more accurate than the *ad hoc* expressions proposed earlier in the literature.

Acoustic field in a horizontally-inhomogeneous waveguide

Consider acoustic field at a point with the horizontal coordinates $(x_2, y_2) = \boldsymbol{r}_2$ and the vertical coordinate z_2 due to a point source at $(\boldsymbol{r}_1, z_1)$. Assuming the unit strength of the source and slow, gradual dependence of environmental parameters on horizontal coordinates, one has [1, Sect. 7.2]

$$p(\boldsymbol{r}_2, z_2; \boldsymbol{r}_1, z_1) = \sum_n \left(\frac{1}{8\pi D_n} \right)^{1/2} f_n(z_1; \boldsymbol{r}_1) \times f_n(z_2; \boldsymbol{r}_2) \exp\left(i \int_{\boldsymbol{r}_1}^{\boldsymbol{r}_2} q_n \, ds - \frac{3\pi i}{4} \right). \quad (1)$$

Here p stands for acoustic pressure, f_n is a normalized shape function of a local mode of the order n, $q_n = q_n(\boldsymbol{r})$ is wavenumber of the mode. Integration in the exponent is along a horizontal ray $\boldsymbol{r}=\boldsymbol{r}(\tau, \psi_1)$ that connects the source and receiver, ψ_1 is the launch angle of the ray, i.e. the angle the ray makes with Ox coordinate axis at the source, τ is a parameter that defines a point along given ray. The quantity D_n in (1) is related to cross section area of a modal ray tube and can be calculated as follows:

$$D_n \equiv \frac{\partial(x, y)}{\partial(\tau, \psi_1)} = q_n(\boldsymbol{r}_2) \left[\left(\frac{\partial y}{\partial \psi_1} \right)_\tau \cos\psi_2 - \left(\frac{\partial x}{\partial \psi_1} \right)_\tau \sin\psi_2 \right]. \quad (2)$$

where ψ_2 stands for the ψ value at the receiver. Equations (1), (2) are exact within the adiabatic approximation but their application requires knowledge of q_n as a function of the 2-D vector $\boldsymbol{r}$ and an extensive ray tracing in the horizontal plane.

A simpler expression for the field was first proposed in the pioneering paper [2] by *Pierce*. It differs from (1) in that q_n is integrated along a radial from the source to receiver and D_n is calculated as

$$D_n = q_n(\boldsymbol{r}_2) |\boldsymbol{r}_2 - \boldsymbol{r}_1|. \quad (3)$$

It can be easily verified that (3) and the exact equation (2) are equivalent in the special case of cylindrically-symmetric medium with acoustic source located on the vertical axis of symmetry. Generally, however, D_n (3) is not invariant with respect to interchange of source and receiver positions, and therefore the resulting expression for acoustic pressure violates the reciprocity principle [1, Sect. 4.2]. To correct this shortcoming, some authors suggest using the expression [3]

$$D_n = \int_{x_<}^{x_>} q_n \, dx \quad (4)$$

instead of (3). To simplify notation, we chose here the coordinate system in such a way that $y_1=y_2=0$. Then integral in (4) is along an interval on the Ox axis; $x_<=\min(x_1, x_2)$, $x_>=\max(x_1, x_2)$. *Brekhovskikh* and *Godin* [1, Sect. 7.2.2] and independently *Porter* [4] proposed another expression:

$$D_n = q_n(x_1) q_n(x_2) \int_{x_<}^{x_>} \frac{dx}{q_n} \quad (5)$$

as an alternative to (3). This expression for D_n is manifestly reciprocal and reduces to the exact result (2) in the special case when environmental parameters are independent of the cross-range Cartesian coordinate y.

Qualitatively, for the expressions (3) - (5) to be useful when applied to a horizontally-inhomogeneous waveguide, true horizontal rays should be close to straight lines. However, the error introduced by using either (3) - (5) instead of (2) in the general 3-D environment has not been quantified in the literature.

Results of a perturbational analysis

To formalize the notion of "almost straight" modal rays, we represent the modal wavenumber squared as

$$q_n^2(\boldsymbol{r}) = k_0^2 + \epsilon g(\boldsymbol{r}), \quad |g|/k_0^2 \le 1, \quad 0 \le \epsilon \ll 1,$$
$$L_x = k_0^2/\|\partial g/\partial x\|, \quad L_y = k_0^2/\|\partial g/\partial y\|. \qquad (6)$$

Here L_x and L_y are representative spatial scales of the wavenumber variation in the range and cross-range directions. The parameter ϵ describes deviation of the horizontally-inhomogeneous ocean considered from a layered medium. The deviation is assumed small. When $\epsilon=0$, the environmental parameters depend on depth z only, and all modal rays are straight lines. When $\epsilon>0$, each modal ray has a nonzero curvature unless ∇g is tangent to the ray. The curvature is small as long as $\epsilon \ll 1$.

For the media described by (6), solutions to the differential equations governing modal rays [1, Sect. 7.2.1] can be found in terms of series in powers of ϵ. At the next step, eigenrays are found analytically for given source and receiver locations. Then, mode phase and amplitude are calculated. It turns out that all the three *ad hoc* expressions (3) - (5) lead generally to $O(\epsilon)$ errors in mode amplitude. That is, (3) - (5) are not generally any more accurate than straightforward approximations $D_n=k_0|x_2-x_1|$ or $D_n=q_n(\boldsymbol{r}_3)|x_2-x_1|$, where $\boldsymbol{r}_3$ is an arbitrary point between the source and the receiver.

A more accurate result is given by

$$D_n = q_n(x_1,0)\,q_n(x_2,0)\left[\int_{x_<}^{x_>}\frac{dx}{q_n(x,0)} - \int_{x_<}^{x_>} dx\,(x-x_<)(x_>-x)\,\frac{\partial^2}{\partial y^2}\,\frac{1}{q_n(x,0)}\right] + O(\epsilon^2). \qquad (7)$$

Among the infinite number of approximations to D_n that have accuracy $O(\epsilon^2)$, we have chosen the one that becomes *exact* in two important special cases of translational and rotational symmetry. Equation (7) reduces to (5) and is equivalent to (2) when the environmental parameters do not depend on the cross-range y. The error term in (7) is also zero when the environment is cylindrically-symmetric and the Ox axis (i.e., the horizontal line connecting source and receiver locations) intersects the vertical axis of symmetry. In the particular case of the source lying on the axis of symmetry, (7) reduces to (3).

The Fermat principle guarantees that the integral of q_n along a straight line between the source and receiver gives mode phase $\theta(\boldsymbol{r}_2,\boldsymbol{r}_1)$ to within $O(\epsilon^2)$. A second-order phase correction arises due to the horizontal ray curvature. The perturbation theory enables one to represent the correction explicitly:

$$\theta(\boldsymbol{r}_2,\boldsymbol{r}_1) = \int_{x_<}^{x_>} q_n(x,0)\,dx - \frac{1}{2\sqrt{q_n(x_1,0)\,q_n(x_2,0)}} \times \int_0^{|x_2-x_1|}\frac{ds}{s^2}\left(\int_0^s \frac{\partial q_n}{\partial y}(x_< + a, 0)\,a\,da\right)^2 + O(\epsilon^3). \qquad (8)$$

The result is invariant with respect to interchange of the source and receiver positions. To determine the mode phase with (8), one needs to know only mode wavenumber and its cross-range derivative along a radial from the source to receiver. The derivative can be easily calculated provided local mode shape functions as well as horizontal environmental gradients are known. An explicit expression for ∇q_n in rather general fluid and fluid/anisotropic solid waveguides can be found in [5]. It is essentially a weighted sum of (i) slopes of ocean floor and internal interfaces within ocean bottom, (ii) horizontal gradients of sound speed and density in water, and (iii) horizontal gradients of elastic parameters of the bottom.

For the perturbation theory to be valid, excursion of the horizontal eigenray from Ox axis should be small compared to L_y. In terms of the propagation range $R=|x_2-x_1|$, this condition can be written as

$$\epsilon R^2 L_y^{-2} \ll 1. \qquad (9)$$

Effects of cross-range variation of environmental parameters on modal amplitude and phase enter (7) and (8) through terms with derivatives of q_n with respect to y. The effects may be very significant under the condition (9). In particular, deviation of the mode phase from the first term on the right side of (8) can be large compared to unity. When the effects of horizontal ray curvature are negligible, one can disregard azimuthal coupling and substitute the 3-D problem by the 2-D problem of sound propagation in the vertical xz plane. From (7) and (8) it follows that the uncoupled azimuth approximation (sometimes also referred to as *N×2-D* approximation) is applicable as long as the inequality

$$10^{-2} k_0 \epsilon^2 L_y^{-2} R^3 \ll 1, \qquad (10)$$

holds in addition to (9).

Implications the conditions (9) and (10) have on mathematical modeling of 3-D acoustic fields in horizontally-inhomogeneous deep- and shallow-water environments, will be discussed in the oral presentation.

Conclusion

The results obtained can be summarized as follows:

1. A new expression for the adiabatic mode amplitude in horizontally-inhomogeneous ocean is systematically derived that is manifestly reciprocal, requires knowledge of the local mode parameters only in the source-receiver vertical plane, and possess higher accuracy than previous formulations.
2. Adiabatic mode phase correction due to horizontal ray curvature is calculated analytically.
3. An applicability condition is obtained for the uncoupled azimuth approximation.

Acknowledgment

This work was supported in part by the Natural Sciences and Engineering Research Council of Canada.

References

1. L.M. Brekhovskikh, O.A. Godin: *Acoustics of Layered Media. II: Point Sources and Bounded Beams,* Springer Ser. Wave Phenom., Vol. 10 (Springer, Berlin, Heidelberg 1992).
2. A.D. Pierce: Extension of the method of normal modes to sound propagation in an almost-stratified medium, *J. Acoust. Soc. Am.* **37**, 19-27 (1965).
3. F.B. Jensen, W.A. Kuperman, M.B. Porter, H. Schmidt: *Computational Ocean Acoustics* (AIP Press, New York 1994). Sect. 5.9.3.
4. M.B. Porter: Adiabatic modes for a point source in a plane-geometry ocean, *J. Acoust. Soc. Am.* **96**, 1918-1921 (1994).
5. O.A. Godin: Acoustic mode reciprocity in fluid/solid systems: Implications on environmental sensitivity and horizontal refraction, in *Theoretical and Computational Acoustics '97*, ed. by Y. C. Teng et al. (World Scientific, Singapore, 1999), p. 59-75.

Simulations Of Full-Field Tomography Of Oceanic Currents In Shallow Areas

Dmitry Yu. Mikhin
Atlantic Oceanographic and Meteorological Lab / NOAA
4301 Rickenbacker Causeway Miami, FL 33149, U.S.A.

Matched Non-reciprocity Tomography (MNT)

According to the acoustical reciprocity principle, the CW acoustic pressures measured in reciprocal transmissions scheme are identical in motionless stationary media [1]. Oceanic currents are relatively slow, but even slow flows break reciprocity. Observing reciprocity breaking effects seems to be the only reliable way of detecting currents by acoustical methods. Usually acoustic tomography of currents relies on measuring non-reciprocity of travel times along acoustic rays. The approach experiences difficulties in shallow water due to problems with ray resolution and identification [2].

MNT [3,4] is an alternative full-field technique that generalizes Matched Field Processing [5] for the problem of flow monitoring. MFP solves inverse problems through multiple solutions of the forward problem. First, the sound propagation is simulated numerically for a large set of possible models of the environment. Then the simulation results are compared to the experimental data using some criterion. The model that provides the best match is taken as a solution of the inverse problem.

To detect currents MNT compares not the acoustic fields, but the differences in some acoustical quantity measured (and simulated) in reciprocal transmissions. In the absence of flows, there is no difference between reciprocal data and the method correctly gives zero current. Any non-reciprocity is transformed into flow field.

Put into practice, this simple idea leads to new problems:

- the computer model must correctly describe acoustical effects of oceanic currents in complicated shallow-water environments
- the method for comparing experimental and numerical results should be sensitive to flows, but not sensitive to uncertainties in other environmental parameters, like bottom topography and sound speed field
- the method is computationally demanding

These issues and possible solutions are addressed in the following sections.

Direct problem

In theory, acoustical fields in motionless and stationary media are symmetric with respect to interchange in source and receiver positions. However, most of numerical models do not preserve this fundamental property for general range-dependent media. (Ray models are a notable exception.) The fields predicted for reciprocal transmissions are different. The discrepancy is often related to bottom topography and sound speed field. For complicated scenarios it becomes comparable or exceeds the effects of flows. MNT inversion with such propagation models will attribute this non-reciprocity to currents and will give erroneous results.

An energy-conserving and reciprocal One Way Wave Equation (OWWE) for motionless fluid was proposed in [6]. For moving media, a closely related Generalized Claerbout PE (GCPE) was derived [7]. Application of OWWE to moving media is discussed in [8]. Efficient algorithm for solving GCPE and OWWE is developed in [8, 9]. The IFD scheme exactly comply with the reciprocity principle and the flow reversal theorem (FRT), which is an extension of reciprocity principle to moving media [1].

To demonstrate GCPE properties consider propagation of sound over a rugged wedge shown in Fig. 1. Sound speed field is defined by three vertical profiles at 3, 18, and 33 km. The profiles (not shown) approximately correspond to conditions in the Strait of Florida in summer. Point transceivers are located at 200 m depth 36 km apart. CW frequency is 50 Hz.

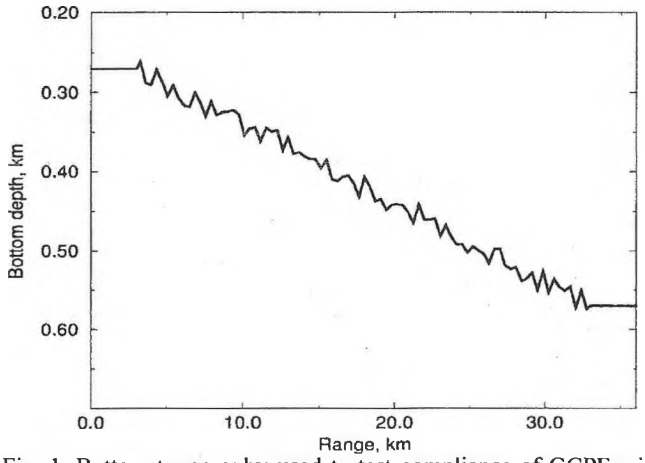

Fig. 1. Bottom topography used to test compliance of GCPE with the acoustical reciprocity principle

The acoustical amplitudes and phases predicted by GCPE for up-slope and down-slope propagation are presented in Fig. 2. The last 40 m of the propagation paths are shown. The fields at the transceivers' locations are identical. The agreement is within the limits of round-off errors: about 10^{-10} dB in amplitude and 10^{-10} degrees in phase.

Complicated bottom topography strongly affects acoustic fields. Acoustical imprints of currents are much smaller. However, the topography effects cancel each other in reciprocal transmissions. The subtle effects of currents are isolated in non-reciprocity.

The developed OWWE and GCPE models are adequate for acoustic monitoring of flows.

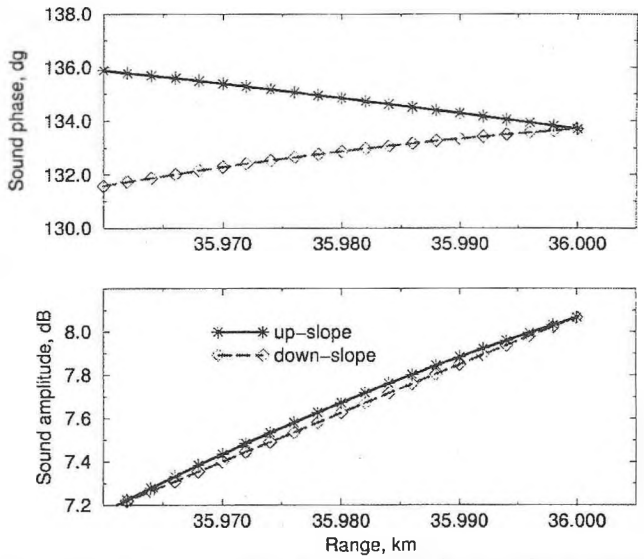

Fig. 2. Sound phases (top) and amplitudes (bottom) for reciprocal transmissions over the wedge of Fig. 1.

Cost functions

Theoretical and experimental non-reciprocities are compared using a measure or norm that in MFP and MNT is referred to as ***cost function***. The simplest cost function is RMS difference of non-reciprocities of complex acoustic pressure. However, this trivial cost function has poor performance [4, 10].

In real experiment, the exact geometry, bottom topography and properties, etc., are never known. Non-reciprocities of various acoustical quantities have different sensitivities to environmental parameters. Corresponding cost functions will have different response to experimental errors.

Theoretical analysis and numerical simulations in [3, 4, 10] revealed that non-reciprocity of acoustical phase does not depend on small variations in sound speed, density, bottom topography and geophysical properties, and horizontal separation between the transceivers. It is still quite sensitive to the vertical distribution of the flow field. On the opposite, non-reciprocity of complex pressure is as sensitive to the above mismatches as the one-way sound field itself. Non-reciprocity of acoustic amplitude reveals only weak dependence on the vertical profile of the flow. Robust cost functions should compare phase non-reciprocities. Auxiliary amplitude information might be used to give larger weight to phase data with good signal-to-noise ratio.

Originally, MNT was formulated for CW signals in accordance with MFP [4]. For CW sound, it is important to collect the data at many depths. A cost function using CW data from a single depth would not provide much resolution. Measuring depth dependence of non-reciprocity requires a vertical array of transceivers. This can be a synthetic aperture array, as MNT in not sensitive to mismatches in propagation range.

Acoustical phase is known with uncertainly of the total number of periods. RMS difference of phases becomes unstable when any phase is close to the limits of $[-\pi,\pi]$ period. A robust cost function is constructed from sine and cosine components of phase difference. A typical MNT cost function is [10]

$$F_{\Delta NT} = 2\left(1-\left[\left\langle I\cos\Delta\vartheta\right\rangle^2+\left\langle I\sin\Delta\vartheta\right\rangle^2\right]^{1/2}\Big/\left\langle I\right\rangle\right). \qquad (1)$$

Here $I=\left|p_e^{(+)}p_e^{(-)}p_t^{(+)}p_t^{(-)}\right|^{1/2}$ and $\Delta\upsilon=\arg\left(p_e^{(+)}\overline{p}_e^{(-)}\overline{p}_t^{(+)}p_t^{(-)}\right)$ are the amplitude weighting multiplier and phase non-reciprocity. Acoustic pressure fields $p^{(\pm)}$ correspond to downstream and upstream propagation; tilde denotes complex conjugation. Indexes "e" and "t" refer to experimental and predicted values. Angular brackets stand for averaging over a transceiver array.

Phase non-reciprocity is a distinct and non-degenerate function of frequency [10, 11]. Therefore, for current velocity inversions, the data on the depth-dependence of phase non-reciprocity can be efficiently combined with its frequency dependence. For realistic problems considered in [10, 11] the inversion was robust with only 3-4 transceivers. Hence, MNT can be implemented using standard tomographic transceivers instead of specialized transceiver arrays. Cost function for multi-frequency MNT is obtained, e.g., by averaging (1) over frequency.

Linearization

Search of the global minimum of MNT cost function requires repeated calculations of sound fields in range-dependent ocean for many times. The number of iterations rapidly increases with dimension of $\mathbf{q}$ space. The problem is strongly non-linear.

To accelerate inversion two linearized methods were developed [12]. For MFP linearization is possible for variations of the sound speed field as small as 1-2 m/s [5]. For temperature tomography this restriction is usually unacceptable. On the opposite, the amplitude of current velocity in the ocean is usually within these limits and linearization looks promising. Moreover, the second order terms mutually cancel in reciprocal values to be used for inversion which favors to linearization.

Non-reciprocity of acoustic phase depends linearly on the parameters of the flow model within some interval of their variation

$$\vartheta_t(\mathbf{q}) \approx \vartheta_t(\mathbf{q}_0)+\nabla\vartheta_t(\mathbf{q}_0)\cdot(\mathbf{q}-\mathbf{q}_0)\,. \qquad (2)$$

The first approach called complete linearization is to substitute (2) in (1) and convert $F_{\Delta NT}$ into a quadratic form of $\mathbf{q}-\mathbf{q}_0$. Good initial estimate $\mathbf{q}_0$ is required. In this approximation the full field phase non-reciprocity measured as a function of depth or frequency is converted into the flow field using existing linear inversion methods. These methods intrinsically provide the estimates of uncertainty of the inversion results.

The second approach is closely related to the normal mode theory. The phases of separate normal modes are calculated with (2) and then substituted into the standard modal formulas for $p_l^{(\pm)}(\mathbf{q})$. The cost function (1) remains non-linear with respect to $\mathbf{q}-\mathbf{q}_0$. However, its computation is much faster. This approach is referred to as partial linearization. Partial and complete linearization can be combined in one scheme.

Summary

The presented methods are essential components of acoustical toolbox for fast, accurate, and robust reconstruction of oceanic currents in shallow water environment. Their capabilities are confirmed by numerical simulations.

References:

[1] Godin, O. A. Reciprocity and energy theorems for waves in a compressible inhomogeneous moving fluid. *Wave Motion*, **25**, p.143-167, 1997.

[2] Palmer, D. R., L. M. Lawson, D. A. Seem, Y. H. Daneshzadeh. Ray-path identification and acoustic tomography in the Straits of Florida. *J. Geophys. Res.*, **90**, p.4977-4989, 1985.

[3] Godin, O. A., D. Yu. Mikhin. An opportunity for improved observation of ocean currents in the coastal zone. *Proc. Oceans '96 MTS/IEEE Conference*, Fort Lauderdale, Florida, p.345-350, 1996.

[4] Godin, O. A., D. Yu. Mikhin, S. Ya. Molchanov. Acoustic tomography of oceanic currents by the matched non-reciprocity method. *Acoust. Phys.*, **42**, p.441-448 (translated from *Akusticheskii Zhurnal*, **42**, p.501-509), 1996.

[5] Tolstoy, A. *Matched field processing for underwater acoustics*. World Scientific, Singapore, 212 p., 1993.

[6] Godin, O. A. Reciprocity and energy conservation within the parabolic approximation. Wave motion, **29** (2), p.175-194, 1999.

[7] Godin, O. A. A wide-angle, energy-conserving parabolic equation for sound in moving medium. *Proc. of the Third International Conference on Theoretical & Computational Acoustics*, Newark, NJ, July 1997, World Scientific, Singapore, 1999.

[8] Mikhin, D. Yu. Energy-conserving and reciprocal solutions for higher-order parabolic equations. *In the same issue*.

[9] Mikhin, D. Yu. Modeling Acoustic Tomography of Ocean Currents in Coastal Regions via Wide-Angle Parabolic Approximation. *Fourth European Conference on Underwater Acoustics (ECUA), Rome, Italy, September 1998*, p.581-586, 1998.

[10] Mikhin, D. Yu., O. A. Godin. Computer Simulations of Acoustic Tomography of Ocean Currents in Coastal Regions. *Proc. of the Third International Conference on Theoretical and Computational Acoustics*, Newark, NJ, July 1997, World Scientific, Singapore, 1999.

[11] 6. O. A. Godin, D. Yu. Mikhin. Numerical simulations of acoustic tomography of ocean currents in coastal regions. *Proc. 3rd European Conference on Underwater Acoustics*, ed. by J. S. Papadakis. Heraklion: FORTH-IACM, **2**, p. 785-790, 1996.

[12] Goncharov, V. V. Matched field processing in ocean acoustic tomography. *Proc. of the 7th Meeting of the Russian Acoustical Society*, Moscow, Russia, May 1998, p. 30-37. GEOS Publishing house, Moscow, 1998.

ENERGY-CONSERVING AND RECIPROCAL SOLUTIONS FOR HIGHER-ORDER PARABOLIC EQUATIONS

Dmitry Yu. Mikhin
Atlantic Oceanographic and Meteorological Lab / NOAA
4301 Rickenbacker Causeway Miami, FL 33149, U.S.A.

Parabolic equations

Conservation of sound energy in non-absorbing media and acoustical reciprocity in stationary fluids at rest are the fundamental properties of acoustic field [1]. Preserving these properties in parabolic approximations is essential for accurate modeling of sound propagation in shallow water environments.

An energy-conserving and reciprocal One Way Wave Equation (OWWE) for motionless fluid was proposed in [2]. OWWE allows improved description of mode coupling without adversely affecting phase accuracy [2]. For moving media a closely related Generalized Claerbout PE (GCPE) was derived [3]. Its solutions preserve the acoustic energy in the absence of dissipation and satisfy the flow reversal theorem (FRT), which is an extension of reciprocity principle to moving media [1].

OWWE of [2] is a pseudo-differential equation for 2D problem

$$\partial\left[\rho^{-1/2}\hat{G}_2\psi\right]/\partial x = ik_0\rho^{-1/2}\hat{G}\hat{G}_2\psi + i\left(2k_0\rho^{1/2}\hat{G}_2\right)^{-1}B\,. \qquad (1)$$

Here ψ is a complex envelope of sound pressure, ρ is density, $k_0 = \omega/c_0$ is a reference wavenumber, B is the source amplitude, and x is the horizontal coordinate along the propagation path. The operators are $\hat{G} = (1+\hat{X})^{1/2} - 1$, and $\hat{G}_2 = (1+\hat{X})^{1/4}$, where $\hat{X}$ is a dimensionless vertical operator defined below.

The GCPE for motionless medium corresponds to [1, 1] Padé approximation of operator $\hat{G}$ and two-term Taylor expansion of $\hat{G}_2$. In [3] it was obtained independently for moving medium by multi-scale asymptotic analysis:

$$\frac{\partial}{\partial x}\left[\left(\rho\beta^3\right)^{-1/2}\left(1+\gamma\hat{X}\right)\psi\right] = \frac{2\alpha ik_0}{\sqrt{\rho\beta^3}}\hat{X}\psi + \frac{i\nu}{2k_0\sqrt{\rho\beta^3}}\left(1+\gamma\hat{X}\right)^{-1}\beta B \qquad (2)$$

where $\beta = 1 - uc_0^{-1}$ is a local Doppler factor, u is an in-plane flow component. We write the equation in general form with arbitrary complex constants α, γ, ν to reveal similarity between OWWE and GCPE solutions. In [3] α and γ were the real coefficients of Padé and Taylor approximations $\alpha = \gamma = 0.25$ and $\nu = 1$. Finally, the vertical operator is

$$\hat{X} = \beta k_0^2\left[\rho\beta^2\,\partial\left(\left(\rho\beta^2\right)^{-1}\partial/\partial z\right)/\partial z + k^2\beta^2 - k_0^2\right]. \qquad (3)$$

OWWE (1) is derived for motionless medium with $\beta \equiv 1$. However, we can solve the equation with the vertical operator (3) with arbitrary β and ρ in (1) replaced by $\rho\beta^3$, in agreement with GCPE (2). Compared to GCPE, such solution does not improve asymptotic accuracy with respect to the Mach number. But it does not deteriorate the accuracy either, and has better wide-angle capabilities. Hence, this generalization is useful.

As with other PE's, there are several numerical approaches for solving (1,2) (e.g., [4, 5]). The existing algorithms can be applied to the new equations. However, the numerical scheme itself must be reciprocal and energy conserving, otherwise these advantages of the original differential PE's will be lost. This is especially important for reciprocity, because oceanic currents are slow and their effects are small. Even minor errors in numerical solution might become comparable with the current-induced effects. The existing IFD and split-step Fourier algorithms were found deficient for the new problem.

Numerical solution

An IFD algorithm preserving the conservation properties of the differential GCPE (2) with real-valued coefficients was proposed in [6]. The numerical solution satisfies discrete analogs of the acoustical reciprocity principle and FRT. Below it is generalized to handle OWWE, as well GCPE with source term and complex Padé coefficients.

Let us re-write (1,2) in terms of new dependent functions

$$U = \rho^{-1/2}\hat{G}_2\psi \;\text{ and }\; U = \left(\rho\beta^3\right)^{-1/2}\left(1+\hat{X}/4\right)\psi \qquad (4)$$

which are the local energy fluxes [2, 3] corresponding to (1,2). In terms of U the equations become

$$\partial U/\partial x = ik_0\left(\rho^{-1/2}\hat{G}\rho^{1/2}\right)U + i\left(2k_0\rho^{1/2}\hat{G}_2\right)^{-1}B \;\text{ and} \qquad (1a)$$

$$\frac{\partial U}{\partial x} = \frac{2\alpha ik_0}{\sqrt{\rho\beta^3}}\hat{X}\left(1+\gamma\hat{X}\right)^{-1}\left(\sqrt{\rho\beta^3}U - \frac{\gamma\beta B}{4\alpha k_0^2}\right) + \frac{i\nu\beta B}{2k_0\sqrt{\rho\beta^3}} \qquad (2a)$$

To convert OWWE into a parabolic equation the operators in (1a) are approximated by Padé series

$$\hat{G} \approx \sum_{l=0}^{L-1}\frac{2\alpha_l\hat{X}}{1+\gamma_l\hat{X}} \;\text{ and }\; \hat{G}_2^{-1} \approx \sum_{l=0}^{L-1}\frac{\nu_l}{1+\gamma_l\hat{X}} = \sum_{l=0}^{L-1}\left(\nu_l - \frac{\nu_l\gamma_l\hat{X}}{1+\gamma_l\hat{X}}\right). \qquad (5)$$

It is important to have the same set of coefficients γ_l in denominators of both approximations. Using decomposition (5), equation (1a) is solved by operator splitting method [7, Sect. 2.13]. The equation for each term of the Padé approximation is identical to (2a) with $\gamma = \gamma_l, \alpha = \alpha_l, \nu = \nu_l$. Then solution of (1a) is $U^{n+1} - U^n = \sum_{l=0}^{L-1}\left(U^{n+(l+1)/L} - U^{n+l/L}\right)$, where each term in the sum is taken from the solution of (2a) with corresponding l.

Consider equation (2a) on a uniform range-depth grid $x_n = n\Delta x, z_j = j\Delta z$ and apply Crank-Nicolson scheme to discretize the equation in range. Then introducing a new dependent function

$$\Theta^{n+1/2} = \frac{1}{2}\left(1+\gamma\hat{X}\right)^{-1}\Big|_{n+1/2}\left\{\left(\rho\beta^3\right)_{n+1/2}\left(U^{n+1}+U^n\right) - \frac{\gamma\nu\beta B^{n+1/2}}{2\alpha k_0^2}\right\} \qquad (6)$$

the differential equation (2a) transforms into an equivalent system of two finite-difference equations [6]:

$$\begin{aligned} U^n &= \left(\rho\beta^3\right)^{-1/2}\left\{\left[1+d^{(-)}\hat{X}\right]\Theta^{n+1/2} + \left(4\alpha k_0^2\right)^{-1}d^{(-)}\nu\beta B^{n+1/2}\right\}\Big|_{n+1/2} \\ U^{n+1} &= \left(\rho\beta^3\right)^{-1/2}\left\{\left[1+d^{(+)}\hat{X}\right]\Theta^{n+1/2} + \left(4\alpha k_0^2\right)^{-1}d^{(+)}\nu\beta B^{n+1/2}\right\}\Big|_{n+1/2} \end{aligned} \qquad (7)$$

$d^{(\pm)} = \gamma \pm ik_0\Delta x\alpha$. Finally, the vertical operator is discretized as

$$\left(\hat{X}\Theta\right)_{z_j} = \frac{\left(\rho\beta^3\right)_j}{\left(k_0\Delta z\right)^2}\left(\tau_j\left(\Theta_{j+1}-\Theta_j\right) - \tau_{j-1}\left(\Theta_j - \Theta_{j-1}\right)\right) + \frac{\beta_j\left(\left(k^2\beta^2\right)_j - k_0^2\right)}{k_0^2}\Theta_j$$

where $\tau_j = 0.5\left(\left(\rho\beta^3\right)_{j+1}^{-1} + \left(\rho\beta^3\right)_j^{-1}\right)$. Assume a point source of volume velocity is located at depth grid j_s within range cell $[n_s, n_s+1]$. Then the source term is presented in discreet form via Kroneker symbols as $B = a_s\omega^2\rho\beta^2\exp(-ik_0x_s)\delta_{j,j_s}\delta_{n,n_s}/\Delta x/\Delta z$.

To solve the equation numerically one determines $\Theta^{n+1/2}$ from U^n using the first equation (7) and then substitutes $\Theta^{n+1/2}$ to the second equation (7) to find U^{n+1}. Each step in range requires one solution of a three-diagonal system of algebraic equations and one back-substitution.

Properties of the new IFD solution

Exact reciprocity of the numerical solution is an inherent property of the IFD scheme [6], which is valid for ***arbitrary*** coefficients $\alpha_l, \gamma_l, \nu_l$. Compare propagation of sound between two point transceivers located in the grid cells $(j_0,0)$ and (j_M,M). It is assumed that direction of flow is changed to the opposite in the reverse propagation. The same derivation as in [6] proves that acoustical fields in direct and reverse transmissions are related by

$$a_{M}\Theta_{j_M}^{M+1/2}\exp(ik_0x_M) = a_0\Phi_{j_0}^{1/2}\exp(-ik_0x_M) \qquad (8)$$

where the value Φ corresponds to Θ in reverse transmission and $a_{0,M}$ are amplitudes of sources. In accordance with the FRT, the fields are symmetric with respect to interchange of source and receiver positions and simultaneous reversal of the flow direction. The same analysis gives the discrete boundary conditions on stair-step interface [6]. Reciprocity of the OWWE solution follows from reciprocity on each split-step. The reciprocal value for point sources of volume velocity, i.e., the discrete analog of acoustic pressure, is $\psi_j^n = \sum_{l=0}^{L-1}\nu_l\Theta_j^{n,l+1/2}$.

Energy conservation and reciprocity are equivalent in case of equations with real-valued coefficients [2, 3]. However, strict energy conservation is more a problem than an asset. Both the field components corresponding to discreet spectrum (normal modes) and the components corresponding to continuous spectrum are advanced in range without losses. In the solution of wave equation the modes should propagate (probably, with some attenuation), while the continuous spectrum should vanish. Cf. analysis in [8], propagation of continuous spectrum does not lead to infinite growth of the solution, because the energy is conserved, hence, always limited. However, the model does not reproduce an important feature of the wave equation and yields erroneous results.

To eliminate the evanescent spectrum in IFD-based PE's the operator $\hat{G}$ is approximated with complex Padé coefficients α,γ. The energy of the discrete solution of proved to be non-increasing for coefficients with $\mathrm{Im}\alpha = 0$, $\mathrm{Im}\gamma < 0$. Attenuation of a field component with horizontal wavenumber ξ is proportional to $\varepsilon^2\mathrm{Im}\gamma$, where $\varepsilon = (\xi^2 - k_0^2)/k_0^2$ is a measure of how wide-angle is the modal spectrum. If k_0 is chosen close to horizontal wavenumbers of propagating modes, than additional attenuation of modes due to complex coefficients is small. Field components with horizontal wavenumbers located far from k_0, including continuous spectrum, are effectively eliminated by IFD solution.

In terms of finite differences precise energy conservation or energy attenuation means the IFD scheme is ***conservative*** [9], hence, the discrete solution is ***stable***. System (7) and corresponding discrete boundary conditions [6] are consistent with the original PE and its boundary conditions [3]. Together with stability this establishes ***convergence*** of the scheme to the true solution for small $\Delta x, \Delta z$ [9].

Analysis of energy conservation for OWWE also demonstrates non-increase of acoustic energy for properly chosen coefficients. However, derivation is beyond the volume of the present paper.

Solution with large range step

The discreet solution presented above uses Crank-Nicolson finite-difference scheme in range. The range step should be small for accurate solution. A numerical technique for solving a parabolic equation with very large steps in range was developed in [5]. Following [5], we write a formal solution of (2a) in operator form:

$$U(x+\Delta x) = \left[\exp(i\hat{R})\right]U(x), \quad \hat{R} = 2\alpha\, k_0\Delta x\left(\rho\beta^3\right)^{-1/2}\hat{X}\left(1+\gamma\,\hat{X}\right)^{-1}\left(\rho\beta^3\right)^{1/2}$$

This operator equation is solved by the method of operator splitting [7]. The exponent is approximated by Padé series as $\exp(iR) \approx \prod_{l=0}^{L-1}(1+\sigma_l R)(1+\tilde{\sigma}_l R)^{-1}$. Then on each sub-step we define

$$U^{n+\frac{l+1}{L}} = \left(1+\sigma_l\hat{R}\right)\left(1+\tilde{\sigma}_l\hat{R}\right)^{-1}U^{n+\frac{l}{L}},\ l = 0,\ldots,L-1.$$

Combining the terms these equations are transformed into the form of (2a) with coefficient α replaced with $-2i\alpha\sigma_l$. The solution is reciprocal for any set of σ_l and its energy does not increase if $\mathrm{Im}\sigma_l > 0$, $l = 0,\ldots,L-1$.

Numerical examples

Due to the format limitations of the paper, all numerical examples are given in the accompanying paper [10].

Conclusions

Exact reciprocity, energy conservation, wide-angle capability and large steps in range are simultaneously achieved in IFD solution of one-way wave equation. The numerical scheme is robust, efficient, and allows generalization to 3D problems. The developed algorithm provides accurate description of acoustical effects of oceanic currents in complicated shallow-water environments. The software package is free for non-commercial and non-governmental use. It is available for download at http://rav.sio.rssi.ru/~dima. This work is partially supported by INTAS and NRC.

References:

[1] Godin, O. A. Reciprocity and energy theorems for waves in a compressible inhomogeneous moving fluid. *Wave Motion*, **25**, p.143-167, 1997.

[2] Godin, O. A. Reciprocity and energy conservation within the parabolic approximation. Wave motion, **29** (2), p.175-194, 1999.

[3] Godin, O. A. A wide-angle, energy-conserving parabolic equation for sound in moving medium. *Proceedings of the Third International Conference on Theoretical & Computational Acoustics*, Newark, NJ, September 1997, World Scientific, Singapore, 1999.

[4] Hardin, R. H., F. D. Tappert. Applications of the split-step Fourier method to the numerical solution of nonlinear and variable coefficient wave equations. *SIAM rev.*, **15**, p.423, 1973.

[5] Collins, M. D. A split-step Padé solution for parabolic equation method. *J. Acoust. Soc. Am.*, **93** (4, Pt. 1), p.1736-1742, 1993.

[6] Mikhin, D. Yu. Modeling Acoustic Tomography of Ocean Currents in Coastal Regions via Wide-Angle Parabolic Approximation. *Fourth European Conference on Underwater Acoustics (ECUA), Rome, Italy, September 1998*, p.581-586, 1998.

[7] Mitchell, A. R., D. F. Griffiths. The finite difference method in partial differential equation. Chichester; New York: Wiley, 1980.

[8] Wetton, B. T. R., G. H. Brooke. One-way wave equations for seismoacoustic propagation in elastic waveguides. *J. Acoust. Soc. Am.*, **87** (2), p.624, 1990.

[9] Samarsky, A. A., A. V. Gulin. Stability of difference schemes. *Nauka*, Moskva, 1973.

[10] Mikhin, D. Yu. Simulations of full-field tomography of oceanic currents in shallow areas. *In the same issue*.

Acoustic Measurements of the Two-Layer Exchange Flow in the Strait of Istanbul

Frank Gerdes
University of Victoria, School of Earth and Ocean Sciences, Victoria, BC, V8W 3P6 &
Institute of Ocean Sciences, Acoustical Oceanography Research Group, Sidney, BC, V8L 4B2

Introduction

Acoustical methods are playing an increasingly important role in the study of oceanographic phenomena. Here we discuss recent results illustrating the power of combining acoustic Doppler profiling, back scatter acoustic imaging and GPS navigation in a study of the exchange flow in the Bosphorus.

The Bosphorus, Dardanelles Straits and Sea of Marmara constitute a system through which an exchange of water takes place between the Black Sea and Mediterranean Sea. Low salinity water from the Black Sea, formed as a result of excess precipitation and river discharge, flows along the surface through the straits to the Mediterranean. A return flow of more saline, denser Mediterranean water returns to the Black Sea as an under current. Complexities of the Bosphorus flow include secondary and eddy circulations induced by the tortuous geometry of the strait, along strait density variations, and entrainment of fluid from one layer into the other [2].

The study of the physical processes affecting the exchange flow in the Bosphorus has become more and more important over the years. Large vessel traffic is likely to increase in future if plans to ship oil from the Caspian Sea to the western countries through the Bosphorus become reality. Furthermore the constantly expanding population of Istanbul causes increasing pollution of the Bosphorus and the adjacent seas. Assessing the effects of the pollution on the seas requires a good knowledge of the physics of the flow in the Bosphorus.

Background

The Bosphorus is a meandering strait about 31 km in length, with widths varying from 0.7 to 3.5 km, averaging about 1.6 km. Average and maximum depth are 35 and 110 m. Its bed is a drowned river channel, on average more than 50 m deep. The important geometrical features affecting the flow are two sills and a contraction. The southern sill has a depth of 33m. The northern sill is located just north of the Bosphorus - Black Sea junction and has a depth of about 60m. At the contraction the strait is only 600m wide. This is also the deepest section ($\approx$ 110m).

The Bosphorus is a strongly stratified two-layer system. Highly saline ($S \approx 38$ psu) Mediterranean water flows north under fresher and therefore less dense Black Sea water ($S \approx 18$ psu) which flows into the opposite direction (see Figure 1).

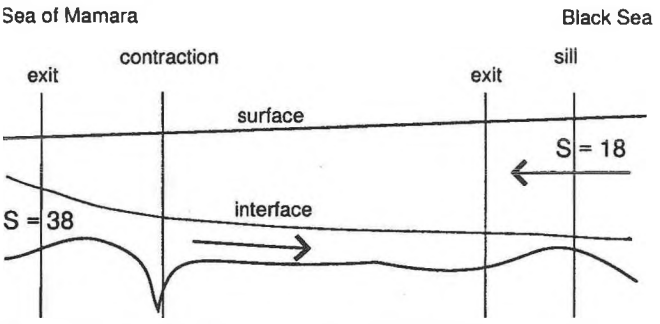

Figure 1: Sketch of the two-layer flow in the Bosphorus.

Experiment

In August 1998 we surveyed the strait with a 300 kHz broadband ADCP in bottom-tracking mode and a 120kHz echo-sounder together with GPS positioning. Available data include runs along the strait, plus several transects across the strait.

The vertical bin size of the ADCP was 2m and the first bin was 4.5m below the surface. With a beam angle of 20 degrees the ADCP missed only a few bins at the bottom. Sometimes high bubble concentrations in the Bosphorus limited the maximum depth of measurement.

High resolution images of the flow structure were obtained with the echo-sounder. The vertical bin size was 0.45m and the first bin was 1.3m below the surface. The beam-angle of the transmitter was 3.6 degrees which gives a good horizontal resolution at even the deepest points in the strait.

The acoustic measurements were supplemented with position data from a differential GPS system. The horizontal position accuracy was better than 2m.

Results

Position in the Bosphorus is given relative to the thalweg. Its origin is at the southern exit at the Sea of Marmara. The thalweg distance increases northwards so that the Black Sea begins at thalweg 32km.

Figure 2 shows the along channel component of the horizontal velocity along the entire strait and the ADCP backscatter intensity. The velocity of the upper layer was about $-0.1\,\mathrm{m\,s^{-1}}$ at the Black Sea side. While moving southward it increased, but varied depending on the width of the strait. Maximum surface velocities of up to $-1.7\,\mathrm{m\,s^{-1}}$ were reached at about 9 to 10 km, south of the contraction. It remained

fairly high (about $-1.3\,\mathrm{m\,s^{-1}}$) until it reached the Sea of Marmara, the reason being the relatively small thickness of the upper layer between the contraction and the Sea of Marmara.

The northward flowing lower layer moved with average speeds ranging from $0.4\,\mathrm{m\,s^{-1}}$ to $0.8\,\mathrm{m\,s^{-1}}$ with highest speeds near the northern exit.

The velocity data as well as the density profiles show that the depth of the interface decreased from north to south. The high vertical resolution of the current data enables us to use the current speed as definition for the interface depth; the interface is defined as the depth of zero current. Then the interface depths are 42 m at 30 km, 40 m at 25 km, 37 m at 17 km, 35 m at 11 km, 28 m at 9 m, and 23 m at 3 km. The interface depth is changing most rapidly between the contraction and the southern sill. While detailed analysis of the acoustic back-scatter images is not discussed here, the coarser resolution ADCP signal is consistent with the interpretation of intense mixing in this region.

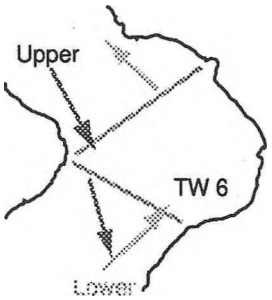

The flow structure along the cross-channel transect TW6, which is located in a highly curved section of the strait, is shown in Figure 3. Because of the curvature the current not only had a vertical velocity gradient but also a horizontal one. The upper layer flow occupies the entire width of the strait but is strongest on the west side. On the other hand, the lower layer flow was confined to the west side. The high resolution echo-sounder image shows instabilities along the interface and also within the upper layer.

Summary

Acoustical measurement techniques were used to study the two-layer exchange flow in the Bosphorus. The vertical resolution of the ADCP measurements is sufficient to clearly define the depth of the interface. The number of missing bins both at the surface and at the bottom is small. This is an important prerequisite for an accurate determination of the layer transports and the change of the layer transports along the channel [1]. The latter will allow us to estimate the amount of mixing and entrainment as a function of position in the Bosphorus. This is currently being undertaken.

The echo-sounder images reveal interesting details about the structure of the flow. Hence they can be used to identify regions of intense mixing and entrainment across the interface and, even more important, they can give insight into the physical processes that occur in the flow.

References

[1] R. Lee Gordon. Acoustic measurements of river discharge. *Journal of Hydraulic Engineering*, 115(7):925–936, 1989.

[2] Ü. Ünlüata, T. Oğuz, M.A. Latif, and E. Özsoy. On the physical oceanography of the Turkish Straits. In L. J. Pratt, editor, *The physical oceanography of sea straits*, pages 25–60. Kluwer Academic Publishers, 1990.

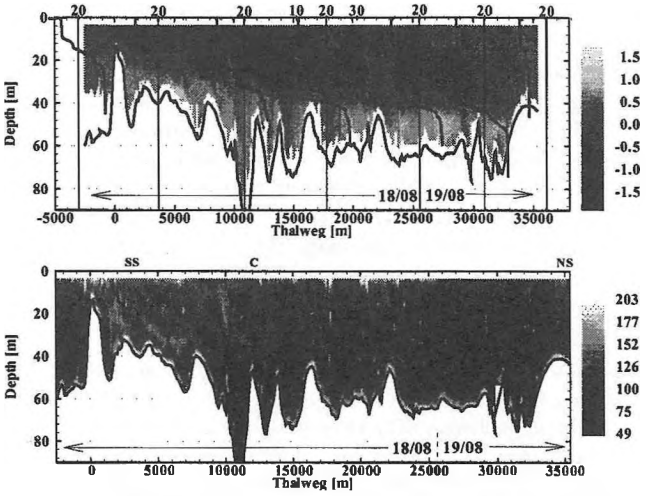

Figure 2: **Upper:** Along channel velocity $[\mathrm{m\,s^{-1}}]$ plotted versus depth and thalweg. Northward flow is positive and southward flow is negative. Vertical profiles of $\sigma_t[\mathrm{kg\,m^{-3}}]$ obtained at thalweg positions -3, 4, 11, 18, 25, 30, and 23 km are superimposed. The data are composed of sections acquired on two days. **Lower:** Average back-scatter intensity from the ADCP.

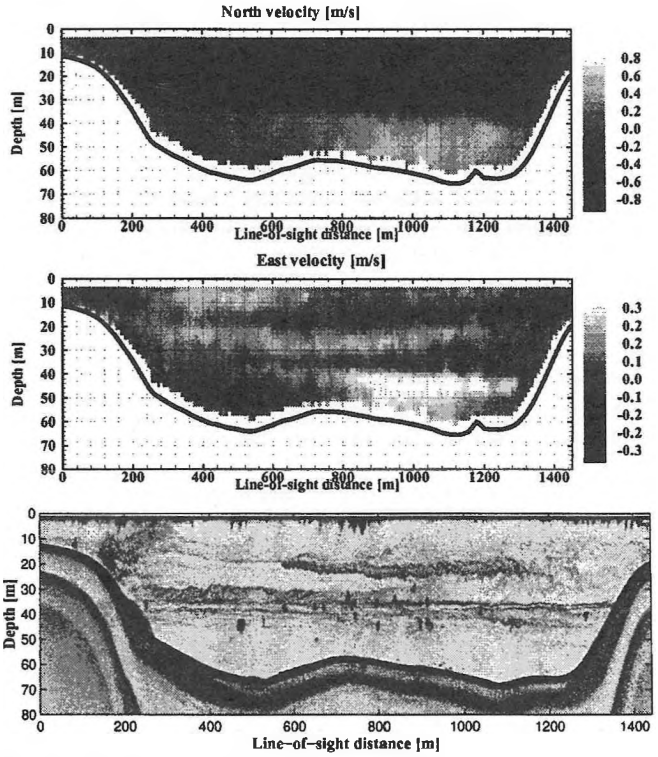

Figure 3: **Upper:** North component of horizontal velocity $[\mathrm{m\,s^{-1}}]$ plotted versus depth and thalweg. **Middle:** East component. **Lower:** Echo-sounder image of the flow.

Radiated Autospectra over [160 Hz, 2000 Hz] of Individual Breaking Ocean Waves

Rex K. Andrew
8361 S.E. 57th St., Mercer Island, WA, 98040: rx.andrew@ieee.org

The radiated autospectrum of breaking wind waves has a broad maximum in [50 Hz, 1000 Hz]: the spectral profile above the peak is believed to be due to the resonant contributions of individual, small, freshly entrained bubbles oscillating in their fundamental mode. The sound source mechanism for the spectral profile below the peak is less certain. The resonant-contribution model is unlikely because it would require large radius (>1 cm) bubbles which have not been heretofore observed. Alternatively, the source must involve some ``off-resonance" mechanism. One such theory is ``collective oscillations"[1].

Collective oscillation theory involves an inclusion of bubbly fluid entrained by a breaker. The inclusion is then considered analogous to a fluidic inclusion with an anomalous sound speed. For the idealized geometry of a hemispherical inclusion, the inclusion acts like a spatial acoustic filter for sound radiated from sources at the hemisphere base (i.e., at the water surface). Oguz [2] analyzed this ideal case and showed that a spectrally smooth source resonant above 1600 Hz yields a radiated (far-field) signal with multiple sharp (i.e., high-Q) harmonic peaks in [50 Hz, 1500 Hz]. These peaks are related to the resonant modes of the fluidic inclusion. Means and Heitmeyer [3] predicted that only the fundamental harmonic would leak through if the sources are concentrated along the leading edge of the breaker. Neither analysis, however, made predictions for a spectral profile involving both resonant and off-resonance regimes.

Such predictions can be tested but comparisons to data are lacking because there have been few experimental measurements in this frequency regime. These measurements are difficult to obtain due to the location of the source, the stormy environment, overwhelming man-made contributions, and inherent signal non-stationarity. We achieved direct measurements using a nearsurface hydrophone array at a fetch-limited site at a wind speed of about 7 m/s [4] . It is important to note that the breaking waves observed during this event were predominantly spilling breakers, as opposed to plunging breakers.

The data presented here are from the array center hydrophone. The (time-domain) radiated signal is nonstationary: at best, it must be partitioned "by eye" into segments that appear quasi-stationary. This is done for two typical waves, W3 (fig. 1) and W5 (fig. 2). The system transfer function is provided in fi.g 3, showing the system high-pass cut-off at »160 Hz. The acquired data are further high-pass filtered with a fifth order Butterworth filter with cut-off frequency 160 Hz to remove residual low-frequency strum energy.

As these segments are short (»200 ms), careful spectral estimation must employ the multi-taper method [5]: 5 tapers are used here with a time-bandwidth product of 3. The results from wave W3 (W5) are shown in figs. 4-7 (figs. 8-12). In each figure, the background ambient noise autospectral estimator is also shown: this was estimated using a much longer data segment judged not to contain nearby breaking wave events. The radiated spectral profiles have a signal excess of up to 6 - 10 dB over ambient. Jackknifed 90% confidence intervals [6] are provided for both the radiated and ambient sound.

These spectral profiles show statistically significant evidence of harmonic structure, with peaks near 500 Hz and 800 Hz. There is some evidence of another peak around 250 Hz. This harmonic structure bolsters the prediction that a bubbly inclusion will act like a spatial acoustic filter.

The autospectral profile has at best, however, only low-Q peaks, with the predominant energy in [250 Hz, 700 Hz]. This cannot be explained if we assume a linear problem with small bubbles resonating at frequencies above 700 Hz. In fact, the profiles above 1000 Hz, where small bubbles are likely to be contributing resonantly, are consistently lower than the spectral peak region. This suggests that the source forcing near and below the spectral peak involves other mechanisms in addition to off-resonance contributions from small bubbles.

[1] W. M. Carey and D. Browning, in Sea Surface Sound, B. R. Kerman, ed., Kluwer Academic, 1988.

[2] H. N. Oguz, J. Acous. Soc. Am. 95(4), 1994.

[3] S. L. Means and R. M. Heitmeyer, submitted to J. Acoust. Soc. Am., 1999.

[4] R. K. Andrew, D. M. Farmer, and R. L. Kirlin, J. Acous. Soc. Am. 101(5), 1997.

[5] D.J. Thomson, Proc. IEEE 70(9), 1982.

[6] D. J. Thomson and A.D. Chave, in Advances in Spectrum Analysis and Array Processing, vol. 1, S. Haykin, ed., Prentice-Hall, New Jersey, 1991.

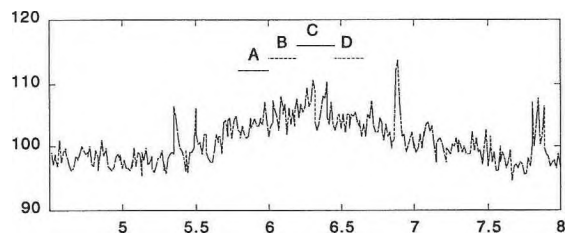

Figure 1. Wave W3. Array depth = 3.1 m, source slant range = 3.7 m.

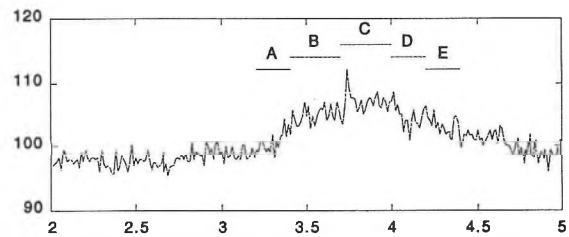

Figure 2. Wave W5. Array depth = 3.1 m, source slant range = 3.7 m.

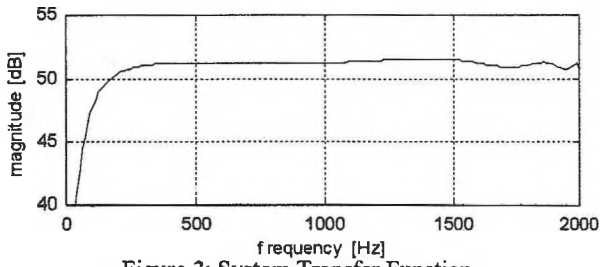

Figure 3: System Transfer Function

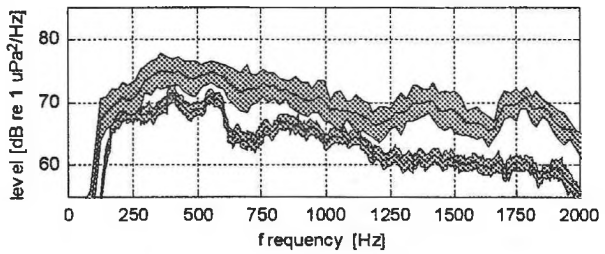

Figure 4: Wave segment W3A.

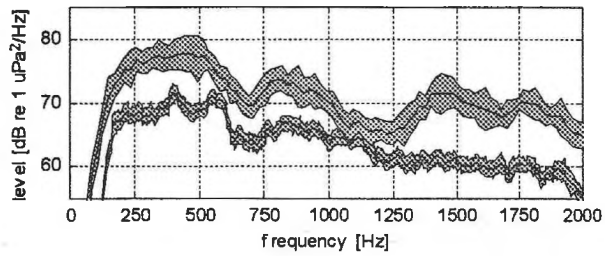

Figure 5: Wave segment W3B.

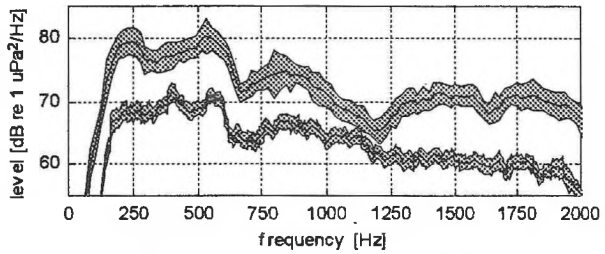

Figure 6: Wave segment W3C.

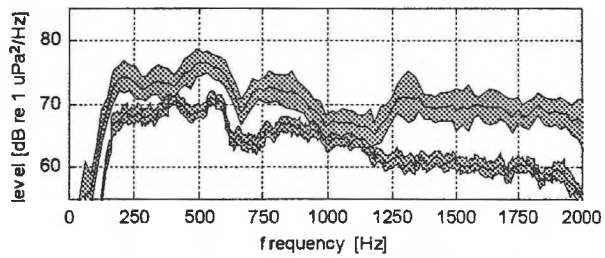

Figure 7: Wave segment W3D.

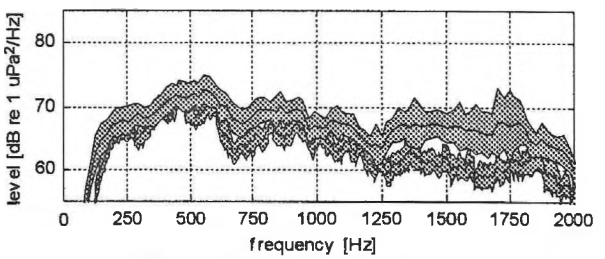

Figure 8: Wave segment W5A

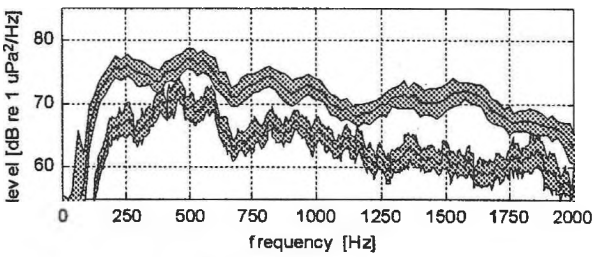

Figure 9: Wave segment W5B.

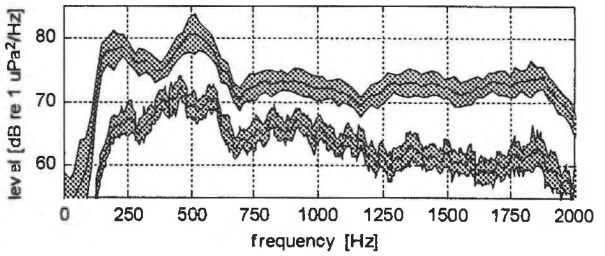

Figure 10: Wave segment W5C.

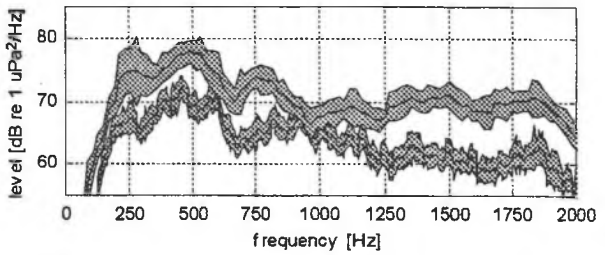

Figure 11: Wave segment WCD.

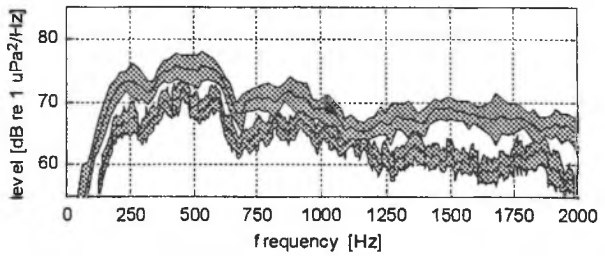

Figure 12: Wave segment W5E.

The Underwater Acoustic Noise Field On Sable Bank

F. Desharnais, G.J. Heard, M.G. Hazen, I.A. Fraser
Defence Research Establishment Atlantic
P.O. Box 1012, Dartmouth, Nova Scotia, Canada, B2Y 3Z7

INTRODUCTION

The ambient noise levels on Sable Bank were investigated, in the vicinity of the oil drilling sites by Sable Island. The goal of the research was to better qualify the background noise levels of the area, in order to assess the impact of the noise arising from the development of the Sable Gas Project. The results presented here are based on historical measurements made at ten different locations on Sable and Banquereau Banks, during various conditions of sea state, and during all four seasons [1-6]. The measurements were made with a range of systems, from commercial sonobuoys to various research array systems.

MEAN NOISE LEVELS

Figure 1 shows the ambient noise spectral data (one-third octave band) in the frequency range of 20-2500 Hz obtained from nine separate data sets [1-6]. Where sufficient data were available, error bars indicating the standard deviation have been included. Figure 2 shows the ambient noise levels at selected third-octave bands for 12 aircraft sorties carried out during the period December 1995 to December 1996 [1]. The year-long study that provided the data of Fig. 2 adds seasonal information to the data from Fig. 1.

The overall noise level in the 10-200 Hz band depends mostly on the number of ships in the area, on their respective source levels, and on propagation conditions. The eastern Canadian shelf is a region of particularly high shipping noise and this is clearly reflected in our data by noise levels in excess of 90 dB//1 μPa2/Hz in the neighbourhood of 50 Hz. These high levels also compare favourably to the high shipping density noise curves from Wenz [7]. The propagation conditions vary according to seabed properties (which in this case do not change), and on the profile of sound-speed as a function of depth (see seasonal variations below).

Above approximately 200 Hz, the noise levels are usually dominated by wind noise. The wind conditions varied greatly over the different data sets included in this report. The mean levels for frequencies above 300 Hz agree to within 5 dB with the levels published by Piggott [8]. Piggott's data set covered an entire year and a full range of wind speeds from light to 18 m/s. The largest differences between our data and Piggott's data are seen for the 316-Hz band at very low wind speed. At this frequency, shipping can influence the noise levels at low wind speeds. Shipping noise contamination is suspected in some of our data sets.

There is a large spread in the 20 Hz data in Figs. 1 and 2. This large variation is believed to be due to finback whales, which are audible in many of the recordings. Finback whales, typically found on the Scotian Shelf and Grand Banks, emit loud calls with centre frequencies near 20 Hz [9]. The noise level in this frequency band can increase by as much as 25 dB if finback whales are in the area.

The lowest noise levels seen in Fig. 2 are representative of the lowest levels that can be expected near Sable Island, at all frequencies. This statement is based on the conditions observed during the recording of these particular measurements: light winds, low sea state, and no shipping in a 100-km radius around the experimental site. The maximum levels are also representative of the highest levels that can be expected near Sable Island under normal conditions, except in the band 100-500 Hz where higher levels could be observed for extreme weather conditions. It should be noted that a nearby ship could produce even higher broadband noise levels, especially if it is large (e.g. a tanker) and very close.

SEASONAL VARIATION

Three different factors can introduce a seasonal variation in the noise levels. At shipping frequencies, the main factor is the seasonal change in the sound-speed profile. In the summer months (mainly May to September), the warm layer near the sea surface redirects the energy from a source near the surface (such as a ship) towards the seabed, and the interaction with the seabed is increased. Therefore, propagation losses for shipping noise are higher in the summer, and the measured noise levels tend to be lower, especially for distant shipping.

The only data set that covers an entire year is that of Fig. 2. Figure 3 shows the third-octave band noise levels as a function of flight date from the data set of Fig. 2. The 20 and 1000 Hz levels show a reduction in noise level during the summer season. The seasonal dependence of the noise is weak at shipping frequencies, especially when compared with other sites on the Continental Shelf [1]. This difference is explained by the noise on Sable Bank from nearby sources, believed to be due to the oil drilling platform within approximately 50 km of the experimental site. (Note that we do not differentiate between the noise from the drilling platform itself and the noise from the shipping traffic that the drilling operation attracts.) The high standard deviations of the noise levels at shipping frequencies (not shown here) are indicative of the importance of nearby sources near Sable Island. The noise levels influenced by a nearby ship are expected to show more variation, and therefore higher standard deviations than the levels influenced by a distant ship. This was observed in the summer months for Sable Bank, when the higher propagation losses reduced the contribution from far-away ships.

Another factor that can induce a seasonal effect is the seasonal variation of the wind speed. Since the noise levels above 200 Hz are mainly dictated by wind speed (sea surface noise), a statistically significant change in wind speed will induce a change in the noise levels. Fig. 3 demonstrates lower noise levels in the summer season (particularly during August) at wind noise frequencies, and the measured winds (not shown here) were on average slightly lower in the summer time. It should be noted that as the wind speed in the North Atlantic is generally lower in the summer season, the seasonal wind speed effect reduces noise levels as does the summer warming effect discussed earlier. On average, the noise levels can be expected to be lower by 2-6 dB in the summer season, in the frequency band of 150-2000 Hz.

The third factor that can produce a seasonal effect is the presence of biological noise sources. We mentioned earlier the strong emissions from finback whales around 20 Hz. The 20-Hz band in Fig. 3

shows the greatest variation and this is attributed to the behaviour of finback whales. A one-year cycle is clearly evident in the data, with a noise level variation on the order of 25 dB from peak to trough. From this figure, the peak whale season is defined as fall (October) to mid-winter (January).

CONCLUSIONS

We have shown here some of the ambient noise data previously analysed that are relevant to predicting the noise levels on the Sable Bank, in particular, in the area of the drilling operations near Sable Island. Mean, maximum, and minimum noise levels have been presented and should form a baseline for evaluating the importance of new noise sources on the Bank.

Data showing the seasonal variability of noise have been presented. Shipping traffic tends to increase during the summer, but surface warming and lower wind speeds result in generally lower levels of ambient noise during the summer. It is also noted that the variation of noise levels can increase during summer, as the importance of individual nearby ships is increased by the loss of energy from distant shipping through increased bottom absorption. Biological sources have also been shown to have a seasonal dependence and can, in the case of finback whales, lead to increases in the noise at 20 Hz in excess of 25 dB.

More information on the directionality of the noise field and the influence of shipping traffic will be presented during AWC 1999.

ACKNOWLEDGMENTS

This work was funded in part by LGL Environmental Research Associates.

REFERENCES

1 Hazen, M.G. and Desharnais, F. (1997) "The Eastern Canada Shallow Water Ambient Noise experiment", in Proceedings of Oceans '97 conference, Halifax, NS, 1, p. 471-476.

2 Bluy, O. (1975) Private communication.

3 Desharnais, F., MacDonald, B.R. and Mah, K.J. (1998) "Vertical noise coherence measurements in shallow water using Lagrangian drifters," J. Acoust. Soc. Am., 103(5), p. 2858.

4 Zakarauskas et al. (1984) Private communication.

5 Zakarauskas, P., Chapman, D.M.F. and Staal, P.R. (1990) "Underwater acoustic ambient noise levels on the Eastern Canada continental shelf," J. Acoust. Soc. Am. 87, p. 2064-2071.

6 Carr, S. (1998) "TTCP Trial RDS-1: Rapidly Deployable Systems - reduction, analysis, and reporting of non-acoustic data from DREA Sea-Test Q239," DREA Contractor's Report CR 98/421 parts 1 and 2, JASCO Research Ltd.

7 Wenz, G.M. (1962). "Acoustic ambient noise in the ocean: spectra and sources," J. Acoust. Soc. Am. 34, 1936-1956.

8 Piggott, C.L. (1964) "Ambient sea noise at low frequencies in shallow water of the Scotian Shelf," J. Acoust. Soc. Am. 36, p. 2152-2163.

9 Watkins, W.A., Tyack, P., Moore, K.E., and Bird, J.E. (1987) "The 20-Hz signals of fin-back whales (balaenoptera physalus)," J. Acoust. Soc. Am. 82, p. 1901-1912.

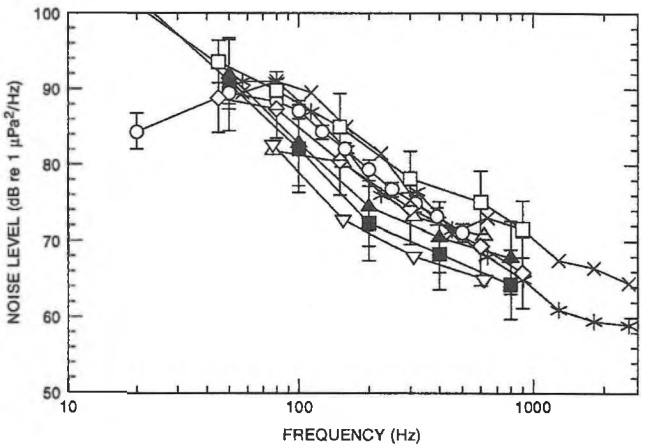

Figure 1. Ambient noise spectra obtained from 9 data sets on the Sable and Banquereau Banks.

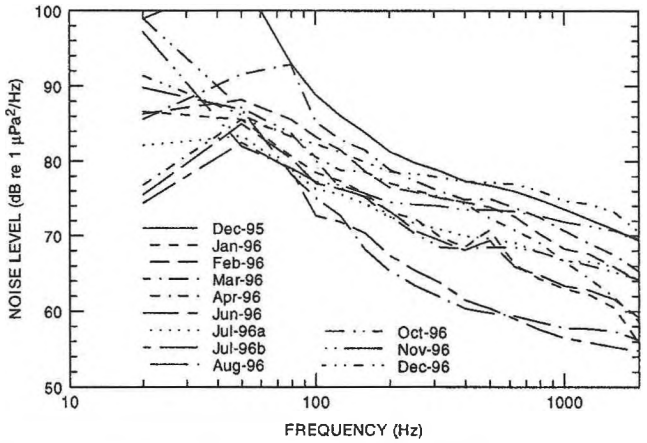

Figure 2. Ambient noise spectra obtained from [1].

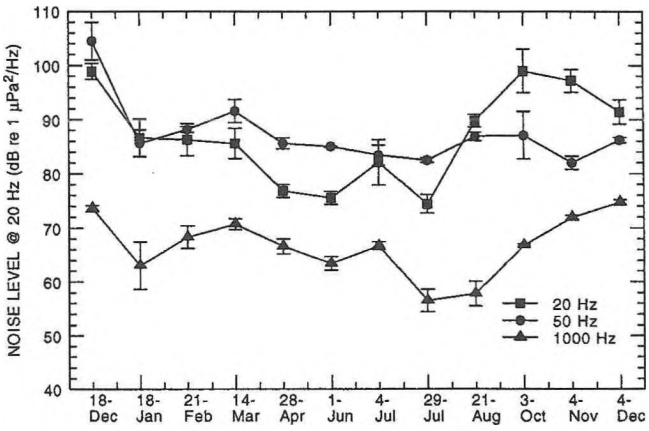

Figure 3. Ambient noise level-vs-time (1995-1996) at 20, 50 and 1000 Hz.

Simulation of Underwater Ambient Noise Time Series

Daniel Hutt, Paul C. Hines and Andrew Rosenfeld
Defence Research Establishment Atlantic
P.O. Box 1012, Dartmouth, Nova Scotia, Canada, B2Y 3Z7

In modern naval surveillance, ships and submarines may be tracked via their underwater acoustic signatures. In both active and passive sonar, arrays of hydrophones are used to enhance the signal-to-noise ratio and to obtain directional information. Various techniques exist to process the acoustical signals from arrays in order to maximize the sensitivity in a desired direction while minimizing the contribution of ambient noise. Two array processing techniques currently being explored at Defense Research Establishment Atlantic (DREA) are superdirective and intensity processing. In order to test these concepts for underwater applications, it is necessary to simulate the response of an array to an acoustic signal in the presence of ambient noise. The results obtained from the signal processing algorithms will be affected by the spatial and temporal characteristics of the noise field. Since real acoustic data may be unavailable or the statistics may not be fully known, simulated noise can be used to probe array performance as a function of quantifiable noise characteristics.

In this paper we present three different approaches for generating synthetic ambient noise time series data which possess controlled statistical characteristics. The noise statistics which are specified are the probability density function, power spectrum, and the complex cross correlation function between pairs of noise time series. The simulated noise time series represent different types of underwater noise fields.

1. Synthetic noise time series for a single hydrophone

To create synthetic ambient noise time series from a single hydrophone, we used the approach of Walker (Ref. 1) where a one dimensional autoregressive moving average (ARMA) filter is applied to discrete Gaussian white noise. ARMA filters, also known as finite impulse response filters, are designed to have frequency responses that approximate the power spectra of different undersea noise conditions. The filtered Gaussian noise yields a time series with the desired spectral properties. ARMA filters have been used successfully to simulate time series representing a wide range of processes from car traffic noise to financial markets (Ref. 2).

ARMA filters have the form

$$y_k = \sum_{i=1}^{m} a_i y_{k-i} + b_0 x_k \ , \qquad (1)$$

where, x_k is the input white noise value at time sample k and y_k is the k^{th} filter output. y_k is determined by previous values of y through the m coefficients $a_1, a_2, \ldots a_m$. The quantity b_0^2 is known as the prediction error variance and is a measure of how well the power spectrum of y matches the spectrum being modelled.

To create a filter, the desired noise frequency spectrum is Fourier transformed to obtain the autocovariance function with elements R_j where j refers to the jth time lag. The filter coefficients a_i are found by solving the equation:

$$R_j = \sum_{i=1}^{m} a_i R_{j-i} \qquad 1 \le j \le m. \qquad (2)$$

Equation 2 defines a set of m simultaneous equations in m unknowns. In matrix form it may be expressed as

$$\begin{bmatrix} R_0 & R_{-1} & R_{-2} & \cdots & R_{1-m} \\ R_1 & R_0 & R_{-1} & \cdots & R_{2-m} \\ \vdots & \vdots & \vdots & \vdots & \vdots \\ R_{m-1} & R_{m-2} & R_{m-3} & \cdots & R_0 \end{bmatrix} \begin{bmatrix} a_1 \\ a_2 \\ \vdots \\ a_m \end{bmatrix} = \begin{bmatrix} R_1 \\ R_2 \\ \vdots \\ R_m \end{bmatrix} . \qquad (3)$$

The m-order system of Eq. 3 can be solved with approximately m^3 operations using Gaussian elimination. However, the matrix **R** has a Toeplitz structure which can be inverted with approximately m^2 operations using the Levinson recursion algorithm (Ref. 3, p. 359-367).

An example of an ambient noise power spectrum is shown in Fig. 1. It is based on the empirical noise model of Merklinger and Stockhausen (Ref. 4) which combines estimated contributions of noise from shipping, surface noise caused by wind and the intrinsic noise of the recording system. The parameters used in the Merklinger and Stockhausen model are wind speed of 40 km/hr and a moderate shipping noise level of 86 dB//μPa^2/Hz. A filter designed to model this noise spectrum was applied to a Gaussian white noise time series resulting in a time series with the power spectrum shown in Fig. 1. Clearly the power spectrum of the simulated noise time series closely resembles the power spectrum being modelled.

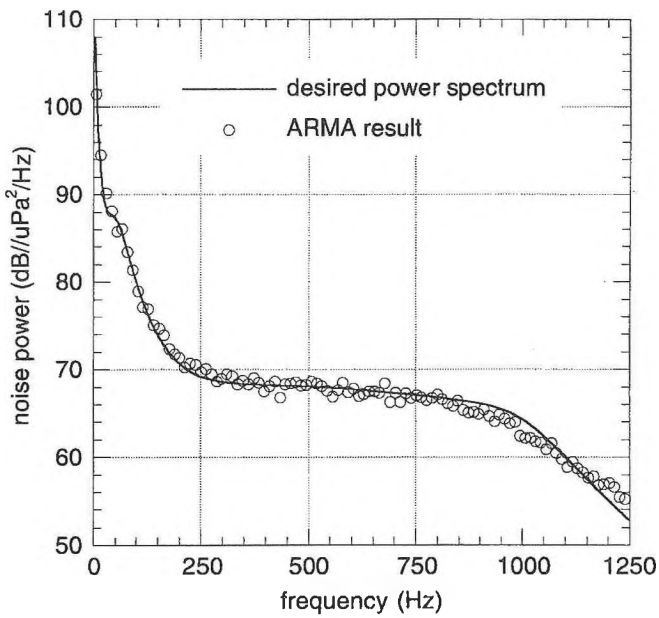

Fig. 1 Example power spectrum from the model of Ref. 4 and power spectrum of simulated noise using an ARMA filter.

2. Synthetic noise time series for a hydrophone array

Although ARMA filters are widely used for time series simulations, they are only appropriate for generating ambient noise for a single hydrophone. For realistic simulation of noise signals from an array of hydrophones, the generated signals must possess the appropriate cross-correlation. The degree of correlation of noise signals $s_1(t)$ and $s_2(t)$ measured at two hydrophones is characterized by the normalized cross-spectrum $S_{1,2}(\omega)$,defined as

$$S_{1,2}^2(\omega) = \frac{S_1(\omega)S_2^*(\omega)}{|S_1(\omega)||S_2(\omega)|} , \quad (4)$$

where S_1 and S_2 are the Fourier transforms of s_1, s_2 and ω is the angular frequency $2\pi f$. The cross-spectrum is a function of the spacing between the hydrophones and the directionality and spatial coherence of the noise field. A non-zero imaginary part of the cross-spectrum indicates an anisotropic component in the noise field. The imaginary part is also proportional to the intensity of the propagating component of the noise field.

For a spatially isotropic noise field, the real part of the normalized cross-spectrum has the simple analytical form

$$S_{1,2}(kd) = \frac{\sin(kd)}{kd} \quad (5)$$

where $k = 2\pi/\lambda$ is the wavenumber, λ is the wavelength and d is the spacing between the hydrophones (Ref. 5). Equation 5 is plotted in Fig. 2 along with the cross-spectrum of two simulated isotropic noise time series.

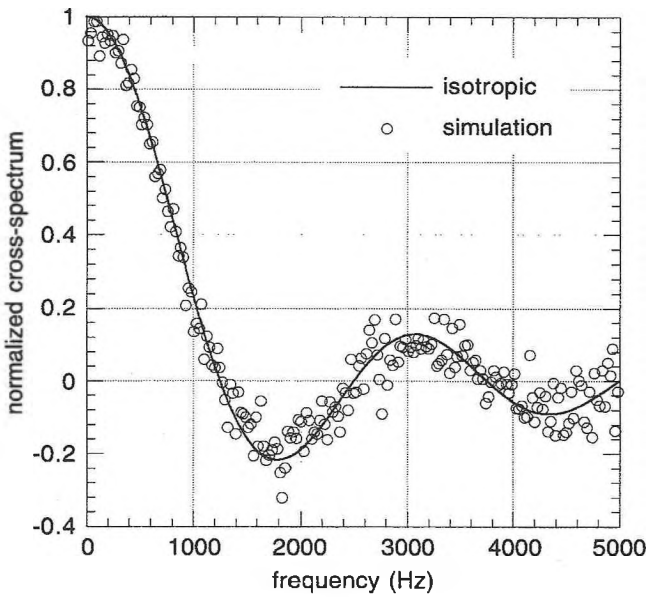

Fig. 2 Real part of cross-spectrum $S_{1,2}(\omega)$ for isotropic noise field and cross spectrum of two simulated time series.

To generate a pair of noise time series with a pre-defined cross-spectrum $S_{1,2}$, two Gaussian time series and their Fourier transforms were created. The phase differences $\Delta\phi$ between the complex Fourier components of S_1 and S_2 at each frequency interval were then found. The phase of the Fourier transforms were then shifted so that $\Delta\phi = \cos^{-1}[\mathrm{Re}(S_{1,2})]$. Thus the relative phases of the frequency components are adjusted so that the real part of the resultant cross-spectrum is equal to $S_{1,2}$ without affecting the magnitude of the Fourier coefficients, or equivalently, the power spectrum of the time series. The imaginary part of the cross-spectrum is a function of the phase shift and is given by $\mathrm{Im}(S_{1,2}) = \sin^{-1}(\Delta\phi)$. For isotropic noise, the time average of the imaginary part of $S_{1,2}$ goes to zero. In our simulation $\mathrm{Im}(S_{1,2})$ is constrained to average out to zero by alternating the signs of the phase shifts applied to S_1 and S_2 on successive iterations. The final step is to reverse Fourier transform S_1 and S_2 yielding two time series with the same individual statistics as $s_1(t)$, $s_2(t)$ but with the desired complex cross-spectrum.

An example of a cross-spectrum of two simulated isotropic noise time series is shown in Fig. 2 along with the theoretical cross-spectrum given by Eq. 5. The imaginary part of the calculated cross-spectrum (not shown) had a mean of 0.001 with a standard deviation of 0.071. The parameters of the simulation were d = 0.6 m and a sampling frequency of 10 kHz. The cross-spectrum shown in Fig. 2 is the average of results from 100 blocks of 4096 time series samples which is equivalent to a total of 41 s of time series data.

The above approach to simulating correlated noise is computationally efficient and can produce time series pairs with an arbitrary real cross-spectrum but the imaginary part of the cross spectrum must be zero. This is sufficient to represent any noise field which is symmetrical about the axis of the hydrophones. Noise with an arbitrary power spectrum can be generated by multiplying S_1 and S_2 by the appropriate weighting function.

3. Monte Carlo method

The noise simulation method described in Sect. 2 is limited to generating noise where the imaginary part of the cross spectrum is zero. However, noise fields are often anisotropic and have non-zero $\mathrm{Im}(S_{1,2})$. To handle these cases a third simulation technique based on the Monte Carlo method was developed.

The Monte Carlo algorithm randomly assigns directions and phases to a uniform distribution of monochromatic sources about a linear array of hydrophones. The resulting plane waves are weighted by an angular distribution of noise power, and then summed in the frequency domain as a "random walk" of phasors. By comparing the resulting phasor sums, the normalized cross-correlation coefficient is obtained. The complex cross-correlation function is then found by repeating the above process while stepping through frequency.

The angular weighting function applied to the noise sources depends on the physical situation being modelled, such as noise from an infinite plane surface above an absorbing bottom. The axis of the array can have an arbitrary orientation allowing anisotropic noise to be modelled for vertical or horizontal arrays. Time series possessing the appropriate cross-correlation statistics for a given angular weighting function can be generated for each hydrophone by distributing the phasor sums over frequency and then taking the inverse Fourier transform. The angular weighting function makes a Fourier transform pair with the desired cross-correlation spectrum, and thus either a cross-correlation or angular weighting function can be adapted as input for the generation of suitable time series.

4. References

1. R. Walker, "Autoregressive time series to simulate undersea acoustic noise", DREA RN/81-4
2. K. D. Hsueh and R. P. Hamernik, "A generalized approach to random noise synthesis: Theory and computer simulation", J. Acoust. Soc. Am. 87 1207-1217 (1990).
3. Bose, N. K., "Digital filters: theory and applications", Elsevier, New York (1985)
4. H. M. Merklinger and J. H. Stockhausen, "Formulae for estimation of undersea noise spectra", J. Acoust. Soc. Am., 65 S88 91979A).
5. H. Cox, "Spatial correlation in arbitrary noise fields with application to ambient sea noise", J. Acoust. Soc. Am. 58, 1289-1301 (1973).

RANGE DEPENDENT MATCHED-FIELD SOURCE LOCALIZATION AND TRACKING IN SHALLOW WATER ON A CONTINENTAL SLOPE

LIEUTENANT (N) MARTIN L. TAILLEFER
Department of National Defence
Meteorology and Oceanography, Victoria BC

DR. N. ROSS CHAPMAN
University of Victoria
School of Earth and Ocean Sciences, Victoria BC

INTRODUCTION

The postwar advances in ocean acoustics has been significant. The ever-growing silent and quiet modern diesel-electric submarine has generated enormous amounts of research and developments in an effort to counter a submarine's greatest strength ... it's covert nature. In passive acoustics, advanced beam-forming techniques have been highlighted as a viable solution to provide useful operational capability against the perpetual threat of a submarine.

The threat has been complicated even further as the tactical setting has migrated to a littoral environment far more difficult than for open ocean regions. The time and distance scales of near shore environmental phenomena are shorter and because the sea is acoustically shallow it creates a more complex acoustic environment.

The aim of this paper is to provide insight on one aspect of adaptive beam-forming, matched field processing, that exploits all environmental conditions to localize a moving underwater target along a coastal region.

MODELLING

Acoustic data were collected using a multi-element vertical line array during the Pacific Shelf experiment off the west coast of Vancouver Island. A 16-element array was suspended from a surface float in water depths of 380-400 m, with the top hydrophone at a depth of 90 m and the elements equi-spaced at 15 m intervals. A CW sound source was towed along specific tracks, projecting three tones in the 45 - 72 Hz band. In this paper, data obtained for a downslope radial track out to a range of 5.5 km and along an arc at the same range are processed to localize the source in range, depth and bearing. The GPS track is shown by the dotted curve in Figure x.

The source location was estimated using a Bartlett matched-field (MF) processor, which acts as a simple correlator between the measured and modelled fields. Its output value is given by [1]:

$$P_B(\hat{\mathbf{m}},\mathrm{r},\mathrm{z},\theta,\mathrm{t}) = \hat{p}_n^*(\hat{\mathbf{m}},\mathrm{r},\mathrm{z},\theta,\mathrm{t})\ \underline{C}_t\ \hat{p}_n(\hat{\mathbf{m}},\mathrm{r},\mathrm{z},\theta,\mathrm{t})$$

- $\hat{p}_n(\hat{\mathbf{m}},\mathrm{r},\mathrm{z},\theta,\mathrm{t})$ is the modelled field for a variable environment model $(\hat{\mathbf{m}})$ and source position r, z, θ in time t.
- $\underline{C}_t$ is cross-spectral matrix for the measured field at time t.

An adiabatic normal mode expression that satisfies reciprocity was used in order to compute the replica field $\hat{p}$ [2]:

$$\hat{p}(\hat{\mathbf{m}},\mathrm{r},\mathrm{z},\theta) \cong \alpha \sum_{m=1}^{M(r,\theta)} \Psi_m(\hat{\mathbf{m}},\mathrm{r}=0,\mathrm{z}_s,\theta_i)\,\Psi_m(\hat{\mathbf{m}},\mathrm{r},\mathrm{z},\theta) \quad * \quad \frac{e^{i\int k_{rm}(\hat{\mathbf{m}},\mathrm{r}',\theta)\,dr'}}{\sqrt{k_{rm}(\hat{\mathbf{m}},\mathrm{r},\theta)\,k_{rm}(\hat{\mathbf{m}},\mathrm{r}_s,\theta)\int_0 \frac{dr'}{k_{rm}(\hat{\mathbf{m}},\mathrm{r}',\theta)}}}$$

- where θ is the azimuth bearing direction and θ_i is the first bearing in an arc of investigation.
- Ψ_m is the mode function of the mth mode and k_{rm} is the associated wave number for a range-dependent environment which is varying slowly in r and range-independent in the segmented, r'.
- α is a constant.

For rapid repetitive computations, the bathymetry, mode functions and wave numbers are pre-computed for a grid of values of the water depth and source depth and stored in "look-up" tables for fast reference [3].

MATCHED FIELD SOURCE LOCALIZATION AND TRACKING

The MF localization results for selected portions of the track are listed in Table 1. Time 1815 was at the start of the tow near the array; the track proceeded to a maximum radial range at 1840 and completed the turn along the arc by about 1842; at 1920 the source had returned upslope to water depths roughly equal to those at the array.

The greatest bearing resolution is expected for the cross slope propagation paths, from about 1910 to 1930. The MF localization in range and bearing are shown in Figure 1 by the crosses (+), based on 38 second samples at one minute intervals. The range-bearing discrimination is very good for the later times along the arc where the change in the field (or transmission loss) per unit angle is greatest. The performance was not as good near the end of the radial; this result may also indicate mismatch in the geo-acoustic model at the deeper portion of the slope.

The source depths estimated by MFP are also plotted in Figure 1; the heavy curve is a polynomial fit. The measured depths, except near the turn, were about 40 to 45 m.

Time	True Range	True Bearing	P_B	MFP Range	MFP Depth	MFP Bearing
1815	1470	288	0.821	1900	69	283
1840	5679	255	0.529	5375	45	253
1855	5459	281	0.716	5850	55	279
1920	5226	327	0.784	5425	39	328
1929	5196	346	0.886	5000	35	346

Table 1: Target Tracking Summary (selected values)

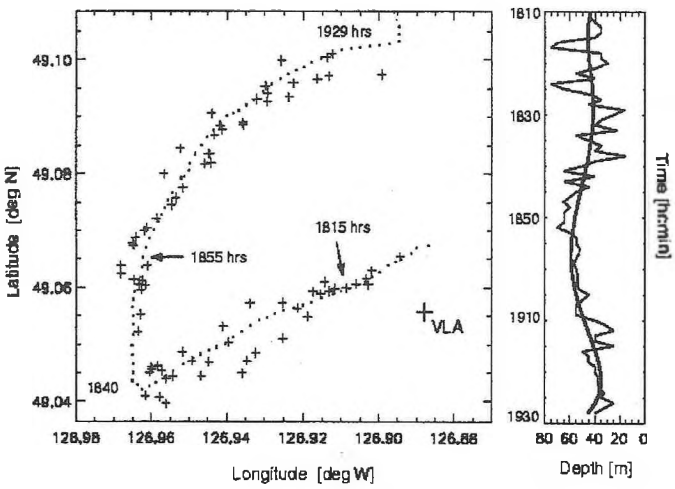

Figure 2: Geographic target tracking (1810 hrs - 1930 hrs)

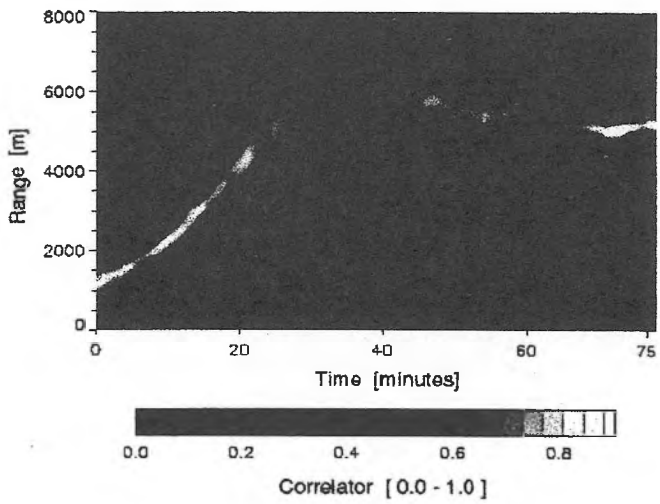

Figure 2: Best Bartlett plotted as Range vs. Time

The results presented at Figure 1 demonstrate remarkably good tracking performance using conventional MFP with a vertical line array over a sloping bottom. The range dependence introduced by the sloping bottom breaks the cylindrical symmetry of the acoustic field, and provides the means for bearing resolution with the VLA.

The tracking results were then further elaborated, Figure 2, showing the best Bartlett correlation plotted as an ambiguity surface of the source range versus time along a known bearing. It demonstrates a dramatic representation of the target's movements.

CONCLUSION

The littoral environment with a complete knowledge and understanding of the bathymetry, geo-acoustic and water column properties provide a powerful tool that exploit all the available parameters to produce accurate and reliable target localization. Specifically related to this experiment, the tracking results sufficiently show the unique tracking over the azimuthally dependent environment. The matched-field localization provided evidence that the breaking symmetry of the continental slope allows the means for bearing resolution with a vertical line array.

Although, not all littoral regions will have a sloping bottom with a gradient sufficient to produce distinct MF bearings, however, the complex nature of shallow water or coastal regions can be exploited to effectively provide enough data to process discriminate tracking along a time-scale.

This paper is meant to demonstrate that the progression of matched field processing and tracking in a complex, spatially varying environment, serves to better refine the tracking capabilities of passive acoustic localization. from conventional beam-forming methods. This is by no means a panacea. The pursuit to counter hostile underwater threats only emphasizes the need to continue these advances.

Acknowledgements: research supported by the Canadian Department of National Defence and the Univeristy of Victoria, Canada.

REFERENCES

1. Tolstoy, A, *Matched Field Processing for Underwater Acoustics*, New York: World Scientific, 1993, ch. 2, p. 15.
2. Brekhovskikh, L,.M., and Godin, O.,A., *Acoustics of Layered Media II*, Moscow: Spinger-Verlag, 1992, ch.7, pp. 247-253.
3. Dosso, et al., Estimation of ocean-bottom properties by matched-field inversion of acoustic field data, IEEE J. Oc. Eng., **18**, 232-239 (1993).

SOURCE LOCALIZATION USING REGULARIZED MATCHED-MODE PROCESSING

Nicole Collison and Stan Dosso
School of Earth and Ocean Sciences, Univ. of Victoria, P.O. Box 3055, Victoria, B.C., CANADA V8W 3Y2

BACKGROUND

Localizing an acoustic source in the ocean is an important problem in underwater acoustics [1]. Matched-field processing (MFP) methods localize a source by matching acoustic pressure fields measured at an array of sensors with modelled replica fields computed for a grid of possible source locations. Matched-mode processing (MMP) consists of first decomposing the measured fields into their constituent modal components, and then matching the resulting mode excitations with modelled replica excitations. An advantage of MMP over MFP is that subsets of the complete mode set can be considered (e.g., in cases where seabed geoacoustic properties are poorly known, the matching can be applied only to low-order modes which interact minimally with the bottom). A disadvantage of MMP involves the modal decomposition itself. Modal decomposition represents a linear inverse problem that is non-unique and can be unstable (small errors on the data can lead to large errors on the solution). In particular, standard modal decomposition methods used in MMP can give poor solutions when the inversion is ill-posed due to an inadequate sampling of the acoustic field [1]. This paper develops a new approach to modal decomposition and MMP, referred to as regularized matched-mode processing (RMMP) [2].

THEORY

The normal-mode model for the acoustic pressure field p at a range r and depth z is given by

$$p(r,z) = \frac{e^{i\pi/4}\sqrt{2\pi}}{\rho(z_s)} \sum_{m=1}^{M} \phi_m(z)\phi_m(z_s)\frac{e^{ik_m r}}{\sqrt{k_m r}}, \qquad (1)$$

where ϕ_m and k_m represents the mth mode function and wavenumber, respectively, and M is the total number of propagating modes. The field recorded at a vertical line array (VLA) of N sensors can be written

$$\mathbf{A}\,\mathbf{x} = \mathbf{p}, \qquad (2)$$

where $\mathbf{p}$ is a vector of the measured acoustic pressures, $\mathbf{A}$ is an $N \times M$ matrix with columns consisting of the sampled mode functions, and $\mathbf{x}$ is a vector of the received mode excitations

$$\mathbf{x} = \left[\ \phi_1(z_s)\frac{\exp[ik_1 r]}{\sqrt{k_1 r}}, \ldots, \phi_M(z_s)\frac{\exp[ik_M r]}{\sqrt{k_M r}}\ \right]^T. \qquad (3)$$

Modal decomposition consists of solving (2) for an estimate $\tilde{\mathbf{x}}$ of the true mode excitations $\mathbf{x}$.

The matrix $\mathbf{A}$ is orthogonal if the orthonormal mode functions $\phi_m(z)$ are adequately sampled over their entire extent. However, such sampling is often not possible. If the array contains fewer sensors than modes, the higher-order modes will be spatially aliased, and the inversion is singular. If the array spans too small a fraction of the water column, the lower-order modes will be poorly sampled, leading to an ill-posed inversion. Typically, singular value decomposition (SVD) or zeroth-order regularization is applied to stabilize the inversion; however, it should be noted these methods are based on determining the "smallest" solution in the sense that $|\tilde{\mathbf{x}}|$ is as close to zero as possible. These smallest-model approaches produce a mathematical solution to the inverse problem (i.e., a stable solution that fits the data), but do not necessarily produce the most physically-meaningful solution.

A more general approach is regularized inversion, which minimizes an objective function Ψ that combines a term representing the data mismatch and a regularizing term incorporating an arbitrary *a priori* estimate $\hat{\mathbf{x}}$

$$\Psi = |\mathbf{G}(\mathbf{A}\,\tilde{\mathbf{x}} - \mathbf{p})|^2 + \theta\ |\mathbf{H}(\tilde{\mathbf{x}} - \hat{\mathbf{x}})|^2. \qquad (4)$$

In (4), $\mathbf{G}$ is a diagonal matrix with the reciprocals of the estimated data standard deviations on the main diagonal, $\mathbf{H}$ is an arbitrary weighting matrix for the regularization, and θ is a trade-off parameter that controls the relative importance of the two terms in the minimization. Minimizing Ψ with respect to $\tilde{\mathbf{x}}$ leads to

$$\tilde{\mathbf{x}} = \hat{\mathbf{x}} + [\mathbf{A}^\dagger\mathbf{G}^\dagger\mathbf{G}\,\mathbf{A} + \theta\,\mathbf{H}^\dagger\mathbf{H}]^{-1}\mathbf{A}^\dagger\mathbf{G}^\dagger\mathbf{G}\,(\mathbf{p} - \mathbf{A}\,\hat{\mathbf{x}}). \qquad (5)$$

An appropriate choice for θ is the value that produces a χ^2 data misfit (first term, right side of eq. 4) equal to $2N$, the expected value for N complex data. Although a closed-form solution for θ does not exist, it can be determined efficiently using Newton's method with analytic partial derivatives [2].

Applying a trivial prior estimate $\hat{\mathbf{x}} = \mathbf{0}$ in (4) and (5) leads to the standard zeroth-order regularized solution. RMMP is based on the conjecture that incorporating a physically-meaningful prior estimate can produce a better solution than standard MMP inversion techniques. The underlying idea makes use of the modelled replica mode excitations calculated for the search grid. The replica excitations for each grid point are computed via a normal-mode forward model, which provides a stable, noise-free solution. Thus, if the source is actually located at a particular grid point, the replica excitations computed for that point provide an ideal *a priori* estimate for the modal decomposition. This observation provides the basis for RMMP: an independent regularized inversion of the acoustic fields for the mode excitations is carried out prior to matching with the replica excitations for each grid point, using the replica itself as the prior estimate $\hat{\mathbf{x}}$. For grid points at or near the actual source location,

using the corresponding replica as an *a priori* estimate and minimizing $|\bar{\mathbf{x}}-\hat{\mathbf{x}}|$ should provide a more meaningful solution than minimizing $|\bar{\mathbf{x}}|$. For grid points away from the source location, this procedure provides a stable inversion, although the regularization may not be particularly physical. At every grid point, RMMP produces the maximum match possible (subject to the data) between the replica and the constructed modal excitations.

EXAMPLE

This section compares source localization results obtained using RMMP, MMP and MFP for a realistic synthetic testcase. The ocean environment consists of a 300-m water column with a typical N.E. Pacific sound-speed profile overlying a 50-m thick sediment layer and semi-infinite basement. The sediment layer has a compressional speed of $c_p = 1650$ m/s, shear speed of $c_s = 300$ m/s, density of ρ=1.6 g/cm^3. The basement has $c_p = 2000$ m/s, $c_s = 800$ m/s and $\rho = 2.1$ g/cm^3. The acoustic source is located at (r, z)=(6 km, 100 m). This environment supports 12 propagating modes at the source frequency of 40 Hz, as shown in Fig. 1. The synthetic data for the testcase were computed using the ocean environment described above; however, all replicas used in inversion were computed for an environment with the basement compressional speed in error by 300 m/s (i.e., using 2300 m/s instead of 2000 m/s). The mismatched environment supports 14 modes (Fig. 1).

Source localization results are considered for signal-to-noise levels SNR = 15, 5, 0 dB, and a variety of different VLA configurations. To compare the different localization approaches for noisy data, 100 different random realizations of spatially-uncorrelated Gaussian noise were added to acoustic field data computed using a wavenumber integration model. The search grid extended from 0–12 km in range with a range increment of 100 m, and 0–300 m in depth with a depth increment of 10 m. The estimated source location for each realization of noisy data corresponds to the grid point at which the match between the measured and replica fields (MFP) or mode excitations (RMMP and MMP) was a maximum, employing the standard Bartlett correlator. The performance of the various methods is quantified by the probability of correct localization P, taken to be the fraction of times that the localization is within ± 200 m in range and ± 10 m in depth about the true source location. For the matched-mode methods, only the eight lowest-order modes were included in the matching process to reduce the effects of environmental mismatch. For RMMP, $\mathbf{H}$ concentrated the regularization on the modes retained. MMP employed a zeroth-order regularization.

The results of this study are shown in Fig. 2 for VLAs consisting of from 6 to 12 sensors spanning the water column (Fig. 2a-c), and for VLAs consisting of 12 sensors with apertures spanning various fractions of the water column from 0.5 to 1 (Fig. 2d-e). Figure 2 shows that RMMP produced substantially better localization results than MMP or MFP for all array configurations, particularly for low to moderate SNRs.

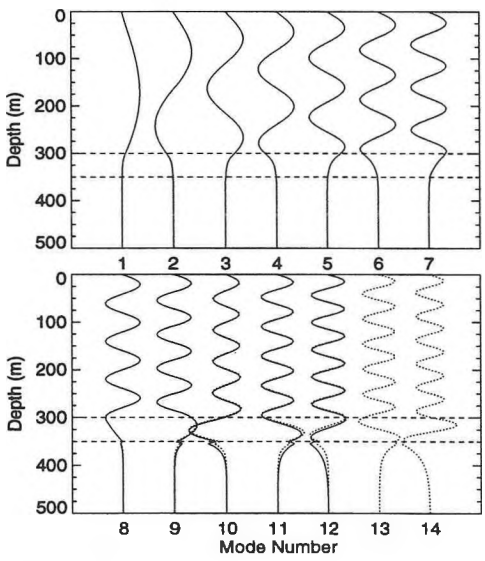

Fig. 1 Normal modes supported by the known and mismatched ocean environments shown by solid and dotted curves, respectively. Dashed lines denote the water-sediment and sediment-basement interfaces.

REFERENCES

[1] A. Tolstoy, 1993. *Matched-field processing for underwater acoustics*, World Scientific, Singapore.

[2] N. E. Collison, 1999. Regularized matched-mode processing for ocean acoustic source localization, *M.Sc. thesis*, University of Victoria, Victoria BC, 90 p.

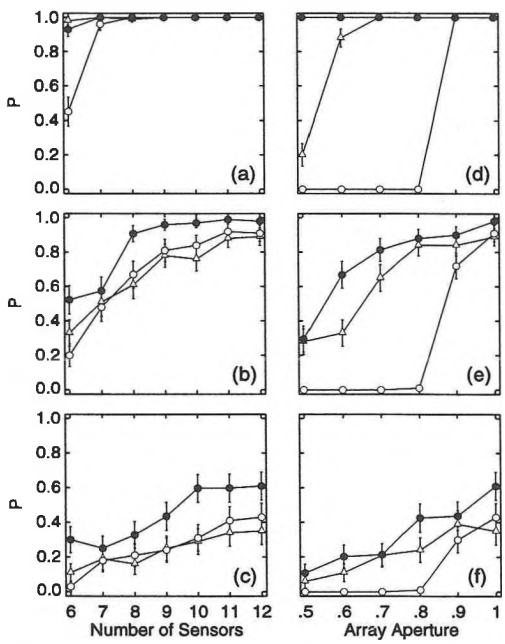

Fig. 2 Probability of correct localization P for MFP (triangles), MMP (open circles), and RMMP (filled circles). Results are given for the under-sampled cases for SNRs of (a) 15 dB, (b) 5 dB, and (c) 0 dB. (d)–(f) are the same as (a)–(c), but give results for short-aperture cases. Error bars denote 90% confidence intervals.

High Resolution Beamforming Applied to a DIFAR Sonobuoy

D. Desrochers and R. F. Marsden
Royal Military College of Canada, P.O. Box 17000, STN FORCES, Kingston, ON, K7K 7B4

Introduction

An important sensor used in Naval acoustic operations is the directional frequency and recording (DIFAR) sonobuoy. The hydrophone component contains three sensors, making it possible to obtain directional acoustic information from a single device. A bender element, on the bottom of the hydrophone, measures the omni-directional component of acoustic pressure. The direction of the signal is obtained from two orthogonal sensors, combined in a separate cruciform-shaped wobbler assembly that measure the *x* and *y* components of acoustic pressure wavenumber. Each has a beam pattern consisting of two circles similar in shape to the well-known acoustic doublet.

Present DIFAR direction processing (Bscan) uses the arctangent of the co-spectra between the omni and two directional channels to estimate target bearing at only a single direction at each frequency. This technique may introduce errors when two sources such as a surface ship and an underwater target radiate energy simultaneously at the same frequency. The resulting bearing estimate will lie somewhere in between, usually closer to the stronger one, an effect known as *bearing bias* [1]. Debiasing algorithms can reduce these effects by removing non-signal components [2]. However, this method only addresses the bias that is introduced by relatively broadband interference masking discrete tonals. With two sources producing narrowband signals at the same frequency, bearing errors are still likely to occur [1].

An alternate approach is to apply beamforming algorithms to the Fourier transformed data in order to resolve energy received from multiple directions. The simplest is the conventional beamformer. It is very broad-banded and incapable of detecting point directional sources. Recently, high resolution, data adaptive techniques have been proposed that are particularly effective for small arrays of omni-directional sensors. The mathematical equivalent to the directional DIFAR buoy is the heave, pitch and roll buoy that has long been used by the oceanographic community to determine directional spectra of surface gravity waves ([5], [6] , [7]) and more recently [8] high frequency internal waves. The first of these is the maximum likelihood (ML) beamformer [3]. A spectral window is designed that favours transmission of point sources, while suppressing sidelobes. A generalization of the ML is the eigenvector (EIG) technique [4]. A noise matrix is defined and a spectral window, similar to that of the ML determined. Iterative improvements to the ML [5] and the EIG [6] have been proposed that further sharpen the directional resolution of these three-element point sensors.

The purpose of this presentation is to apply high resolution beamforming to DIFAR data and to assess its efficacy in resolving multiple direction point sources.

Theory

The DIFAR hydrophone provides three time series:

$$x_{ok}$$

$$x_{xk} = x_{ok} \sin\theta$$

$$x_{sk} = x_{ok} \cos\theta$$

where: x_{ok} is the time series from the omni-directional receiver, and x_{sk} and x_{ck} are the time series of the wave pattern travelling to the $+y$ and $+x$ directions respectively. Defining a look-of-direction vector as:

$$\beta^T = (1, \sin\theta, \cos\theta)$$

the conventional beamformer ($\hat{E}_{CB}$)is given by [9]:

$$\hat{E}_{CB} = \beta^T \hat{Q} \beta$$

where $\hat{Q}$ is the 3 x 3 cross-spectral matrix between the three channels. The ML beamformer ($\hat{E}_{ML}$) is given by:

$$\hat{E}_{ML} = [\beta^T \hat{Q}^{-1} \beta]^{-1}$$

To calculate the EIG beamformer, the cross-spectral matrix is partitioned into signal ($\hat{S}$)and noise ($\hat{N}$)components:

$$\hat{Q}_{ij} = \hat{S}_{ij} + \hat{N}_{ij} = \sum_{m=1}^{P} \lambda_m \phi_i^m \phi_j^m + \sum_{m=P+1}^{M} \lambda_m \phi_i^m \phi_j^m$$

where λ_μ is the eigenvalue and ϕ_m the eigenvector of the mth eigenmode of with $\lambda_1 > \lambda_2 \ldots$ Thus the signal is defined as the portion of defined by the P largest eigenmodes and the noise by the M-P smallest eigenmodes. The EIG beamformer ($\hat{E}_{EV}$) is:

$$\hat{E}_{EV} = [\beta^T N^{-1} \beta]^{-1} = [\sum_{m=2}^{3} \frac{1}{\lambda_m} | \vec{\beta}^T \cdot \vec{\phi}^m |^2]^{-1}$$

An iterative improvement [5] has been proposed for any general beamformer. The estimate $\hat{E}^i$ at step *i* is:

$$\hat{E}^i = \hat{E}^{i-1} + \delta^i$$

$$\delta^i = \frac{|\mu|^{\xi+1} \hat{E}^{i-1}}{\mu\varphi}$$

$$\mu = 1.0 - \frac{\hat{T}^{i-1}}{\hat{E}^0}$$

$\hat{T}^{i-1}$ is the estimated beamformer calculated from the cross-spectral matrix determined from $\hat{E}^{i-1}$, ξ=1.0 and φ=5.0.

Simulations

The data adaptive algorithms were tested for *np* simulated beams travelling towards directions θ_n at angular spreads of σ_n and isotropic noise level E_N defined by:

$$E = \sum_{n=1}^{np} P_n \exp(-\frac{(\theta - \theta_n)^2}{2\sigma_n^2}) + E_N$$

The simulations demonstrated that: a. none of the beamforming algorithms could detect a signal emanating from three directions simultaneously; b. E_{CB} could not separate a signal emanating from two directions; c. the data adaptive methods could distinguish two peaks separated by an angular spread of 120^0; d. the iterative improvement used with E_{EV} could resolve peaks to 90^0 separation but tended to over-resolve sharp peaks in high signal-to-noise situations.

Field Data

The high-resolution beamforming methods were applied to field data collected in an open ocean situation. Three ships were present. Contact 1, north of the study site, was traveling from west to east at over 20 kts, contact 2, south of the study site, was moving at over 15 kts in a southwest direction, and contact 3, the deployment vessel, was travelling to the southeast.

Several acoustic tonals were detected. At 25 Hz (fig 1), for example, a strong source at 340^0 (contact 1) and a weaker one at 195^0 (contact 2) were found by all the techniques except the E_{CB}. At 42.5 Hz (fig 2) contact 2 was correctly identified by E_{ML} and E_{IML} along with a weak indication of contact 1 to the North. E_{EV} indicated a contact at bearing 110, matching contact 3, with a smaller hump for contact 2. E_{IEV} separated those two contacts, resulting in a strong bearing for contact 3, and a weaker one for contact 2. These last two methods could not discern contact 1, and although they detected contact 3, the relative strengths seem to be in error. The ability to provide accurate directional information from broadband noise was also a desired feature for target detection and localization. The frequency spectrum between 150 and 250 Hz contained no tonals and was used to compare the performance of the techniques. The Bscan showed a concentration of dots along bearing 180^0 and 340^0 with a wide bearing variation between estimates. The high-resolution beamforming techniques indicated two distinct contacts corresponding to contact 1 to the North and contact 2 to the South. The direction estimates showed considerably less variation between frequency bins than the Bscan.

Summary

High-resolution beamforming techniques have been successfully applied to DIFAR data to provided accurate directional information. Although the current processing techniques are adequate for most situations, the presence of multiple contacts, or strong directional noise, may hinder target detection, and localization. Simulations and experimental results from field data showed that E_{ML} provided the best overall results in terms of accuracy, peak-to-trough visibility and processing time, for a range of parameters. E_{IML} improved the peak-to-trough difference at the expense of processing time, but in most cases, the weaker contact was

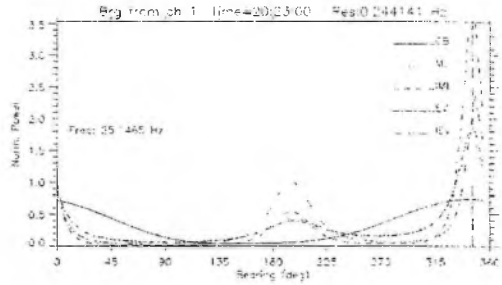

Fig. 1. Direction estimates at 25 Hz. Vertical line is the Bscan.

already visible with E_{ML}, making the gain minimal. It was also found that E_{EV} may produce spurious peaks, or create double peaks, in isolated cases. E_{EV} is otherwise accurate, with E_{IEV} providing marginal improvement.

References

[1] A.J. Collier, 1984: The DIFAR Bearing Debiasing algorithm in the Aurora, *DREA research note DWA/84/4.*

[2] 14 Software Engineering Squadron, circa 1980, Program Description Document for the Passive Program PD5924507G7, Greenwood, NS.

[3] J. Capon, 1969: High-Resolution Frequency-Wavenumber Spectrum Analysis , *Proc. IEEE*, 57 , 1408-1419.

[4] D.H. Johnson and S.R. DeGraaf, 1982 : Improving the Resolution of Bearing in Passive Sonar Arrays by Eigenvalue Analysis, *IEEE Trans. Acoust. Speech Signal Process.* , ASSP-30, 638-647.

[5] S.S Pawka, 1983: Island Shadows in Wave Directional Spectra, *J. Geophys. Res.* 88, 2279-2591.

[6] J. Oltman-Shay and R.T. Guza, 1984: A Data-Adaptive Ocean Wave Directional-Spectrum Estimator for Pitch and Roll Type Measurements, *J. Phys. Oceanogr.* , 14, 1800-1810.

[7] R.F. Marsden and B.-A. Juszko, 1987: An Eigenvector Method for the Calculation of Directional Spectra from Heave, Pitch and Roll Buoy Data, *J. Phys. Oceanogr.* , 17, 2157-2167.

[8] R.F. Marsden, B.-A. Juszko, and R.G. Ingram, 1995: Internal Wave Directional Spectra Using an Acoustic Doppler Current Profiler, *J. Geophys. Res.*, 100, 16179-16192.

[9] W.S. Burdic, 1991: Underwater Acoustic System Analysis, 2nd edition, Prentice Hall, 466 pp.

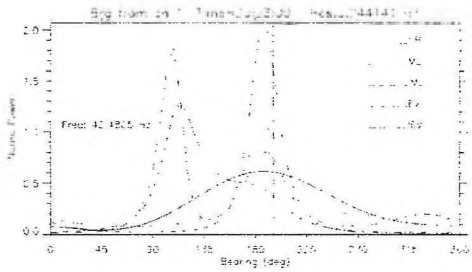

Fig. 2. Same as fig. 1 at 42 Hz. Note *bearing bias* of the Bscan.

REGULARIZED ACOUSTIC INVERSION FOR TOWED-ARRAY SHAPE ESTIMATION

Nicole Collison and Stan Dosso
School of Earth and Ocean Sciences, Univ. of Victoria, P.O. Box 3055, Victoria, B.C., CANADA V8W 3Y2

BACKGROUND

This paper considers the inverse problem of determining the shape of a ship-towed hydrophone array using the relative travel times of direct and reflected arrivals from acoustic sources deployed by a pair of consort ships [1]. To date, this inversion has been solved as a least-squares problem (minimizing the squared data error), assuming straight-line acoustic propagation in the ocean and neglecting the inevitable errors in the source positions. This paper develops a new approach based on an iterated linearized inversion of the ray-tracing equations, which is solved using the method of regularization [2]. The 3-D positions of both sources and sensors are treated as unknowns, subject to *a priori* information. For the sources, the prior information consists of position estimates and uncertainties. For the sensors, the prior information is that the array shape is expected to be smooth; this is applied by minimizing the 3-D curvature of the array to obtain a minimum-structure solution. An example is given comparing least-squares and regularized inversion.

THEORY

The set of acoustic arrival times $\mathbf{t}$ measured in an acoustic positioning survey can be written in general vector form as

$$\mathbf{t} = \mathbf{T}(\mathbf{m}) + \mathbf{n}. \tag{1}$$

In (1), the forward mapping $\mathbf{T}$ represents the arrival times of the acoustic signals along ray paths between sources and receivers . The model $\mathbf{m}$ of unknown parameters consists of 3-D position variables x, y, z for each sensor, position variables x', y', z' for each source, and the source instant t_0 for each source. Finally, $\mathbf{n}$ represents the data errors (noise). The inverse problem of determining an estimate $\tilde{\mathbf{m}}$ of $\mathbf{m}$ is functionally nonlinear; however, a local linearization can be obtained by expanding $\mathbf{T}(\tilde{\mathbf{m}}) = \mathbf{T}(\mathbf{m_0} + \delta\mathbf{m})$ in a Taylor series to first order about an arbitrary starting model $\mathbf{m_0}$ to yield

$$\mathbf{t} = \mathbf{T}(\mathbf{m_0}) + \mathbf{J}(\mathbf{m_0})\,[\tilde{\mathbf{m}} - \mathbf{m_0}], \tag{2}$$

where $\mathbf{J}$ represents the Jacobian matrix of partial derivatives $J_{ij} = \partial T_i / \partial m_j$ (analytic expressions for these are derived in [2]). Equation (2) can be written

$$\mathbf{J}\,\tilde{\mathbf{m}} = \mathbf{t} - \mathbf{T}(\mathbf{m_0}) + \mathbf{J}\mathbf{m_0} \equiv \mathbf{d}, \tag{3}$$

where the explicit dependence on $\mathbf{m_0}$ has been suppressed. Note that $\mathbf{d}$ consists entirely of known or measured quantities, and may be considered modified data for the problem. Equation (3) represents a linear inverse problem for $\tilde{\mathbf{m}}$. Since nonlinear terms have been neglected in (3), the linearized inversion may need to be repeated iteratively until the solution converges (i.e., update $\mathbf{m_0} \leftarrow \tilde{\mathbf{m}}$ and repeat the inversion until $\tilde{\mathbf{m}} = \mathbf{m_0}$).

Solving the linear inverse problem (3) at each iteration requires some attention. By treating both source and sensor positions as unknown, a straightforward application of least-squares yields an ill-posed solution. The method of regularization provides a unique, stable inversion by explicitly including *a priori* information regarding the solution. This is typically accomplished by minimizing an objective function Ψ which combines a term representing the data misfit and a regularizing term that imposes the *a priori* expectation that the model $\tilde{\mathbf{m}}$ in some manner resembles a prior estimate $\hat{\mathbf{m}}$:

$$\Psi = |\mathbf{G}\,(\mathbf{J}\,\tilde{\mathbf{m}} - \mathbf{d})|^2 + \mu\,|\mathbf{H}\,(\tilde{\mathbf{m}} - \hat{\mathbf{m}})|^2. \tag{4}$$

In (4), $\mathbf{G}$ is a diagonal matrix with the reciprocals of the estimated data standard deviations on the main diagonal, $\mathbf{H}$ is an arbitrary weighting matrix for the regularization, and μ is a trade-off parameter controlling the relative importance of the two terms in the minimization. The regularized solution is obtained by minimizing Ψ with respect to $\tilde{\mathbf{m}}$ to yield

$$\tilde{\mathbf{m}} = \left[\mathbf{J}^T\mathbf{G}^T\mathbf{G}\mathbf{J} + \mu\mathbf{H}^T\mathbf{H}\right]^{-1}\left[\mathbf{J}^T\mathbf{G}^T\mathbf{G}\mathbf{d} + \mu\mathbf{H}^T\mathbf{H}\hat{\mathbf{m}}\right]. \tag{5}$$

The value for μ is generally chosen so that the χ^2 misfit (first term of eq. 4) achieves its expected value of N for N data, which applies the *a priori* information subject to ensuring that the data are fit to a statistically appropriate level.

The regularization matrix $\mathbf{H}$ in (4) and (5) provides flexibility in the application of *a priori* information in the inversion. For instance, if prior model parameter estimates $\hat{\mathbf{m}}$ are available, an appropriate weighting is given by

$$\mathbf{H} = \mathrm{diag}[1/\xi_1, \ldots, 1/\xi_M], \tag{6}$$

where ξ_j represents the uncertainty for jth parameter estimate $\hat{m}_j$. Alternatively, the *a priori* information can be applied to derivatives of the model parameters. For instance, if the *a priori* expectation is that the parameters are well approximated by a smooth function, then an appropriate choice is $\hat{\mathbf{m}} = \mathbf{0}$ and

$$\mathbf{H} = \begin{bmatrix} -1 & 2 & -1 & 0 & 0 & 0 & 0 & \cdots & 0 \\ 0 & -1 & 2 & -1 & 0 & 0 & 0 & \cdots & 0 \\ \vdots & & & & \ddots & & & & \vdots \\ 0 & \cdots & 0 & 0 & 0 & -1 & 2 & -1 & 0 \\ 0 & \cdots & 0 & 0 & 0 & 0 & -1 & 2 & -1 \end{bmatrix}. \tag{7}$$

For this choice of $\hat{\mathbf{m}}$ and $\mathbf{H}$, minimizing (4) effectively minimizes a discrete approximation to the second derivative of $\mathbf{m}$ (i.e., minimizes model curvature), subject to fitting the data.

The inverse problem considered here involves both types of *a priori* information described above. In particular, prior estimates are available for the source locations, and the prior expectation that the array shape is smooth can be applied by minimizing the curvature. A solution incorporating both regularizations can be written

$$\tilde{\mathbf{m}} = \left[\mathbf{J}^T\mathbf{G}^T\mathbf{G}\,\mathbf{J} + \mu_1\,\mathbf{H}_1^T\mathbf{H}_1 + \mu_2\,\mathbf{H}_2^T\mathbf{H}_2\right]^{-1} \times \left[\mathbf{J}^T\,\mathbf{G}^T\mathbf{G}\,\mathbf{d} + \mu_1\,\mathbf{H}_1^T\mathbf{H}_1\,\hat{\mathbf{m}}_1 + \mu_2\,\mathbf{H}_2^T\mathbf{H}_2\,\hat{\mathbf{m}}_2\right]. \quad (8)$$

In (8), the first regularization term is taken to represent the *a priori* source-position estimates. Hence, $\hat{\mathbf{m}}_1$ consists of the prior estimates for these parameters, (with zeros for the remaining parameters), and $\mathbf{H}_1$ is of the form of (6). The second regularization term is taken to represent the *a priori* expectation of a smooth array shape. Hence, $\hat{\mathbf{m}}_2 = \mathbf{0}$, and $\mathbf{H}_2$ is of the form of (7) for the sensor position parameters.

EXAMPLE

This section illustrates the regularized approach to towed array shape estimation with a realistic synthetic example. The ocean is 1300 m deep, with a typical N. E. Pacific sound speed profile. The towed array consists of 32 sensors, each separated by 10 m, towed at a nominal depth of 300 m. The sources deployed by the two consort ships are nominally located at 200-m depth, 500-m range (from the array centre), and at angles of $\pm 45°$ with respect to array broadside. The errors on the source positions are taken to be Gaussian-distributed random variables with a standard deviation of 10 m in x', y' and 5 m in z'. The data consists of the relative travel times of the direct and bottom-reflected acoustic arrivals, computed via 1D raytracing, with additive (Gaussian) errors. Cases are considered with data standard deviations of 1 ms and 0.5 ms. The (linearized) localization inversion was solved two ways: (i) using the regularized solution (8), treating source and sensor positions as unknown and solving for the smoothest array shape, as outlined in the previous section; and (ii) by applying standard least-squares inversion to minimize the misfit to the data, treating the source positions as known quantities. In each case, the linearization and inversion were applied to the 1-D raytracing equations.

The results of the inversions are shown in Fig. 1. Figure 1(a) and (b) show the array shape in the horizontal (x-y) and vertical (x-z) planes, respectively, for data errors of 1 ms. Figure 1(c) and (d) show the same results for data errors of 0.5 ms. The fairly large offsets of the inversion results are due to the errors in the source positions. Note, however, that by treating the source positions as (constrained) unknowns, the regularized solutions achieve significantly smaller offsets. In addition, the regularized inversion provides smooth models, with substantially less structure (random fluctuations) than

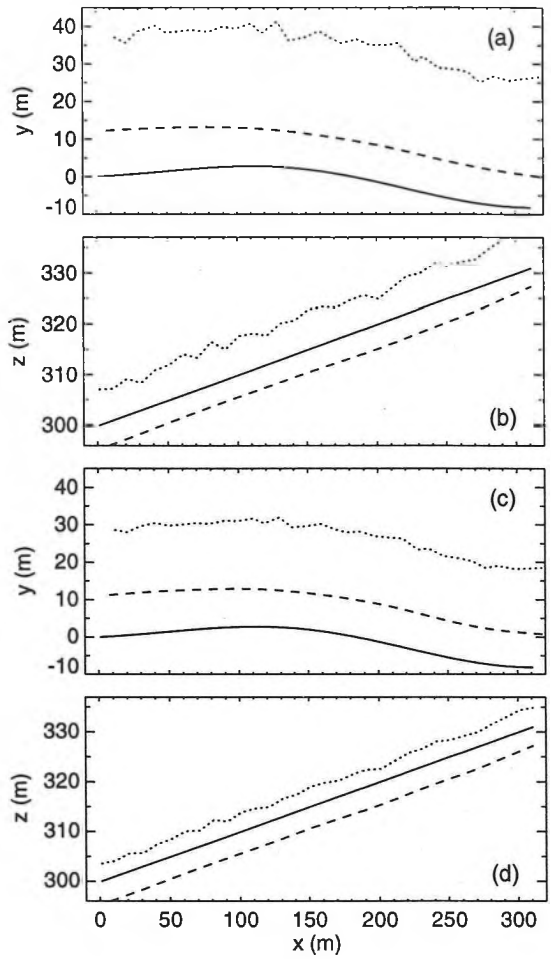

Fig. 1 Comparison of regularized and least-squares inversion for the synthetic test case described in text. Solid line indicates true array shape, dashed and dotted lines indicate the regularized and least-squares solutions, respectively. In (a) and (b) the data errors are 1 ms; in (c) and (d) they are 0.5 ms.

the least-squares solution. The fluctuations in the least-squares solution result from the tendency of a minimum-misfit approach to over-fit the data, in effect fitting the noise as well as the data. The regularized inversion avoids this by trading off data misfit with physical *a priori* information.

ACKNOWLEDGMENTS

This work was supported by the Defence Research Establishment Atlantic, Dartmouth NS.

REFERENCES

[1] E. C. Ballegooijen et al., 1989. Measurement of towed array position, shape and attitude, IEEE J. Ocean. Eng., **14**, 375–383.

[2] S. E. Dosso, M. R. Fallat, B. J. Sotirin and J. L. Newton, 1998. Array element localization for horizontal arrays via Occam's inversion. J. Acoust. Soc. Am., **104**, 846–859.

Array Element Localization of the Haro Strait Experiment Using a Two-Step Inversion Mehtod

Vanessa Corre, Ross Chapman and Mike Wilmut
School of Earth and Ocean Sciences, University of Victoria, Victoria, B.C., CANADA V8W 3P6

OVERVIEW OF THE PROBLEM

The Haro Strait experiment [1] was designed for ocean and geoacoustic tomography inversion. Three vertical line arrays (VLAs) were deployed at sea to record acoustic pressure fields generated by light bulb explosions over a period of several days. Tomography inversion requires an accurate knowledge of the receiver and source locations. Such knowledge is usually not available and this is particularly true in the case of the Haro Strait experiment. GPS measurements of the ship position were done during the deployment of the VLAs and sources. The uncertainty of these measurements varies from 5 to $20m$. The source depth was estimated by the length of the immersed cable carrying the light bulb (uncertainty $\pm 3m$). In addition, due to strong tidal currents, the arrays were expected to be tilted and a GPS measurement at one VLA while being recovered revealed a drift of about $100m$ from the original position. It is thus necessary to localize the VLAs as continuously as possible (ideally at each explosion time). Localization is usually done by inverting the measured travel times of the direct paths between one source and the receivers. For the Haro Strait data, the large number of unknowns in the problem (x,y and z coordinates of each receiver and each source, and the absolute time of the explosions) requires additional information (data) in order to obtain an accurate solution. In this paper, we present a method for array element localization that takes advantage of additional travel times provided by the use of multiple sources and multiple paths. To overcome the lack of exact knowledge of the source positions, this method includes 2 inversion steps : a relative localization of the receivers which depends on the depth of the sources, and then the absolute localization of both sources and receivers.

INVERSIONS

Relative localization Inversion of travel times for localization is a nonlinear problem. However it is not highly nonlinear and local linearization using Newton's method has been applied successfully. Since the source and receiver x and y coordinates are not known, we first concentrate on their relative positions and define $\mathbf{m}$, the model of parameters to be determined, as follow:

$$\mathbf{m} = \{Z_j^r, D_{ij}, t_i'; \quad j = 1, N_{rec}, i = 1, N_{src}\},$$

where N_{src} and N_{rec} are the number of sources and receivers respectively, Z_j^r is the depth of the j^{th} receiver, D_{ij} is the horizontal distance between the i^{th} source and the j^{th} receiver and t_i' is the time delay for the i^{th} source. The total number of parameters is $M = N_{rec}(1+N_{src})+N_{src}$.

The source depths Z_i^s are assumed to be known. Given a constant sound speed c in the water, the relative onset travel times of the direct (d) and surface (s) reflected paths between the i^{th} source and the j^{th} receiver are given by eqs. 1 and 2 respectively:

$$t_{ij}^d = (\sqrt{d_{ij}^2 + (Z_i^s - Z_j^j)^2} - ct_i')/c, \tag{1}$$

$$t_{ij}^s = (\sqrt{d_{ij}^2 + (Z_i^s + Z_j^j)^2} - ct_i')/c. \tag{2}$$

The measured travel times of both paths define the vector of data: $\mathbf{t} = \{\mathbf{t^d}, \mathbf{t^s}\}$ ($N = 2N_{src} \times N_{rec}$ elements). Eqs 1 and 2 can be written in the more general form $\mathbf{t} = \mathbf{T(m)}$, where $\mathbf{T}$ is a nonlinear function. The expansion of $\mathbf{T(m)}$ in a Taylor series (linearization) to first order about an arbitrary starting model m_0 gives:

$$\mathbf{T(m)} = \mathbf{T(m_0 + \Delta m)} \simeq \mathbf{T(m_0)} + \mathbf{J\Delta m}$$

where $J_{kl} = \delta T_k(\mathbf{m_0})/\delta m_l$ is a Jacobian matrix. Applying the jumping method [2]($\mathbf{\Delta m = m - m_0}$) leads to:

$$\mathbf{Jm} = [\mathbf{t} - \mathbf{T(m_0)}] + \mathbf{Jm_0} \equiv \mathbf{t_o}. \tag{3}$$

This equation defines a linear problem (the right side of the equation is known). At this stage, it is possible to invert for $\mathbf{m}$. However, the solution is nonunique and the inversion can be unstable. One way to adress this problem is regularization i.e. including *a priori* information about the model to stabilize the inversion. Regularized inversion consists in minimizing the objective function Φ that combines a least square data misfit term and a regularizing term :

$$\Phi = |\mathbf{G(J\,m - t_o)}|^2 + \mu\,|\mathbf{H(m - \hat{m})}|^2. \tag{4}$$

In this equation, $\mathbf{G}$ is a diagonal matrix whose diagonal elements are the inverse of the estimated data standard deviations (the noise is assumed Gaussian with zero mean), $\mathbf{H}$ is the regularization matrix, $\hat{\mathbf{m}}$ is the *a priori* estimate of $\mathbf{m}$, and μ is a trade-off parameter controlling the relative importance of the 2 terms in the minimization. Minimizing Φ with respect to $\mathbf{m}$ leads to the solution:

$$\mathbf{m} = \hat{\mathbf{m}} + [\mathbf{J^\dagger G^\dagger G\,J} + \mu\,\mathbf{H^\dagger H}]^{-1}\mathbf{J^\dagger G^\dagger G}\,(\mathbf{t_o} - \mathbf{J}\,\hat{\mathbf{m}}). \tag{5}$$

Since nonlinear terms are neglected during the linearization, the solution $\mathbf{m}$ may not be satisfactory (large misfit $\chi^2 = |\mathbf{G(T\,(m) - t)}|^2$). The inversion is then repeated by updating the starting model ($\mathbf{m} \rightarrow \mathbf{m_0}$) until $\chi^2 = N$.

Absolute localization The result of the inversion described in the previous part is the estimate of receiver depths and horizontal distances between sources and receivers. The next step is to estimate the absolute position (x and y coordinates) of the acoustic elements. However, the new model $\mathbf{m}'$ of parameters to be determined is reduced to the $2N_{src}$ source coordinates (X_i^s, Y_i^s) since analytical expressions of the receiver coordinates (X_j^r, Y_j^r) can be derived from (X_i^s, Y_i^s) and the distances D_{ij}. The candidate models are sampled on a grid covering the uncertainty surface of the source locations. For each model, the receiver positions are determined and a coefficient β is calculated to characterize the shape of the array:

$$\beta = \sum_{j=1}^{N_{rec}-1} \sqrt{|X_{j+1}^r - X_j^r|^2 + |Y_{j+1}^r - Y_j^r|^2 + |Z_{j+1}^r - Z_j^r|^2}. \quad (6)$$

The model $\mathbf{m}'$ corresponding to the minimum β (minimum structure in the array shape) is the estimate of the source x and y coordinates.

If the depths of the source are known, it is thus possible to determine the absolute positions of the sources and receivers ($\mathbf{m}'' = \{X_i^s, Y_i^s, X_j^r, Y_j^r, Z_j^r\}$). However, this is not true for the Haro Strait data and using different sets of source depths in the inversion would result in different estimates of $\mathbf{m}''$ that could still fit the data. In order to reduce the number of these solutions, a second inversion is done. This inversion consists in 1) repeating the estimation of $\mathbf{m}''$ for different sets of source depths and 2) for each estimate, predicting the onset travel times of the bottom (b), surface-bottom(sb) and bottom-surface (bs) reflected paths. Similar equations to eqs 1 and 2 do not exist to calculate the travel times of these additional paths. Instead, this 2^{nd} inversion is a model-based inversion: the modeled travel times $\tau = \{\tau^d, \tau^s, \tau^b, \tau^{bs}, \tau^{sb}\}$ are computed using a ray code. The travel times of the bottom interacting paths $(\tau^b, \tau^{bs}, \tau^{sb})$ are then compared to the corresponding measured travel times $(\mathbf{t}^b, \mathbf{t}^{bs}, \mathbf{t}^{sb})$:

$$\chi_b^2 = \sum_{i=1}^{N_{src}} \sum_{j=1}^{N_{rec}} 3/\sigma_{ij}(|\tau_{ij}^b - t_{ij}^b|^2 + |\tau_{ij}^{bs} - t_{ij}^{bs}|^2 + |\tau_{ij}^{sb} - t_{ij}^{sb}|^2), \quad (7)$$

where the modeled travel times τ have been preliminary calibrated such that $\tau_{i0}^d = t_{i0}^d$, and σ_{ij} is the uncertainty of the travel time between the i^{th} source and the j^{th}. The estimate of the source depths (and by extension $\mathbf{m}''$) is given by the model that minimizes $|\chi_b^2 - N_b|$ where N_b is the number of data ($N_b = 3N_{src} \times N_{rec}$).

RESULTS

For each VLA localization, 2 sources were selected such that 1) they were close enough in time, 2) their positions relative to the VLA would allow good x and y resolution (ie not in line with VLA) and 3) the 5 paths were easily identifiable. Picking the measured onset travel times $\mathbf{t} = \{\mathbf{t}^d, \mathbf{t}^s, \mathbf{t}^b, \mathbf{t}^{bs}, \mathbf{t}^{sb}\}$ of the different paths from the time series was done using an adaptative matched filter calculating correlation between the time series and a reference waveform (direct path). For the regularization, $\hat{\mathbf{m}}$ was set to the preliminary estimates of the parameters at the deployment and $\mathbf{H}$ was a diagonal matrix whose diagonal elements are the inverse of the uncertainties of these preliminary estimates. Table 1 shows the result of localization for 2 of the VLAs (noted NW and SW) as well as the *a priori* model $\hat{\mathbf{m}}$. X and Y coordinates are minutes of longitude 123^o and latitude 48^o respectively. Results for the top, middle and bottom receivers are given. In figure 1, the travel times τ calculated for the various paths from the final estimate of source and receiver locations are compared to the measured travel times. A good agreement can be observed.

	NW		SW	
param.	a priori	estimate	a priori	estimate
$X_1^r(min)$	12.880	13.140	12.880	12.778
$X_8^r(min)$	12.880	13.137	12.880	12.778
$X_{15}^r(min)$	12.880	13.131	12.880	12.778
$Y_1^r(min)$	38.700	39.479	38.700	38.741
$Y_8^r(min)$	38.700	39.478	38.700	38.735
$Y_{15}^r(min)$	38.700	39.470	38.700	38.717
Z_1^r (m)	30.00	40.94	50.00	66.98
Z_8^r (m)	73.75	84.32	93.75	110.10
Z_{15}^r (m)	123.75	132.54	143.75	150.02
$X_1^S(min)$	13.195	12.680	13.195	12.681
$Y_1^S(min)$	38.985	39.017	38.985	39.020
Z_1^S (m)	70.00	71.00	70.00	71.00
$X_2^S(min)$	13.195	13.184	13.195	13.186
$Y_2^S(min)$	38.985	38.982	38.985	38.986
Z_2^S (m)	70.00	71.00	70.00	71.00

Table 1: Result of localization for 2 arrays.

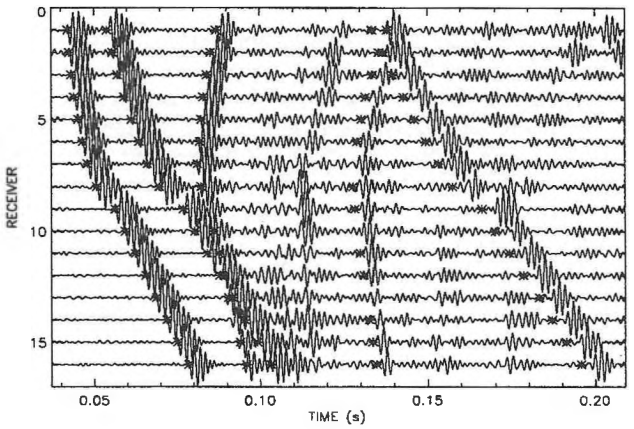

Figure 1: Pressure field recorded at the SW array for source 1. The modeled onset travel times τ are indicated by asterisk.

REFERENCES

[1] N.R. Chapman, M.A. McDonald and L. Jaschke, "Haro Strait Experiment 1996-Low frequency tomography experiment: 17-21 June '96. Cruise Report", University of Victoria (1996).

[2] S.E. Dosso, M.R. Fallat, B.J. Sotirin and J.L. Newton,"Array element localization for horizontal arrays via Occam's inversion,"J. Acoust. Soc. Am. **104**,846-859 (1998).

AVO Investigations Of Shallow Marine Sediments

M. Riedel[1] and F. Theilen[2]

[1] School of Earth and Ocean Science, University of Victoria, B.C. Canada

[2] Institute of Geosciences, Department of Geophysics, University Kiel, Germany

AVO/AVA (Amplitude Versus Offset/Angle) analysis has been used to determine the physical characteristics of shallow marine sediments. The parameter that can be constrained, are P- and S- wave velocity, bulk density and acoustic attenuation. Shear modulus and other geotechnical properties such as grain size can be inferred from these parameters. The theory of AVO investigations is given by the Zoeppritz equations (Zoeppritz, 1919), which allow the computation of the reflection and transmission coefficients as a function of angle of incidence. AVO has been widely used in the petroleum industry, usually for frequencies of 20-100 Hz. High frequency shallow sediment AVO studies require special analysis including careful geometry and source and receiver directivity corrections.
In the past, marine sediments have been modeled as elastic materials. However, viscoelastic models with absorption are more realistic. At large angle of incidence, AVA-functions derived from viscoelastic models differ significantly from those with purely elastic properties. The influence of S-wave velocity on the reflection coefficient is rather small (especially for the low S-wave velocities encountered at the seafloor). On the other hand, P-wave velocity and density show a considerably stronger effect (Fig. 1). Thus, it will be difficult, or nearly impossible, to extract the S-wave parameter from AVA trends, especially when the signal-to-noise ratio is low.

In order to measure the reflection coefficient in a seismogram, the peak amplitudes of the direct wave and the seafloor reflection in a CMP (Common Mid Point) gather are determined and corrected for spherical divergence, and source and receiver directivity (Fig. 2). At CMP locations showing different AVA characteristics, the sediment parameters P- and S-wave velocity, density and absorption are determined by using a Sequential Quadratic Programming (SQP) inversion technique. The use of the viscoelastic model within the inversion gives better results in fitting the data than the elastic model without absorption.

The introduction of constraints, e.g. empirical relationships given by core investigations, can improve and stabilize the inversion results.

Parameter	CMP 570	CMP 4000
P-wave [m/s]	1453	1622
S-wave [m/s]	*92*	*358*
density [kg/m^3]	1220	1380
Q P-wave	*14*	*787*
Q S-wave	*9*	*25*

Table 1. Inverted sediment properties of CMP-Bin 570 and CMP-Bin 4000.

In Fig. 2, a soft mud layer, with a typical low P-wave velocity close to water velocity, forms the seafloor at CMP-Bin 570 whereas at CMP-Bin 4000 the seafloor contains boulder clay, a mixture of sand and gravel with a higher P-wave velocity and density.
In both cases the inversion gives reasonable results for the first three sediment parameters. Note that the value of the S-wave velocities have an uncertainty of more than 100% due to the insensitivity of the reflection coefficient to this parameter.

The investigation of deeper sediment layers by AVA requires a good estimate of the absorption (described by the Q-factor) within the first sediment layer.

The influence of Q on the reflection coefficient is enhanced in the wide-angle domain. However, our measurements were restricted to a maximum angle of incidence of 60°, which results in relatively high uncertainties in the inversion result with respect to the absorption factor Q. Further investigations on the absorption in shallow marine sediments, e.g. by spectral division methods of broadband multichannel seismic data, must be carried out in the future.
A posteriori probability distributions for linearized inversion and non-linear approaches (simulated annealing and Gibbs sampling) are subject of ongoing research.

REFERENCES

Zoeppritz, R., 1919. On the reflection and propagation of seismic waves, Erdbebenwellen VIIIB, Göttinger Nachrichten, I, 66-84

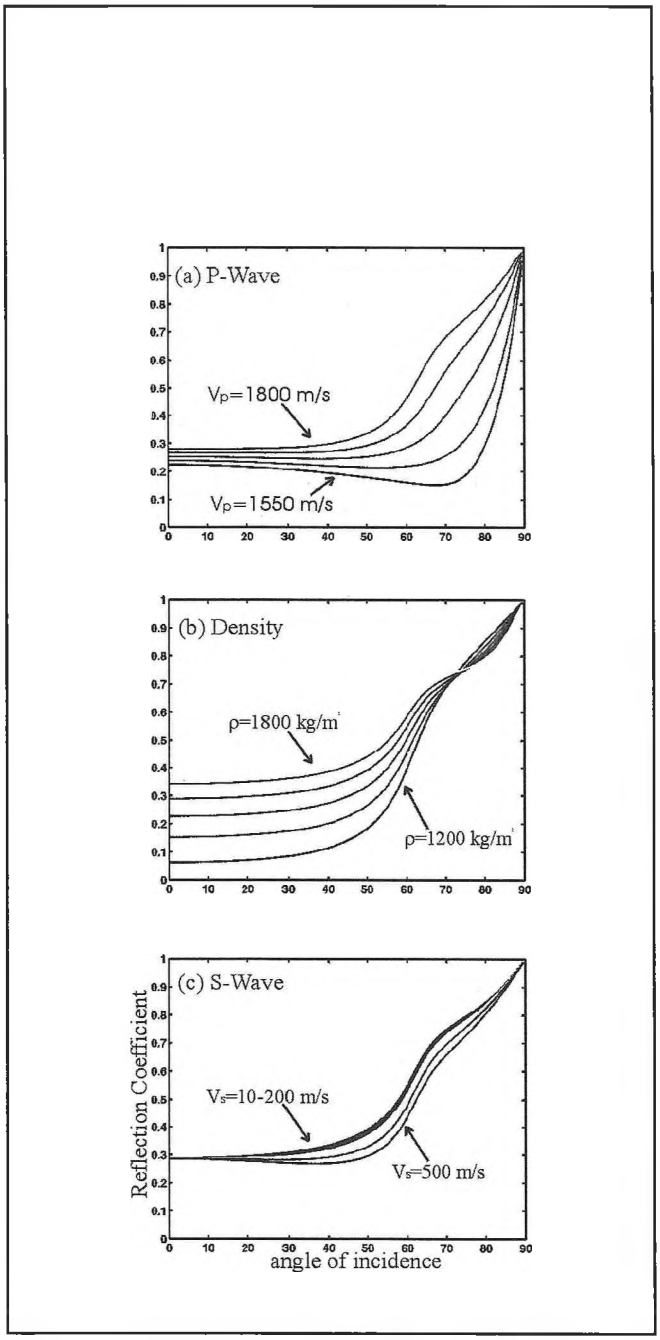

Fig. 1. Influence of (a) P-wave velocity, (b) density, and (c) S-wave velocity on the reflection coefficient as a function of angle of incidence. The parameters of the viscoelastic sediment model are: P-wave velocity = 1700 m/s, S-wave velocity = 100 m/s, density = 1300 kg/m3, and Qp = Qs = 10.

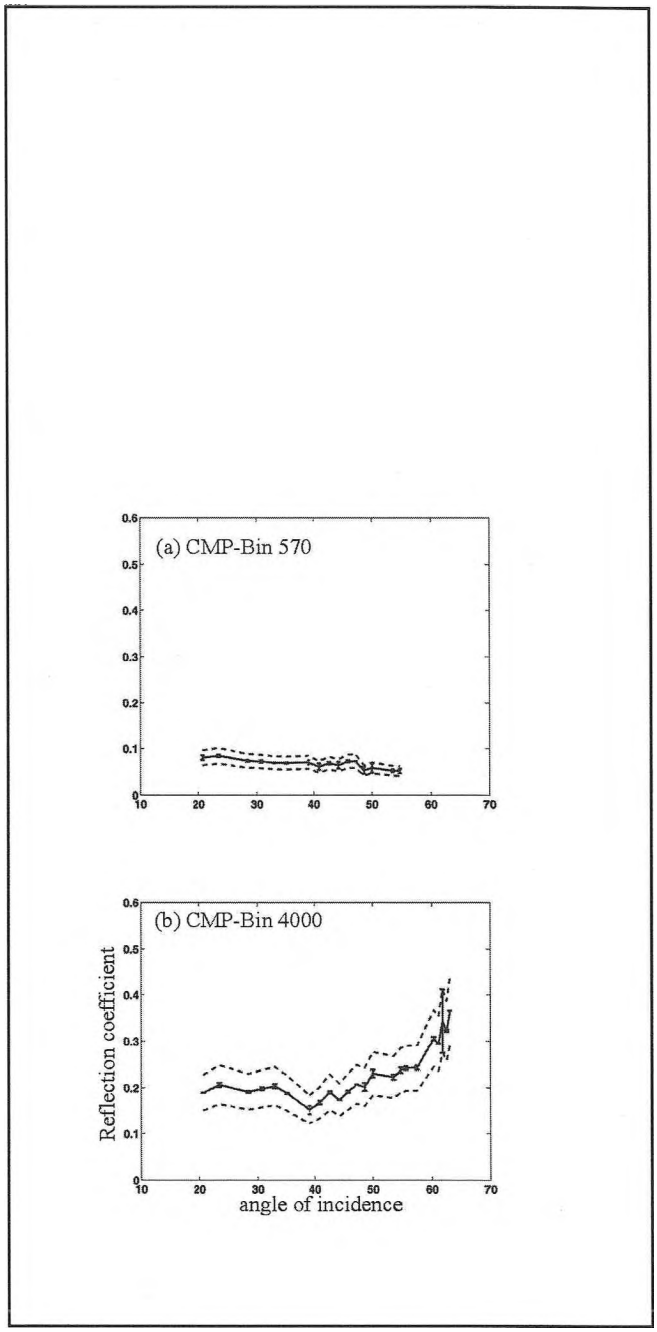

Fig. 2. Calculated reflection coefficient at (a) CMP-Bin 570 (mud), and (b) CMP-bin 4000 (boulder clay). Error bars indicate variability within each bin. Lower and upper bounds for the reflection coefficient have been included based on an uncertainty in the source directivity of 20%.

The Effect of Thin Beds on Attenuation Estimates for Shallow Subbottom Classification

Stephen F. Bloomer, N. Ross Chapman
School of Earth and Ocean Sciences, Univ. of Victoria, P.O. Box 3055, Victoria, B.C., CANADA V8W 3P6

William T. Collins
Quester Tangent Corp., 9865 West Saanich Rd., Sydney, B.C.,CANADA V8L 5Y8

Acoustic seabed classification from sonar data has generally focussed on attributes of the return echo from the seafloor. For many engineering applications such as the dredging and monitoring of navigable waters, building of major structures such as bridges, pipelines, and dams requiring the support of the subbottom, and research into regional tectonic activity, a detailed knowledge of the subbottom is also required. The development of high-resolution seismic systems such as chirp sonars (1) and the IKB SEISTEC^{TM} system (2) this decade has allowed the mapping of the subsurface in shallow water to become cost-effective, and provides the potential for rapid, subbottom classification.

These shallow-water high-resolution seismic profilers operate in water depths of 10-15 metres with bandwidths up to 1-12 kHz. Subsurface penetration in excess of 10 metres can be achieved. Often, in cases where seismic reflectors appear to be well resolved, it is inviting to assume a frequency-dependent loss of amplitude between seafloor and subbottom reflectors. Methods, such as the spectral-ratio technique, that can utilize the wide bandwidth of these profilers, can be then used to estimate attenuation coefficients between successive reflectors. These estimates in turn could be then used to classify subbottom sediment types.

In many cases, however, an apparently well-resolved reflector may be the result of the constructive interference between reflected energy (including multiples) from closely spaced interfaces. This paper will present the results of a model study investigating the effects on apparent attenuation due to thin bed interaction.

ACOUSTIC ATTENUATION IN SEDIMENTS

When an acoustic signal passes through sediments, attenuation typically causes the amplitude of the signal to decrease with the distance traveled. Hamilton (3) demonstrated from a large database of field measurements that compresssional attenuation varies linearly with frequency. Therefore, we can write the average attenuation between two consecutive reflectors as (4):

$$A_2(f) = G \times A_1(f) \times \exp\left(\frac{-\beta \times (t_2 - t_1) \times f}{20 \times \log_{10}(\exp(1))}\right) \qquad (1)$$

where $A_1(f)$ and $A_2(f)$ are the amplitude spectra of the shallower and deeper reflector signals, f is the frequency, t_2-t_1 is the travel-time between the two reflectors, β is the attenuation coefficient in dB/wavelength (dB/λ), and G is a frequency independent term dependent on the reflection coefficients at the interfaces associated with the two reflectors. A least squares fit of the logarithm of the ratio of the amplitude spectra versus frequency over the source bandwidth results in a line with a slope related to the attenuation coefficient and intercept related to approximately the ratio of the reflection coefficients (for a small upper reflection coefficient).

There are a few studies in which the values of attenuation coefficients in near surface sediments have been published. Schock (1) summarizes the results of these few studies, and the attenuation coefficient ranges typically from 0.05 to 0.35 dB/λ, and is well resolved (approximately 0.05 dB/λ) for the sediment types of interest, suggesting that this property is useful for classification purposes.

However, in many cases, interference from overlapping subbottom reflectors creates a "hole" in the spectrum of the subbottom arrival in the useful source band (see (6)), and consequently degrades the fit of the least-squares relationship described above. At the expense of classifying less of the subbottom, rejecting estimates where the correlation coefficient of the least-squares fit falls below the 95% confidence level can overcome potential misclassification. The effectiveness of this criterion in the following model study will also be examined.

MODELING PROCEDURE

To test the effect of thin beds on attenuation coefficient estimates, the impulse response of a series of acoustic models containing a near-surface thin bed (depicted in Figure 1) was calculated at a sample rate of 50 KHz by varying the attenuation coefficient (α), the thin bed reflection coefficient (z_{tb}), the thin bed thickness (Δx), and the thickness of the bed below the thin bed (x-Δx) over the ranges shown in Figure 1, while holding the surface and subsurface reflection coefficient constant (0.20 and 0.05 respectively. A synthetic seismogram for each case was created by convolving a ~2-8 KHz source wavelet with the impulse response. 64 point FFT's of the apparent seafloor and subsurface reflectors (as shown in Figure 2) were calculated (the thin bed reflector was eliminated and the data zero-padded if it was well-resolved from the seafloor reflector). The attenuation coefficient and reflection coefficient ratio between the reflectors were then estimated by fitting a straight line between the log of the amplitude spectra ratio versus frequency over the source of range 2-8 KHz.

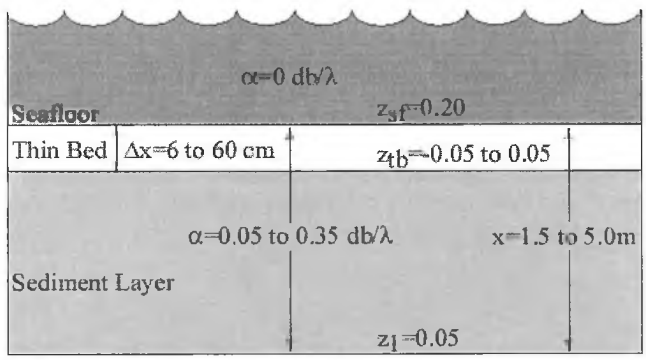

Fig. 1. Geoacoustic model used for this study. The parameters varied are the attenuation of the sediment layer (α), the reflection coefficient of the thin bed-sediment layer interface (z_{tb}), the thin bed thickness (Δx), and the overall thickness of sediment (x).

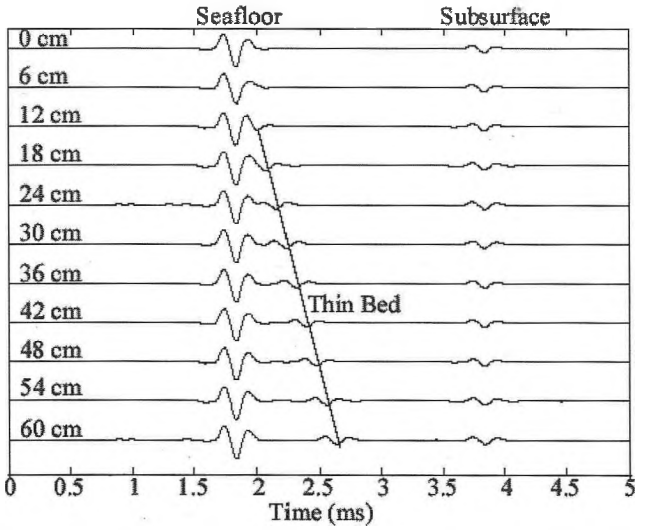

Fig. 2. Arrivals resulting from a geoacoustic model with α=0.05 dB/λ, x=1.5m, z_{tb}=0.04, for various thin bed thicknesses Δx. Note for very thin beds, an arrival from a single interface is nearly indistinguishable from one resulting from the interaction of two interfaces.

RESULTS

To attempt to isolate the sensitive parameters influencing attenuation estimates, histograms of the estimated attenuation coefficients and reflection coefficient ratios were generated with the value of one model variable held constant, while letting the other variables span their entire tested range. Figure 3, as an example, shows the histograms of the estimated attenuation coefficient by holding the attenuation coefficient constant (for various values of a), while letting ztb, x, and Dx vary. Also shown (in solid) are the histograms of estimates that were generated from a least-squares line with a goodness-of-fit significant at the 95% confidence level.

From all these histograms, some general patterns can be observed concerning the attenuation coefficient estimates.

1. The attenuation coefficient has little effect on the accuracy of the estimated values, except that the number of estimates that pass the 95% confidence level increases as the attenuation increases. This is not surprising, as the influence of the thin-bed will be increasingly suppressed as attenuation increases.
2. The reflection coefficient of the thin bed, ztb, has a strong influence on the accuracy of the estimation. For |ztb|<0.2, the estimates form histograms that are not widely dispersed (<0.03 dB/l) from the true value. As the value of |ztb| increases, the histograms about each of the true attenuation coefficients have wider tails and lower peaks, and develop bimodal distributions for |ztb|=0.03 and higher.
3. The total thickness of the sediments, x, has little effect on the shape of the histograms about the true attenuation coefficients when considering all the estimates. For the histograms generated from estimates from least-square fits with a 95% confidence, the dispersion about the true values decreases for thinner sediment thickness and lower attenuation coefficients, but the number of estimates satisfying that criteria also decreases.
4. The estimated attenuation coefficient is very sensitive to thin bed thickness, but the relationship is not simple. For thin bed thickness of 18 cm., and 30 cm. and greater, the histograms about the true attenuation coefficient are narrow, indicating accurate estimates regardless of the value of the other parameters. For a bed thicknesses of 24cm., the histograms are bimodal and have a width of .10 dB/l on either side of the true value. For bed thickness of 6 and 12 cm., the width of the histograms is even wider. Again the histograms generated from estimates from least-square fits with a 95% confidence are narrower for lower attenuation coefficients, though the number of estimates satisfying that criteria also decreases. This is undoubtedly the result of zeros in the amplitude spectra of the apparent surface reflector for thin bed thicknesses of 6 and 12 cm. The result for a 24 cm. thin bed is curious.
5. This study shows that a difference in the attenuation coefficient of 5 dB/l between two sediment layers can be distinguished with some confidence, especially if a goodness of fit criterion is used to limit problems that can be caused by thin bed interaction.

ACKNOWLEDGEMENTS

S.F. Bloomer and N.R. Chapman wish to acknowledge support for this study by NSERC through the Industrial Chair in Ocean Acoustics, and for Dave Hannay for supplying the program used to generate the impulse response from a geoacoustic model.

REFERENCES

1. Schock, S.G., "The Chirp Sonar - A High Resolution, Quantitative Subbottom Profiler", PhD Thesis, University of Rhode Island. (1989).
2. Toth, T. and Simpkin, P., Leading Edge, pp. 1691-1695 (1997).
3. Hamilton, E.L., Journal of the Acoustical Society of America, 68, 1313-1340 (1980).
4. Maroni, C.S. and Quinquis, A., "Estimation of chirp sonar signal attenuation for classification of marine sediments: Improved Spectral Ratio Method", in Proceedings of the Conference on High Frequency Acoustics in Shallow Water, NATO SACLANTCEN, pp. 347-354, 1997.

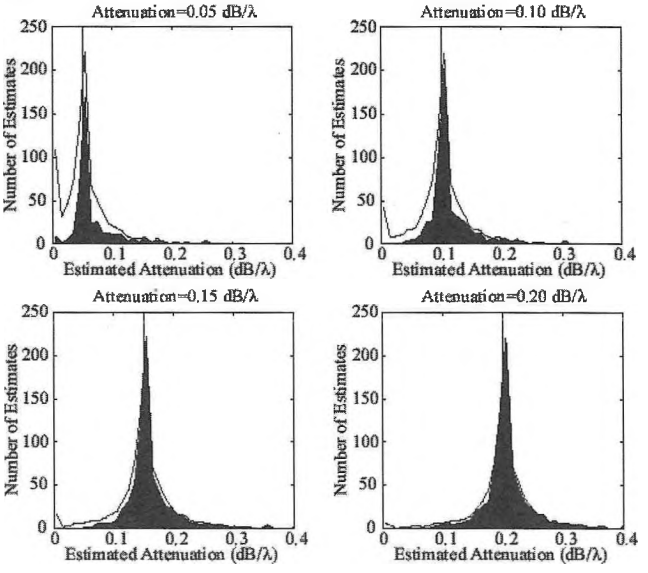

Fig. 3. Plot of histograms of the estimated attenuation for all the model runs with the attenuation equal to 0.05 (upper left), 0.10 (upper righ), 0.15 (lower left), and 0.20 dB/l (lower right). The dark shaded histograms are those that the goodness-of-fit is significant at the 95% confidence level.

FREQUENCY-DEPENDENT SEABED SCATTERING ON BROWNS BANK

Yan Jia and Robert Courtney
Geological Survey of Canada Atlantic

INTRODUCTION

Most marine seismic systems do not measure a calibrated estimate of the backscatter response of the seabed. To better predict the physical properties of the seabed, recent efforts at the Geological Survey of Canada Atlantic have attempted to bring a more quantitative approach to seismic surveying. Frequency-dependent seabed scattering was studied in a frequency domain from 1 to 6 kHz over two small areas with different surface conditions in Browns Bank (south of Yarmouth, Nova Scotia) using a broad-band, impulsive source and a calibrated hydrophone.

THEORY

A Huntec Deep Tow boomer was used as a point source in this study.

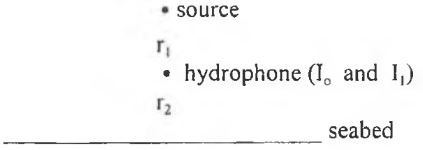

I_o and I_1 are the calibrated source intensity and the scattered wave intensity recorded by hydrophone. The backscattering strength (BBS) is:

$$BSS = \log_{10} \frac{I_1}{I_0} \frac{(r_1+2r_2)^2}{r_1^2} .$$

The backscattering coefficient m_{bs} [1] which is related to the back-scattering strength is defined as:

$$BSS = \log_{10} m_{bs} ,$$

$$m_{bs} = m_f + m_\mu + m_v ,$$

where m_f describes the scattering contribution from fine scale components of the bottom roughness,

$$m_f = M(k,\sigma_\mu)F(\delta_f,\theta_i) ,$$

$$M(k,\sigma_\mu) = R_0^{\,2} \exp(-4\sigma_\mu^{\,2} k^2 \cos^2\theta_i) ,$$

$$F(\delta_f,\theta_i) = \frac{1}{8\pi\delta_f^{\,2}\cos^2\theta_i} \exp(-\frac{\tan^2\theta_i}{2\delta_f^{\,2}}),$$

$$R_0 = [\frac{m\cos\theta_i}{(n^2-\sin^2\theta_i)^{1/2}} - 1] / [\frac{m\cos\theta_i}{(n^2-\sin^2\theta_i)^{1/2}} + 1]$$

where $k=\omega/c_1$ is the acoustic wave number, c_1 is the acoustic wave velocity in the sea water, f is the frequency, θ_i is the incident angle for the $i-th$ trace, σ_μ is the rms height of the micro roughness, δ_f is the rms slope of the fine-scale facets, and R_o is the pressure-reflection coefficient of the seabed, $m=\rho_2/\rho_1$ (ρ_1 and ρ_2 are the densities of the water and sediment) and $n=c_1/c_2$ (c_1 and c_2 are the acoustic velocities of the water and sediment). m_μ is the contribution from the micro scale roughness,

$$m_\mu = R_0^{\,2} k^4 \cos^4\theta_i W(\frac{k}{\pi}\sin\theta_i) / \pi^2 ,$$

$$W(\frac{k}{\pi}\sin\theta_i) = a^2(\frac{k}{\pi}\sin\theta_i)^{-2b} ,$$

where a and b are constants. m_v is the contribution from the inhomogeneities within the volume of the sediments,

$$m_v = \frac{160\pi m^2 m_0}{knK_p c_2 \ln 10} \frac{\cos^4(\theta_i-\alpha_f)[1-\frac{\sin^2(\theta_i-\alpha_f)}{n^2}]^{1/2}}{\{m\cos(\theta_i-\alpha_f)+[n^2-\sin^2(\theta_i-\alpha_f)]^{1/2}\}^4}$$

$$\alpha_f = \tan^{-1}\delta_f ,$$

where m_o is the volume scattering coefficient, K_p is the attenuation factor for the compressional waves.

The unknown parameters θ_i, δ_f, σ_μ, a, b and K_p were the model parameters of the inversion for the BSS data.

DATA

Two areas with different surface conditions in Browns Bank were studied. The first area (Site 2) is a broadly smooth and it is covered by very coarse sand and gravel, while the other site (Site 3) has high amplitude bedforms, covered with medium to fine sand. The scattered wave amplitudes at Site 2 can be easy detected for every trace, while some seabed reflections on Site 3 are very weak and difficult to detect. Fig. 1 shows both high and low amplitude examples of scattered waveforms from each site.

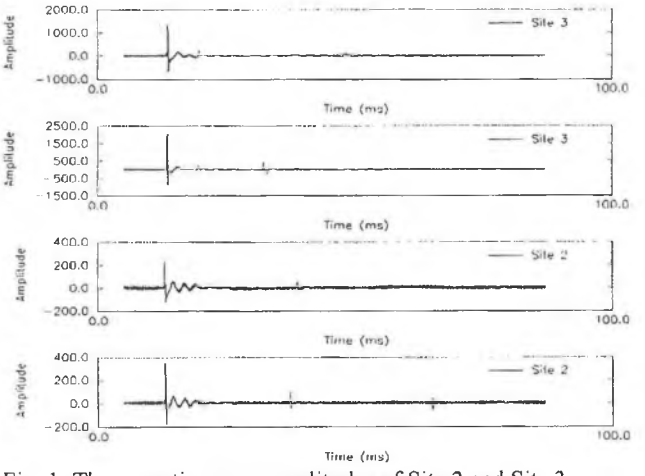

Fig. 1: The acoustic wave amplitudes of Site 2 and Site 3 recorded at the hydrophone

RESULTS AND DISCUSSION

Fig. 2 shows the measured BSS data as a function of frequency. The BSS data of Site 2 concentrate near -30 dB, while the data of Site 3 show a large variation at each frequency.

For the inversion, we used m=2.23, n=0.80 for Site 2 and m=1.45, n=0.90 for Site 3.As the velocity, we chose c_1=1480 m/s, c_2=1850 m/s for Site 2 and c_2=1639 m/s for Site 3. Table 2 lists the inversion results for two sites (file1, file2 for Site 2, and file21, file23 for Site 3). The volume scattering coefficients and the attenuation factors for these four files are similar. The last column in Table 2 describes the data variance of the inversion. In order to illustrate how well the inversion results fit the data, Fig. 3 gives four examples of the comparison between the real data and the theoretical data calculated from the inversion results. These four examples have derived incident angles around 10 degrees. At the same incident angle, the backscattering strength of the two files from Site 2 are significantly stronger than the other files from Site 3.

The inverted incident angles mostly vary between 5 and 20 degrees. There are some angles for Site 3 which are anomalously large. These estimates are likely less accurate due to the relatively higher noise contribution to the recorded signal at lower scattered amplitudes.

Table 2: Inversion results

	δ_f	σ_μ	a	b	mo	K_p*	σ^2_d
file1	1.47°	0.07	0.14	1.02	3.0e-6	0.100	0.02827
file2	1.28°	0.06	0.11	1.10	3.5e-6	0.096	0.02430
file21	1.00°	0.04	0.045	1.32	1.7e-5	0.099	0.01373
file23	1.03°	0.04	0.068	1.40	1.8e-5	0.099	0.03460

* units of dB/m/Hz.

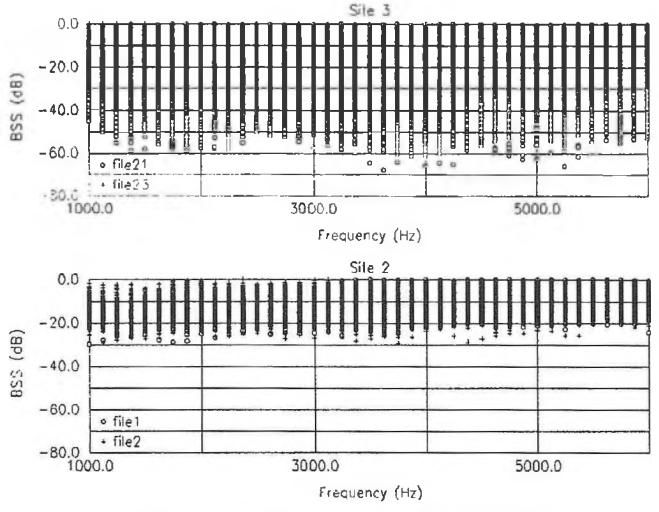

Fig. 2: The BSS results for Site 2 and Site3.

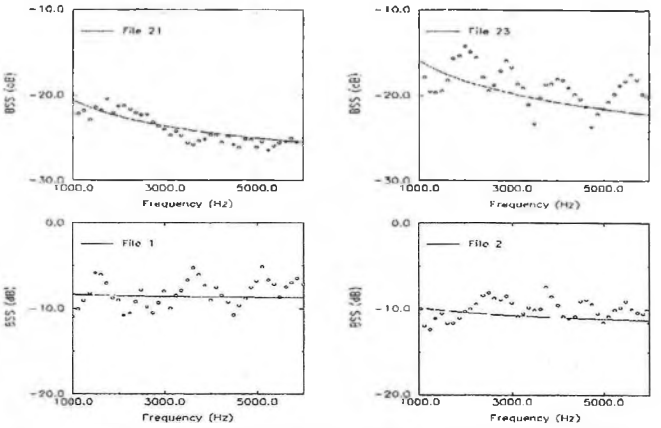

Fig. 3: Comparison between the theoretical values calculated from the inversion results and the measured data.

The apparent seabed bathymetry was calculated by integrating the incident angle information derived from the inversion. Fig. 4 shows examples of the comparison between the calculated seabed bathymetry and the seabed depths measured from the arrival times of the scattered waves. The calculated estimates are close those derived from measured arrival times.

CONCLUSION

The backscattering strength is largely dependent on the gradient of the long-wavelength bathymetry and the in-situ values of the primary geo-acoustic parameters (e.g, velocity and density). Near-normal incidence acoustic parameters (δ_f, σ_μ) and volume scattering coefficient (m_o) have less effect on the scattered signal and show little relative variation for the sites examined in this study.

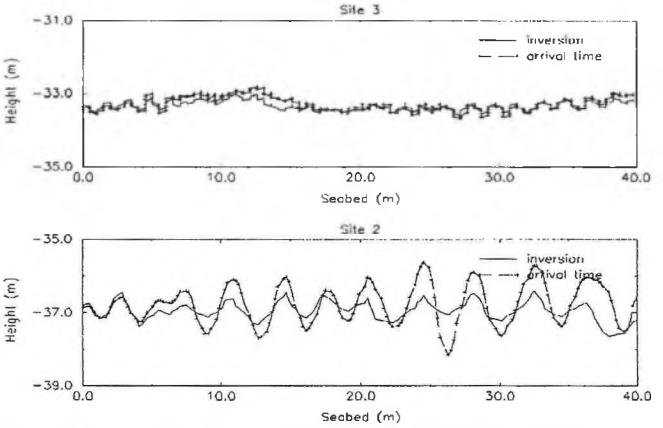

Fig. 4: The simulated seabed shape is similar to the seabed bathymetry estimated by the arrival time of the scattered waves.

REFERENCE

[1] J. C. Novarini and J. W. Caruthers, "A simplified approach to backscattering from a rough seafloor with sediment inhomogeneities," IEEE Vol. 23, pp 157-166 1998.

A Whole Lotta Shakin' Going On: The Peculiar Seismo-Acoustics Of Soft Marine Sediments

David M.F. Chapman (1) and Oleg A. Godin (2)

1) Defence Research Establishment Atlantic, P.O. Box 1012, Dartmouth, N.S., B2Y 3Z7. (dave.chapman@drea.dnd.ca)

2) School of Earth and Ocean Sciences, University of Victoria, P.O. Box 3055, Victoria, B.C., Canada V8W 3P6. (ogodin@uvic.ca)

From both experimental and theoretical investigations, it is evident that soft marine sediments such as mud, clay, and silt have profiles of shear wave speed vs. depth that can be described by a "power-law" relation of the form

$$c_s(z) = c_0 z^{\nu},$$

in which c_s is the shear speed, z is the depth below the seafloor, and c_0 and ν are constant parameters. The parameter c_0 represents the shear speed at unit depth, while ν is a dimensionless parameter in the range $0<\nu<1$. We have determined that seismo-acoustic wave propagation in such profiles exhibits some peculiar features that depend critically on the value of ν.

Power-law profiles are mathematically singular, in the sense that the shear speed goes to zero with infinite slope at zero depth. Conventionally, one models seismo-acoustic wave propagation in a stratified elastic medium by dividing the layer into a stack of homogeneous sub-layers. In this way, physical effects associated with gradients of material properties are approximated by discrete coupling terms at the boundaries between the sub-layers. With an appropriate layering scheme, one expects results obtained with the stacked-layer model to converge to the presumed results of the continuous model as the number of layers is increased. However, for the power-law profile such convergence is glacially slow, owing to the very large gradients near the singularity. We have developed analytical techniques to model seismo-acoustic phenomena in power-law shear speed profiles, avoiding the pitfalls of stacked-layer models, provided that the shear speed is small in comparison with the compressional speed. Mathematically, this corresponds to "low-speed" elastic waves in the limit of infinite compressional speed. One could call these materials "incompressible solids". Some surprisingly simple results emerge, which we can only sketch in this summary paper.

Chapman (1997) and Godin and Chapman (1999) have shown that an ocean bottom seismometer placed on the seabed over a layer of soft sediment with a high-impedance basement will show very large resonances in horizontal displacement. These resonances are excited by the infrasonic ambient noise field in the ocean, the energy having been converted from compressional waves to shear waves at the sediment/basement interface. Naturally, the spacing of the resonances is governed by a referecne frequency that is the inverse of the two-way travel time of shear waves within the sediment; however, the precise location of the fundamental frequency is strongly dependent on the value of the parameter ν, as indicated in Figure 1.

In the same medium, there may exist seismo-acoustic interface waves at the water/sediment boundary. Osler and Chapman (1996) observed these at the same site that displayed the ambient noise resonances, using the same instrument. They modelled the dispersion of these waves (i.e. curves of group speed vs. frequency) using a stacked-layer model, and the resulting shear speed staircase implied a continuous power-law profile with $c_0 = 23$ and $\nu = 0.61$. The new analytic approach allows inversion of these two profile parameters directly from the dispersion data. Moreover, the analytic approach provides the elegant result that both the phase speed and the group speed of interface waves in power-law profiles scale with frequency according to $f^{\nu/(\nu-1)}$. This scaling law is observed not only in our own data but in data of other researchers, as shown in Figure 2. The full details of this last result are being prepared for journal publication.

Chapman, David M.F. (1997), "Shear speed gradients and resonances in ocean seismo-acoustic modelling", Proceedings of the 3rd International Conference on Theoretical and Computational Acosutics, Newark, New Jersey (July, 1997).

Frivik, S.A., *et al.* **(1997)**, 155-162, in *High Frequency Acoustics in Shallow Water*, edited by N.G. Pace *et al.* (NATO SACLANT Undersea Resarch Centre, La Spezia, Italy).

Godin, Oleg A., and Chapman, David M.F. **(1999)**, "Shear speed gradients and ocean seismo-acoustic noise resonances", accepted by J. Acoust. Soc. Am.

Osler, John C., and Chapman, David M.F. **(1996)**, Canadian Acoustics **24**(3), 11–22.

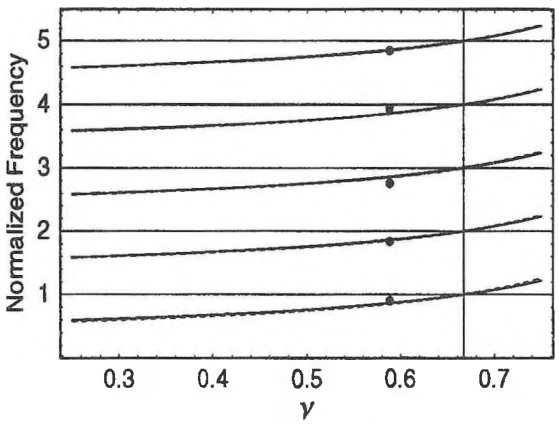

Figure 1. Normalized frequencies of shear resonances in a power-law shear speed profile. Solid circles are experimental measurements from a site off Nova Scotia's Eastern Shore.

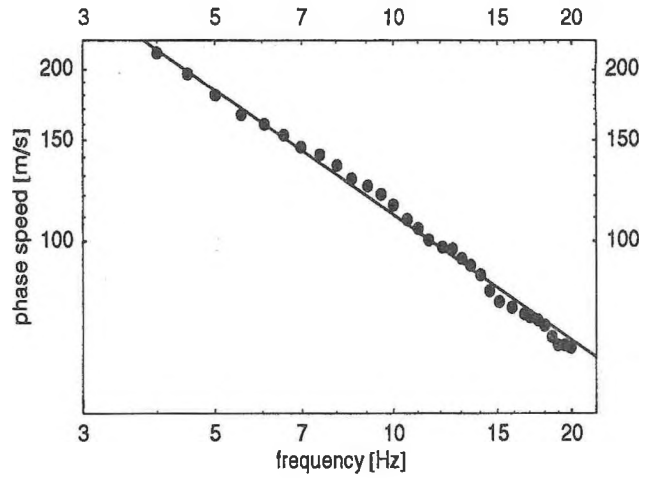

Figure 2. A log-log plot demonstrating the frequency scaling of interface wave phase speed in a power-law profile with $c_0 = 79$ and $\nu = 0.42$. (after Frivik *et al.* 1997).

Inversions for Geoacoustic and Geometric Parameters Using a Full-wave, Range-dependent Forward Modeling Technique

J. Viechnicki and N. R. Chapman
School of Earth and Ocean Sciences, University of Victoria, Victoria BC V8W 3P6

Inversion of acoustic field data using a range-dependent, full-wave forward modeling technique and matched-field processing (MFP) is considered. Data examined were collected as part of the Matched Field (MF) tomography component of the Haro Strait PRIMER Experiment of June/July 1996[1]. Solutions to a discrete forward model parameter vector, $\mathbf{m} = m_j$ for $j = 1..., M$, are sought where each element of $\mathbf{m}$ is bounded and is either a geoacoustic or a geometric parameter. Assuming a bottom consisting of two homogeneous layers, parameters of interest are source depth, sediment compressional sound speed, sediment density, basement compressional sound speed, and basement density. Multiple iterations of the forward model seek to minimize the discrepancy between discrete sampling of synthetic, $q(\mathbf{m}, t)$, and measured, $p(t+\tau)$, waveforms through an objective function, $E(\mathbf{m})$ where

$$E(\mathbf{m}) = 1 - \frac{\sum_{i=1}^{N} max_{\tau_i} \int q_i(\mathbf{m}, t) p_i(t+\tau_i) dt}{\left(\sum_{i=1}^{N} \int q_i^2(\mathbf{m}, t) dt\right)^{1/2} \left(\sum_{i=1}^{N} \int p_i^2(t) dt\right)^{1/2}}.$$

With absolute travel time being difficult to measure, relative, discrete time histories of s and q are compared by finding the offset, τ, which gives the smallest E. The use of broadband, range-dependent forward models has long been considered computationally inefficient in inversion methods where thousands of runs must be done to accurately sample the parameter space.

Two trends have expedited this process to the point where inversions can be accomplished for $j \sim 5 - 10$ in a reasonable amount of time. Synthetic waveforms are constructed using broadband split-step (FFT) parabolic equation runs and the c_o insensitive propagator which gives full second-order accuracy [4,5]. These simulations are computationally intensive as the sampling in depth and range must be fine enough to account for wide-angle propagation and the number of individual frequency runs must be large enough to accurately match the experimental source shape. Advancements in computer processing speed and memory size are rapidly occuring. For example, two thousand forward simulations in the Haro Strait environment takes two to three days on a 128 Mhz processor but can now be done overnight on a 512 Mhz processor. The second improvement involves the efficiency of inversion techniques. The latest hybrid inversion techniques combining global and local inversion techniques dramatically reduce computation time[3]. The simplex simulated annealing method of Fallat and Dosso[3] is used in this study.

The use of full-wave, range-dependent modeling is examined for two reasons. First, inverting real data to converge on a unique solution for $\mathbf{m}$ is inherently difficult due to noise, receiver array location uncertainty, and model simplifications in approximating the natural environment. The more data used during the inversion, the more accurate the estimation of $\mathbf{m}$. Therefore, we examine broadband MFP where simulations are done for many frequencies and the simulated wavefield is matched to the entire receiver array domain in relative travel time and depth. Comparisons are made to previous studies such as Chapman et. al. [2] for evidence of a decrease in ambiguity manifested by a reduction in the number of local minima in $E(\mathbf{m})$ and a decrease in sensitivity to correlation between parameters. Second, full-wave, range-dependent modeling allows for inversion studies in more complex environments where bathymetry or range-dependent water sound speed structure are observed. The complex bathymetry of the Haro Strait environment conducted just off of Stuart Island in Washington State is ideal. The MF tomography component of the experiment involved a grid network of light bulb sources with center frequency of 600 Hz and an overlapping grid network of vertical arrays such that each transmission was roughly 0.5 to 3.0 km.

REFERENCES

[1] Chapman, N.R., M.A. McDonald and L. Jaschke,"Haro Strait Experiment 1996-Low frequency tomography experiment: 17-21 June '96. Cruise Repor", University of Victoria (1996).

[2] Chapman, N.R., L. Jaschke, M.A. McDonald, H. Schmic and M. Johnson (1998) "Matched field geoacoustic tomography experiments using light bulb sound sources in the Haro Strait Sea Trial," *J. Acoust. Soc. Am.* **77**, 1248-1249.

[3] Fallat, M.R. and S.E. Dosso (1999) "Geoacoustic inversions via local, global and hybrid algorithms," *J. Acoust. Soc. Am.* **105**, 3219-3230.

[4] Tappert, F.D., J.L. Spiesberger and L. Boden (1995) "New full-wave approximation for ocean acoustic travel time predictions," *J. Acoust. Soc. Am.* **97**, 2771-2782.

[5] Tappert, F.D. and M.G. Brown (1996) "Asymptotic phase errors in parabolic approximations to the one-way Helmholtz equation," *J. Acoust. Soc. Am.* **99**, 1405-1413.

GEOACOUSTIC INVERSION OF MEDITERRANEAN SEA DATA

Mark Fallat (1) and Stan Dosso (2)
1) Macdonald Dettwiler and Associates, Richmond BC
2) School of Earth and Ocean Sciences, University of Victoria, Victoria, B.C., CANADA

BACKGROUND

Determining seabed geoacoustic properties from measured ocean acoustic fields is a challenging nonlinear inverse problem with no direct solution. Typically, global search methods, such as simulated annealing and genetic algorithms, have been applied to provide a practical solution. Recently, a hybrid inversion algorithm which combines the local (gradient-based) downhill simplex method with simulated annealing has been developed and shown to be more effective than global searches alone [1, 2]. In this paper, the hybrid inversion, referred to as simplex simulated annealing (SSA) is applied to invert measured acoustic fields [3] for geoacoustic properties at at a site off the west coast of Italy where previous acoustic and geophysical studies have been performed [4, 5].

EXPERIMENT AND INVERSION

Figure 1 shows the location of the acoustic experiment, referred to as PROSIM'97. Acoustic fields were recorded on a 48-sensor vertical line array (VLA) due to a swept-frequency source (300–850 Hz) towed at a nominal depth of 12 m over a series of tracks. In this paper, data recorded while the source was towed over a 10-km section of relatively constant water depth is analyzed (Fig. 1). Environmental parameters such as ocean sound speed and current velocity were recorded throughout the experiment; however, the precise bathymetry along the source track was poorly constrained due to experimental difficulties.

Based on the known geology, the seabed was modelled as a sediment layer overlying a semi-infinite basement with parameters consisting of the sediment thickness h, sediment and basement sound speeds c_s and c_b, source range and depth r and z, array tilt ψ, and water depth at source and receiver D_1 and D_2. The geoacoustic parameters were estimated using matched-field inversion which determines the set of model-parameter values that minimizes the mismatch between the measured acoustic fields and modeled replica fields computed using a numerical propagation model. The measure of the mismatch used here is based on the (normalized) Bartlett correlator for a broad-band signal:

$$E(\mathbf{m}) = 1 - \frac{1}{F}\sum_{i=1}^{F}\frac{|\mathbf{p}(f_i)\cdot\mathbf{p}^*(\mathbf{m},f_i)|^2}{|\mathbf{p}(f_i)|^2\,|\mathbf{p}(\mathbf{m},f_i)|^2}, \qquad (1)$$

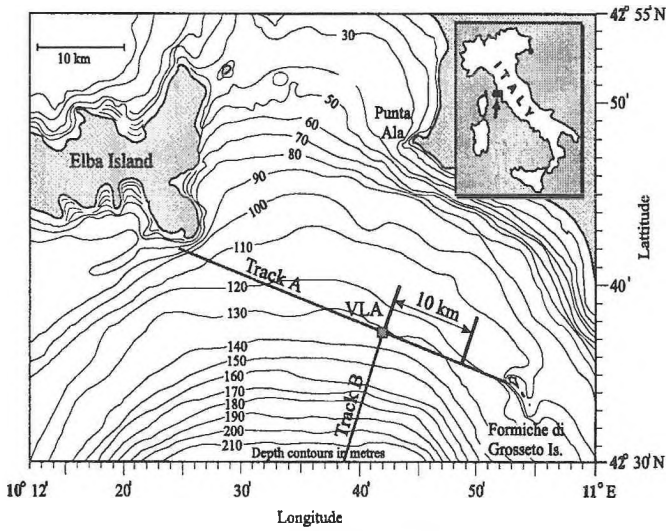

Fig. 1 Experiment site and ship tracks.

where $\mathbf{p}(f_i)$ is a vector of acoustic pressures measured at the VLA at a frequency f_i, $\mathbf{p}(\mathbf{m},f_i)$ is a vector of replica pressures computed for a model $\mathbf{m}$, and F is the number of frequencies. With the normalization applied in Eq. (1), the mismatch has a value $E \in [0, 1]$, with zero indicating a perfect match. The replica acoustic fields were generated using an adiabatic normal-mode acoustic propagation model known as PROSIM. The mismatch was minimized using SSA, a hybrid inversion algorithm that incorporates the local downhill simplex method into a fast simulated annealing global search [1, 2].

Acoustic data for 17 ranges from 0.7–10 km along the source track were selected for inversion. The goal of inverting data from multiple ranges was not to determine a range-dependent geoacoustic model, but rather to consider a large enough number of independent measurements to provide an indication of the consistency of the inversion results for the various model parameters. Several independent SSA inversions were carried out for the acoustic data at each range, for a total of 52 inversions (each inversion required approximately 3 hours on a 500-MHz DEC Alpha workstation). Figure 2 shows the model parameters determined in all inversions plotted as a function of the source longitude, with the inversion results that produced the lowest mismatch at each range connected by a solid line.

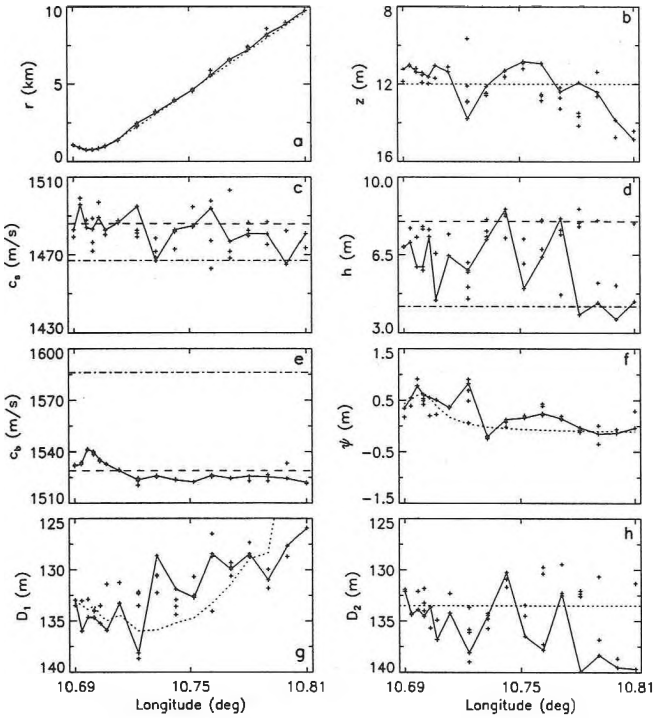

Fig. 2 SSA inversion results as a function of source longitude. Crosses represent all results, with solid lines connecting the lowest mismatch results. Dotted lines represent independent estimates (when available); dashed and dash-dotted lines represent results from Refs. [4] and [5].

The SSA inversion results for the source range r are shown in Fig. 2(a), with the dotted line representing the nominal range calculated using differential GPS measurements. The lowest-mismatch results closely track the nominal range, and the variation between inversion results at each range is small. Figure 2(b) shows the inversion results for the source depth z. The dotted line at 12 m indicates the nominal source depth. With a small number of exceptions, the inversion results are within approximately 1 m of the nominal depth, and exhibit a moderate amount of variation.

Figure 2(c)–(e) show the results for the seabed properties (sediment sound speed c_s, sediment thickness h, and basement sound speed c_b) compared to the results obtained in previous studies of the same region [4, 5]. The results for c_s generally fall between the previous results, and exhibit a moderate amount of variation from inversion to inversion. The results for h also fall between the two previous results, but with a relatively large variation. The results for c_b are in excellent agreement with the results of [4], and are highly consistent from inversion to inversion.

Figure 2(f) shows the inversion results for the array tilt ψ. The dotted line represents the estimated (relative) tilt, calculated by projecting the measured current vector onto the radial vector between the source and VLA. With the exception of a few points, the inversion results are highly consistent and are in excellent agreement with the estimated tilt.

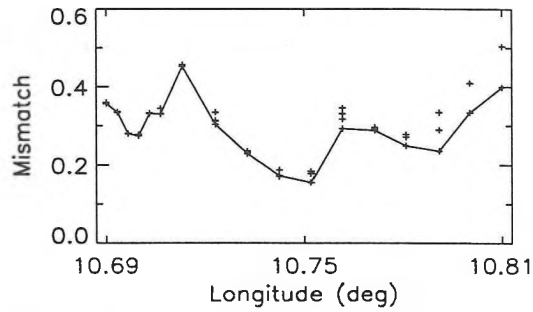

Fig. 3 Mismatches for inversion results shown in Fig. 2.

Figure 2(g) and (h) shows the inversion results for the water depth at the source and receiver D_1 and D_2, with the dotted lines representing the measured water depths. The general features of the inversion results for D_1 are in reasonably good agreement with the measured bathymetry. The inversion results for D_2 are in reasonable agreement for the first 8–10 points, but are in poorer agreement beyond. The results for both water depths D_1 and D_2 show a substantial amount of variation from inversion to inversion.

The relatively large amount of variation in the results for the sediment thickness and water depths is likely due to inter-parameter correlations that arise because the low-speed sediment layer appears similar acoustically to the water column (sound speed 1510 m/s). Correlated parameters cause difficulty in reliably estimating individual parameter values, as different parameter combinations produce very similar (low) mismatch values. The mismatches obtained by the SSA inversions of Fig. 2 ranged from 0.15–0.5, and are shown in Fig. 3.

REFERENCES

[1] M. R. Fallat, 1999. Simplex simulated annealing, a hybrid approach to geoacoustic inversion with application to Mediterranean Sea acoustic data, *M.Sc. thesis*, University of Victoria, Victoria, B.C., Canada.

[2] M. R. Fallat and S. E. Dosso, 1999. Geoacoustic inversion via local, global and hybrid algorithms, J. Acoust. Soc. Am. **105**, 3219–3230.

[3] P. L. Nielsen, F. Bini-Verona, and F. B. Jensen, 1999. Environmental and acoustic data collected south of the island of Elba during the PROSIM'97 experiment, Report SM-357, SACLANT Undersea Research Centre, La Spezia, Italy.

[4] J.-P. Hermand and P. Gerstoft, 1996. "Inversion of broad-band multitone acoustic data from the YELLOW SHARK summer experiments," IEEE J. Oceanic Eng. **21**, 324–346.

[5] M. Siderius and J.-P. Hermand, 1999. Yellow Shark Spring 95: Inversion results from sparse broad-band acoustic measurements over a highly range dependent soft clay layer, IEEE J. Oceanic Eng. In Press.

PROBABILITY DISTRIBUTIONS FOR GEOACOUSTIC INVERSION

Stan Dosso
School of Earth and Ocean Sciences, Univ. of Victoria, P.O. Box 3055, Victoria, B.C., CANADA V8W 3Y2

BACKGROUND

Determining seabed geoacoustic properties from ocean acoustic fields represents a strongly nonlinear inverse problem with no direct solution. Global inversion methods, such as simulated annealing (SA) and genetic algorithms (GA), provide a practical approach based on searching the multi-dimensional parameter space for the geoacoustic model that minimizes the mismatch between measured and modelled fields [1–3]. However, these approaches provide only the best-fit solution, with no indication of the range of acceptable model parameters. Recently, GA have been used as an importance sampling technique to estimate properties of the *posteriori* probability distribution (PPD) for the geoacoustic inverse problem [4]. However, the sampling distribution of GA is unknown, and hence the PPDs constructed in this manner can suffer from both unknown errors and biases.

An alternative approach, based on SA at a fixed temperature (i.e., sampling rather than minimizing), samples directly from the PPD [5]. This procedure, known as the Metropolis Algorithm (MA) in statistical mechanics, can be used to construct an accurate and unbiased PPD, which can then be displayed in terms of marginal distributions for individual parameters. This procedure is described and illustrated here for geoacoustic inversion.

THEORY

Both SA inversion and the procedure described here for constructing PPDs for inverse problems are based on an analogy with statistical mechanics. In statistical mechanics, the probability P of a system $\mathbf{m}$ being in an energy state $E(\mathbf{m})$ is given by the Boltzmann distribution

$$P(\mathbf{m}) = \frac{\exp\left[-E(\mathbf{m})/T\right]}{\sum_{\mathbf{m}} \exp\left[-E(\mathbf{m})/T\right]}, \tag{1}$$

where T is the absolute temperature. In the early days of scientific computing, Metropolis *et al.* devised a simple numerical procedure to simulate $P(\mathbf{m})$. The MA consists of applying random perturbations to the system (or model) $\mathbf{m}$, and accepting these perturbations if

$$\xi \leq \exp[-\Delta E/T], \tag{2}$$

where ξ is a random number drawn from a uniform probability distribution on [0, 1]. It can be proved that this procedure converges asymptotically, i.e., in the limit of a large number of perturbations, the MA samples accurately and without bias from the Boltzmann distribution [5]. The evolution of the system to its global-minimum energy configuration can be simulated by applying the MA while slowly reducing the temperature T to collapse $P(\mathbf{m})$ about its groundstate.

To apply these concepts to data inversion and appraisal, consider a data set $\mathbf{d}$ with the error on each datum consisting of an independent, zero-mean, Gaussian-distributed random variable with standard deviation σ, and assume that the *a priori* information regarding the model $P(\mathbf{m})$ consists of a uniform distribution between known upper and lower limits. The model PPD is given by Bayes theorem which, for the above assumptions, can be written

$$\begin{aligned} P(\mathbf{m}|\mathbf{d}) &= P(\mathbf{d}|\mathbf{m})\, P(\mathbf{m})/P(\mathbf{d}) \\ &= \frac{\exp\left[-E(\mathbf{m})\right]}{\int_{\mathbf{m}} \exp\left[-E(\mathbf{m})\right] d\mathbf{m}}, \end{aligned} \tag{3}$$

where

$$E(\mathbf{m}) = [\mathbf{d} - \mathbf{d}(\mathbf{m})]^T\, \mathbf{C}_\mathbf{D}^{-1}\, [\mathbf{d} - \mathbf{d}(\mathbf{m})]. \tag{4}$$

In (4), $\mathbf{C_D} = \langle \mathbf{n}\mathbf{n}^T \rangle$ represents the data covariance matrix containing all sources of uncertainty, and $\mathbf{d}(\mathbf{m})$ represents the replica data computed for model $\mathbf{m}$. Noting the similarity between eqs (3) and (1), two approaches to the inverse problem are available: (i) Maximize $P(\mathbf{m}|\mathbf{d})$ by minimizing $E(\mathbf{m})$ using the MA while slowly reducing T. This defines the method of SA, and yields the maximum-likelihood solution. (ii) Construct $P(\mathbf{m}|\mathbf{d})$ by applying the MA at a fixed temperature $T = 1$. This approach yields the full PPD for the model.

Typically, for acoustic matched-field inversion, the amplitude and absolute phase of the acoustic source are not known, i.e., we must treat

$$\mathbf{d}(\mathbf{m}) = A e^{i\theta}\, \mathbf{w}(\mathbf{m}) \tag{5}$$

where $\mathbf{w}(\mathbf{m})$ represents the modelled acoustic field and A and θ represent the unknown amplitude and phase. For $\mathbf{C_D} = \sigma \mathbf{I}$, the source characteristics can be removed by optimizing $E(\mathbf{m})$ over $Ae^{i\theta}$ to obtain [4]

$$E(\mathbf{m}) = [1 - B(\mathbf{m})]\, |\mathbf{d}|^2/\sigma, \tag{6}$$

where B is the normalized Bartlett processor

$$B(\mathbf{m}) = \frac{|\mathbf{d}^* \cdot \mathbf{w}(\mathbf{m})|^2}{|\mathbf{d}|^2\, |\mathbf{w}(\mathbf{m})|^2}. \tag{7}$$

Ideally, an independent estimate of the data error σ is available; however, if σ is unknown, optimizing over σ leads to the following maximum likelihood solutions [4]

$$\hat{\mathbf{m}} = \arg \min_{\mathbf{m}} [1 - B(\mathbf{m})], \tag{8}$$

$$\hat{\sigma} = |\mathbf{d}|^2[1 - B(\hat{\mathbf{m}})]/N, \tag{9}$$

and the model PPD is given by

$$P(\mathbf{m}|\mathbf{d}) \propto \exp\{[1 - B(\mathbf{m})]\,|\mathbf{d}|^2/\hat{\sigma}\}. \tag{10}$$

To apply the above procedure, the maximum-likelihood solution $\hat{\mathbf{m}}$ is computed according to (8) using an optimization scheme such as SA, $\hat{\mathbf{m}}$ is then used to define $\hat{\sigma}$ according to (9), and finally the MA is applied to construct the model PPD by sampling (10), i.e., by sampling an energy function

$$E(\mathbf{m}) = [1 - B(\mathbf{m})]\,|\mathbf{d}|^2/\hat{\sigma} \tag{11}$$

at temperature $T = 1$. An efficient method to achieve equilibrium for the MA is to start at high T, cool rapidly to $T = 1$, and then accumulate results for a large number of iterations. The efficiency can be further improved by reducing the perturbation sizes during cooling in a manner that reflects the various parameter sensitivities (this reduces the number of perturbations rejected during sampling). We have developed an efficient scheme based on using a perturbation size of 10× the running average of the last 30 accepted perturbations to scale Cauchy perturbation distributions for each parameter.

EXAMPLE

To illustrate the calculation of PPD for geoacoustic inversion, this section considers data collected by the SACLANT Undersea Research Centre in the Mediterranean Sea off the west coast of Italy [6]. Acoustic fields were recorded on a 48-sensor vertical array due to a swept-frequency source (300–850 Hz) towed over a track with nearly constant bathymetry (average water depth approximately 135 m). Based on known geology of the region, the geoacoustic model is taken to consist of the sediment thickness h, sediment and basement sound speeds c_s and c_b, source range and depth r and z, water depth at the source and array D_1 and D_2, and array tilt T (measured as a horizontal displacement of the top hydrophone). A hybrid inversion algorithm that combines SA with the local downhill simplex method [7] was applied to determine the parameter values that minimize the Bartlett mismatch with the measured acoustic fields for a frequency range of 300–400 Hz. Independent inversions were carried out for six source ranges from 2 to 7 km to examine the variability of the results. Given that the environmental parameters are expected to remain relatively constant with range, this variation should provide a rough indication of the relative parameter uncertainties. The model PPD was computed using the MA with unknown σ, as described above, for the acoustic data recorded for a source range of 4 km.

The results of the inversion and appraisal are shown in Fig. 1. The marginal PPDs in Fig. 1 show considerable variation in the relative uncertainty of the various parameters. For instance, the basement sound speed c_b is determined with much less uncertainty (narrower marginal distribution) that the sediment sound speed c_s. The results of the six independent inversions (crosses)

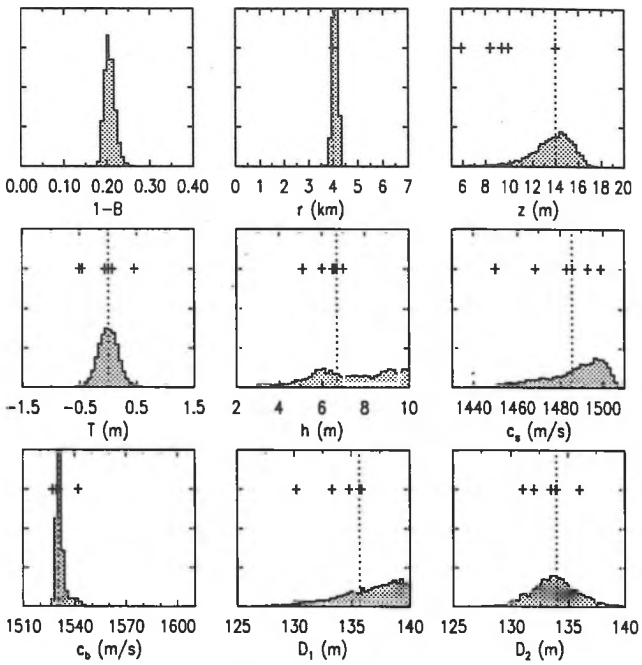

Fig. 1 Marginal PPDs for mismatch and geoacoustic model parameters for the source at 4-km range. Crosses indicate the parameter values determined for data collected at all six ranges; dotted lines indicate values determined for the 4-km source. For the geoacoustic parameters, the range of ordinate values indicates the parameter search interval.

support this, with a much greater variation between the inversion results for c_s than for c_p.

REFERENCES

[1] M. D. Collins, W. A. Kuperman & H. Schmidt, 1992. Nonlinear inversion for ocean-bottom properties, J. Acoust. Soc. Am. **92**, 2770–2783.

[2] S. E. Dosso, M. L. Yeremey, J. M. Ozard & N. R. Chapman, 1993. Estimation of ocean-bottom properties by matched-field inversion of acoustic field data, IEEE J. Oceanic Eng. **18**, 232–239.

[3] P. Gerstoft, 1995. Inversion of acoustic data using a combination of genetic algorithms and the Gauss-Newton approach, J. Acoust. Soc. Am. **97**, 2181-2190.

[4] P. Gerstoft & C. F. Mecklenbrauker 1998. Ocean acoustic inversion with estimation of *a posteriori* probability distribution, J. Acoust. Soc. Am. **104**, 808–819.

[5] M. K. Sen & P. L. Stoffa, 1996. Bayesian inference, Gibbs' sampler and uncertainty estimation in geophysical inversion, Geophys. Prosp. **44**, 313–350.

[6] M. R. Fallat, P. L. Nielson & S. E. Dosso, 1999. Hybrid geoacoustic inversion of broadband Mediterranean Sea data, Submitted: J. Acoust. Soc. Am.

[7] M. R. Fallat & S. E. Dosso, 1999. Geoacoustic inversion via local, global and hybrid algorithms, J. Acoust. Soc. Am. **105**, 3219–3230.

Measuring The In-Situ Airborne Sound Insulation Using The Acoustic Intensity Technique

T.R.T. Nightingale and R.E. Halliwell
Institute for Research in Construction, National Research Council, Ottawa, Ontario, Canada K1A OR6

INTRODUCTION

Currently, the ASTM and ISO standards organizations are writing standards to facilitate the measurement of airborne sound insulation using the acoustic intensity technique. Working groups in both organizations have nearly completed prescriptions for applying the technique under laboratory conditions where there is suppressed flanking transmission. Both standards organizations are now writing parts that describe methods for making in-situ measurements to allow the assessment of individual building elements in the field.

This paper will compare estimates of the in-situ transmission loss (TL) of an individual building element measured using the acoustic intensity technique and traditional two-room method (ASTM E336). These comparisons are used to show that the accuracy of TL measurements using the intensity technique are very sensitive to the presence of flanking transmission and reverberant energy in the receive room. In some cases it may be necessary to add absorption and shield flanking surfaces in the receive room in order to obtain reasonable TL estimates. This paper also shows that quality control indicators should be used to help assess the suitability of measurement conditions in the receive room.

MEASUREMENT TECHNIQUE

The TL of a building element is defined as the ratio of the incident sound power on the element in the source room to the radiated sound power in the receive room. An estimate of the sound power radiated by a building element is obtained by measuring the acoustic intensity over a measurement surface that completely encloses it. The intensity may be sampled using either a series of discrete points or a scanning action. The radiated sound power is simply the intensity multiplied by the area of measurement surface. If the sound power radiated by each surface in the receive room is measured then it is possible to determine the dominant transmission paths as well as rank the individual flanking paths.

The most common intensity probe (P-P type) uses two phase-matched microphones that are closely spaced to measure both the particle velocity and the acoustic pressure. The product of these two quantities is a vector: the acoustic intensity. The measured acoustic intensity is the resultant vector parallel to pick-up axis of the probe (i.e., the sum of the intensity flowing toward the probe minus the intensity flowing in the opposite direction).

It is widely assumed that, since the probe measures a vector, the probe's directional characteristic is sufficient to discriminate against adjacent radiating surfaces. This has lead to the misconception that accurate estimates of the TL for individual building elements can be obtained without special treatment(s) to the receive room. Often, this is not the case, especially for lightweight constructions. Significant difficulties can be encountered when measuring the intensity of a building element that is physically connected at right angles to another building element that is also radiating. An example is shown in Figure 1 where the continuous subfloor represents a flanking surface that is connected to the element under test; the partition wall.

Since, the partition wall is bounded on all four sides by reasonably rigid surfaces (ceiling, floor, and two walls) the measurement surface would be a single planar surface. Typically, located about 150 mm from the partition wall as shown in Figure 1.

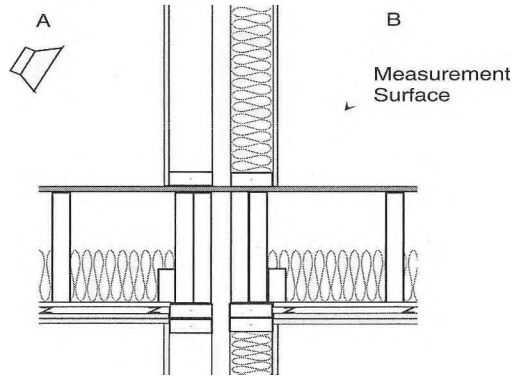

Figure 1: Sketch showing the construction and the partition wall that was measured. Note the location of the measurement surface and the portion of the floor that is contained in the measurement volume. The measurement volume is the space defined by the specimen under test, the measurement surface and all bounding surfaces.

MEASUREMENT PRECISION

In this section the accuracy with which the intensity technique can reproduce the TL of the two-room technique (ASTM E336) is examined. From Figure 2, it is evident that treatments to the receive room (absorption and shielding of flanking surfaces) can significantly affect the TL estimate given by the intensity technique. These treatments are now discussed.

In general, flanking transmission will tend to increase the amount of reverberant energy in the receive room which is very undesirable. Depending on the amount of absorption in the receive room and the severity of the flanking transmission, it is possible that there can be more energy flowing toward the specimen under test than there is radiated by it, (i.e., flowing away from it). This situation typically results in the measurement of a negative intensity or greatly reduced positive intensity (where the sign indicates the direction of the intensity vector). Figure 2 shows this well, since the TL estimate for the partition wall measured with the floor exposed and no absorption is considerably greater than that obtained using ASTM E336. The TL can not be computed at frequencies at which the intensity is negative. This explains the missing data points in the figure.

Absorption can be placed in the receive room to reduce the amount of reverberant energy. Figure 2 shows that with the floor exposed and absorption (25m2 of 25 mm thick open cell foam) added to the receive room the estimate of the TL changes radically. It changes from being a significant overestimation at most frequencies to being a significant underestimation. This change indicates the absorption effectively controlled the reverberant field, resulting in a more accurate estimate of the intensity flowing across the measurement surface.

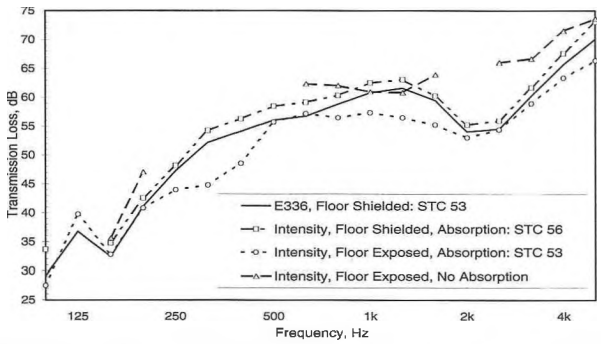

Figure 2: Measured in-situ transmission loss of the partition wall of Figure 1 using the intensity method and ASTM E336. (Measurements using ASTM E336 were conducted with the floor of the receive room shielded and other flanking paths suppressed). Data are not shown at frequencies where the acoustic intensity was negative, i.e., sound power was flowing into the wall.

Despite this apparent improvement in accuracy of the sound power estimate with the floor unshielded, the agreement between the TL reported by the two methods remains poor. The intensity technique significantly underestimates the TL at many frequencies. This underestimation can be explained by recognizing that a portion of the floor is contained in the volume formed by the measurement surface. Thus, the sound power measured by the probe will be the sum of two contributions: one from the wall and the other from the portion of the floor contained in the measurement volume. This leads to an overestimation of the sound power of the wall and an underestimation its TL. Thus, an accurate estimation of the sound power radiated by a building element can only be obtained if it is the only radiating surface contained in the measurement volume. For the situation shown in Figure 1, the portion of the floor contained inside the measurement volume must be shielded. Shielding in the form of 13-mm thick gypsum board over 50-mm fibrous material works very well.

With the floor shielded and absorption, the TL estimate obtained using the intensity technique approaches the TL measured using ASTM E336. The agreement is reasonable over most of the frequency range although there is a consistent overestimation.

QUALITY CONTROL INDICATORS

Draft standards produced by both organizations include indicators to help the operator judge the quality, and hence accuracy, of the TL estimates. These indicators will be briefly discussed and results presented for the cases with shielding and absorption and no shielding and no absorption. The first indicator, FpI, assess the amount of reverberant energy in the receive room. Reverberant energy should not be a problem if,

$$(F_{pI} = L_p - L_I) < 10\ dB \qquad (1)$$

where L_p and L_I are the average measured pressure and intensity over the measurement surface. The second indicator ensures that the measuring system (probe and analyzer) has sufficient dynamic capability for the receive room conditions. It requires that,

$$\delta pIo - Fpl > 10\ dB \qquad (2)$$

where δ_{pIo} is the pressure-residual intensity index. δ_{pIo} is defined as the difference between the measured pressure and intensity when the probe is placed a sound field that has zero intensity. If the intensity was sampled at discrete points, then a third indicator, CF_4, can be used to determine if a sufficient number of sample points were used to attain a prescribed degree of accuracy,

$$CF_4 < N \qquad (3)$$

where N is the number of measurement points used. A thorough definition of CF_4, and degree of accuracy implied when equation 3 is satisfied, is beyond the scope of this paper. The reader is referred elsewhere[1] .

From Figure 3 it is evident that with no shielding and no masking the receive room conditions are very unsuitable. The F_{pI} indicator is much greater than 10 dB suggesting that the field is excessively reverberant, so much so that the measurement system has insufficient dynamic capability (i.e., δ_{pIo}-F_{pI}<<10 dB) Finally, the CF_4 indicator shows that many more points were required than the 132 that were used. All indicators suggest the measurement should be discarded and the receive room treated.

With the floor shielded and absorption added to the receive room the quality control indicators improve significantly. From the change in F_{pI} it is easy to see the improvement due to the absorption. Ideally, F_{pI} would be near zero which would occur in a perfectly anechoic environment. More low frequency absorption should be added since the criterion is not satisfied in the 100 and 125 Hz one-third octave bands.

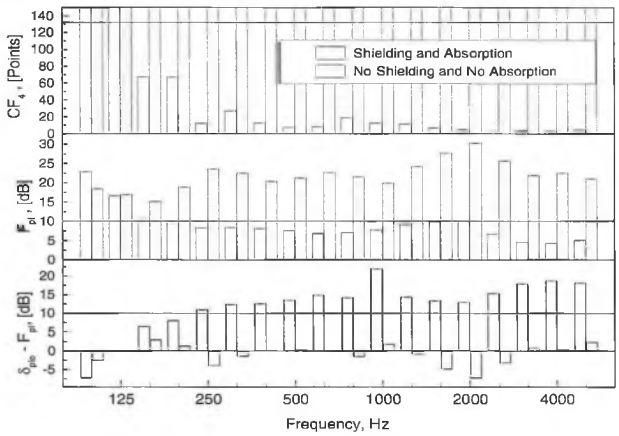

Figure 3: Measured indicators for the cases with no shielding and no absorption and shielding and absorption. The solid lines are the pass-fail points for the three criteria (equations 1, 2, 3).

Conclusions

Flanking transmission, which is inevitable for in-situ measurements, will adversely affect the accuracy of the TL estimate. Significant amounts of absorption may have to be placed in the receive room to control the resulting reverberant field. Flanking surfaces must not be contained inside the measurement volume as this typically results in an underestimation of the TL. In many cases it may be necessary to shield the flanking surfaces. Quality control indicators can be used to determine when poor receive room conditions (excessive reverberation, insufficient dynamic capability, and insufficient measurement points) will affect the estimate of the TL.

References

ISO 9614-1, "Acoustics - Determination of sound power levels using noise sources using sound intensity," Part 1: Measurement by discrete points, 1996.

Preliminary Results Of A Systematic Study Of Sound Transmission Through A Cavity Wall Assembly

T.R.T. Nightingale and J. D. Quirt
Institute for Research in Construction, National Research Council, Ottawa, Ontario, Canada K1A OR6

INTRODUCTION

This paper examines trends from a parametric study that examined the transmission loss (TL) of simple cavity walls without framing. This paper is restricted to examining the effect associated with doubling the depth of a simple wall constructed from two sheets of 3 mm thick LEXAN (1.2 x 2.4 m, density 1183 kg/m^3, and modulus of elasticity 4.8x10^9 Pa). The LEXAN wall specimen was placed in a filler wall that had a very much greater TL so no correction to the measured data was necessary. Fibrous material, when installed, was placed vertically (i.e., parallel to the LEXAN leaves) and was supported by thin wires to prevent the material from touching the leaves. The LEXAN was supported only at the perimeter; there was no framing interior to the cavity. Measured trends are compared to predictions from a lumped-impedance (T-Matrix) model to provide insight into the transmission mechanism(s).

Simple cavity walls like the one described above can be modelled using the T-Matrix method if each element (LEXAN sheets, and the cavity) can be considered to be semi-infinite. LEXAN sheets and the cavity approximate these conditions reasonably well, since the cavity perimeter is hard and reflective and the LEXAN has a very high critical frequency.

Lumped impedance models show that the TL of a cavity wall will exhibit different trends in three frequency regions: below the mass-spring-mass (MSM) resonance, between the MSM resonance and the first cavity cross-mode, and above first cross-mode.
The MSM resonance is caused by the air in the cavity coupling the wall leaves. The air acts like a spring and the resonance frequency, F_{MSM}, is given by,

$$F_{MSM} = \frac{1}{2\pi}\left[\left(\frac{\rho c_c^2}{d}\right)\left(\frac{\rho s_1 + \rho s_2}{\rho s_1 \rho s_2}\right)\right]^{\frac{1}{2}} \qquad (1)$$

where ρ is the density of air, C_c is the speed of sound in the cavity, d is the cavity depth and ρs is the surface density of the leaf indicated by the subscript. The frequency of the first cross-mode is given when n=1 by,

$$F_{CM} = \frac{n\,c}{2d\,\cos(\theta)} \qquad (2)$$

where θ is the angle of incidence.

The formulation of the T-Matrix model for a cavity wall has already been given[2] and will not be repeated here. Recently, it has been shown that accuracy of T-Matrix predictions can be greatly improved if a Gaussian weighting function[3] is used when computing the angular average TL. This was incorporated in this work.

EMPTY CAVITY RESULTS

Figure 1 shows the measured TL for the wall with an empty cavity of varying depth. Shown for comparison are the data for a single sheet of LEXAN. From the figure is easy to see the detrimental effect of the MSM resonance. The 25-mm cavity shows this very well, since the TL is higher for the single sheet in the frequency range 250 Hz to 1000 Hz than for two sheets spaced by 25 mm. Increasing the air space reduces the MSM frequency and shifts the frequency at which the single sheet out-performs the cavity wall to lower frequencies. It is for this reason that separating impermeable materials in walls or floors by a small air space should be avoided, where possible.

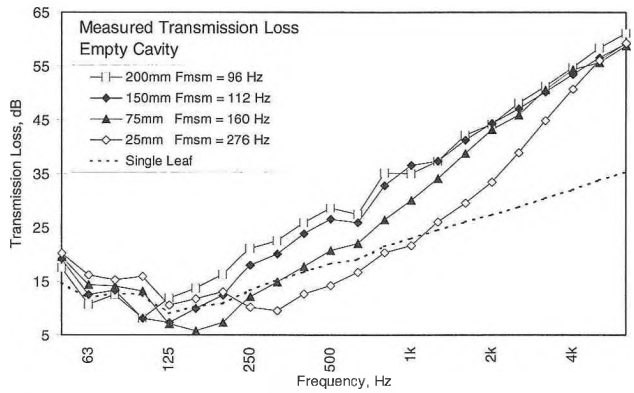

Figure 1: TL for the LEXAN wall with an empty cavity of varying depth measured in accordance with ASTM E90. Shown for comparison are the TL data for a single LEXAN sheet.

Figure 2 shows the measured and predicted change in the TL for doubling the cavity depth. From the figure it is evident that the below F_{MSM} there is no improvement. This should be expected since, for both the larger and smaller cavity depths, the air appears to be a very stiff spring that couples the two leaves. For frequencies well below F_{MSM}, the resulting TL is the same as if the leaves were glued together, without a cavity.

Both the measured and predicted results indicate that increasing the cavity depth causes a very significant change in the TL near F_{MSM}. There will be a reduction in the TL at F_{MSM} for the deeper cavity and then there will be a rapid improvement with increasing frequency to a maximum at F_{MSM} for the original cavity depth before doubling. Above F_{MSM} for the smaller of the two cavities, the benefit of depth doubling is diminished with increasing frequency. The predictions show that the TL will tend to converge to a limiting value and increasing the cavity depth will have only a very marginal improvement. The measured data exhibit this trend too, although not as clearly. Inspection of Figure 1 suggests that the once the cavity depth is greater than approximately 1-1/2 wavelengths there is little benefit to increasing the depth.

The trend of diminishing TL improvement with increasing frequency shown in Figure 2 can be explained by noting that above F_{MSM}, the transmission loss increases rapidly with increasing frequency (18 dB/octave for normal incidence) to the point at which the cavity depth is equal to one-half wavelength, F_{CM}. At this frequency, and all multiples of it, (e.g., n=2, 3, 4... in equation 2) the TL will take an abrupt drop because of efficient coupling across the

cavity. Since, the sound field is incident at all angles, there will be at least one angle for which this half-wavelength condition is satisfied at each frequency. Thus, in a given frequency range, there should be a minimum cavity depth above which the number of cross-mode conditions (equation 2) remains nearly constant with increasing frequency. This explains the presence of an upper limit for the transmission loss for an empty cavity and the strong dependence of the TL on the angular distribution of the incident sound field[3].

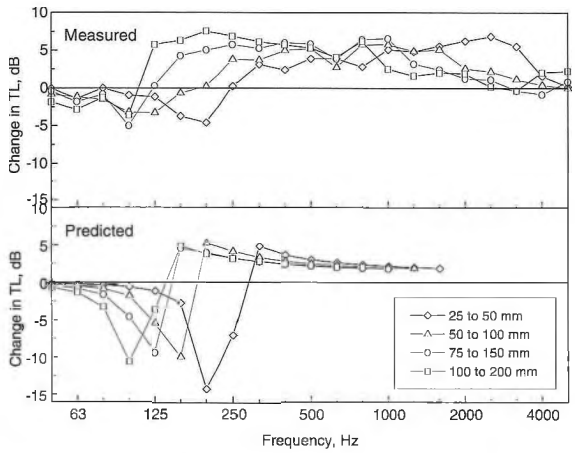

Figure 2: Measured and predicted change in the TL due to doubling of the cavity depth of the LEXAN wall without absorption. Predictions above 1600 Hz are not shown due to difficulties in obtaining solution convergence.

FILLED CAVITY RESULTS

The same series of measurements were conducted with the cavity filled with a rigid fibrous board material having an airflow resistivity of 7800 mks rayls/m. Both the measured and predicted results of Figure 3 show that F_{MSM} shifts to lower frequencies when cavity is completely filled with absorption. This is because the speed of sound in the fibrous material is slower than in air, and can be approximated by,

$$C_c = \frac{C_o}{1 + 0.0978\left(\rho \frac{f}{R}\right)^{-0.700}} \qquad (3)$$

where C_0 is the speed of sound in air, and R is the airflow resistivity of the fibrous material filling the cavity.

For frequencies well below F_{MSM}, the effect of doubling the depth of a completely filled cavity is the same as if the cavity were empty; there is no improvement.

In the frequency region near F_{MSM} the measured and predicted results are in reasonable agreement as shown in Figure 3.

Just as in the empty cavity case, for frequencies above F_{MSM} of the original cavity, the improvement due to doubling the cavity depth diminishes with increasing frequency. However, unlike the empty cavity, the data to not converge to a limiting value. There is a frequency at which there is a very pronounced TL improvement with increasing depth. From Figure 3 and using equation 3 it can be shown that if the depth of the original cavity is at least 1/5 of a wavelength then there will be a very significant increase in the TL due to doubling the cavity depth.

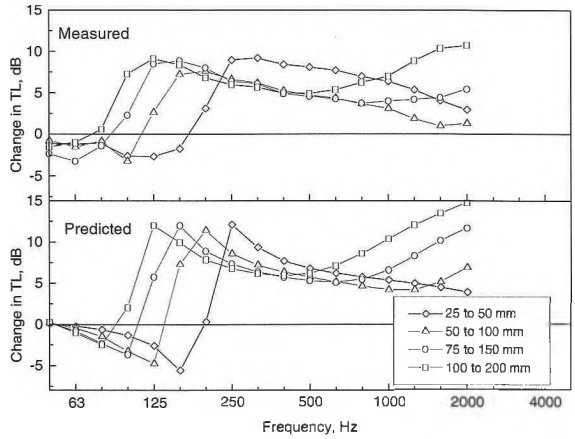

Figure 3: Measured and predicted change in the TL due to doubling of the cavity depth of the LEXAN wall that was completely filled with fibrous material having an airflow resistivity of 7800 mks rayls/m. Measured data are not shown above 2000 Hz since the measured results proved to be very sensitive to edge conditions and unreliable.

CONCLUSIONS

Cavity depth is an important factor in determining the sound insulation of double leaf walls. The trends due to doubling the cavity depth are similar for cavities with and without fibrous material. Measured and predicted results show that there is no improvement for frequencies well below F_{MSM} even if the cavity has absorption. Absorption tends to shift the F_{MSM} to lower frequencies and, in this sense, it can be thought of as effectively increasing the cavity depth. Increasing the cavity depth should not be relied upon as a method to improve the high frequency TL of a wall with an empty cavity. However, if the cavity is completely filled with fibrous material and the wavelength is less than 5 times the depth of the cavity, doubling the cavity depth will offer significant TL improvement.

REFERENCES

Quirt J.D., Warnock A.C.C. "Influence of sound absorbing material, stud type and spacing, and screw spacing on sound transmission through a double-panel wall specimen", Proceedings of InterNoise'93, pp. 971-974. 1993

Ookura, K., Saito,Y., "Transmission loss of multiple panels containing sound absorbing materials in a random incidence field," Proceedings of InterNoise'78, pp. 637-642. 1978.

Kang, H.J., Ih., J.G., Kim, J.S., Kim, H.S., Kim, S.R., "Directional dependence of the incident energy in measuring and predicting the sound transmission loss through partitions," Proceedings Sixth International Congress on Sound and Vibration, Copenhagen, Denmark, July, pp. 305-312, 1999.

VIBRATION TRANSMISSION AT FLOOR/JOIST CONNECTIONS IN WOOD FRAME BUILDINGS

Ivan Bosmans and Trevor R.T. Nightingale

National Research Council Canada, Institute for Research in Construction, Acoustics, Montreal Road, Ottawa, Ontario, K1A 0R6

INTRODUCTION

Floors in wood frame buildings usually consist of a number of Oriented Strand Board (OSB) sheets supported by a series of parallel wood joists. The OSB subfloor is connected to the joists by a number of equally spaced screws. When predicting flanking transmission in wood frame buildings using statistical energy analysis (SEA), two issues need to be addressed. Firstly, one needs to determine whether the joist should be treated as a beam or as a plate strip. Secondly, the frequency dependent behaviour of the joist/floor connection should be characterized. Both topics will be discussed in the following paragraphs, which deal with structure-borne sound transmission in the direction normal to the joists.

MODELLING THE JOISTS

In SEA, beams at plate/beam junctions are often considered as undamped coupling elements and not as subsystems [1-2]. The influence of a beam is taken into account when calculating the coupling loss factor, since the presence of the beam changes the impedance of the junction and therefore also the energy flow between the coupled plates. As cross-section deformation is typically not included, this approach is particularly suited for beams having a rectangular cross-section and an aspect ratio close to 1.

However, since the aspect ratio of a joist cross-section is usually larger than 6, some deformation is likely to occur at relatively low frequencies. As a result, the impedance at the junction is considerably overestimated when the cross-section is modelled as infinitely rigid. In fact, it is more appropriate to model the joist as an undamped plate strip [3]. Also in this case, the joist is not included as a subsystem in the SEA model. Figure 1 illustrates that a plate strip model allows the joist to bend in the plane of its cross-section, whereas, in the traditional plate/beam model, the cross-section behaves as a rigid body.

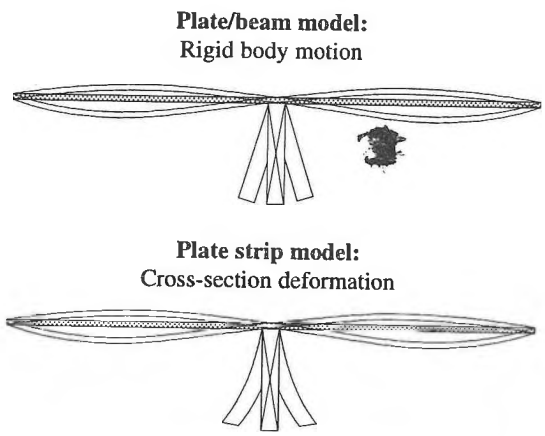

Figure 1: Plate/beam model versus plate strip model. (View: cross-section normal to the joist.)

Modelling the joist as an undamped plate strip is justified as long as the energy dissipation in the joist is negligible compared to the damping of the OSB plates. This implies that the plate strip model should be applied in a frequency range where the joists support only few modes. At high frequencies, the dissipation cannot be ignored and the joists should be modelled as plate subsystems in order to obtain the correct energy distribution in the floor. In this case, coupling loss factors are calculated by modelling the floor/joist junction as a T-joint.

The three models were applied to a subfloor/joist junction and compared to experimental data obtained in laboratory. One OSB sheet (2.4 x 1.2 x 0.0148 m) was connected to a wood joist (1.2 x 0.235 x 0.038 m) by a combination of glue and 17 equally spaced screws. The joist divided the OSB sheets into two identical plates measuring 1.2 x 1.2 m. The calculations were carried out using thin plate theory for homogeneous and isotropic plates and by assuming a line connection between the plate and the stiffener. In view of the anisotropic nature of OSB and the wood joist, the presented comparison is not entirely justified, but tendencies can still be compared.

Figure 2 shows the theoretically and experimentally obtained velocity level difference between both plates as a function of frequency. At low frequencies, the predictions of the plate/beam model and plate strip approach are essentially the same. However, the results of both models deviate at mid and high frequencies, where the plate/beam model clearly overestimates the velocity level difference. The plate strip prediction shows a pronounced maximum near 1250 Hz. A similar feature can be observed for the measured data at 1600 Hz. The T-joint model works well at high frequencies, but underestimates the transmission considerably at low and mid frequencies. In general, there is a reasonable agreement between the trends of the plate strip calculations and the measurements.

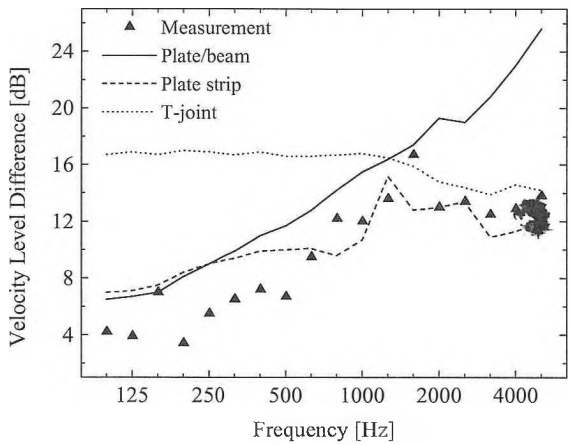

Figure 2: Predicted and measured velocity level difference for a subfloor-joist connection.

Modelling the joist/floor connection

Characterizing structural connections using nails or screws represents a major difficulty of modelling flanking transmission in wood frame buildings. In the context of lightweight walls, it has been sug-

gested to treat the joint between a gypsum board sheet and a wood stud as a line connection at low frequencies and a point connection at high frequencies [4]. The transition between both regimes was found to be the frequency at which the spacing between the nails matched half the bending wavelength in the gypsum board. This simplified approach assumes an infinitely small contact area between the plate and the beam element. In addition, it treats the plate as one entire subsystem and therefore neglects the vibration attenuation across the stud. Consequently, the simplified theory is not suited for the purposes of this paper.

The influence of the screw spacing on structure-borne sound transmission at a floor/joist connection is investigated experimentally by two series of measurements on the same floor section as considered in the previous section. In the first series, the OSB sheet was attached to the joist by 5, 9 and 17 equally spaced screws, corresponding to a screw spacing of 0.3, 0.15 and 0.075 m. In the second series of tests, the same number of screws was considered, but a thin aluminum plate (0.038 x 0.038m) was positioned between the joist and the OSB sheet at each of the fasteners. The aluminum spacers were applied to create a well defined contact area at the joint. The results of the two series are shown in Figures 3 and 4. All results were compared to a line junction, which corresponds to a combination of glue and 17 screws.

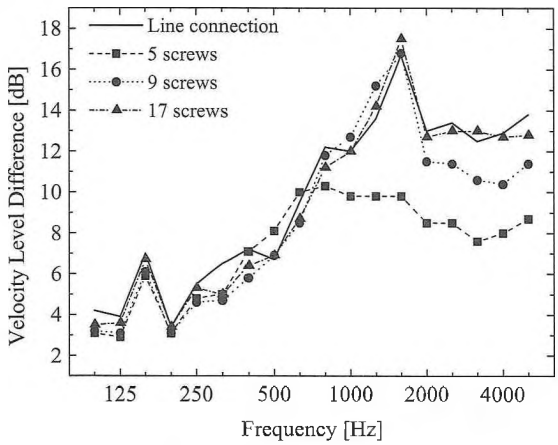

Figure 3: Measured velocity level difference between the OSB plates for the connection using screws only.

Figure 3 shows that the 17 screw connection behaves as a line junction over the entire frequency range. The case with 9 fasteners approximates a line connection up to 2 kHz, whereas the case with 5 screws does the same up to 800 Hz. Above these cut-off frequencies, the velocity level difference drops, indicating a weakened coupling between the joist and the plate. By comparing Figures 3 and 4, it can be observed that the connections with spacers are characterized by a considerably lower cut-off frequency. This leads to the conclusion that the transition from line to 'local' connection is not determined exclusively by the spacing between the fasteners. Moreover, the results indicate that the effective contact area between the joist and the plate is considerably greater that the thickness of the fastener.

As a first step toward modelling the effective contact area, the measured data for the junctions with spacers are compared to calculated results based on the theory presented in [5]. The agreement between measured and predicted data in Figure 5 for the cases with 17 and 5 fasteners is reasonable, but large discrepancies can be observed for the remaining case. However, further research is required to determine the influence of the anisotropy of the materials.

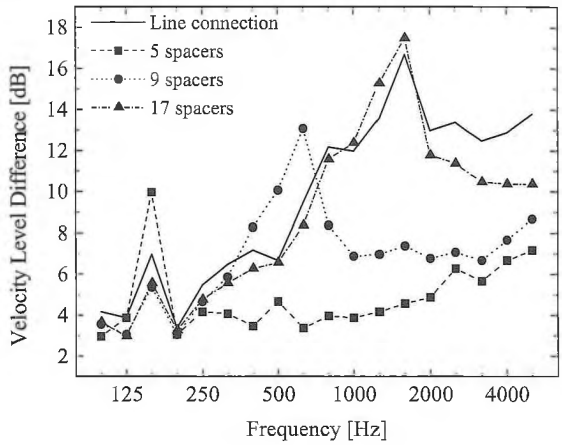

Figure 4: Measured velocity level difference between the OSB plates for the connection using screws and spacers.

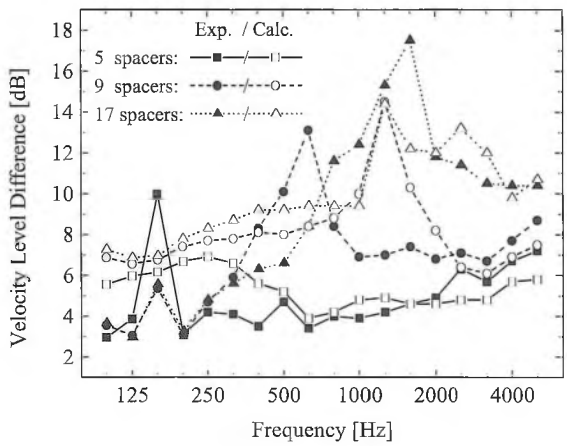

Figure 5: Measured and predicted velocity level difference for the three cases with spacers.

CONCLUSIONS

Structure-borne sound transmission at a floor/joist connection was studied theoretically and experimentally. It was shown that the joist should be treated as a plate strip rather than as a beam. It was further demonstrated that the transition from line to local connection is not only determined by the fastener spacing but also by an effective contact area between the plate and the joist. However, a more complete analysis is required to include anisotropic characteristics of the subfloor and joist material.

REFERENCES

1. Langley, R.S. and Heron, K.H. J. Sound Vib. 143, pp. 241-253 (1990).
2. Steel, J.A. J. Sound Vib. 178, pp. 379-394 (1994).
3. Fahy, F.J. and Price, W.G., IUTAM Symposium on Statistical Energy Analysis, Dordrecht, Kluwer Academic Publishers, 1999, pp. 107-118.
4. Craik, R.J.M. and Smith, R.S. Accepted for publication in Appl. Acoust. Sound transmission through lightweight plasterboard walls. Part II: structure-borne sound (1998).
5. Bosmans, I. and Vermeir, G. J. Acoust. Soc. Am. 101, pp. 3443-3456 (1997).

SkyDome Acoustical Model

Jeffery S. Bamford
Engineering Harmonics Inc., 61 Dixon Avenue, Toronto, Ontario, M4L 1N5

INTRODUCTION

In 1996, Engineering Harmonics was retained to investigate, test and re-tune the current sound system for Toronto's SkyDome. On the basis of this work and insight into the sound system, in 1997 SkyDome retained Engineering Harmonics again to prepare cost estimates and a plan to upgrade the systems. After receiving approval, Engineering Harmonics began a project to upgrade, replace and improve the system. This project involved the replacement and addition of loudspeakers, replacement of amplifiers and implementation of a digital audio transportation and DSP system. This article discusses the EASE computer model that was used to model the new loudspeakers for the lower two tiers of seating.

The existing sound system has long suffered from a balanced coverage problem. Due to architectural concerns during the construction of the building, the loudspeakers for the 100 and 200 Levels were not optimally placed. The loudspeaker placement lead to the creation of "hot spots" underneath the balconies and very poor coverage by the field.

While a centre cluster could easily cover the entire stadium, the moveable roof does not allow a speaker cluster to be permanently hung. Thus, a distributed system was designed. A series of loudspeakers were to be placed on the front of the 500 Level. These would provide coverage to the 100 and 200 Levels below. Each loudspeaker cabinet would have several drivers to cover the areas. As balconies obscure part of the 100 and 200 Levels, additional loudspeakers were to be installed underneath these overhangs. These speakers provide coverage for areas not covered by the new main loudspeakers.

In order to assist in the placement and design of the custom loudspeaker cabinets, the EASE computer program was used.

MODEL DEVELOPMENT

The model was constructed from architectural plans of the building. Using the AutoCad program, a complete three-dimensional model was developed. Once completed in AutoCad, the model was then imported into the EASE program. Once in EASE, the painstaking process of defining acoustic surfaces began. Although the model only used a small number of different acoustic surfaces, for example smooth concrete, glass and Hussey Seating, the total number of surfaces totalled over 1500. Each one had to be set by hand.

After all of these surfaces were labelled, approximately eighty audience investigation areas were defined. However, once all of these acoustic surfaces and audience areas were defined it was determined that there was not sufficient memory left to add any of the loudspeakers.

Based on the symmetry of the building, it was thought that the building could be chopped in half along its North-South axis. As this would cut the surface and volume in half, it would have no effect on any reverberation calculations from the model. An acoustical mirror was added along the cut-axis; it had an absorption co-efficient of zero and hence did not add any surface area to the model.

A series of loudspeakers were then added to the model. Several areas were under investigation; they include the uncovered and covered parts of Level 100 and 200 and some loudspeakers at the North end of the building. These North end speakers were dropped from the project. Loudspeakers were added to the face of the 500 Level to cover the majority of Levels 100 and 200. As the areas near the concourse are covered, separate speakers were to be installed in those areas. Although two rings of speakers were designed for Level 100, for simplicity only one was modelled.

Each loudspeaker's exact position was computed using a spreadsheet program. Data for each loudspeaker type was supplied by the manufacturer from an existing product. Although these would not be the exact loudspeakers installed, the data would allow for an initial gauge of their placement and aiming.

Figure 1 shows the model as a wire frame; this gives a rough idea of its shape.

INITIAL USE

Once all of the acoustic properties were defined and all of the various types of loudspeakers were entered, the model was useable. As a test of the model, an existing loudspeaker pair was entered into the model. It showed that there was an extreme build-up of energy near the top of the sections, especially 121. Closer to the field, the coverage dropped off drastically, as shown in Figure 2, for Sections 121 and 219. In all of these figures, the field is at the top of the picture. The bottom corresponds to the area closest to the con-course. Level 100 is the first seating level above the field; in the figure it is the larger of the two. The loudest areas correspond to the light

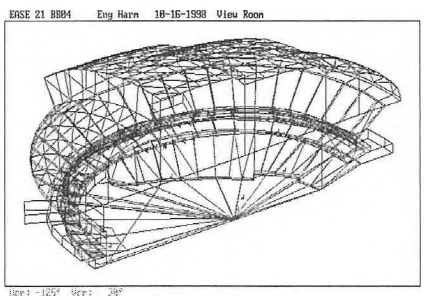

Figure 1: Wireframe Model

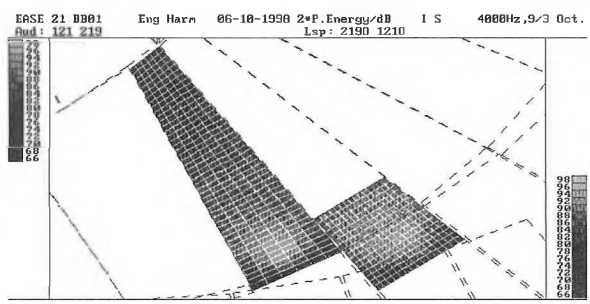

Figure 2: Coverage of Existing System

colour, the quieter areas are darker. It is easy to see that the Level 100 coverage has a severe hotspot close to the loud-speaker. Patrons close to the field would not hear the program very well.
For the proposed system, initial runs indicated that the system would be able to cover both the 100 and 200 Levels with no more than a 5 dB variance. Figure 3 shows the predicted coverage with the new system for Sections 121 and 219. The drop-off of coverage in Section 121 near the concourse is expected. Two rings of underbalcony speakers will be installed in that area; only the inner ring appears in the model. Thus, the coverage drops, as this loudspeaker is not in the model. Note that the overall coverage is even throughout the whole section.

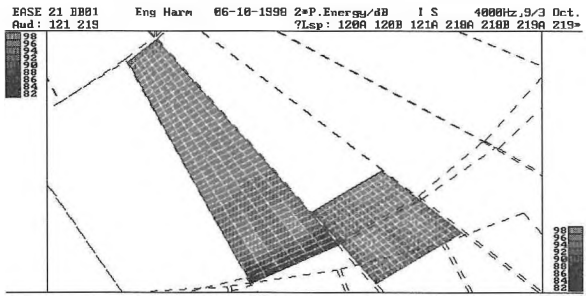

Figure 3: Predicted Coverage of New System

SOUND TESTS

To gauge the effectiveness of the model, the companion program to EASE, called EARS, was used. A ray-tracing reflectogram was created in the EASE model. This was then imported into the EARS program. It is then possible to convolve this room response with a "dry" signal. This process took approximately 36 hours of computation on our computer. The initial result was less than satisfactory.

As we were familiar with the room response of the SkyDome, we were able to listen to the model and realise that it was not as reverberant as the actual room. We determined that the model was simply not carrying the ray-tracing far enough. It was truncating the result, which caused it to underestimate the reverberation time. We adjusted the settings and forced EASE to follow through on the rays until they were really "gone". Once this was done, EARS was much better able to show the interaction of the loudspeaker system with the room.

REFINEMENTS

Having obtained results from the model and thoroughly examining them to determine their validity, we were assured that the model was predicting correctly. The manufacturer had now constructed the custom cabinet for the loudspeaker drivers. Up until this point, we were using "prototype data". The drivers for the cabinet were existing and well documented but in the model, they were in a standard cabinet - not the custom one for this project.

After they were constructed, the manufacturer measured them in their plant and we received new data for the main loudspeaker. Various tests were then conducted with this data. It led us to believe that the cabinets were not angled properly. The cabinets were about 5 degrees off; the coverage pattern did not reach to the end of the 100 Level well enough.

Various tests were run by changing the down angle of the loudspeaker enclosure. It was determined that they would need to be roughly 4 degrees steeper. While the coverage for the mid-range driver was fine at the built angle, the more directional horn was not achieving its target level of coverage. With this information, we realised that they would have to be mounted differently. A wedge was developed that would allow the loudspeaker to be moved out such that the entire level would be covered properly.

Figure 4 shows the coverage for the 100 and 200 Levels with the face aimed down 36 degrees. The coverage is much stronger near the field and drops off by the concourses. This is of concern because the loudspeaker would be too loud on the field. At 42 degrees, as in Figure 5, the coverage is more even. After careful examination of the coverage over all frequency bands, it was determined that the optimal angle was around 42 degrees.

CONCLUSIONS

The model was a massive undertaking. It frequently taxed the limits of the EASE program. It was not used as the end authority for loudspeaker placement. It was used as a design tool to quickly evaluate different placements and aiming angles. It was also used to evaluate the performance of loudspeakers from several different manufactures.

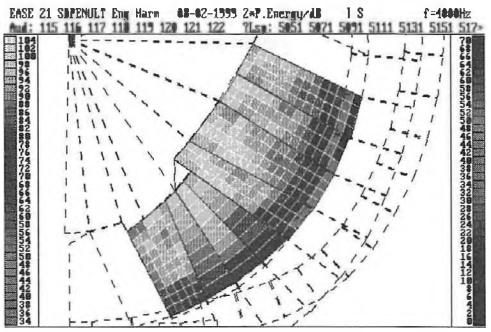

Figure 4: 4kHz at 36 degrees

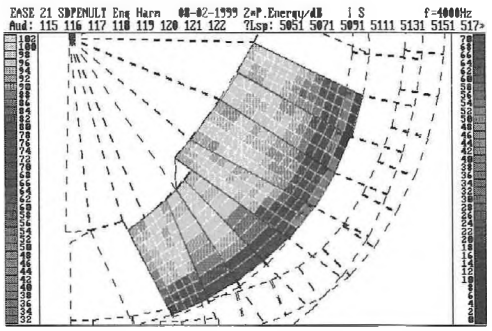

Figure 5: 4kHz at 42 degrees

Localized Sound Reproduction Using A Directional Source Array

David I. Havelock and Anthony J. Brammer
Institute for Microstructural Sciences, National Research Council, Ottawa, Ontario K1A 0R6

INTRODUCTION

By localized sound reproduction we mean the generation of a sound field that is clearly audible by a few people within a small region and substantially less audible outside this region so as not to cause interference with the surrounding environment. There are many practical applications for such a system. One example is the presentation of information at a museum exhibit where current techniques require the use of earphones. The notion of an "acoustic spotlight" that provides a localized beam of sound is considerably more appealing.

Figure 1a depicts a conventional loudspeaker array arranged in end-fire configuration. Each loudspeaker is driven by an appropriately modified signal replica to form a beam that may be steered. The replicas may be simply delayed versions of each other, with delays determined so that coherent summation of the loudspeaker outputs occurs in the desired beam direction. Alternatively, each loudspeaker may receive a filtered replica to control beamwidth and sidelobe levels. The design flexibility of these arrays is obtained at the cost of considerable system complexity, with separate signal processing and amplification required for each array element. Diffraction around the loudspeakers and supporting structure must also be considered.

In principle, a linear end-fire array can form a narrow beam along its axis but the beam becomes conical if steered off axis. A steerable 'spotlight' beam may be generated by a planar array (not illustrated), however planar arrays involve considerably more transducer elements, and associated system complexity, compared to line arrays with the same baseline.

We consider here two alternative approaches to achieving localized sound reproduction (i) an array of point sources, and (ii) a virtual source array [1].

DUCTED POINT-SOURCE ARRAY

A ducted point-source array is represented schematically in figure 1b. The single transducer is coupled to multiple ducts. Each duct terminates at a desired point source location in the array. The delay at each point source is adjusted by altering the length of the ducts, forming a beam in the (fixed) desired direction. For demonstration, an eight-element ducted point-source array, 1.35 meters long, was constructed using flexible hoses.

Acoustic coupling efficiency into the ducts, radiation efficiency at the point source, reflections within the duct system, and diffraction from the hoses and support structure are the principal challenges of this approach. Benefits include requiring only a single transducer and being very simple to construct.

A manifold is required to couple sound from the transducer into each of the ducts. Impedance mismatch at the branches will reduce the coupling efficiency and cause internal reflections. A cylindrical branching manifold was constructed with a 2.5 cm source aperture at one end and eight 1.5 cm branch ports on the circumference. The dimensions of the cylinder were kept as small as possible (about 12 cm long by 2.5 cm diameter). The coupling efficiency of the cylindrical manifold was adequate to achieve substantial output and the individual array elements combined coherently to beamform over a bandwidth from 200 to 5000 Hz.

Internal reflections occur at the end of each duct, where the radiation impedance does not match the duct impedance.
Since each duct has a different length, and a uniform spacing between the ends (i.e. the point sources) was avoided, the resulting reflections sound less like the echo from a series of pipes and more like a 'diffuse' reverberation.

To obtain accurate phase coherence from the eight point sources, the ducts were first cut to their nominal lengths and the position of their ends was then carefully adjusted along the array. Deviations of a millimeter were evident in the arrival time of sound impulses ("clicks"), as measured at the focal point two meters in front of the array. Constructed in this way, the propagation time to the focal point through each duct was identical.

Figure 2 shows the beam pattern of the demonstration array at 250 Hz (dotted curve) and 4000 Hz (dashed curve). The heavy solid line shows the directivity of the total power for white noise over the frequency band from 500 to 5000 Hz. The main beam becomes increasingly wide at lower frequencies due to the short array length relative to the wavelength. Away from the main axis, partially coherent summation of the point sources causes sidelobes. At higher frequencies, random errors in the point source spacing limit the narrowness of the mainlobe and tend to smooth out the sidelobes. For a broadband signal the peaks and troughs of the sidelobes average out. There is some asymmetry in the response due to the ducts and their support structure.

PARAMETRIC ACOUSTIC ARRAY (PAA)

A high intensity sound traveling though air will be distorted due to nonlinear wave propagation. If the signal consists of two frequencies, f1 and f2, then the nonlinear effects will generate, among other distortion products, a signal at the difference frequency ½f1-f2½. The difference frequency signal is generated locally in the medium along the propagation path of the high intensity sound and so it forms a 'virtual acoustic source'. There has been much interest in using high intensity ultrasound to generate a parametric acoustic array by choosing f1 and f2 in the ultrasonic region with ½f1-f2½ in the audio region. A narrow ultrasonic beam will produce a virtual linear end-fire array of sources in the audio frequency range [2,3].

A high power, four element ultrasonic transducer with primary frequency 28 kHz was amplitude modulated at audio frequencies to produce a PAA [4]. Figure 3 shows the beam pattern of the PAA at frequencies close to the extremes of its useable audio range (250 and 4000 Hz) as measured 4 m from the transducer. Comparison of Figures 2 and 3 shows that the PAA is capable of generating an

extremely narrow beam (localized sound field) even at low frequencies. There are no significant sidelobes in the PAA directivity pattern and no audio output could be detected in the rear hemisphere (i.e., from 90° to 270°). Substantial harmonic distortion was observed that increased with modulation depth.

Although the virtual array generated along the ultrasonic beam has a fixed end-fire direction, the PAA may be steered by physically aiming the ultrasonic transducer. Harmonic distortion due to the nonlinear generation of the audio can be reduced by pre-distorting the modulation signal, however this requires a wide bandwidth ultrasonic source. It is difficult to obtain simultaneously adequate output power and bandwidth from available transducers. Care must be exercised in the development of loundspeakers employing a PAA to ensure no health hazard arises from exposure to the high power ultrasound.

REFERENCES

[1] D.I. Havelock and A.J.Brammer, "Highly directional sound beams for audio and multimedia," (in preparation for AES.)

[2] M. Yoneyama and J. Fujimoto "The audio spotlight: An application of nonlinear interaction of sound waves to a new type of loudspeaker design," J. JASA 73(5):1532-1536, 1983.

[3] M.B. Bennett and D.T. Blackstock, "Parametric array in air," JASA 57(3): 562-568, 1975.

[4] A.J. Brammer and D.I. Havelock, "Performance of airborne parametric end-fire source array," (in preparation for JASA.)

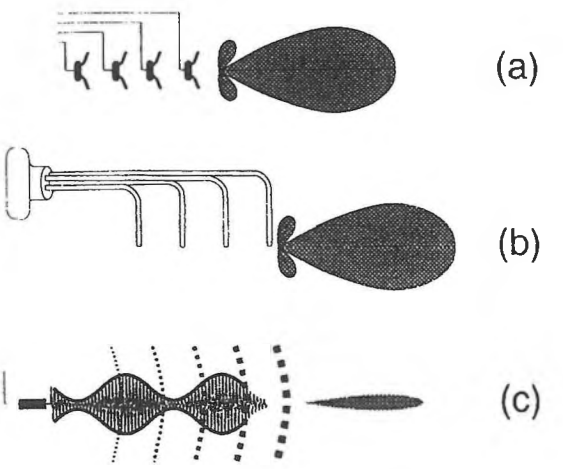

FIGURE 1. End-fire arrays: (a) loudspeakers, (b) ducted point sources, (c) parametric acoustic array.

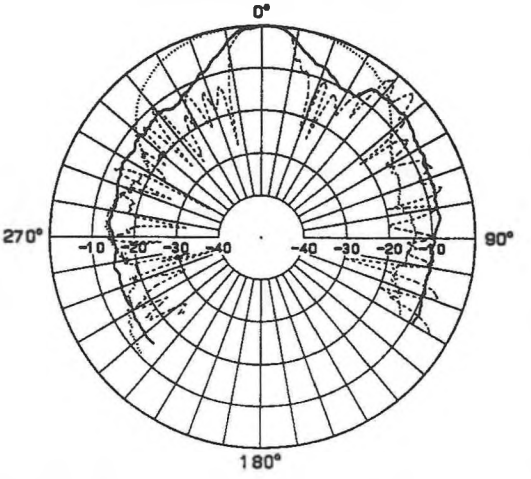

FIGURE 2. Directivity of point source array for signals of 250 Hz (dotted), 4000 Hz (dashed), and 500-5000 Hz white noise (heavy solid).

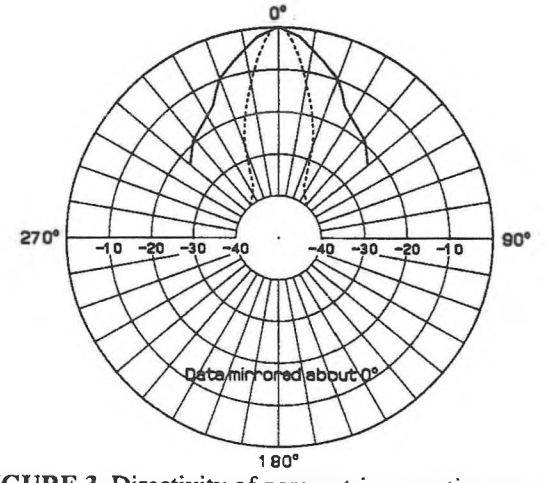

FIGURE 3. Directivity of parametric acoustic array at 250 Hz (solid) and 4000 Hz (dashed).

SYSTEM 824 SLM/RTA

Five sophisticated acoustical instruments in One!

1 **Integrating Sound Level Meter** meeting Type 1 Standards with simultaneous measurement of sound pressure levels using fast, slow, and impulse detector, and simultaneous A, C, and flat weighting. It measures 48 sound pressure parameters at once! All this with a 105 dB linearity range!

Simple Sound Analyzer with simultaneous sound pressure level measurement and real-time 1/3 octave frequency analysis.

Logging Sound Level Meter permits data gathering of broadband sound pressure levels and frequency spectra over user-defined time intervals.

Real Time Frequency Analyzer with 1/1 and 1/3 octave analysis over a 20kHz frequency range and optimized for characterizing steady-state or high speed transient events.

Fast Fourier Transform Analyzer with 100, 200, and 5 400 lines resolution and 20kHz range for specific frequency investigations.

Listen with Larson•Davis

For use in a wide variety of applications

Research and Development

- Building Acoustics
- Sound Power Determination
- Vibration measurements
- Statistics
- Simple Point Shoot
- Transient Capture

Environmental

- Aircraft Noise
- Industrial Noise
- General Surveys
- Transportation Noise
- Community Noise

Worker Safety

- Noise Exposure Measurements
- Work Place Surveys
- Machinery Noise
- Audiometric Calibration
- Simultaneous C minus A Measurements

Dalimar Instruments Inc.

at your service since 1986

193, Joseph Carrier, Vaudreuil-Dorion, Quebec, Canada J7V 5V5 Tel.: (450) 424-0033 Fax: (450) 424-0030
90 "C" Centurian Drive, Suite 206, Markham, Ontario, Canada L3R 8C5 Tel.: (905) 948-8345 Fax: (905) 948-8344
E-mail: info@dalimar.ca Website: www.dalimar.ca

Choice. Convenience. Cost.
No one else compares.

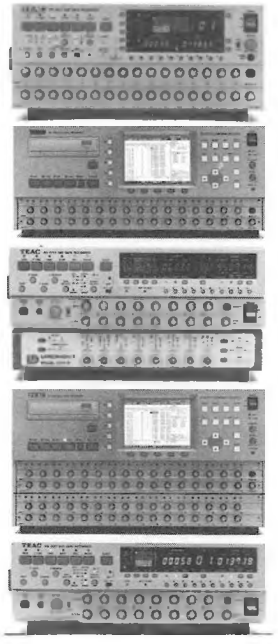

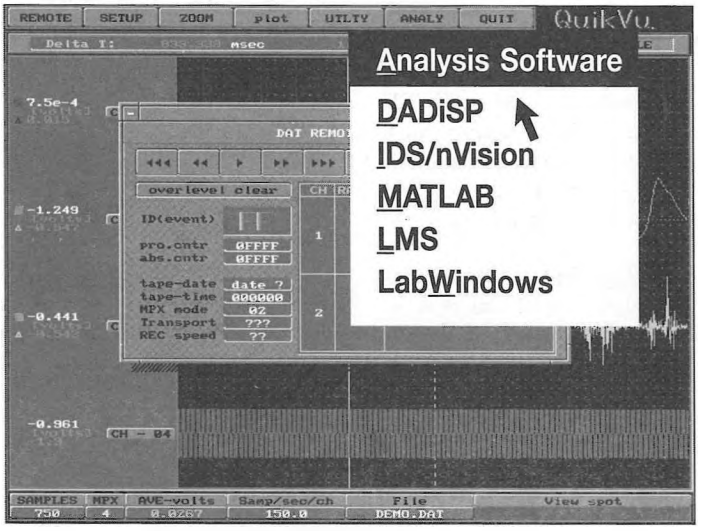

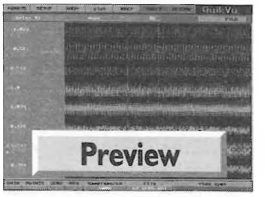

Record

Accurately recording test data is a critical issue for every test engineer. You only get one shot, because repeats are expensive, if not impossible. That's a fact we understand. That's why TEAC offers more combinations of affordable recorders, data analysis programs and downloading options than anyone else. For digital recording we have seven different compact, portable DAT models with extended dynamic range and high signal-to-noise ratios.

Download

For Hi-8mm recording, our RX series offers a very low cost-per-channel, in either a 16 or 32 channel model. Using multiple units, you can synchronously record up to 128 channels. These units feature S/N ratios greater than 80dB, a 20kHz bandwidth and up to 60 minutes of record time. And using on-board, menu-driven programming, you can easily record up to 7GB of data.

And you'll appreciate TEAC QuikVu®, a real-time PC or PCMCIA software program that lets you preview test data before you record. It allows you to monitor data in real time as well as archive or transfer data to other systems. And speaking of software, TEAC offers another major advantage.

Analyze

We have relationships with all the major data analysis software companies, so our recorders are compatible with their programs. That makes your data analysis much easier ... much faster. Just pick your favorite analytical program and go to work.

Choice. Convenience. Cost.

We're the only one who can give you a total solution for virtually any application. In fact, if we don't have it, you probably don't need it.

TEAC®

INSTRUMENTATION DATA RECORDERS

Dalimar Instruments Inc.

At your service since 1986

193, Joseph Carrier, Vaudreuil-Dorion, Quebec, Canada J7V 5V5 Tel.: (450) 424-0033 Fax: (450) 424-0030
90 "C" Centurian Drive, Suite 206, Markham, Ontario, Canada L3R 8C5 Tel.: (905) 948-8345 Fax: (905) 948-8344
E-mail: info@dalimar.ca Website: www.dalimar.ca

NUMERICAL MODELING OF POROUS-ELASTIC MATERIALS USING HIERACHICAL ELEMENTS

S. Rigobert[1], N. Atalla[2] and F.Sgard[1]

1) Laboratoie des sciences de l'habitat, DGCB URA CNRS 1652, ENTPE, rue Maurice Audin, 69518 Vaulx en Velin cedex, France

2) G.A.U.S, Université de Sherbrooke, Sherbrooke, Québec, J1K 2R1, Canada

INTRODUCTION

Porous materials are increasingly used in many industries such as aeronautics, automobile, building acoustics to improve the reverberent properties of rooms and increase the transmission loss of multilayered structures. Recently, FE models based on either {u,U}[1] or {u,P}[2] formulation have been extensively used to model such structures. These models, based on classical linear finite elements, require refined meshings to insure convergence, and consequently a great number of degrees of freedom.

The present approach aims at reducing the number of degrees of freedom while keeping the accuracy of the results. To achieve that goal, a {u,P} formulation based on hierarchical elements (high interpolation order shape functions) is implemented. The results for a single porous material bonded onto a rigid wall are presented in the case of acoustical and mechanical excitations, and different boundary conditions on the lateral faces. The performance of the approach is underlined through a comparison with classical poroelastic linear elements. The effect of different interpolation orders for the solid and the fluid phase is discussed in the oral presentation.

THEORY

In the following, the case of a single porous material is considered. The weak {u,P} formulation is given by:

$$\underbrace{\int_{\Omega p} \underline{\underline{\widetilde{\sigma}}}^S(\underline{u}^S) : \underline{\underline{\epsilon}}^S(\underline{u}^S) d\Omega - \widetilde{\rho}\omega^2 \int_{\Omega el} \underline{u}^S \cdot \delta \underline{u}^S d\Omega}_{\text{solid phase}} + \underbrace{\int_{\Omega p} \Big[\frac{h^2}{\omega^2 \widetilde{\rho}_{22}} \nabla p \cdot \nabla \delta p - \frac{h^2}{\widetilde{R}} p \delta p\Big] d\Omega}_{\text{fluid phase}}$$

$$\underbrace{- \int_{\Omega p} \Big[\gamma + h\Big(1 + \frac{\widetilde{Q}}{\widetilde{R}}\Big)\Big]\Big[\nabla p \cdot \delta \underline{u}^S + \underline{u}^S \cdot \nabla \delta p\Big] d\Omega - h\Big(1 + \frac{\widetilde{Q}}{\widetilde{R}}\Big) \int_{\Omega p} \Big[p \cdot div(\delta \underline{u}^S) + div(\underline{u}^S) \cdot \delta p\Big] d\Omega}_{\text{symetrical volume coupling terms}}$$

$$\underbrace{- \int_{\partial \Omega p} \Big[\underline{\underline{\sigma}}^t \cdot \underline{n}\Big] \cdot \delta \underline{u}^S dS - \int_{\partial \Omega p} h\big(U_n - u_n\big) \delta p dS}_{\text{natural boundary terms}} = 0 \qquad (1)$$

In equation (1), Ωp and $\partial \Omega p$ represent the poroelastic domain and its boundary, $\underline{u}^p$ is the solid phase displacement, p is the fluid pressure in the pores, $\underline{\underline{\widetilde{\sigma}}}^S$ and $\underline{\underline{\epsilon}}^S$ are the strain and stress tensors of the solid phase *in vacuo*, $\widetilde{\rho}$ and $\widetilde{\rho}_{22}$ are the complex dynamic solid and fluid phase mass density, h porosity, γ the coupling coefficient between the two phases, $\widetilde{Q}$ and $\widetilde{R}$ are poroelastic coeficients. Equation (1) is slightly different from the original form[2]. It allows for an easier application of the boundary conditions and coupling conditions through the natural boundary terms.

The theoretical foundation of hierarchical elements lies in the way the pressure in the pores and the displacement of the solid phase are interpolated at any point of the subdomain. On one 8-nodes brick element, the pressure in the pores is given by:

$$P(\xi, \eta, \zeta) = \sum_j \mathcal{N}_j q_j^{ph} + \sum_k \mathcal{G}_k q_k^{gen} \qquad (2)$$

Where ξ, η, ζ are the coordinates on the parent element and vary from -1 to 1. In equation (2), $\mathcal{N}_j$ and $\mathcal{G}_k$ are polynomial shape functions defined on the parent element. The associated variables q_j^{ph} and q_k^{gen} stand for the amplitude of these functions. Amplitudes q_j^{ph} $(1 < j < 8)$ are the amplitudes of the pressure in the pores at the element nodes, and $\mathcal{N}_j$ are the classical shape functions used in finite elements. The values of $\mathcal{N}_j$ are 1 at node j and 0 at any other node of the considered element. Amplitudes q_k^{ph} have no simple physical meaning, and are not used in classical finite element. The associated generalized functions $\mathcal{G}_k$ are divided in several categories: side modes, face modes, and internal modes. These functions are selected to make complete polynomials of ascending order p. Namely, the basis functions of the hierarchical variables are constructed using Legendre polynomials. Their number depend on the interpolation order p. For further details on the selection process, the reader is invited to refer to Babuška[3]. The approximation of the solid phase displacement on one element is achieved in the same way as for the pressure in the pores.

In the results section, two indicators are considered. For the solid phase, the mean square velocity in the three directions is computed. The mean quadratic velocity along the i direction is practically computed using the formula:

$$< v_i^2 >= \frac{\omega^2}{2\Omega_p} < u_n^{ph} \vdots u_n^{gen} >^* [M_i^S] \begin{Bmatrix} u_n^{ph} \\ \cdots \\ u_n^{gen} \end{Bmatrix} \qquad (3)$$

Where $< u_n^{ph} \vdots u_n^{gen} >$ is the row vector of the physical and generalized amplitudes relative to the solid phase displacement along direction i. $[M_i^S]$ is the mass matrix for the solid phase divided by $\widetilde{\rho}$. It contains coefficients corresponding to the direction of the displacement. In equation (3), (*) means

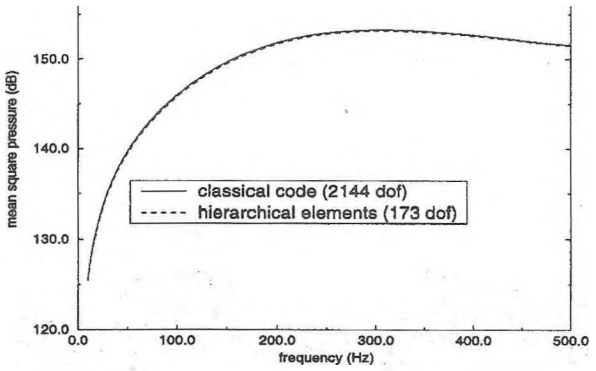

Figure 1: Single porous material on rigid wall with free edges, excited by piston motion

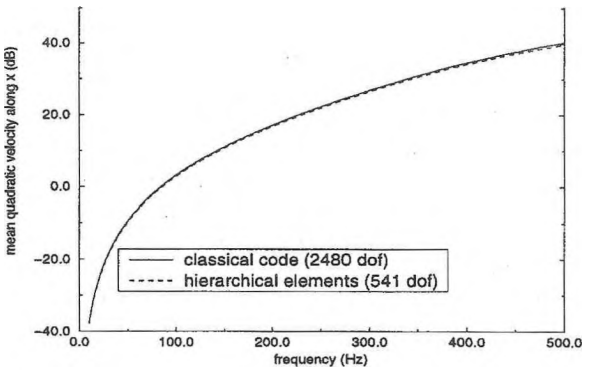

Figure 2: Single porous material on rigid wall with bonded edges, excited by incoming plane wave under normal incidence

Material	h	σ (kN.s/m^4)	α_∞	Λ (μm)	Λ' (μm)	ρ_S (kg/m^3)	N (kPa)	ν	η_S
FM2	0.90	25	7.8	226	226	300	286	0.4	0.265

Table 1: Properties of the material

complex conjugate.
For the fluid phase, the mean quadratic pressure is computed using the folowing formula:

$$< P^2 >= \frac{1}{2\Omega_p} < q_n^{ph} . q_n^{gen} >^* [M^f] \left\{ \begin{array}{c} q_n^{ph} \\ \cdots \\ q_n^{gen} \end{array} \right\} \qquad (4)$$

Where $< q_n^{ph} . q_n^{gen} >$ is the row vector of the physical and generalized amplitudes relative to the pressure in the pores. $[M^f]$ is the mass matrix divided by $h^2/\tilde{R}$.

RESULTS

The case of a single porous material of dimensions 0.35m*0.22m*0.05cm bonded onto a rigid wall is studied here. The properties of the material are given in Table 1. Two configurations are considered. First, the porous material is submitted to a piston motion and its lateral edges are free. Then, the material is excited by an incoming plane wave under normal incidence and the lateral edges of the porous material are bonded. The computed indicators, either the mean square velocity or the mean square pressure are compared to the results given by a FE code developped at the GAUS. This latter code based on classical poroelastic linear elements is chosen as reference and is insured to converge for the meshing considered. The results are presented on Figure 1 and 2. The number of degrees of freedom has been chosen so as to insure the convergence of all the indicators within 0.5dB from the results given by the classical code. For both cases, hierarchical elements enable to get very accurate results using only a reduced number of degrees of freedom. Actually, 2144 dof are needed for the first configuration and 2480 for the second configuration when the classical code is used. In comparison, the present approach requires 173 dof for the first configuration and 541 dof for the second configuration. The indicator chosen for the latter, namely the mean quadratic velocity along x direction is the one that has the most difficulties to converge.

CONCLUSION

In this paper, a FE code based on the $\{u, P\}$ formulation for a porous material and using hierarchical elements has been designed. The response for a single porous material has been computed and compared to the results given by classical elements. Hierarchical elements prove to give accurate results with less degrees of freedom.

REFERENCES

(1) Panneton, R. and Atalla, N. "Numerical prediction of sound transmission through finite multilaye systems with poroelastics materials." J.Acoust.Soc.Am., 100(1), **1996**
(2) Atalla, N. Panneton, R. and Debergues, P. "A mixed displacement pressure formulation for poroelastic materials" J.Acoust.Soc.Am., 104(3), **1998**
(3) Szabò, B. Babuška, I. "Finite element analysis", John Wiley and Sons, New York

IBANA - Insulating Buildings Against Noise from Aircraft

J.S. Bradley and J.A. Birta
Institute for Research in Construction, National Research Council, Montreal Rd. Ottawa, K1A 0R6

INTRODUCTION

IBANA is a new research project to develop a computer-based procedure for designing the sound insulation of a building against aircraft noise. Work in the 1970s led to a design guide [1] that has been widely used in Canada to design the sound insulation of residential buildings against aircraft noise. Unfortunately it is now very much out of date. Aircraft noise has changed, construction techniques have changed and it is now possible to produce a more accurate and a more convenient computer based procedure. This paper is a status report of this ongoing new project.

There are three main components to this project: (1) laboratory measurements of sound transmission loss (TL) of building façade components, (2) field measurements of TL, and (3) development of the computer software for sound insulation calculations. Laboratory measurements of TL are made for approximately diffuse field conditions and are more precise than field measurements. However, aircraft noise is incident on building facades from particular angles of incidence. It is known that TL varies with angle of incidence and it is intended to derive corrections for the laboratory TL results so that they are representative of the reduction of aircraft noise by real buildings. This will be accomplished by systematic comparisons of laboratory measurements with those in a simple test structure at Ottawa airport.

LABORATORY MEASUREMENT PHASE

The laboratory measurements of a large number of exterior wall and roof constructions are now complete and will be compiled into a data report. There are many combinations of construction details to be found in exterior walls and roofs of buildings near Canadian airports. The list of constructions to be tested was developed with advice from Canadian consultants (See acknowledgements). The focus of these measurements was on common types of residential constructions. However, a few tests related to commercial buildings were also included.

Table 1 lists the construction variables that were considered for four basic types of roof-ceiling systems. Not all possible combinations were tested but a total of 43 different roof-ceiling systems were measured. Both 2" by 10" wood joist and 14" wood truss systems were tested where the outer and inner surfaces were parallel as in flat roofs and cathedral ceilings. The raised heel wood truss (RHWT) was a sloping roof as illustrated in Figure 1. The steel deck roof systems were representative of light-weight commercial roof systems.

Type	Outer layer details	Insulation	Inner surface
2" by 10" wood	Shingles	None	1 gyp
14" wood truss	Steel sheet	R20	2 gyp
Raised heel wood truss (sloping)	Roofing - membrane	R40	RC+1 gyp
Steel deck	Roof vents		RC+2 gyp
	Ridge vent		

Table 1. Roof Construction Variables

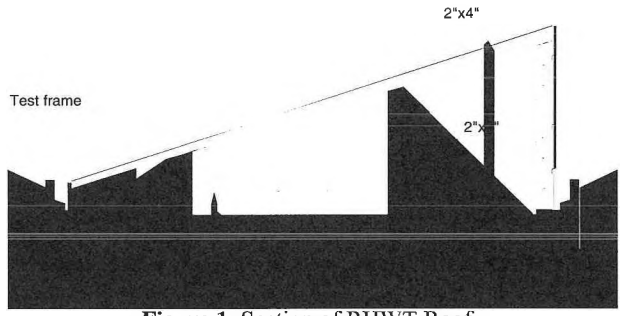

Figure 1. Section of RHWT Roof.

Figure 2 is one example of these roof-ceiling system tests and illustrates the effects of various ceiling treatments for the roof illustrated in Figure 1. Increased layers of gypsum board and the addition of resilient channels (RC) both have the expected effects on the measured TL. Figure 3 shows the change in measured TL for this same roof system with the addition of roof vents. The effect of the roof vents is quite dependent on the amount of attic insulation.

Table 2 summarises the construction details that were considered for the wood stud exterior walls tested in the laboratory. Although most walls were built using 2" by 6" wood studs at 406 mm (16") spacing, tests also included 610 mm (24") spacing and 2" by 4" stud constructions. A total of 29 different exterior wall constructions have been tested. In addition 6 different conventional windows have been tested, some both with and without an additional storm window. The windows included aluminum, wood, vinyl and vinyl clad wood frames and the double glazing units from the windows were also tested separately to help to identify the effects of the different window frame constructions.

As an example of these measurements, Figure 4 compares the effects of three different types of resilient channels (RC) when added to a wood stud wall construction. The differences among the different designs of RC are much less than the average effect of adding the RCs.

Table 2. Wall Construction Variables

FIELD MEASUREMENTS

The project will include two different types of field measurements. The first is intended to make it possible to derive conversions from laboratory TL measurements to the attenuation of aircraft noise by real buildings. A simple test structure has been constructed at

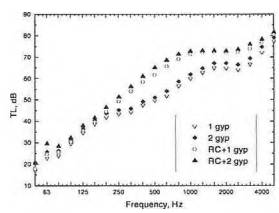

Figure 2. RHWT Roof with varied ceiling treatment.

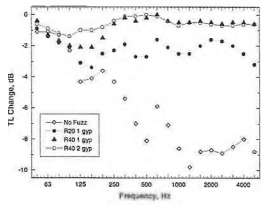

Figure 3. Effects of roof vents on RHWT roof.

Ottawa airport and a systematic series of tests will compare the TL of a number of constructions obtained for aircraft noise with results from the same constructions tested in the laboratory. Measurements in the test structure are recorded using two exterior microphones and 3 microphones in each of the two receiving rooms. All equipment is battery powered. The plan of the test structure is illustrated in Figure 5 showing a configuration that includes windows.

The second type of field measurements that are planned will consist of sound insulation measurements in homes near a major airport. The purpose is to validate the complete computer based design procedure under completely realistic conditions. The same measurement equipment and procedures as used at the Ottawa airport test structure will be used.

Outer layer	Outer insulation	Ext. Sheathing	Insulation	Inner layer
Vinyl Aluminum Brick Stucco (cement) Stucco (acrylic)	none air glass fibre Styrofoam	OSB Fibre board	Glass fibre Cellulose fibre Mineral fibre	1 gyp 2 gyp RC+1 gyp RC+2 gyp

TABLE 2. Wall Construction Variables.

COMPUTER PROGRAM

The computer design software is intended to perform quite simple calculations but in a very convenient manner so that the design process is both more accurate and more efficient. The program is written in Visual Basic and is intended to have the look and feel of typical Windows based software. Users first select details describing the type and level of the source. They then calculate a sound

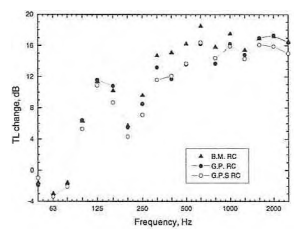

Figure 4. Incremental effects of 3 types of RCs.

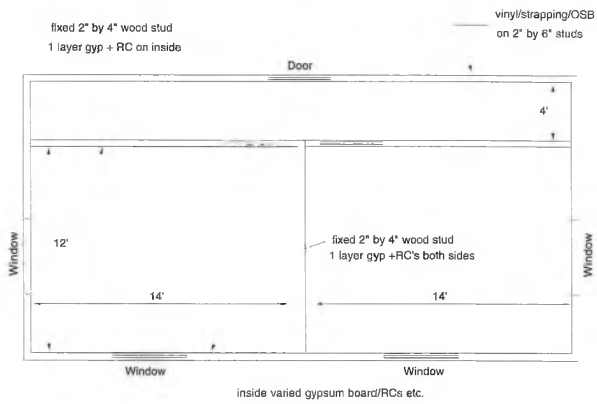

Figure 5. Plan of Ottawa airport test structure.

insulation scenario by selecting combinations of façade elements from lists. Calculations are performed for all 1/3 octave band frequencies from 50 to 5000 Hz and the expected indoor sound levels are determined. Multiple scenarios can be compared so that the user can rapidly determine the desired combination of façade elements to meet the design goals. The program will include a data base of TL measurements including those obtained as part of this project. The software has been beta tested and its development is now mostly complete.

CONCLUSIONS

It is hoped that the data base, field measurements and design software will be complete and available for use by the summer of 2000.

ACKNOWLEDGEMENT

This project is jointly sponsored by Transport Canada, the Department of National Defence and the National Research Council. The helpful advice of the following consultants is very gratefully acknowledged: Valcoustics Canada Ltd., Aercoustics Engineering Ltd., BKL Ltd. and Griffiths Rankin Cook Architects.

REFERENCES

[1] Anon, "New Housing and Airport Noise", Canada Mortgage and Housing (1981).

ACTIVE NOISE CONTROL IN ENCLOSED SPACES

Jignan Guo and Murray Hodgson
Occupational Hygiene Programme and Department of Mechanical Engineering,
University of British Columbia, Vancouver, B.C., Canada V6T 1Z4

Introduction

Much of the progress on active noise control (ANC) has been achieved in the case of one-dimensional sound-fields, as found in ducts or very small enclosed spaces, such as hearing protectors. The possibility of using ANC to attenuate noise in free-field environments has been studied. ANC in three-dimensional enclosed sound fields, such as rooms and aircraft cabins, though relatively difficult, has also attracted increased studies. though the special cases of a low modal density[1-4] or a diffuse sound field[5-10] are always assumed. When the enclosed space is very small (that is, the wavelength at the frequency of interest is large compared with its size), the sound field consists of a few dominant modes, and the modal-depression method is often used. The sound energy can be significantly attenuated by reducing the energy of each mode. This is the mechanism normally involved in active air-mufflers and active noise control in small cabins. However, when the enclosure is large (that is, the wavelength at the frequency of interest is much smaller than its size), there are too many modes to be controlled. An approach that assumes that the enclosure contains a diffuse sound field demonstrates that the noise can be controlled only over a very small area. However, in many practical enclosed environments, the sound field is neither of low modal density nor diffuse - examples are workshops, offices, and classrooms[11]. The noise in these environments is usually difficult, or even impossible, to control by traditional means. The application of ANC in such non-diffuse environments is an option that needs to be investigated theoretically, and with respect to practical implementation.

In this paper, the effectiveness of ANC in enclosed environment is studied using an image-source model developed in this study. Both global and local control strategies are investigated with different configurations of the primary source, control source and error microphone. The total power output of the sources, and the size of quiet zone created by the local control strategy, are the two indicators of control efficiency used in this study.[12]

Image-source model

To calculate the effectiveness of ANC in an enclosure, a sound prediction model is necessary. There are many such models based on ray-tracing, image-source, and modal analysis. However, most of the existing models are either too time-consuming, or are unable to provide phase information that necessary for ANC analysis.

A computer model based on the image-source approach has been developed for the general analysis of ANC in enclosed spaces. According to the image-source method, for a rectangular enclosure, the steady-state sound pressure at a position X generated by a point sound source located at X' can be expressed by[13]

$$p(X,X') = qA\sum_{p=0}^{1}\sum_{r=-\infty}^{\infty}\beta_{x1}^{|n-q|}\beta_{x2}^{|n|}\beta_{y1}^{|l-j|}\beta_{y2}^{|l|}\beta_{z1}^{|m-s|}\beta_{z2}^{|m|}\frac{e^{-ik|R_p+R_r|}}{|R_p+R_r|}$$

Theoretically, an infinite number of reflections from the walls (infinite image sources) needs to be included in the calculation. However, this is impossible in practice. One of the main tasks of the model development was to determine the least number of images that is accurate enough to describe the sound field. It has been found in this study that the least number of images depends on many room parameters, such as the room dimension, reflection coefficients of the walls, and the location of the sound source. Figure 1 shows how the calculated sound power output of the source W changes with increased number of images included N. The enclosure in this example is a rectangular room with dimension of 15×20×6 m^3. The reflection coefficients of the six walls are chosen to be the same, and to take the values B indicated.

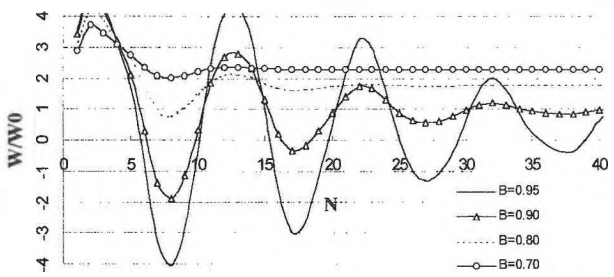

Fig. 1. Power output via the number of images.

It can be shown that the calculated sound-power output gradually converges with the increase of the reflections included. The lower are the reflection coefficients of the walls, the less is the number of the images needs to be calculated. In the example above, more than 40 reflections needed to be included when the reflection coefficient is B=0.90. This number reduced to 21 and 12 when the reflection coefficient decreased to 0.80 and 0.70, respectively.

Sound energy reduction

The reduction of total sound energy in the enclosure was studied through the reduction of total sound-power output when a control source was introduced into the enclosure, using the image-source model. The power-output reduction in a room considered by Bullmore et al.[2] which is of the dimensions of 2.264×1.132×0.186 m^3 is shown in Fig. 2 for both global and local control strategies. The primary source is at (0,0,0), the control source at (2.264,0,0), and the error microphone at (1.132,0.566,0) for local control. The reflection coefficients of all six walls were chosen to be the same at B=0.9. It shows that both global and local control strategies reduce the sound energy in the enclosure significantly at low frequencies (f<120 Hz). At high frequencies, while the local-control strategy increases the sound energy, the global-control strategy is still effective in some frequency ranges.

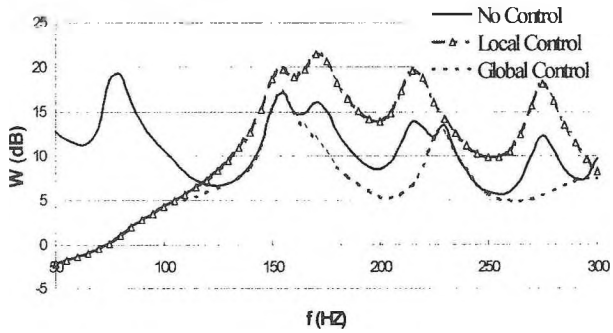

Fig. 2. Total energy reductions with both control strategies.

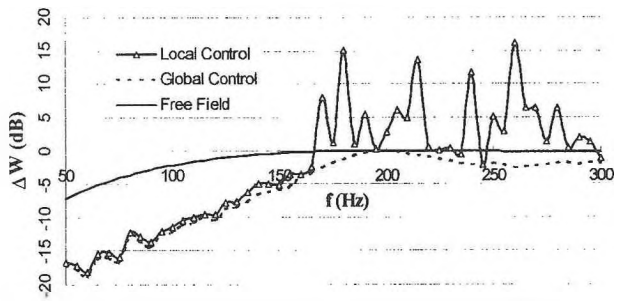

Fig. 3. Energy reduction with primary source at (0,0,0).

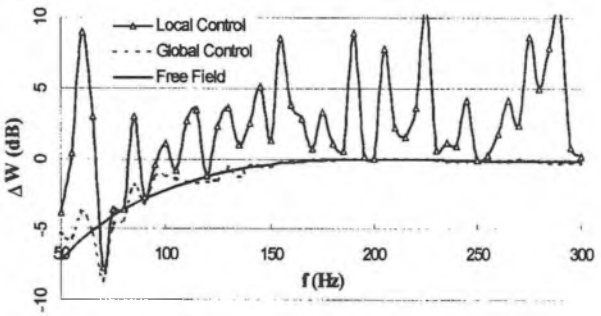

Fig. 4. Energy reduction with primary source at (7.5,10,3).

However, it has been found in this study that the performance of the control system depends not only on the relative position of the primary and control sources, but also on their positions in the enclosure. A rectangular room with dimensions of 15×20×6 m^3 is chosen to illustrate this fact. Figure 3 shows the total sound-power output reduction for both global and local control strategies. The global reduction in free-space is also included as a reference. The primary source is at (0,0,0), the control source is at (0.5,0.5,0.5), and the error microphone is at (7.5,10,3). The reflection coefficients of the walls have the same value of B=0.90, and 41 reflections are included in the calculation. A significant total sound-power output reduction is seen for both control strategies at low frequencies (f<150 Hz), and the reduction in the enclosure is much larger than that in free-space for the same separation of the primary and control sources. Figure 3 also implies that the local control strategy works as well as global control strategy does in achieving big reduction of sound energy at low frequencies, which is much easier to be implemented.

When the primary source is at (7.5,10,3), and the control source is at (8,10.5,3.5) and the error microphone is at (15,20,6), the power-output reduction at low frequencies for both control strategies decreases, as shown in Fig. 4. The difference between the results of Fig. 3 and Fig.4 are very evident at low frequencies, even though the distance between the primary and control sources is the same in these two configurations.

More analysis indicates that, in most cases, the sound-energy reduction is more significant for both control strategies when the primary source is in a corner or close to a wall of the enclosure.

Sound-pressure reduction

The same enclosure of 15×20×6 m^3 with the same reflection coefficients of the six walls, B=0.90, is chosen to demonstrate the sound-pressure reduction. Figure 5 shows the sound-pressure reduction in the enclosure by the global-control strategy when the primary source is at (0,0,0), the control source is at (0.5,0.5,0.5), and the error microphone is at (7.5,10,3). A sharp reduction of sound pressure (more than 10 dB) occurs almost everywhere within the enclosure. The reduction by the local control strategy in this case is very similar.

However, the large reduction of sound pressure in the whole enclosure disappears when the primary source is located at (7.5,10,3) when the local-control strategy is applied, as shown in

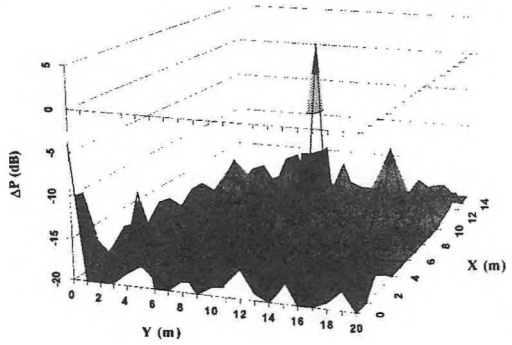

Fig. 5. Pressure reduction with primary source at (0,0,0).

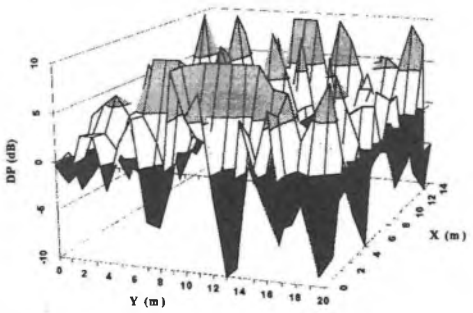

Fig. 6. Pressure reduction with primary source at (7.5,10,3).

Fig. 6, even when the separation of the primary and control sources is the same as in the case shown in Fig. 5. The control source makes the sound field very non-uniform in this case. It reduces sound pressure at some places, but increases it in other places. No large quiet zones exists.

It has been found in this study that the size of the quiet zone created around the error microphone is also dependent on the positions of the sources and error microphone, as well as the frequency of interest and the reflection coefficients of the walls. Figure 7 shows the size of the quiet zone created by the control system when the primary source is at (7.5,0,3), the control source is at (7.5,10,3), and the error microphone is at (7.5,15,3). It is obvious that the size of the quiet zone is much larger than an area with maximum diameter of λ/10, a typical size of the quiet zone predicted in a diffuse field.

Conclusions

The image-source model works well in the analysis of ANC in enclosures, and can accurately describe the sound field with not many images when the reflection coefficients of the walls are not very large.

The total sound energy can be greatly reduced, or a large quiet zone can be created in the enclosure when the control system is suitably arranged. However, the control efficiency is highly dependent, not only on the relative positions of the primary and control sources, but also on the positions of the sources and error microphone in the enclosure. There are preferable locations for the primary source for which the control system works much better.

References

1. P.A. Nelson *et al.*, J. Sound and Vib., **117** (1), 1-13 (1987).
2. A.J. Bullmore *et al.*, J. Sound and Vib., **117** (1), 15-33 (1987).
3. M. Tohyama & A. Suzuki, J. Sound and Vib., **119** (3), 562-564 (1987).
4. C. Bao *et al.*, J. Sound and Vib., **161** (3), 501-514 (1993).
5. A. David & S.J. Elliott, Applied Acoustics, **41**, 63-79 (1994).
6. P. Joseph *et al.*, J. Sound and Vib., **172** (5), 605-627 (1994).
7. P. Joseph *et al.*, J. Sound and Vib., **172** (5), 629-655 (1994).
8. J. Elliott and J. Garcia-Bonito, J. Sound and Vib., **186**(4), 696-704 (1995).
9. J. Garcia-Bonito and S. J. Elliott, ***ISVR Technical Memorandum* 745** (1994).
10. J. Garcia-Bonito & S.J. Elliott, J. Acoust. Soc. Am., **98** (2), 1017-1204 (1995).
11. Murray Hodgson, Applied Acoustics, **49**, 197-207 (1996).
12. Jingnan Guo *et al.*, J. Acoust. Soc. Am. **101** (3), 1492-1501 (1997).
13. J.B. Allen & D.A. Berkley, J. Acoust. Soc. Am., **65** (4), 943-950 (1995).

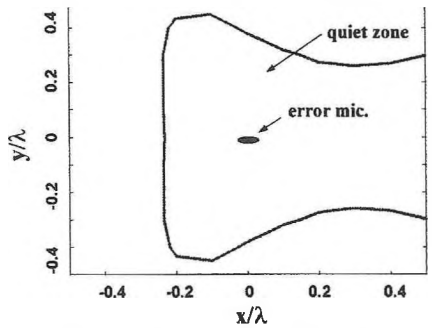

Fig. 7. Quiet zone around error microphone.

PRELIMINARY INVESTIGATION OF ACTIVE CONTROL OF AIRPORT RUN-UP NOISE

Pierre Germain, Jignan Guo, Murray Hodgson and Mark Cheng
Occupational Hygiene Programme and Department of Mechanical Engineering,
University of British Columbia, Vancouver, B.C., Canada V6T 1Z4

INTRODUCTION

Nighttime run-ups at the Vancouver International Airport (YVR) often occur between the hours of 11 pm and 6 am, creating noise in the neighboring communities to the north and south of the airport [1]. These run-ups consist of revving up the engine, sometimes to full power, as part of normal maintenance of the aircraft.

The purpose of this research is to determine the feasibility of using an Active Noise Control (ANC) system in order to reduce run-up noise that travels to neighboring communities. Propeller aircraft are commonly the source of most complaints, most likely due to the tonal nature of the noise produced by exposed propellers. In this paper, the selection of ANC strategies, run-up noise analysis, and computer simulations of a local control ANC system are discussed.

EXPERIMENTAL MEASUREMENTS

A Beech-1900D twin-engined turboprop aircraft was provided by Central Mountain Air for the noise measurements. During the full power run-up of this aircraft, the four bladed propeller rotated at approximately 1700 rpm. Two microphones captured the near field run-up noise, positioned at approximately 73 (Position 1) and 98 m (Position 2) away from the aircraft. The purpose of the second microphone is to enable a correlation analysis to be performed for the sound field at two different points in space. This analysis, however, will not be covered in this paper. A third microphone was positioned in a community north of the airport, approximately 3 km (Position 3) from the aircraft. (see Figure 1).

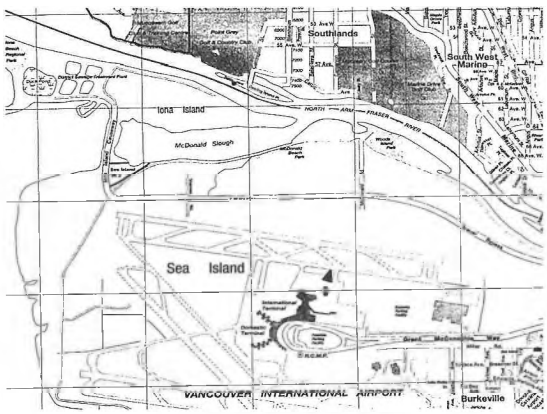

Figure 1. Map of YVR showing microphone positions (aircraft denoted by triangle)

ANALYSIS

An analysis of the run-up noise measured at Position 1 revealed a fundamental frequency of 111.7 Hz, along with several harmonics at an equally high level as the fundamental (see Figure 2). This run-up measured approximately 103 dB at Position 1, and measured approximately 80 dB at Position 3 (Figure 3). Note that at Position 3, the fundamental frequency is the only frequency to measure 80 dB and the harmonics registered lower. This creates desirable situation for ANC, as a system can be designed to attenuate this frequency only, resulting in a lower overall level in the community.

COMPUTER SIMULATIONS

In order for ANC to be used in this situation, it is evident that a global control system is not feasible, since the control sources would have to be within ¼ wavelength of the propellers in order to be effective [2,3]. This would correspond to a distance of 0.77 m to attenuate the 111.7 Hz fundamental frequency. Therefore a local control strategy must be adopted, with a zone of attenuation pointed towards the affected communities. A multiple input, multiple output (MIMO) ANC system would also be required in order to extend the quiet zone over an area of several square kilometers.

An adaptive ANC system was simulated using 21 control sources and 21 error microphones, arranged in parallel straight lines. The run-up noise source was first assumed to be a point source, and the noise was assumed coherent enough in order for ANC to be effective. The control-source-array is 20 m away from the run-up source, and the error-microphone-array is 20 m away from the control-source-array.

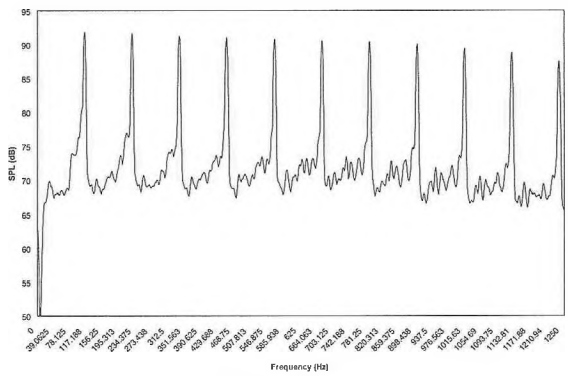

Figure 2. Noise spectrum of Beech-1900D aircraft at a heading of 255°, as measured at Position 1

It can be calculated that the optimal spacing between the control speakers and error microphones ranges from 0.5 - 0.7λl [4].

A spacing of 0.65λ was chosen for this simulation, which works out to a distance of 2 m. First, an assumption of free-field conditions was simulated, and the results of this system are shown in figure 4. A very large zone of attenuation of at least 10 dB can be achieved using this assumption. However, the presence of nearby asphalt aprons and runways would create a situation closer to a half-space condition. This condition was also simulated using 21 control speakers and 21 error microphones, and assuming a reflection coefficient of 0.8. The results are shown in Figure 5.

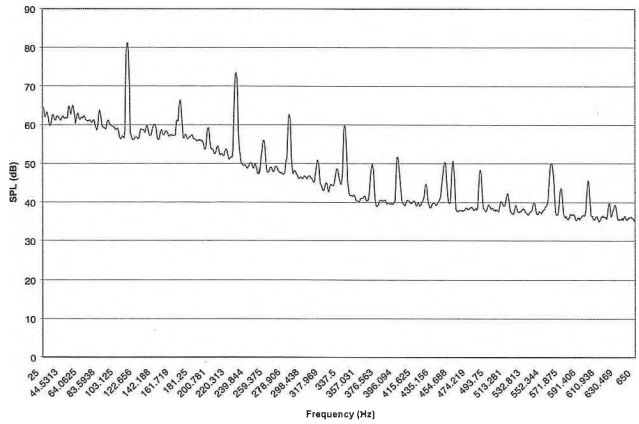

Figure 3. Noise spectrum of Beech-1900D aircraft at a heading of 255°, as measured at Position 3

It is important to note that a local control strategy will produce a redistribution of sound energy, meaning that in order for sound to be reduced in one area, it will mean that sound will increase in other areas. This is a key point, since the intent is to mitigate noise complaints in some areas without increasing the number of complaints in other areas. As can be seen in Figures 4 and 5, there is only a slight increase of 1-2 dB in areas away from the quiet zone. Most of the redistributed sound energy is localized around the control sources themselves, away from communities.

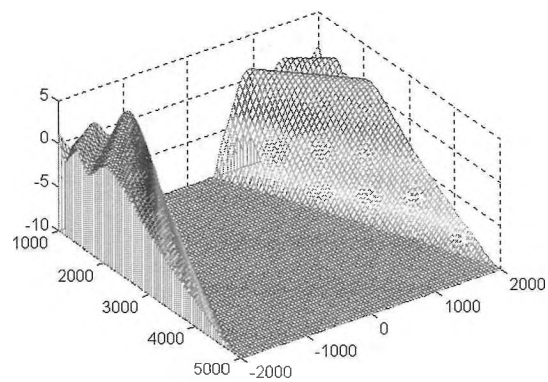

Figure 4. ANC simulation of local control using 21 control speakers and 21 error microphones in free space

CONCLUSIONS

The results of this preliminary investigation show that a very wide zone of at least 10 dB attenuation can be achieved using a local ANC system with 21 control speakers, using either a free space or half-space simulation. This attenuation can be attained without a significant increase in noise in other areas. A larger quiet area can be obtained using more control channels arranged both in a line and in a plane. Further research needs to be performed in order to determine the coherence of the Beech-1900D aircraft noise, and thus its compatibility with an ANC system. A laboratory setup of this experiment will be performed on a smaller scale in order to verify the theoretical findings.

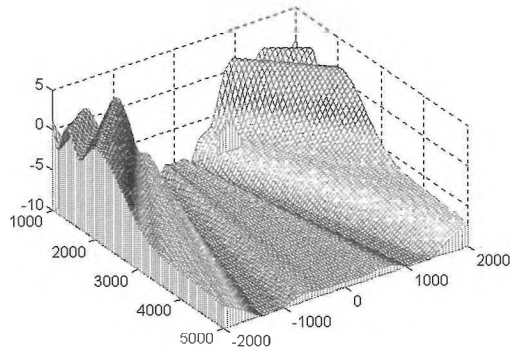

Figure 5. ANC simulation of local control using 21 control speakers and 21 error microphones in half space

ACKNOWLEDGEMENTS

The authors would like to thank Central Mountain Air for providing the aircraft, as well as Mark C. Cheng, Edward Haboly and Natsumi Valerga from the Vancouver International Airport Authority and Doug Kennedy from BKL Consultants for their co-ordination of and help with the noise measurements.

REFERENCES

1. "YVR Aeronautical Noise Management - 1997 Annual Report", Vancouver International Airport Authority.
2. Guo J., Hodgson M., and Pan J., "Active noise control in outdoor environment," Innovations in Noise Control for the Energy Industry--Spring Conference on Environmental & Occupational Noise, Banff, Alberta, Canada, April 1998.
3. Nelson P.A. and Elliott S.J. (1992). Active control of sound, Academic Press, San Diego, CA, USA.
4. Guo J., Pan J. and Bao C., "Actively created quiet zones by multiple control sources in free space," J. Acoust. Soc. Am. 101(3), 1492-1501 (1997).

The Evolution Of Environmental Noise Legislation For Alberta's Energy Industry Over Three Decades

David C. DeGagne
Alberta Energy & Utilities Board
640 Fifth Avenue S.W., Calgary, Alberta, T2P 3G4

INTRODUCTION

The energy industry in Alberta is pervasive as development extends across the entire province. Over the years the energy industry and the Alberta economy have in turn attracted many tens of thousands of new citizens to its borders. Since 1970, Alberta's population has doubled to almost three million people. This, of course, is coincidental to an order of magnitude increase in the number of energy industry related facilities. Consequently, conflict between an expanding population and the booming surface-based energy industry is inevitable as they compete for land use. One of the most significant and common impacts to arise from this problem of proximity is the increase in environmental noise.

BACKGROUND

Environmental noise is simply unwanted sound where people live, socialize or participate in recreational activities. The challenge in trying to limit environmental noise is to establish what is an acceptable level of unwanted sound given that it is impossible to eliminate all sources of environmental noise. When the Alberta Energy and Utilities Board (EUB), the Alberta energy industry regulator, first started addressing environmental noise in 1969, it took a very simplistic approach in using a single day-time and night-time noise level maximum measured in dBA. These levels were later published in the first EUB Noise Control Guideline in 1973. This one-page guideline stated that energy industry facilities could not exceed a 65 dBA day-time or 55 dBA night-time sound levels at nearby residences. It was felt that a receptor-based criterion would be best, as this could take advantage of the already existing buffer which existed between industrial facilities and rural residences.

It was only a few short years before the EUB conceded that measuring and ultimately controlling environmental noise was much more complicated than first realized. To be effective, a noise control guideline for industrial facilities would need to consider many technical challenges, as well as show a better understanding of human psychological response to environmental noise. A task force was formed of academics, acoustical engineering consultants, members of the public, knowledgeable industry, government, and EUB representatives to develop the next generation of Noise Control Directives. After a very lengthy process, the task force presented its recommendations for a new guideline that included the following:

· Criteria for instrumentation and measurement techniques.
· The adoption of A-weighted level energy equivalent (Leq) as the new metric system.
· A stepwise process for determining the permissible environmental sound level at a receptor location which was based on dwelling unit density and proximity to transportation corridors.
· Adjustment factors for unique ambient conditions, and the quality and duration of the noise.
· A detailed guide, including technical glossary, example problems, and flowcharts to assist the user.
· A requirement for conducting a noise impact assessment for proposed new facilities to ensure the permissible sound levels could be met.
· A mandatory two-year review process.

After lengthy deliberation and requests for further refinement, the EUB adopted the task force's recommendations and published what was believed to be an unprecedented comprehensive environmental noise control regulation. Known as Interim Directive ID 88-1 and companion Guide 38, the new policy provided the public with a consistent and fair process to ensure noise impacts would be kept to and acceptable minimum.

WHAT'S NEW

Since its first publication the Noise Control Directive ID 88-1 has undergone several reviews and revisions. The most recent of these has concluded with the publication of ID 99-8. The new edition reflects many significant changes in the structure and format of the directive. Highlighted below are areas where the most significant change occurred:

Noise Impact Assessments: As part of the energy facility application process, operators must prepare an appropriate noise impact assessment (NIA) when noise is a consideration for the proposed facility. New requirements and protocol for an NIA will help reduce common errors such as using near field manufacturers sound data to calculate far field estimates and underestimating the overall sound level as a result of not considering all noise sources.

Complaint Investigation: A facility that was not subject to a noise impact assessment because it predated the issuance of ID 88-1, are not required to determine compliance with the directive unless a noise complaint is filed against it by a nearby resident. Comprehensive surveys conducted as a result of a complaint must be performed under representative conditions, similar to those of when the noise is a problem. Matching these conditions is often difficult, and it is necessary to get from the complainant a clear understanding of what they are. The expectation is to not get the absolute worst case but rather a time when conditions are similar.

Measurement Instrumentation: The condition of measurement instrumentation is critical to the credibility of any noise survey. The new directive requires both the meter and calibrator to be calibrated and certified on a regular basis in accordance with ANSI S1.4 - 1983, S1.4A - 1985 or later revisions, and ANSI S1.40 - 1984.

Construction Noise: Operators are encouraged to take mitigative measures during construction to reduce any exceptional impacts, as this phase of the project is not required to be included in the noise impact assessment. Such steps include limiting construction to daylight hours, scheduling noisy activities with nearby residents, fitting all combustion engines with suitable mufflers, and using existing screening to shield residences from equipment noise.

Heavy Industrial Area Designation: The directive recognizes that some areas of the province will present unique challenges. One of these is heavy industrial areas, because within them are EUB-regulated facilities and, alternatively, non-EUB-regulated facilities which are not required to adhere to the EUB Noise Control Directive.

Compliance and Enforcement: It is essential that operators know and understand the consequences of failing to meet the established environmental noise criteria. The directive lays out what are considered "major" and "minor" noncompliance events, along with the action that will be taken by the EUB accordingly. This action ranges from immediate suspension of operations to requiring a written response from the operator. However, too many minor events can escalate matters to a serious level if necessary.

FUTURE DIRECTIONS

One portion of the directive and guide which have changed little since the issuance of ID 88-1 are the technical requirements used to establish the permissible sound level, the metrics, or how to conduct measurements. With the possible exception of the metrics, changes are not being contemplated or pursued in the other technical sectors.

As stated earlier, the directive uses an A-weighted Leq measurements, which are able to average the sound over time in a way that approximates the way the human ear hears different frequency sounds. The current Noise Control Directive fails to properly account for the presence of low-frequency noise (LFN) in survey data. This is primarily due to the use of A-weighted energy equivalent sound levels, which do not accurately account for LFN. Since most energy facilities are located in rural areas, the noise they produce will predominantly travel over acoustically soft and very soft surfaces. Therefore, whatever noise reaches the survey field (receptor) from an energy facility will consist mostly of LFN. The psychoacoustic research has shown that LFN can have serious negative effects on an individual's quality of life. Unlike high-frequency noise, LFN is difficult to suppress. Closing doors and windows in attempt to diminish the effects of LFN will often make the noise worse for the affected individual. This is due to the propagation characteristics of LFN and the low-pass filtering effect of structures. Individuals often become irrational and anxious as attempts to control LFN fails, serving only to increase their awareness of the noise.

For this reason, the Noise Control Directive should in some way account for LFN. Methods that are currently being investigated are loudness (as described by ISO 532 Method B), C-weighting (including dB(C) minus dB(A)), and appropriate maximum SPL's for one-third octave bands below 200 Hz. The advantages and disadvantages of each method must be fully considered before implementing a course of action. Work to date has been slow and sometimes frustrating as limitations in each new measurement system are discovered. Most probably, a hybrid approach will have to be developed. Modifying one of these methods might make it more applicable to the field conditions and the current approach adopted in ID 99-8. Inevitably, the work will be the main focus of the next directive review in 2002.

CONCLUSION

The Noise Control Directive ID 99-8 continues to serve industry, the public, and the EUB as a useful tool to control environmental noise. Continued review and improvement will guarantee its effectiveness and acceptability as a fair regulatory approach. The Directive can be viewed on the EUB Web site http//www.eub.gov.ab.ca

REFERENCES

Noise Control Directive ID 99-8, Alberta Energy and Utilities Board (September 1999)

ISO 532, Acoustics - Method for Calculating Loudness Level, (1975)

H. Moller, T. Watanabe, Low Frequency Hearing Thresholds in Pressure Field and in Free Field, Journal of LFN and Vibration, Vol. 9, No. 3 (1990)

K. Holmberg, U. Landstrom, A. Kjellberg, Low Frequency Noise Level Variations and Annoyance in Working Environments, Journal of LFN, Vibration and Active Control, Vol. 16, No. 2 (1997)

D. C. DeGagne, J. G. Farquharson, The Application of Loudness in Environmental Noise Legislation for the Energy Industry, Inter-Noise '95 (July 10-12 1995)

A message from John Hemingway - The Role of a CAA TREASURER

After serving several years as Treasurer of the CAA, I have decided that the time has come to pass the reins on to someone else. As Past President I am also responsible for finding a replacement! If you would be interested in taking on the post of Treasurer or know of someone who might be interested, please call me at (416) 798-0522. The following is a listing of the Treasurers duties:

- Update the CAA Ledger for the Operating and Capital Funds from Monthly Bank Statements;
- Receive paying in slips from the Secretary who does the banking of membership fees;
- Write Cheques for Prizes, Student Travel Subsidy, Journal expenses etc.;
- Liaise with the Advertising Sub-Editor re payment of Journal advertising fees;
- Receive and bank cheques (mainly advertising fees); and
- Present the Ledger, receipts, vouchers, statements, etc. annually to the Auditor.

PREDICTION, VISUALIZATION AND AURALIZATION OF NOISE IN INDUSTRIAL WORKROOMS DURING COMPUTER 'WALK-THROUGH'

Murray Hodgson, Nelson Heerema and Kurtis Halingten
Occupational Hygiene Programme and Department of Mechanical Engineering,

1. INTRODUCTION

In industrial workrooms, in order to limit the risk of hearing loss as well as to promote the adequate recognition of speech and warning signals, it is necessary to limit noise levels and reverberation times to acceptable levels at work positions. The distribution and levels of noise generated by sources in industrial workrooms are affected by room geometry, construction materials and equipment layout. Acousticians can implement noise-control measures at the design stage of new workrooms by appropriately controlling these factors, as well as by specifying quiet machinery. Noise reduction is also achieved by the use of noise-control measures such as barriers, acoustical enclosures and sound-absorbing surface treatments. In order to achieve sufficient noise control in the most cost-effective way, the acoustical designer needs to be able to evaluate and compare design options. Prediction of the workroom noise can provide useful objective information to a designer who is responsible for ensuring that the acoustical conditions are satisfactory. However, subjective information about the sound field, obtained by listening to the noise, can also be very useful in demonstrating the need for adequate noise control. Subjective experiences can be realized using acoustical-virtual-reality (auralization) techniques.

This paper presents a new approach to industrial-noise modeling, which takes the form of a combined industrial-noise prediction, visualization and auralization system, called PlantNoise. The system is designed to predict and present noise to a listener in a way that accurately simulates the noise levels that a worker in a workroom would be exposed to. A graphical user interface allows the user to visualize virtual location within the workroom and to 'walk-through' it, experiencing the noise updated in real time. Total and octave-band noise levels and octave-band reverberation times are displayed to the user. New empirical models are used to predict the noise levels and reverberation times. A major objective of this work was to develop a system that is readily accessible to acoustical consultants, industrial hygienists and other professionals.

2. SOUND-FIELD PREDICTION

Noise levels and reverberation times, in octave bands from 125 to 4000 Hz, were predicted using novel empirical models. These were developed using multivariable linear-regression analysis of experimental data from 30 'typical' industrial workrooms. The workrooms were either empty or fitted. Some contained sound-absorptive treatments. Details of the models and their derivations and evaluation are presented elsewhere [1].

3. INPUT DATA AND SYSTEM OPERATION

The operation of PlantNoise is straightforward. A data-file contains all workroom-specific information, including dimensions, surface types, source sound-power levels and information on the workroom fittings. All other information required by the PlantNoise system, including headphone and soundcard calibration constants (see below), surface absorption coefficients and A-weighting constants, is contained within the main executable. Input data describing the workroom are grouped into three categories, as detailed below along with the adjustable input parameters for each case:

- Fittings - proportion of floor area covered, average fitting height, number of fittings;
- Sound sources - description, coordinates, octave-band sound-power levels;
- Surfaces and absorption - area of hard (concrete, etc.) surfaces, area of paneled (steel-deck roof, metal cladding, doors, etc.) surfaces, area of acoustically treated surfaces, octave-band absorption coefficients of the acoustically treated surfaces, octave-band air-absorption exponents. Presumed absorption coefficients for the hard and paneled surfaces are built into the prediction models; those for the treated surfaces are user-defined.

After first reading in the workroom data, the program visualizes the workroom floor plan, with sound sources and a 1-m receiver grid superimposed, and the sound-level / reverberation-time displays. Noise levels at the default receiver position, and reverberation times, are calculated and displayed. The program initializes the soundcard, loads octave-band noise files, and commences noise generation based on the predicted noise levels at the receiver position. The user can then 'walk-through' the workroom by moving the receiver icon to any grid position bounded by the four walls. The user is able to interact with the simulation, and experience the visualized and auralized noise levels, while 'walking-through' the virtual workroom on the screen. Noise contour maps can be plotted at any time. Furthermore, the workroom can be modified - for example, to simulate and test noise-control measures - at any time by adjusting the workroom parameters; the new noise is visualized and auralized and new contour maps are plotted.

Figure 1a is a simulated PlantNoise visual display, showing the floor plan of a moderately-densely-fitted workroom with dimensions of 61 m by 34 m by 5 m high, containing four noise sources (total sound-power levels of 95, 95, 100 and 105 dB, respectively). The workroom has 3024 m^2 of hard surfaces (the floor and walls), 2074 m^2 of paneled surfaces (the steel-deck ceiling) and no acoustical treatment. The smiley-face icon represents the receiver position. The lower central portion of the screen displays graphically the octave-band sound-pressure levels at the receiver position. The levels are updated in real time during 'walk-through', and after parameter adjustments. Also displayed are the predicted octave-band reverberation times, which do not change with receiver position. They are updated only when workroom parameters are adjusted - for example, to reflect the effect of the addition of acoustical treatment to the workroom.

4. AURALIZATION

Noise generation consists of a sound-card replaying anechoic, octave-band noise corresponding to the predicted octave-band sound-pressure levels at the current receiver position, using octave-band noise files resident in the card's DRAM memory. The objective of the auralization component of the system was to replicate octave-band noise levels as accurately as possible. To this end, calibration is required for the sound-output devices used in system - the Sennheiser HD480 headphones and the SoundBlaster sound-card. Both devices exhibit non-linear responses in both frequency and magnitude, requiring compensation to achieve a linear input/output transfer function for the system as a whole. A more significant problem is that of the filtering of sound by the external ears. The assumption of a diffuse sound field was made. The objective was effectively, therefore, to simulate levels corresponding to a diffuse sound field at a listener position, using diffuse-field head-related transfer functions. In order to achieve the desired diffuse-field simulation, the headphone/ear transfer function and hardware non-linearities must be removed from the overall system transfer function, and the diffuse-field head-related transfer functions applied.

5. SIMULATING NOISE-CONTROL MEASURES

There are two common workroom noise-control measures that can be simulated and tested using PlantNoise. The first is the application of sound-absorbing acoustical treatments to the room surfaces to increase the average surface-absorption coefficient. The second consists of installing acoustical enclosures around noisy equipment. To illustrate how such treatments can be simulated with the PlantNoise system, consider the noisy workroom shown in Figure 1a and discussed above. As indicated by the noise contours, levels in the untreated workroom varied from 77 to 93 dBA, being highest in the vicinity of source 4. The reverberation time was about 1.8 s. Subjectively, the noise was very loud, and was annoying due to its dominant high-frequency content. Acoustical treatments were applied as follows:

1. Absorptive surface treatment - covering the ceiling with an absorptive treatment was accomplished by modifying the relative areas of the paneled and treated surfaces. 2074 m^2 were subtracted from the panel-surface area and added to the treated-surface area. The absorption coefficients of the treatment were also entered - in this case values increasing with frequency from 0.4 to 0.8 were used to represent suspended baffles;
2. Enclosing a sound source - enclosing a sound source was accomplished by reducing the source sound-power levels by an amount equal to the attenuation expected from the enclosure. In the present example, the total sound-power output of source 4 was reduced by 15 dB.

The simulated PlantNoise display in Figure 1b shows the noise levels and reveberation times after the addition of the surface treatment and the enclosure of source 4. Noise levels have been reduced by 10-15 dBA. The reverberation time has been reduced to about 0.6 s. Subjectively, the loudness was more than halved and the noise was less annoying, since the acoustical treatments resulted in the high-frequency noise being less dominant.

6. CONCLUSION

Numerous improvements in PlantNoise are planned or currently being implemented. It could be extended to predict noise exposure from worker time/motion information [2]. There is considerable potential for improving the realism of the subjective experience provided by the auralization component of the system. For example, the system could be extended to allow simulation of the radiation by noise sources of pure-tone and impulsive sounds. Equipment-noise signatures could be recorded, digitized and stored in the system for replay at predicted levels. Reverberation could be superimposed on the predicted noise.

1. N. Heerema, M. Hodgson, *Appl. Acoust.* **57**(1) 51-60 (1999).
2. A. M. Ondet, *Proc. Internoise '96*, 3035-3038 (1996).

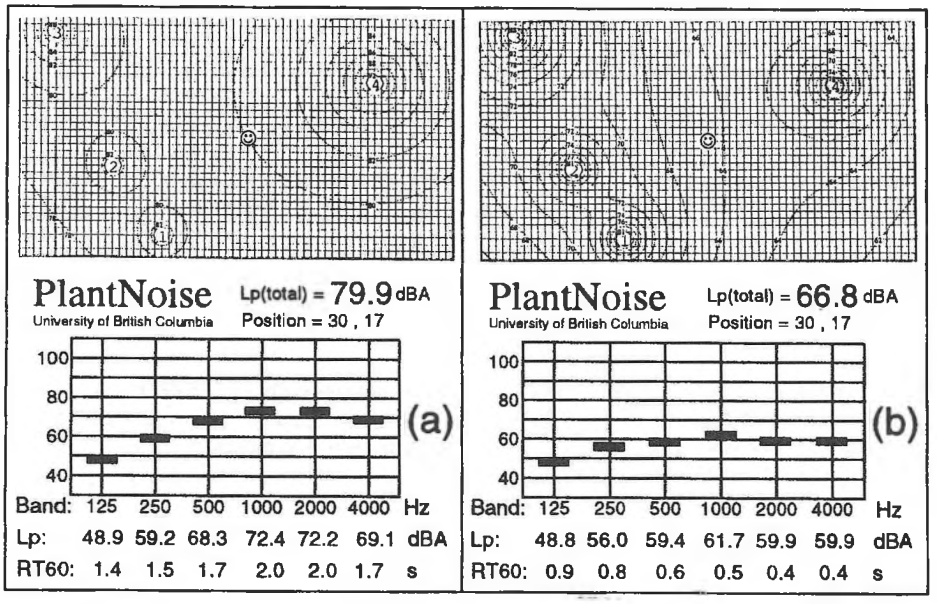

FIGURE 1. Simulated PlantNoise visual displays, showing A-weighted noise levels, and reverberation times, in a large, fitted workroom: (a) before treatment; (b) after treatment.

Broadband Acoustic Absorber Panel

Sid-Ali Meslioui
Aiolos Engineering Corp.
51 Constellation Court, Toronto, Ontario, Canada, M9W 1K4

SOMMAIRE

Cet article décrit comment la largeur de bande d'absorption d'un revêtement absorbant passif, qui souvent consiste d'une couche de matériau fibreux ou poreux tel que laine de verre ou mousse, peut être étendue au domaine des basses fréquences en combinant ce dernier à un système absorbant réactif à base de résonateurs de Helmholtz. Le système réactif, qui peut être composé d'un ou de deux couches de resonateurs, est à son tour couplé à ce qu'on appelle des "plaques résonateurs" qui fournissent un autre pic de résonance dû au couplage de la rigidité de plaque à la rigidité du volume de la cavité. Par un choix judicieux des dimensions des résonateurs de Helmholtz et des plaques résonateurs, les pics de résonances sont combinés de façon à élargir la largeur de bande d'absorption et par ce faite couvrir le domaine des basses fréquences. Cependant, un couplage positif du système réactif avec le système passif est achevé grâce à un choix approprié des caractéristiques du matériau et d'une couche de lame d'air séparant les deux systèmes. Différentes combinaisons ont été testées dans un tube d'impédance et un outil de calcul prévisionnel a été développé et validé. Dans une application pratique, les panneaux absorbants seront accordés à différentes fréquences pour assurer une bonne absorption couvrant tout le domaine des fréquences souhaité. Le coefficient d'absorption moyen varirait alors de 0,8 à 1 dans la gamme des fréquences 50 Hz à 10 kHz.

INTRODUCTION

A bulk absorber panel usually consists of a single layer construction with a solid back plate and a porous face sheet. The cavity is filled with a porous or fibrous material such foam or fiberglass. This passive panel has a wide absorption bandwidth and can absorb sound effectively at all frequencies above the first quarter wave resonance. Its acoustic performance depends mainly on the material thickness and on its resistivity which is a function of the fiber or pore diameters and density of the fills. It can easily be confirmed that the low frequency absorption is poor even for a thick layer of material. This absorber type is the most commonly used and is known as a "conventional acoustic panel".

A reactive acoustic panel can be designed as a Helmholtz resonators panel. In this case, the acoustic performances depend on the physical sizes of the resonators and on their mechanical characteristics. In addition, the acoustic excitation, under which those resonators are exposed and their location inside the circuit, will also affect its performances. Moreover, a one layer resonator panel design consists of inserting partitions between perforate plate and solid back plate. This reactive system absorber is acoustically effective over the narrowest range of frequencies and must be tuned to the frequency of greatest concern. Thus, to increase the effectiveness range, a second peak of resonance can be obtained by adding another layer of resonators and/or by choosing an appropriate plate thickness. This latter resonator is known as a "plate resonator" and its peak of absorption is due to a combination of the plate stiffness and volume stiffness of the cavity.

This paper describes how the absorption bandwidth of a conventional acoustic panel can be expanded to the low frequency domain by coupling it to a reactive panel. The coupling of the two systems is accomplished by a judicious choice of the material properties, an air gap layer, and a proper dimensioning of the Helmholtz resonators (cavity dimensions, plate thickness, hole diameter) with the plate resonators (plate resonator type) [1]. The peaks of resonance are combined in order to widen the absorption bandwidth and thus cover the low frequency range. Different combinations have been tested in impedance tube and a design program has been developed and validated.

VALIDATION

Different samples consisting of single and double layer resonators have been made with different materials and have been tested in an impedance tube by the two microphone technique [2].

The calculation method of the absorption coefficient and the acoustic impedance is based on transfer impedance procedures. The impedance of the overall system is evaluated in stages. The impedance is transferred from one layer to another until the final passive layer which may have a protective skin or a perforated plate.

The "plate resonator" impedance is calculated by solving the equations for the plate motion. The firsts modes of vibrations are then determined and the impedance is calculated [3]. The impedance of the plate resonator is combined with the Helmholtz resonators impedance. The passive layer impedance is calculated using Allard's and Delany & Bazley's models [4,5] in case of a fibrous material. For an elastic porous material, a semi-empirical model is used [6].

The panel's absorption characteristics are dependent on the following:
¨ two coupled resonance given by the Helmholtz resonance and by the combination of the plate stiffness and volume stiffness of the cavity
¨ additional coupling of these two resonances by a passive layer of porous or fibrous material
¨ exact tuning of the system as influenced by the air-gap between the passive layer and the resonators which in turn depend on the material density and its thickness

The coefficients are evaluated from the mass, stiffness and internal damping of the panel, the stiffness of the cavity, the air gap and the characteristic parameters of the passive material.

CONCLUSION

The prediction scheme developed to evaluate the absorption coefficient of a layered passive/reactive absorption panel was validated by conducting impedance tube tests. An example of test results compared to the prediction of the absorption coefficient of a double layer resonator is shown in figure 1. The results show the prediction

compares well with actual test data. Figure 2 shows an example of test results of a passive/reactive system absorber. Furthermore, it is important to mention that the passive system absorber can also be coupled to a plate resonator system alone. The cavity's volume of the plate resonator can be filled with porous or fibrous material to increase the absorption.

In real applications, the panels will be tuned to different frequencies to ensure a high absorption over the frequency range of concern. The proposed broadband absorber acoustic panels would present a mean absorption coefficient of 0.8 to 1 from 50 Hz to 10 kHz.

REFERENCES

[1] U. Ingard, "On the Theory and Design of Acoustic Resonators", J. Acoust. Soc. Amer. (1953), Vol. 25(6).

[2] J.Y. Chung & D.A. Blaser, "Transfer Function Method of Measuring in-duct Acoustic Properties", J. Acoust. Soc. Amer. (1980), Vol. 68(2).

[3] R.D. Ford & M.A. McCormick, "Panel Sound Absorbers", J. of Sound and Vibration (1969), Vol. 10.

[4] J.F. Allard, "Propgation of Sound in Porous Media - Modelling Sound Absorbing Materials", Elsevier Applied Science, 1993.

[5] M.E. Delany & E.N. Bazley, "Acoustical Properties of Fibrous Absorbent Materials", Applied Acoustics (1970), Vol. 3.

[6] U. Ingard, "Sound Absorption Technology", Institute of Noise Control Eng., NY, USA.

Figure 2: One Helmholtz resonator combined with 4" foam.

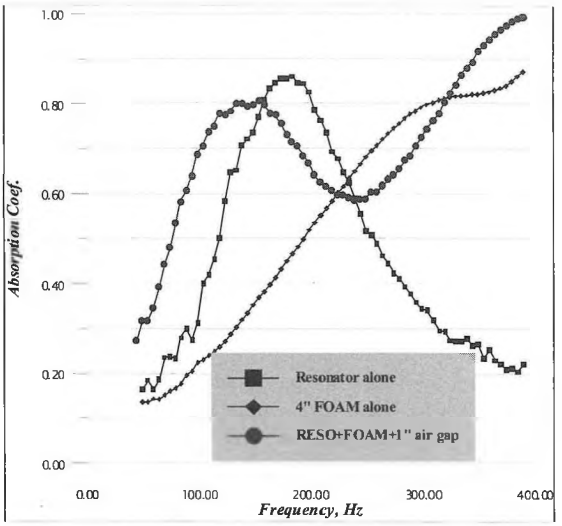

Measured in impedance tube.

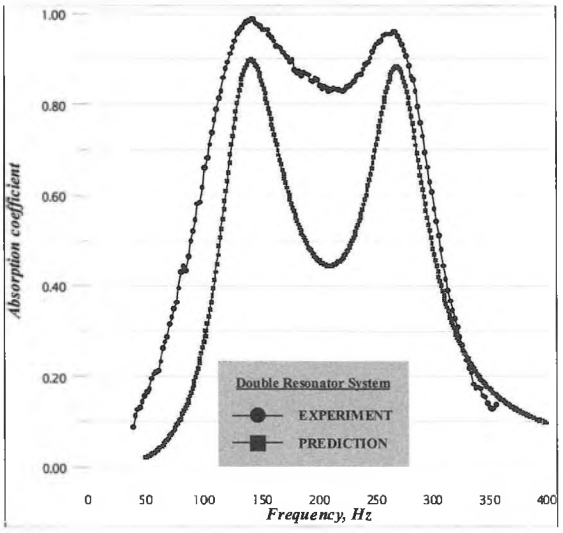

Comparison between measurement in impedance tube and prediction of a double layer Helmholtz resonator system.

Description of Speech Produced by Infants with Bronchopulmonary Dysplasia: Methodological Issues and Preliminary Data

Susan Rvachew, Dianne Creighton, Naida Feldman, and Reg Sauve
Alberta Children's Hospital

1. INTRODUCTION

Up to seventy percent of infants born prematurely and of low birth weight develop significant medical complications (1). One relatively common and serious complication is BPD, a form of chronic lung disease that can have persistent effects on respiratory function through at least early childhood (6). Infants who have suffered BPD are at especially high risk for poor developmental outcomes, even in comparison with other groups of high-risk infants, and there is some evidence that the risk of language delay is higher for infants who develop BPD, relative to other complications (5). Recent research suggests phonetic development during the first year of life impacts on later language development and clinical observations suggest that infants with BPD have difficulty producing good quality canonical babble at the expected age. Therefore, the purpose of this pilot study is to: 1) obtain a comprehensive description of the vocalizations produced by full-term infants, preterm infants without BPD, and preterm infants with BPD; 2) determine the reliability of measures of babbling ability for each of these subject groups; 3) examine the relationship between maturity of babble and aspects of development that may impact on babbling ability (i.e., cognitive ability, hearing acuity, oral motor skills, and respiratory function).

2. METHOD

2.1 Subjects

The subjects are 13 children who were born prematurely and who have been diagnosed with BPD (BPD group), 8 children who were born prematurely but who have not experienced any major medical complication such as BPD or intraventricular hemorrhage (HP group), and 10 healthy children who were born at term (HT group). For the BPD, HP, and HT groups respectively, mean birthweights were 834, 1027 and 3408 grams; mean number of days on supplemental oxygen to 12 months of age were 149, 3, and 0; and mean Blishen scores were 41, 40 and 52.

2.2 Procedure

The children were assessed at 8 and 12 months adjusted age. At 8 months, cognitive function, muscle tone, and pulmonary function were assessed. At 12 months auditory function and feeding skills were assessed. At both ages, a sample of babble was audiorecorded from the infants. Twelve samples were re-recorded within one week of the original recording in order to assess test-retest reliability. Each sample contained 50 to 100 utterances. Details of analyis procedures have been previously described (4) and will be summarized briefly here. Each utterance is coded according to 5 discrete categories: canonical babble (CB), marginal babble (MB), fully resonant vowel (FRV), quasiresonant vowel (QRV), and other (rasperries, growls, squeals etc.). A count of the number of canonical syllables in the entire sample is obtained. Canonical syllables are characterized by the presence of at least one consonant combined with a vowel, normal phonation and resonance and mature timing characteristics (2). The canonical syllable ratio (CSR) is calculated as the number of canonical syllables divided by the number of utterances (3). Efforts to replicate the more recent procedure of taking the ratio of CB syllables to the total number of syllables failed. We were unable to reliably identify the number of noncanonical syllables in a sample, although reliability for canonical syllable counts was good as described below. The ratio of MB syllables with abnormal phonation to the total number of utterances was also calculated as the abnormal phonation ratio (APR). Finally, the frequency of the second formant (F2) of vowels contained within canonical syllables was determined, and the standard deviation (SD) of F2 frequencies was calculated as an indicator of the size of the infant's vowel space.

3. RESULTS

3.1 Reliability

Inter-rater and intra-rater reliability was examined for coding of individual utterances in 12 samples (600 utterances in all). The percent agreement and kappa statistics are shown in Table 1. The Kappa statistics indicate good inter-rater reliability and very good intra-rater reliability, although percent agreement between raters is not as good as we would like. Inter-rater, intra-rater, and test-retest reliability was determined for CSRs, APRs and SD of the F2, using 12 additional samples. Mean differences, range of differences, and Pearson correlation coefficients for these pairs of scores are shown in Table 2. When this study is complete, we will determine intraclass correlations as a more appropriate measure of reliability than the Pearson r. In the meantime however, the information in Table 2 indicates excellent inter-rater and intra-rater reliability for CSRs and APRs. Test-retest CSRs and APRs indicate reasonably good temporal stability for these measures. The mean difference between the SD of the F2s is greater than desired but there is only one pair of samples yeilding a large difference between raters. When this outlier is removed the mean difference between raters is reduced to 50 Hz, with the range 0 to 221 Hz and r = .92. Intra-rater and test-retest reliability is poor for the SD of the F2 frequencies.

Table 1. Inter-rater and intra-rater reliability for coding of individual utterances as CB, MB, FRV, QRV, or OTHER.

	Inter-rater	Intra-rater
Percent agreement	78%	89%
Kappa statistic	0.70	0.85

Table 2. Inter-rater, intra-rater and test-retest reliability for sample level analyses.

	Inter-rater	Intra-rater	Test-retest
CSRs			
M Difference	.05	.03	.10
Range	0 - .12	0 - .08	0 - .28
Pearson r	.97	.98	.71
APRs			
M Difference	.03	.03	.05
Range	0 - .10	0 - .06	0 - .12
Pearson r	.91	.95	.77
SD of F2s			
M Difference	87	108	230
Range	0 - 505	19 - 303	23 - 478
Pearson r	.69	.64	-.54

3.2 Phonetic Development

Figure 1 shows mean CSRs for the three groups at 8 and 12 months. There are significant differences as a function of group [$F(2,28) = 5.10$, $p = .01$], but not age. Tukey pair-wise comparisons indicate that the HT group produces more canonical babble than the BPD group [$t(20) = 3.17$, $p = .01$]. Differences between the BPD and HP groups and between the HT and HP groups are not statistically significant. There are no between group differences in the frequency of marginal babble produced with abnormal phonation. Mean APRs are .12, .13, and .18 at 8 months and .12, .10 and .09 at 12 months for the BPD, HP, and HT groups respectively. Between group differences for size of the vowel space were not observed either. The SD of F2 is 388 Hz, 564 Hz, and 420 Hz at 8 months and 451 Hz, 461 Hz, and 570 Hz at 12 months for the BPD, HP, and HT groups respectively.

3.3 Correlates of the Canonical Syllable Ratio

Table 3 shows for each group the mean and standard deviation for the following variables: feeding score, Bayley Mental Development Index, and number of episodes of otitis media. The feeding score is based on a videotape of the infant eating. Drooling, biting, chewing, and lip closure/movement were rated as normal (score 0), suspect (score 1) or abnormal (score 2).

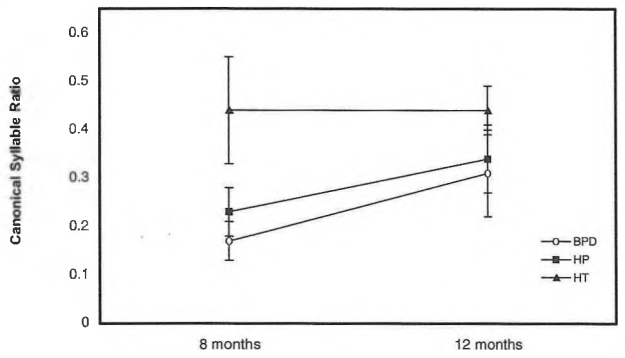

Figure 1. Mean CSRs at 8 and 12 months for the BPD, HP, and HT groups (standard error bars shown).

Table 3. Mean (standard deviation) of feeding scores, Mental Develoment Index, and number of episodes of otitis media.

	BPD	HP	HT
Feeding	2.00 (1.50)	1.38 (1.19)	0.90 (0.99)
MDI	94.85 (5.15)	97.50 (9.35)	97.2 (5.05)
Otitis Media	0.92 (1.66)	0.13 (0.35)	0.70 (1.25)

There are no significant between-group differences or predictor relationships between any of these variables and babbling ability. There may be some threshold effects: infants who received more than 28 days of supplemental oxygen produced less canonical babble than infants who required less oxygen (M summed CSR = 0.48 vs. 0.75). Infants who experienced more than 3 episodes of otitis media produced less canonical babble than infants who experienced fewer episodes (M summed CSR = 0.45 vs. 0.65).

4. CONCLUSIONS

Inter-rater, intra-rater, and test-retest reliability for Canonical Syllable Ratios and Abnormal Syllable Ratios is good or excellent. Reliable determination of F2 frequencies is difficult. Infants born prematurely who have BPD produce less canonical babble than healthy infants born at term. CSRs may also be impacted by otitis media history but are not correlated with feeding and cognitive abilities. Correlational analyses are suspect due to restricted range and small sample size, however.

5. REFERENCES

1. Landry, S.H., Fletcher, J.M., & Denson, S.E. (1993). Longitudinal outcome for low birth weight infants: Effects of intraventricular hemorrhage and bronchopulmonary dysplasia. Journal of Clinical and Experimental Neuropsychology, 15, 205-218.
2. Oller, D.K. (1986). Metaphonology and infant vocalizations. In B. Lindblom & R. Zetterstrom (Eds.) Precursors of early speech (pp. 21-36). New York: Stockton Press, Inc.
3. Oller, D.K. & Eilers, R.E. (1988). The role of audition in infant babbling. Child Development, 59, 441-449.
4. Rvachew, S., Slawinski, E.B., Williams, M., & Green, C. (1999). The impact of early onset otitis media on babbling and early language development. Journal of the Acoustic Society of America, 105, 467-475.
5. Sauve, R.S. & Singhal, N. (1985). Long-term morbidity of infants with bronchopulmonary dysplasia. Pediatrics, 76,725-733.
6. Vohr, B.R., Coll, C.G., Lobato, D., Yunis, K.A., O-Dea, C., & Oh, W. (1991). Neurodevelopmental and medical status of low-birth-weight survivors of bronchopulmonary dysplasia at 10 to 12 years of age. Developmental Medicine and Child Neurology, 33, 690-697.

6. ACKNOWLEDGEMENT

This research supported by the Alberta Children's Hospital Foundation.

Relationship Between F2/F1 Vowel Quadrilateral Area And Speech Intelligibility In A Child With Progressive Dysarthria

Megan M. Hodge
Department of Speech Pathology and Audiology, 2-70 Corbett Hall, University of Alberta, Edmonton, Alberta, T6G 2G4

1. INTRODUCTION

Kent [1] identified several acoustic correlates of speech production (e.g., point vowel precision, size of vowel area/space, obstruent spectral parameters, intersegmental timing) that predict speech intelligibility and that also characterize "clear speech" [2]. As children develop their speech production skills, their speech intelligibility (i.e., the ability to make the linguistic information contained in their auditory speech signal understandable to listeners) also increases [3]. Childhood progressive neurogenic conditions that reduce function of the muscular components of the speech mechanism resulting in dysarthria present the atypical situation where speech intelligibility may decrease during the period of speech development. This paper addresses the relationship between speech intelligibility scores and the acoustic correlate "vowel area" for a child with a progressive developmental dysarthria. The objectives of this initial step in investigating the relationship between acoustic correlates of speech production and speech intelligibility for this child were to:

1. Describe the observed changes in the child's vowel quadrilateral F2/F1 planar area between 3 and 10 years of age using a log Hz scale for comparison.
2. Describe the relationship between the vowel quadrilateral F2/F1 planar area and the child's speech intelligibility scores across this 7 year span.

2. METHOD

2.1 Subject

The child had bilateral facial paresis and a sensorineural hearing loss that were apparent by 14 months of age. She was aided binaurally at age 19 months for her moderate bilateral sensorineural hearing loss which has remained stable to the time of this report. Formal neurological testing at age 2 yr 11 mos confirmed the absence of facial muscle activity manifested as a complete lack of facial expression and no movement of her lips for speech production or swallowing. She used her tongue and jaw for speech and swallowing actions typically performed by the lips. During her late preschool/early school years, muscle wasting in the tongue and shoulder girdle became apparent. Dysfunction of the velopharyngeal mechanism for speech production was evident at age five years. Her cognitive and language skills and school progress have been age-appropriate throughout her development. At age 8.5 yr she was diagnosed with infantile onset facioscapular humeral muscular dystrophy.

2.2 Speech Intelligibility Measures

Audio recordings of the child's productions of single word and sentence formats of the Test of Children's Speech or TOCS [3] were obtained at yearly intervals between ages 3 and 10 yr. The single word format of this test contains 78 English words that are contrastive in vowel, place and length and consonant manner, place and voicing with one or more possible minimal pair words [4]. The stimuli for the TOCS sentence format are randomly selected from pools of word combinations, ranging from 2 to 6 words in length, to create a test that contains 160 words in total. The longest utterance pool selected is based on the child's spoken language level. The TOCS provides intelligibility scores for each test format (single word and sentence) that are based on listener identification of the child's recorded test utterances and that are expressed as the percentage of words correctly identified, averaged across three unfamiliar adult listeners.

2.3 Formant Measures

For each of the point vowels [i], [ae], [a] and [u], 6 words were selected that contained the vowel from the single word items of the TOCS , giving 24 words in total. These words are listed in Table 1. The first (F1) and second (F2) formant frequencies were measured for each word from the recordings obtained at 3 yr, 4 yr, 6 yr, 7 yr, 8 yr, 9 yr and 10 yr. Formant frequencies were measured from spectrograms generated using CSpeech 4.0 [5]. Each word was digitized at 22 kHz and 16 bit quantization size. A 600 Hz analyzing bandwidth was used to generate a spectrographic display of the word. The center frequency of each formant was estimated manually. The point where the formant measures were estimated varied depending on the word and vowel but for a given word, the same measurement point was maintained across the 7 recordings. The mean F1 and F2 values in Hz were determined for the 6 words for each of the 4 point vowels at each recording time (reported in Appendix 1). These F1 and F2 means were then transformed to log Hz [6] and plotted to generate a vowel quadrilateral for each recording year. The planar area for each vowel quadrilateral, expressed in log Hz^2, was then calculated.

[i]	[ae]	[a]	[u]
heat	hat	hot	hoot
seat	bad	top	Sue
sheet	badge	jaw	chew
beat	hash	hawk	two
eat	hatch	chop	shoe
Dee	pad	stop	zoo

Table 1. TOCS word items measured for point vowel F1 and F2 values.

3. RESULTS

3.1 Speech Intelligibility Scores

The child's intelligibility scores for the word and sentence formats of the TOCS are reported in Table 2 for each of the 7 test recordings. On the single word format of the TOCS, the child's scores increased between 3 and 8 years (10% gain) and then decreased between 8 and 10 years (20%) loss. On the sentence format of the TOCS, the child's score increased monotonically from 3 to 8 years (20% gain) and then did not change. As age increased, the difference between the child's word and sentence scores also increased, ranging from an 11% difference at age 3 yr to a 42% difference at

age 10 yr.

3.2 F2/F1 Vowel Quadrilateral Area

The F2/F1 vowel quadrilateral areas obtained from the test words for the point vowels at each recording age are reported in Table 2. The correlation matrix for the variables age, TOCS word score, TOCS sentence score and F2/F1 area are reported in Table 3.

Age (yr)	TOCS Word Score (%)	TOCS Sentence Score (%)	F2/F1 Area (log Hz^2)
3	55	66	0.451
4	55	72	0.513
6	57	77	0.472
7	60	85	0.374
8	65	90	0.410
9	55	90	0.280
10	46	88	0.260

Table 2. TOCS intelligibility scores (% words correctly identified) and F2/F1 vowel quadrilateral areas for the single word recordings measured for the point vowels.

	TOCS Word Score	TOCS Sentence Score	F2/F Area
Age	-0.234	0.948	-0.864
TOCS Word Score		0.061	0.470
TOCS Sentence Score			-0.758

Table 3. Correlations (r values) between pairs of variables.

In contrast to children with normal speech production and children with nonprogressive dysarthrias [3], this child did not exhibit a significantly positive relationship between her TOCS word and TOCS sentence intelligibility scores as her age increased. In addition, a significantly negative relationship was found between her age and her F2/F1 vowel area which is also not typical of talkers with normal speech development, based on previous investigations of vowel development in children at comparable ages [7]. A moderately weak positive relationship was found between TOCS single word intelligibility scores and F2/F1 vowel area; i.e., 22% of the variance in the TOCS single word test scores across the 7 recordings was accounted for by the change in F2/F1 vowel area.

4. CONCLUSIONS

1. A log Hz scale was used for comparing F2/F1 vowel quadrilateral planar areas across time as the child increased in age (and vocal tract size). This scale appeared sensitive to reductions in vowel quadrilateral area associated with progressive neuromuscular deterioration affecting lingual and velopharyngeal function.

2. The significant negative correlation obtained between F2/F1 area and TOCS sentence intelligibility scores suggests that factors other than vowel area are contributing to the child's maintenance of relatively high intelligibility scores on the sentence test format. In contrast, the moderately weak positive relationship between F2/F1 area and TOCS single word intelligibility scores suggests that some of the decrease in the single word intelligibility scores for the later test recordings can be accounted for by a reduction in F2/F1 vowel area.

3. Future questions will address 1) the relative contributions of F2/F1 vowel quadrilateral area and acoustic correlates of obstruent articulation to the child's TOCS intelligibility scores, and 2) attempt to identify acoustic correlates that account for the increasing discrepancy between the child's TOCS single word and sentence intelligibility scores.

5. REFERENCES

[1] R. D. Kent, J. F. Kent, G. Weismer and J. Duffy, "Selected acoustic measures for various aspects and components of normal and disordered speech production", presented at the Annual Convention of the American Speech-Language-Hearing Association, San Antonio, TX, November, 1998.

[2] M. A. Picheny, N. I. Durlach and L. D. Braida, "Speaking clearly for the hard of hearing II: Acoustic characteristics of clear and conversational speech", Journal of Speech and Hearing Research, 29, 434- 446, 1986.

[3] M. M. Hodge, "Measuring speech intelligibility in young children with dysarthria", presented at the Biennial Conference on Motor Speech, Amelia Island, FL, February, 1996.

[4] R. D. Kent, G. Weismer, J. F. Kent & J. C. Rosenbek, "Toward phonetic intelligibility testing in dysarthria", Journal of Speech and Hearing Disorders, 54, 482-499, 1989.

[5] P. H. Milenkovic & C. Read, CSpeech 4.0, Laboratory Version [Computer Program], Department of Electrical and Computer Engineering, University of Wisconsin, Madison, WI, 1992.

[6] T. M. Nearey, "Applications of generalized linear modeling to vowel data", Proceedings, 1992 International Conference on Spoken Language Processing, 583-586.

[7] S. Eguchi & I. Hirsh, "Development of speech sounds in children", Acta Oto-laryngologica, suppl. 257, 5-43, 1969.

APPENDIX 1: Mean F1 and F2 values obtained from the TOCS word items measured for the point vowels at each recording.

Age (yr)	Formant (Hz)	[i]	[ae]	[a]	[u]
3	F1	627	1323	1018	503
	F2	2961	2230	1574	1229
4	F1	506	1302	1108	544
	F2	3037	2389	1749	1253
6	F1	506	1181	1016	526
	F2	2817	2324	1507	1236
7	F1	481	1113	992	499
	F2	2836	2202	1762	1611
8	F1	482	1134	967	537
	F2	2851	2057	1564	1218
9	F1	485	1018	956	545
	F2	2599	2243	1593	1486
10	F1	546	1014	876	585
	F2	2597	1977	1392	1358

AN ACOUSTIC ANALYSIS OF BOUNDARY-SIGNALING DIFFERENCESBETWEEN LANGUAGES WITH CONTRASTIVE AND NON-CONTRASTIVE DURATION

Zita McRobbie-Utasi
Department of Linguistics, Simon Fraser University, Burnaby,British Columbia. V5A 1S6

1. INTRODUCTION

Languages with contrastive duration tend not to utilize duration for additionalgrammatical functions (Engstrand and Krull 1994). It may thus be expectedthat they will behave differently from languages with non-contrastiveduration, with regard to boundary signalling. The acoustic analysis undertaken in the present study aims atproviding further support for this assumption by examining the temporalpatterns apparent within the paragraph. In this paper it is hypothesizedthat, in the above two types of languages, paragraph-boundary signalling differences correlate with differencesevident in the realization of temporal patterns within these speech units.It is argued that, in languages where duration is not contrastive, thedurational increase signalling aboundary co-occurs with a greater degree of durational variation within theparagraph.

The project reported on here is a direct continuation ofa pilot study examining the issue indicated above in six languages: threewith contrastive, and three with non-contrastive duration (McRobbie-Utasi 1999). In that study it wasconcluded that the two observed tendencies -- (i) durational variationsrealized in connection with sentences in different positions as well as inintersentential pauses, and (ii) preboundary lengthening -- are realized differently, depending on the languagetype (i.e., on whether duration is contrastive or non-contrastive).Further, it was hypothesized that languages with contrastive duration tendto maintain durational ratios betweenlong and short segments. Consequently, in languages where duration is notlinguistically significant, a greater degree of variation could be expectedat the segmental level. It is in connection with this latter issue thatthe present study further explores temporal patterns by way of (i) identifying segment durational patterns in both types of languages, and (ii) relating these patterns to the tendencies reported on in McRobbie-Utasi 1999.

2. THE EXPERIMENT

Recordings of six paragraphs by eight speakers wereacoustically analyzed. Each paragraph consisted of three sentences(henceforth A, B and C). The sentences in the six paragraphs were thesame, except in their ordering. Each speaker was asked to translate the same paragraph. In the experimentthere were nine languages in total, five with contrastive, four withnon-contrastive duration. The languages with contrastive duration wereHungarian, Latvian, Hindi, Finnish, and Korean; those with non-contrastive duration were English, Cantonese,Brazilian Portuguese, and Russian. The experiment was designed with the objective of first making thesubjects familiar with the text. They were informed as to the purpose ofthe study only after the recording had taken place. Altogether 108paragraphs were analyzed.

3. RESULTS AND DISCUSSION

3.1 TEMPORAL PATTERNS

The general tendency that was observed insentence duration will be summarized here in relation to the sixconfigurations of sentence ordering. Mean durations and standarddeviations were obtained for each of the three sentences separately in the three positions.These durational values were examined by relating them to the mean sentenceduration (i.e., Ýx of A sentences, Ýxof B sentences, and Ýx of C sentences, in allthree positions). Divergences from the mean, indicating the degree ofvariation associated with the ordering of the sentences within theparagraph, are summarized in Figure 1. It may be observed that (i) it is the third positionin which durational variations are most apparent, and (ii) these variationsare greater for languages with non-contrastive duration.

In connection with the two intersentential pause durations, the patternthat emerges in 69 out of the 108 paragraphs implies the existence of aninteresting tendency: first, it was observed that paragraph durationstend to have relatively small standard deviation values; second, it is in the third sentence position thatthe greatest degree of variation was observed (see Figure1). If we assume that speakers tend to conform to a durational target (the experiment being designedin such a fashion that speakers were familiar with the text), we mayhypothesize that towards the end of the paragraph the durational variationsobserved may function as timing adjustments. Further, the 69 sentences (a number indicating greater thanchance occurrences) confirm the assumption that the duration of the secondintersentential pause also plays a role in this timing adjustment.Keeping to a durational target for theparagraph, as indicated by the degree of variability associated with theparagraph-final sentence and the second intersentential pause duration, isvalid for languages with contrastive and non-contrastive durationalike.

Variations in duration of the last word in the paragraph were examined withthe objective of discovering a possible pattern indicating an increase induration in paragraph-final sentence positions. In comparing thesemeasurement values with those in the first and second sentence positions, the following tendency could be observed: (i) while durationalvariations were manifested in all positions, it is in the paragraph-finalposition that they register mainly as increases in duration; (ii) theseincreases, while apparent in both language types, are of a greater degree in languages with non-contrastiveduration. Subsequently, variations in duration of the last syllablein the paragraph were related to last syllable durations in the threesentences in different positions. The results emerging from the present project are comparable to those reported inMcRobbie-Utasi 1999. Measurements from three additional languages confirmthe existence of a distinct pattern in the two language types. Languageswith contrastive duration havea lesser degree of durational increase in the last syllable than dolanguages with non-contrastive duration.

3.2 SEGMENT DURATIONS

In examining segmental durations, the hypothesistested in this project was that languages with non-contrastive duration will manifest a greater variation in segments than those languages withnon-contrastive duration. The rationale that underlines this assumptionwas that the maintaining of distinctions between short and longsegments -- such distinctions being linguistically significant -- would constrain thevariations in duration in languages with contrastive durations. It wasthus further hypothesized that the durational distance between long andshort segments would have to be

kept preserved -- variations at thesegmental level being constrained by the grammatical function ofduration.

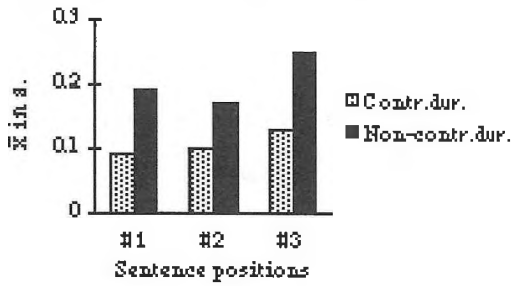

Figure 1. Sentence level durationalvariations

At this stage of the project only vowel segments have been examined. Inlanguages where duration is contrastive, vowels were divided into fourgroups (due to the fact that only three sentences were analyzed, not allthe texts contain representatives of each of these groups for the same vowel): stressed long vowels, unstressedlong vowels, stressed short vowels, andunstressed short vowels. In languages with non-contrastive duration it wasthe stressed vowels (both primary and secondary stressed) that weremeasured.

In connection with durational variation at the segmental level in languageswith contrastive duration the following tendencies were identified: (i)long stressed vowels occur with the greatest degree of durationalvariation, and (ii) the smallest degree of variation occurs in connection with short unstressed vowels. Anexample from Latvian illustrates this tendency: the durational increase or decrease observed forlong stressed vowels is within the range of +/- 41 msec, for longunstressed vowels +/- 26 msec, for short stressed vowels +/- 30 msec, andfor short unstressed vowels +/- 13 msec. In examining the additional three languages, it was observed that themaintenance of durational distance between short and long segments may berealized differently in relation to the degree of the durational variationsobserved. The range of the variation may be similar to that observed in Latvian (see example above); or itmay be larger (such as, for example, in Finnish, where the durational increase or decrease for long stressed vowel is withinthe range of 67 msec, for long unstressed vowels +/- 48msec, for short stressed vowels +/- 60 msec, and for short unstressedvowels +/- 59 msec). It appears that differences in terms of the range ofthese variations are language specific. The manifestation of durational variationimplies the presence of a pattern that assures the keeping of durationaldistance between long and short vowels within values serving thelinguistically significant distinguishingfunction.

Durational measurements of primary stressed vowels in languages whereduration is non-contrastive show a noticeably high degree of variation;measurement values in Brazilian Portuguese indicate an increase or decreasewithin the range of +/- 76 msec, in Cantonese +/- 91 msec, in Russian +/- 103 msec, and in English+/- 80 msec. The degree of variation attested to vowel segments bearingsecondary stress is lesser (in Brazilian Portuguese within the range of+/- 51 msec, in Cantonese +/- 78msec, in Russian +/- 90 msec, and in English +/- 67 msec).

Figure 2 summarizes the differentdurational patterns as described above in connection with the two languagetypes.

In evaluating the tendencies with regard to thedurational variations associated with segments as presented above, it may be stated that

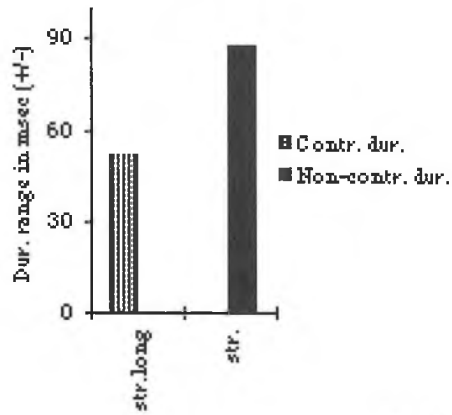

Figure 2 . Differences in vowel durationalvariations between the two types of languages

languages withcontrastive duration behave according to two distinct patterns: (i) thosewhere there is clear evidence of keeping the durational ratios ofthe segment constant, such as in Estonian (Krull and Engstrand 1994, Krull 1999) and in Saami(McRobbie-Utasi 1994), and (ii) those where it is important to maintain aclearly identifiable durational distance between short and long segments(such as in those languages examined in thepresent project).

4. CONCLUSIONS

A comparison of the realization of temporal patterns evident within theparagraph elicited during the course of this controlled experiment showsthat the two language types -- those with contrastive duration, and thosewith non-contrastive duration -- differ in the degree of variation associated with the paragraph constituentsexamined, and that this difference correlates with the degree of durationalincrease signalling boundaries. The apparent tendency for the maintaining of durational differences between long and short segments impliesthat, in languages with contrastive duration, durational increase plays alesser role in signalling the paragraph boundary than in languages withnon-contrastive duration where paragraph-final lengthening is more evident. (Because of the relatively smalldata base these conclusions can be considered as no more than tentative).

5. REFERENCES

Engstrand, O. and D. Krull. (1994). Durationalcorrelates of quantity in Swedish, Finnish and Estonian: Cross-languageevidence for a theory of adaptive dispersion. Phonetica, 51, 80-91.

Krull, D. (1999). Foot isochrony in Estonian. InProceedings of the 12th International Congress of PhoneticSciences, San Francisco. Vol. 2, 1063-1066.

McRobbie-Utasi, Z. (1994). Timing strategieswithin the paragraph. In Proceedings of the InternationalConference of Spoken Language Processing, Yokohama. Vol. 1,383-386.

McRobbie-Utasi, Z. (1999). Contrastive vs.non-contrastive duration in relation to temporal patterns within theparagraph. In Proceedings of the 12th International Congress ofPhonetics Sciences, San Francisco. Vol. 1, 249-252.

The Effect Of Noise On Foreign-Accented Speech: An Acoustic Analysis

Herman Chi Nin Li
Department of Linguistics, Simon Fraser University, Burnaby, BC V5A 1S6

1. INTRODUCTION

Etienne Lombard in 1911 reported that in the presence of noise, people with normal hearing increase their vocal intensity in order that their speech can be better heard by themselves or others [2]. This phenomenon is known as the Lombard reflex. It is well documented that speech produced in a noisy environment exhibits increases in vowel duration, fundamental frequency, and amplitude. The extent to which the Lombard reflex varies may be associated with the language, the type of noise, and the gender of speaker. Previous studies of the Lombard effect have been carried out mostly with native speakers. However, there has been limited research in accented speech under noisy condition. In addition, it has been noted that there is little research in investigating the influence of speaker-specific factor, like gender of speakers, on speaking rate [1]. Native Mandarin speakers of English have been found to speak at a slower rate in ideal (laboratory) environment than native English speakers do [6,7], but little is known about the speaking rates of native Cantonese speakers of English. The goal of this exploratory project was to investigate and compare the effect of noise on speaking rates of native Cantonese speakers with those of native English speakers in producing English sentences. Gender difference, if any, exhibited in speaking rate for the groups under the two conditions would also be examined.

2. METHOD AND EXPERIMENT

Speakers. Individual recordings were made of four adult native speakers of Hong Kong Cantonese (two male, two female). All had been born and raised in Hong Kong, and had moved to Canada after completing at least part of Form Five (secondary) in Hong Kong. Their mean age was 21.3 years. They had been living in Canada for a mean of 27 months. A comparison group of native speakers of Canadian English was also recruited. They were all born and raised in western Canada. Their mean age was 24 years. All participants had passed a hearing screen before recordings.

Recordings. A list of 12 true and 12 false statements was created as stimulus. Similar sets of statements had been used in other earlier studies [4,5,7]. Each item was a single-clause sentence of four to eight high-frequency words. The number of syllables ranged from five to 12. Having been instructed to try to produce the sentences in a conversational manner, participants read aloud to the researcher, who sat in front of the speakers at a fixed distance of two meters, the list of sentences once under each of the two conditions: quiet and noise. Participants wore a pair of headphones with an attached microphone throughout the experiment. Under the noise condition, cafeteria-like masking noise of 70 dB SPL(A), measured with a B&K sound level meter, was fed through the headphones to the speakers. No noise was presented to the speakers in the quiet condition. Participants were randomly assigned into two groups with balanced first language and gender. One of the groups read the list first under quiet and then under noise condition, while the other group read all the sentences in reverse order of condition. All the sentences had been randomized and no participant read the same version in the two conditions. Fluent utterance without noticeable pause or hesitation was elicited; otherwise, participants were asked to repeat the sentences. All recorded speech samples were digitized, and syllable rate (syll/s), obtained by dividing the syllables in each utterance by the duration, was computed.

3. RESULTS AND DISCUSSION

Mean speaking rates (syll/s) for utterances spoken in quiet and noisy conditions are shown for the two groups of speakers in Figure 1. An ANOVA was conducted to determine if first language (Cantonese and English) and condition (quiet and noise) had any effect on speaking rates. Results revealed significant effects of first language and condition on speaking rates, $Fs(1, 6) = 8.216$, and 28.912, $ps < 0.05$, respectively. No significant interaction between first language and condition was found. All these confirmed one of the manifestations of the Lombard effect that speakers generally have a tendency to speak slower in a noisy condition [3]. Moreover, the results indicated that Cantonese speakers in this experiment, like Mandarin speakers in earlier studies, speak reliably more slowly than their English counterparts. This may be due in part to the fact that a reduced speaking rate may sometimes lead to an increase in intelligibility, because nonnative speakers of English have more time to execute good articulations [6].

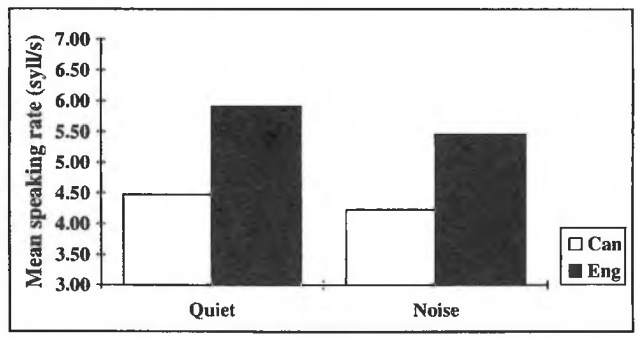

Figure 1. Mean speaking rates for Cantonese and English speakers in quiet and noise conditions

Figure 2 shows the mean speaking rates for statements spoken by females and males under the quiet and noise conditions in each of the two speaker groups. For the group of Cantonese speakers, no significant differences were found between female speakers in both quiet and noise conditions ($M = 4.52$ and 4.25 syll/s) and male Cantonese speakers ($M = 4.41$ and 4.20 syll/s), $ts(1, 94) = 0.582$ and 0.247, $ps > 0.05$. In contrast, female English speakers in both quiet and noise conditions ($M = 6.23$ and 5.91 syll/s) speak significantly faster than male English speakers ($M = 5.59$ and 5.00 syll/s), $ts(1, 94) = 3.088$ and 4.629, $ps < 0.05$. The latter findings might appear contradictory to results of some research where adult female English speakers are found to speak at a slower rate than male English speakers [1].

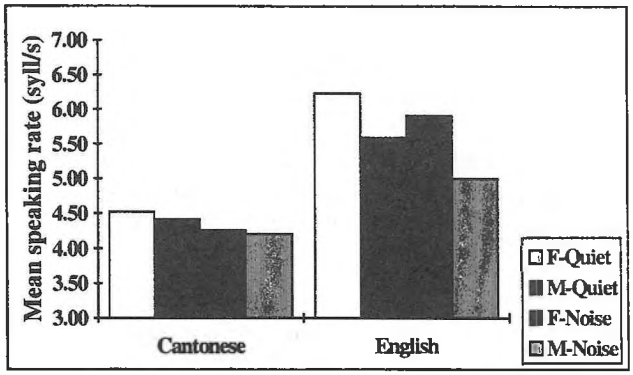

Figure 2. Mean speaking rates for females and males in the two speaker groups in quiet and noise conditions

4. CONCLUSIONS

In this experiment, the masking noise and the first language were found to have strong effects on speaking rates for the set of simple true and false English statements spoken by the native Hong Kong Cantonese and the native English speakers. The results suggest that under the influence of cafeteria-like noise, speakers with normal hearing probably slow down their speaking rates. One of the reasons may be that while speaking in such an adverse condition, the speakers modify their vocal output in order to maintain intelligible communication. Moreover, it is not surprising to find that native speakers of Cantonese speak more slowly than the English speakers in both the quiet and noise conditions. Further, although no gender difference in speaking rates was observed among the Cantonese speakers, female English speakers spoke faster than male English speakers in both conditions. No conclusive statement at this stage can be drawn, as it has been suggested that an account of such a sex-dependent difference needs further research [1]. Because of the limited number of participants and above all, the highly speaker-dependent and inter-speaker variability nature of the Lombard reflex, the results reported here cannot be extended too far. It is hoped that future research can involve more nonnative speakers of English and other types of noise to have a better understanding of the effect of noise on foreign-accented speech.

5. REFERENCES

[1] Byrd, D. (1992). Preliminary results on speaker-dependent variation in the TIMIT database. Journal of the Acoustical Society of America, 92(1), 593-596.

[2] Egan, J. (1971). The Lombard reflex: Historical perspective. Archives of Otolaryngology, 94, 310-312.

[3] Hanley, T., & Steer, M. (1949). Effect of level of distracting noise upon speaking rate, duration and intensity. Journal of Speech and Hearing Disorders, 14(4), 363-368.

[4] Munro, M. (1998). The effects of noise on the intelligibility of foreign-accented speech. Studies in Second Language Acquisition, 20, 139-154.

[5] Munro, M., & Derwing, T. (1995). Processing time, accent, and comprehensibility in the perception of native and foreign-accented speech. Language and Speech, 38(3), 289-306.

[6] Munro, M., & Derwing, T. (1998). The effects of speaking rate on listener evaluations of native and foreign-accented speech. Language Learning, 48(2), 159-182.

[7] Munro, M., & Derwing, T. (1999). The effects of speaking rate on the comprehensibility and accentedness of L2 speech. Manuscript submitted for publication.

6. ACKNOWLEDGEMENT

The author would like to thank Dr. Murray Munro for his advice on this research. This work was supported by the Social Sciences and Humanities Research Council of Canada.

A message from John Bradley - The Role of a CAA DIRECTOR

A director of the Canadian Acoustical Association is expected to enthusiastically and energetically support and promote the interests of the association wherever possible. Directors are responsible for managing theaffairs of the association and are expected to attend two board of directors meetings each year. Directors are expected to take an active role in the association including helping to organise sessions at our annual conference and by encouraging authors to submit contributions to our journal Canadian Acoustics.

Acoustical Correlates for Seven Styles of Singing

Laura Anne Bateman
University of Victoria, McPherson Library, Victoria, BC V8W 3H5

Legend has it that one day Garcia was strolling down the street. He was thinking of his sister, a famous opera diva and wondering how people could create such beautiful sounds. Could he find a way to look inside the instrument and see how it worked? Just at that moment, the sun caught the tip of his walking stick and the light was reflected onto his face. The idea of the laryngeal mirror was conceived and voice science born. These early efforts in voice research took place in the first half of the 19C. By the late 1800's incandescent light was used with stroboscopy to provide more answers, but it wasn't until the development of microtechnology such as fiberoptics, digital analysis and imaging techniques in the 20C that voice science has made the greatest strides.

This century William Vennard, was one of the American pioneers in singing research. He looked at the acoustics and physiology of the classical singing voice. (Vennard, 1967) Johan Sundberg, has also provided much information about the classical singing voice from his continuing research at KTH Voice Research Centre in Sweden. (Sundberg, 1987). The first singing qualities studied were "trained" singers vs "untrained" singers. These early studies provided some answers but, as Jo Estill, an American voice teacher and researcher pointed out in a recent email correspondence "...they are trained or untrained. But trained to do what." (Estill, 1997). Sundberg has since become more specific with the type of voice quality and expanded his focus to include choral, belt and twang qualities. Jo Estill has broadened the scope further to include six basic voice/singing qualities: speech, falsetto, sob, opera, twang, and belt. (Estill, 1996) Ingo Titze has also written extensively on the physics of the singing voice. (Titze, 1994) However, many of the voice qualities people use in contemporary popular music remain somewhat of a mystery acoustically and physiologically.

Voice quality research also has another branch in the field of Linguistics. The most comprehensive taxonomy comes from John Laver, University of Edinburgh. (Laver, 1980). Some is quite specific to the speaking voice, but the concepts can be adapted to the singing voice. Voice quality in speech "is the auditory colouring of an individual speakers voice" (Laver, 1980 pg 1) and involves voice quality settings. For example, a speaker might have a tendency to keep the lips rounded throughout speech. This colours the speaker's utterance. Laver further divides voice quality settings into laryngeal and supralaryngeal settings. These are present for the duration of the speech sequences. For example, the previous subject may have used modal voice with labial protrusion. Modal voice would refer to the laryngeal setting and labial protrusion would refer to the supralaryngeal setting. These settings have corresponding diacritics. In singing, the same concepts can also be applied. For example, using Laver's taxonomy, a belter might use modal voice with a pharyngealized tongue body notated as a capital V with two horizontal wavy lines through it. This describes a physiological configuration, but it is also an auditory label with an acoustic correlate. Phonetic taxonomy also describes speech as having specific units called segments (vowels and consonants). These segments have articulatory, acoustic and perceptual features. As with a speech dialect, segmental features can be analysed in singing style for acoustic correlates. For example, the pop style may use a less aspirate "t" than the classical style. The classical "ah" may be darker than the bright country "ah". This presentation will focus on the acoustic correlates of voice quality settings however, segmental features may also be discussed.

Jo Estill refers the combination of features as a "recipe" and trains singers to make a series of physiological adjustments to obtained a prescribed voice quality. Her list of parameters include: onset, constriction and retraction of the false vocal folds, vocal fold plane, vocal fold mass, laryngeal tilt, soft palate control, anchoring, pharyngeal width, pharyngeal length, tongue control aryepiglottal constriction. Dang and Honda (1996) also clarified the strong effect that the piriform sinuses have in voice quality. Physiological correlates for this presentation are currently under investigation and will not be discussed, however, acoustic results may be compared to the existing literature.

Much acoustic description of the voice still uses a model developed by Fant. (Fant, 1960) He described the voice using a linear model involving a source and three filters. He assumed the glottal source to be white noise filtered at the glottis to produce a source function which decreases by 12dB per octave in strength, the vocal tract as a single tube closed at one end which acts as a second filter producing the odd numbered formants at approximately 500Hz, 1500Hz, 2500Hz etc. and the radiation effect as a third filter with a function increasing by 6dB per octave. This is the model which analysis algorithms such as LPC use so it is worth mentioning. Whether this model is "good enough" is always a contentious issue and the development of other models (Titze, 1997) and analysis algorithms is ongoing. The analysis methods used in this investigation are Spectrograms generated using Fast Fourier Transform algorithm in 3D graphic format (CSL software), and LPC using the auto-regressive model and autocorrelation (solved using the Levinson function). Transfer function plotted using z-transform digital filter frequency response. (Matlab software). Decisions as to sampling rate, order number, windowing, preemphasis and other settings will be discussed.

The data for this presentation comes from a case study of Lisa Popeil, a singing teacher and performer, who can produce seven voice quality settings: pop, jazz, R&B, belt, opera, legit, country. Ms. Popeil has been a Los Angeles studio musician for many years and her singing styles have been heard on radio, advertising, cd, video and in live performance with such notable artists as Frank Zappa and Weird Al Yankovic; therefore, the samples obtained are believed to approximate the norm for the singing styles under consideration. This presentation will focus on formant placement. Steady state and running sample vowels were sampled and analysed to determine formant frequencies and approximate energy in each formant. The values were then compared. Similarities and differences between the styles were noted. The styles will be related to labelling schemes by Jo Estill and John Laver. Perceptual testing has not been included in this investigation.

This type of research has been a great help to singing teachers as well as engineers for producing voice enhancement and education-

al tools for singers.

REFERENCES:

DANG, J. and HONDA, K. (1996). Acoustic characteristics of the piriform fossa in models and humans. J.Acoust.Soc.Am. 100, 3374-3383.

ESTILL, J., FUJIMURA O., SAWADA A. AND BEECHLER K. (1996), Temporal Perturbation and Voice Qualities in P. Davis and N Fletcher (Eds) Vocal Fold Physiology: Controlling Complexity and Chaos, V.9 Ch. 16 237-252 San Diego: Singular Publishing Group.

ESTILL, J. (1997) Email correspondence Feb. 5/97.

FANT, G. (1960), Acoustic Theory of Speech Production. The Hagues:Mounton.

LAVER, J (1980). The Phonetic Description of Voice Quality. Cambridge: Cambridge University Press.

TITZE, I. (1994). Principles of Voice Production. New Jersey: Prentice Hall.

TITZE, I. and STORY, B. (1997) Acoustic Interactions of the Voice Source with the Lower Vocal Tract. J.Acoust.Soc.Am. 101(4), 2234-2243.

SUNDBERG, J. (1987). The Science of the Singing Voice.. Illinois: Northern Illinois University Press.

VENNARD,W. (1967). Singing The Mechanism and the Technic.. New York: Fischer.

Relation between Performance and Confidence Ratings for Sound Localization in Free-Field and Virtual Acoustic Space

G.R. Arrabito, J.R. Mendelson, S.L. Van Blyderveen, R.B. Crabtree and M.J. Boultbee
DCIEM, 1133 Sheppard Ave. W., P.O. Box 2000, Toronto, ON M3M 3B9

INTRODUCTION

A relatively new technology, the three-dimensional (3-D) audio display, is being explored for improving aircrew performance. The presentation of virtual auditory cues over headphones to serve as warnings (e.g., weapons, other aircraft) to the aircrew is one application. Accurate localization of the virtual cues necessitates that the aircrew exhibit a high degree of confidence when making localization judgements.

In general, individuals are overconfident in their performance on knowledge-based tasks [1]. This overconfidence is exacerbated the more difficult the knowledge-based task becomes [2]. Underconfidence is more common in perceptual-based tasks, particularly when the task is not difficult [1]. If the perceptual task is comparable in difficulty to a knowledge-based task, then overconfidence is exhibited [1].

It could be detrimental if a pilot, who is in error of his/her localization judgements, is nonetheless extremely confident in making that judgement. To the best of our knowledge, there is no reported study on confidence ratings for localization judgements. The use of confidence ratings on localization judgements in free-field and virtual acoustic space was investigated in this study. Subjects made confidence ratings on a seven-element Likert scale after each localization judgement.

METHOD

Subjects. Five females and five males participated (mean age was 28.1 years). All subjects had normal hearing as verified by audiometric screening.

Stimuli and Apparatus. The stimuli were low-pass 4 kHz and 14 kHz, and high-pass 4 kHz white noise with duration of 300 ms with a 50 ms onset and decay. These were chosen to allow an assessment of the effectiveness of binaural and spectral cues.

Testing was performed in an Industrial Acoustics Company sound-attenuating listening booth. The booth contained a chair that was positioned in the centre of eight Axiom Millennia loudspeakers (model AX1.2) arranged in a circle with a radius of one metre centered at the seated listener's head. Each loudspeaker was mounted on a Yorkville adjustable microphone stand so that the vertical midpoint of each speaker was at the same height as the listener's ear level. The loudspeakers were placed at 45° intervals ranging from 0° to 315° azimuth increasing clockwise on the horizontal plane with 0° positioned directly in front of the listener. The transmitter of a Polhemus 3Space Fastrak magnetic head tracker was suspended from the ceiling of the sound booth at approximately 12cm directly above the listener's head to monitor the subject's head position. The tracker's receiver was placed on the top of the listener's head and was held in position by a headband worn by the listener. Localization judgements were made on a response box whose buttons were arranged in the same configuration as the loudspeaker array. A separate seven button response box was used for collecting confidence ratings. These buttons were labeled -3 (very unconfident), -2 (moderately unconfident), -1 (somewhat unconfident), 0 (neutral), +1 (somewhat confident), +2 (moderately confident), and +3 (very confident).

A Stax electrostatic headphone (model SR-l Signature) was used to present the stimulus in virtual acoustic space (VAS). The head-related transfer functions (HRTFs), digital filters for synthesizing the location of a sound in VAS, used in this study were measured from the first author. The Tucker-Davis Technologies system in conjunction with custom software running on a personal computer was used to present the stimulus in free-field and VAS.

Experimental Design. A 2 (auditory presentation mode) X 3 (acoustic stimulus) X 8 (azimuth) X 4 (session) within-subject repeated measures design was employed to measure localization performance and confidence ratings. Each acoustic stimulus condition was presented in both free-field and VAS at the eight azimuth positions on the horizontal plane described above. A Latin Square was employed to counterbalance auditory presentation modes, acoustic stimuli, and azimuth positions across subjects and sessions.

Procedure. On each day of testing the subject completed the three acoustic stimuli conditions in free-field and VAS. After all three acoustic stimuli conditions were completed in the same auditory presentation mode (e.g., free-field), the subject proceeded to the other auditory presentation mode. The ordering of auditory presentation modes was randomly determined. Each acoustic stimulus condition consisted of 8 practice trials followed by 104 experimental trials, with each azimuth position used once in the practice trials and 13 times in the experimental trials. Each trial began by flashing a 0.5 second light on the wall in front of the subject followed by a 0.5 second delay prior to the presentation of the stimulus. The subject's task was to identify the perceived location of the stimulus followed by a confidence rating on the seven-element Likert scale for that localization judgement.

Localization judgements and confidence ratings were made on the response boxes described above. If, during the presentation of the acoustic stimulus, the subjects moved their heads more than 2° in any direction of yaw, pitch or roll as monitored by the head tracker, then the subjects were notified by flashing LEDs to reposition their heads to the "straight-ahead" position. The trial was discarded and was presented again at the end of the current block of trials. No feedback was given to the subjects. Subjects completed two practice and four experimental sessions, each on separate days.

RESULTS AND DISCUSSION

A preliminary analysis of the pooled data on the four experimental sessions revealed that localization performance as measured by percent correct localization judgements was better in free-field (95.9%) than VAS (76.1%). Subjects made more reversals (i.e., perceiving the mirror image of the presented sound source) in VAS (9.2%) compared to free-field (1.6%). Performance was nearly identical regardless of the acoustic stimulus. These findings appear to be in partial agreement with those reported in [3].

Figure 1 shows the confidence ratings corresponding to correct

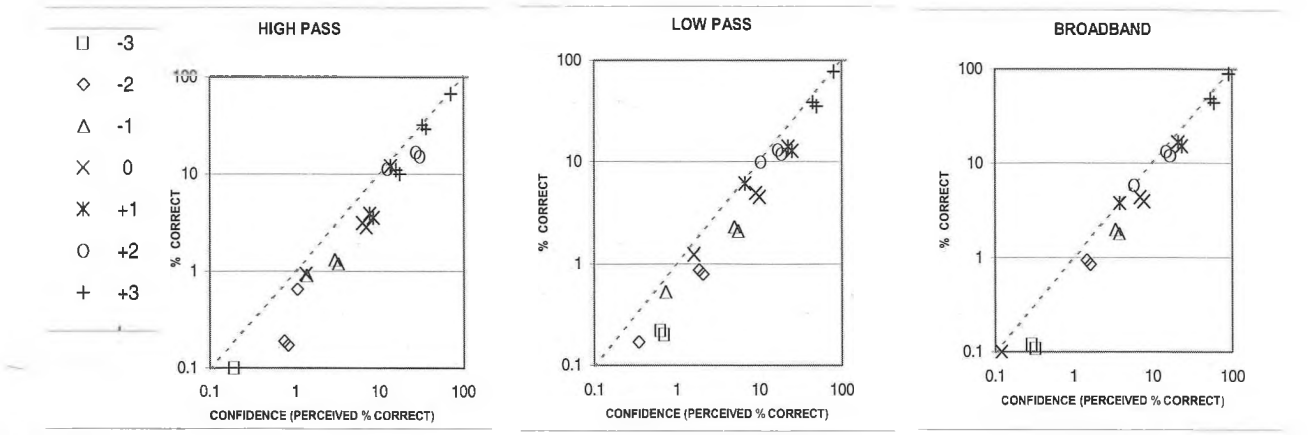

Figure 1. Confidence ratings corresponding to correct versus perceived localization performance. Data are shown for each acoustic stimulus condition in free-field (non-shadowed) and VAS (shadowed). The dotted line represents perfect calibration.

localization judgements as a function of confidence ratings corresponding to perceived localization performance. Subjects had higher confidence in their free-field responses compared to those made in VAS. In the free-field, subjects were close to "perfect calibration". An individual is said to be well calibrated if, in the long run, for all propositions assigned a given probability the proportion correct is equal to the probability assigned [2]. However, subjects were overconfident in VAS, which suggests that the choice of the HRTFs made the localization task too difficult.

The VAS localization performance of the first author, who was one of the subjects, was nearly identical to his free-field performance. He had closer to perfect calibration than all the other subjects. This was most likely due to the fact that he was the only subject who used his own HRTF. Indeed it has been argued that listeners localize a virtual sound better when using HRTFs measured from their own heads ("personal"), as compared to HRTFs measured from a different head ("generic") [3].

The present results suggest that if virtual auditory cues are to serve as warnings to the aircrew then the use of generic HRTFs may convey an inaccurate sense of confidence for making correct localization judgements. They further suggest that the use of personal HRTFs may provide closer to perfect calibration compared to generic HRTFs. However, acquiring personal HRTFs requires a substantial investment in infrastructure and equipment and is currently impractical in many applications. Methods need to be developed to quickly and accurately select a generic HRTF for conveying accurate localization.

REFERENCES

1. Keren G. On the ability of monitoring non-verdical perceptions and uncertain knowledge: Some calibration studies. Acta Psychologica 1988; 67:95-119.

2. Lichtenstein S, Fischoff B & Phillips D. Calibration of probabilities: The state of the art to 1980. Chapter 22, In: D. Kahneman, P. Slovic and A. Tversky, eds. Judgement under uncertainty: Heuristics and biases, Cambridge University Press, Cambridge, 1982.

3. Wightman FL & Kistler DJ. Headphone simulation of free-field listening part II: Psychophysical validation. J Acoust Soc Am 1989; 85(2): 868-878.

A Comparative Study On Cantonese Rising Tones: Native Cantonese Speakers And Canadian Raised Cantonese Speakers

Connie Kwok Lai So
Department of Linguistics, Simon Fraser University, Burnaby, BC V5A 1S6

1. INTRODUCTION

The two Cantonese rising tones, the High Rising (Tone 2) and the Mid-Low Rising (Tone 5), are traditionally described as Tone 35 and Tone 23. Recent studies, however, show that the High Rising tone has changed from Tone 35 to Tone 25 (Bauer, 1997). It starts at a pitch level similar to that of the Mid-Low Rising tone. The High Rising tone is also described to have a long and sharp rise from the midway of its fundamental frequency (Fo) contour pattern (Bauer 1997: 133). There is also a temporal difference among all the lexical tones in Cantonese. The High rising has the longest duration (Kong, 1987: 396). Cantonese rising tones produced by Canadian Born/ Raised Cantonese speakers seem to be under-investigated (So 1997, 1998). The present study aims to assess the above phenomena in these speakers.

2. THE EXPERIMENT

This study recruited 12 adult speakers in two groups, (3 females and 3 males in each group). The first group consisted of those who were either Canadian Born Cantonese speakers, or who had immigrated to Canada before age of seven (hereafter, I called them as CRC, since all of them were raised in Canada). The second group is a comparison group formed with Native Hong Kong Cantonese speakers (NC), who had moved to Vancouver within two years. Productions of their rising tones in citation forms were acoustically analyzed and compared in the aspects of temporal and fundamental frequency (Fo) contour patterns.

Four target words with the High and the Mid-Low rising tones on two root-words /si/ and /fu/ were used. These words were /si 2/ "history" , /si 5/ "city'', /fu 2/ "tiger'' and /fu 5/ "woman". Totally, 480 tokens of these four target words produced by the speaker groups (i.e., 10 tokens of each target from individual speaker) were examined.

3. RESULTS AND DISCUSSION

3.1. TEMPORAL PATTERNS

The temporal patterns between the two rising tones and between the speaker groups were compared. Durations were measured in three different domains of the words - whole syllable (S), prevocalic consonant (C), and vowel (V). Table 1 shows the mean durations and standard deviations of Tone 2 and Tone 5 on /si/ and /fu/ in the NC and the CRC. The data were submitted to three separated ANOVAs for the three domains to see if speaker groups, rising tones, and root-word types had any effect on the duration in the three respective domains (S, C, and V). For all these three domains, no main effects of any factors and no interactions of the factors were found (*ps* > 0.05). The results suggest that durational differences at syllable, prevocalic consonant, and vowel do not play an important role in differentiation between the two tones and between the speaker groups, at least in citation forms. However, there was a non-significant tendency that the durations of Tone 2 were slightly longer than those of Tone 5, except the pairs in /fu/ at S and C in the CRC, and the pair in /fu/ at V in the NC (see Table 1).

3.2. Fo CONTOUR PATTERNS

The method to compare Fo contour patterns between the two rising tones and between the speaker groups has been used in earlier studies (So, 1997, 1998). Fo contours of individual tokens were first obtained through pitch extraction. Then, their durations were normalized using five temporal reference points (at 0%, 25%, 50%, 75% and 100%). Since the mean Fo contour patterns of Tone 2 and Tone 5 on /si/ and /fu/ in each group were very close to each other, the data were collapsed and were averaged to form two mean contours for Tone 2 and Tone 5 in each group. The contour patterns of the two rising tones of groups are shown in Figure 1. The onsets of Tone 2 and Tone 5 in both the NC and the CRC started at a similar level of Fo height, and had a falling pattern from 0% to 25%. In the NC group, the mean contour of Tone 2 began to rise from 25%, and had a sharp rise from 50 to 100%. The mean contour of Tone 5 only rose gently from 25% toward 100%. As a result, the Fo differences between Tone 2 and Tone 5 gradually increased toward the end. Similar to the contour patterns of the NC, the contour of Tone 2 in the CRC was also located on top of the one of Tone 5. However, the Fo height of Tone 2 was close to that of NC's Tone 5, and the slope of Tone 2 in the CRC was less steeper than that of the NC's. It was also noted that the range of Fo height for the two tones in the NC was observed to be much larger than that of the CRC.

		NC		CRC	
Domains	**Tones**	**/si/**	**/fu/**	**/si/**	**/fu/**
S	T 2	511.51 (61.49)	499.97 (48.60)	506.28 (90.79)	476.29 (81.92)
	T 5	503.97 (62.09)	494.97 (57.67)	496.06 (93.85)	476.88 (85.10)
C	T 2	206.80 (43.65)	175.22 (29.69)	205.44 (47.09)	176.95 (52.85)
	T 5	201.26 (40.97)	174.94 (45.34)	205.21 (47.29)	181.93 (57.99)
V	T 2	304.71 (39.73)	317.73 (38.12)	300.83 (61.78)	299.34 (63.15)
	T 5	302.71 (38.69)	320.04 (40.63)	290.85 (66.17)	294.95 (61.30)

Table 1. Speaker groups' mean durations and standard deviations (in parentheses) of Tone 2 and Tone 5 on /si/ and /fu/.

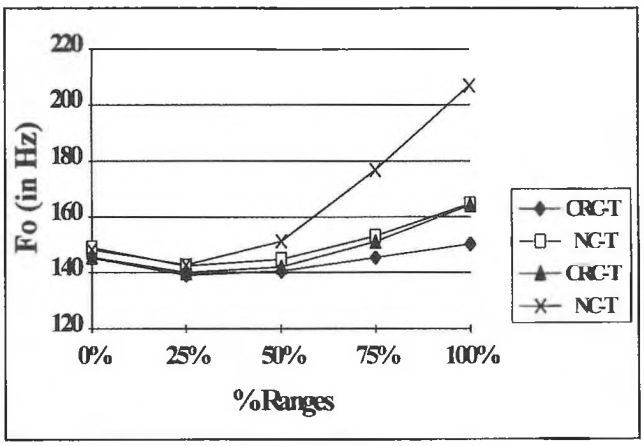

Figure 1. Fo contours for Tone 2 and Tone 5 in the CRC and the NC groups.

In order to compare the relative slopes of the contours between the speaker groups, the differences in changed Fo (ΔFo) among the five reference points, [i.e., four ranges; hereafter R1(0-25%), R2 (25-50%), R3 (50-75%), and R4 (75%-100%)], were investigated. Since durations of individual contours had been normalized, the slopes of these ranges could be interpreted as a function of ΔFos in the four durational ranges. Thus, comparison of ΔFos in the ranges might be fruitful.

The ΔFos data of the rising tones for the NC and the CRC were submitted to a mixed-design ANOVA with speaker groups (G) as between-subjects factor, and durational ranges (R) and tones (T) as within-subjects factors. The result revealed significant main effects of G [F (1, 22) = 18.007, p <0.01], R [F (3, 66) = 49.157, p < 0.01], and T [F (1, 22) = 74.800, p < 0.01]. The results also indicated significant G x R [F (3, 66) = 20.472, p < 0.01], G x T [F (1, 22) = 18.892, p < 0.01], and R x T [F (3, 66) = 47.820, p < 0.01] interactions. Moreover, significant G x R x T interaction was found [F (3, 66) = 8.872, p < 0.01].

Two separated 1-way ANOVAs with durational ranges (R) and tones (T) as within-subjects factors for the CRC and the NC were also conducted to explore the effects of R and T on the ΔFos in each group. The analyses revealed significant main effects of R [Fs (3, 33) = 6.032 and 56.436, ps < 0.01], and T [Fs (1, 11) = 20.091 and 54.852, ps < 0.01], as well as significant R x T [Fs (3, 33) =15.736 and 33.236, ps <0.01] interactions in the NC and the CRC respectively. Individual t-tests for the CRC and the NC further indicated that the differences in ΔFos at R1 and R2 (i.e., the first 50%) between Tone 2 and Tone 5 in CRC were non-significant (ps > 0.05), but significant at R3 and R4 (ps < 0.01). On the other hand, the differences in ΔFos between the two rising tones in the four ranges in the NC group were all significant (ps < 0.01), except at the R1 (p > 0.05) (i.e., the first 25%). (See Figure 2 and 3). All these statistical results suggest that Tone 2 and Tone 5 can be differentiated within each group on the basis of ΔFos in the four durational ranges. Nevertheless, the timing for the NC to differentiate the two tones is earlier than that of the CRC (i.e., R2 vs. R3).

4. CONCLUSIONS

In this exploratory experiment, it is found that Tone 2 did not have durational patterns significantly longer than Tone 5 at the three domains (i.e., syllable, prevocalic consonant and vowel) in both the NC and the CRC. With respect to the onsets of the two rising tones, the contour patterns in Figure 1 clearly demonstrate that the onsets of the two tones are very close to each other in both speaker groups. However, the overall range of Fo height for Tone 2 and Tone 5 in the NC is wider than that of the CRC. It is surprising that the differences of the changed Fo height in the four durational ranges between the two rising tones for the CRC was found to be different from those of the NC in this study. Lastly, since the timing associated with ΔFos in differentiating the two tones is found to be different in productions between the two speaker groups, it is not unreasonable to suggest that Canadian Raised Cantonese speakers may also exhibit deviation from Native Cantonese speakers in perception of the two rising tones. However, this issue awaits further research.

REFERENCES

Bauer, R. (1997). *Modern Cantonese Phonology.* New York: Mouton de Gruyter.

Kong, Q. M. (1987). "Influence of tone upon vowel duration in Cantonese", *Language and Speech.* 30 (4) p. 387-399.

So, C. K. L. (1997) "An acoustic study of Cantonese tonal patterns in young Canadian Chinese", (manuscript), SFU.

_____. (1998) "Difference in tonal productions between Canadian raised Cantonese and native Cantonese speakers", In Lee, K. and Oliveira, M. (eds.), *Proceedings of the 14th North West Linguistics Conference*, held at Simon Fraser University on March 7-8, 1998, Department of Linguistics, SFU, 156 - 165.

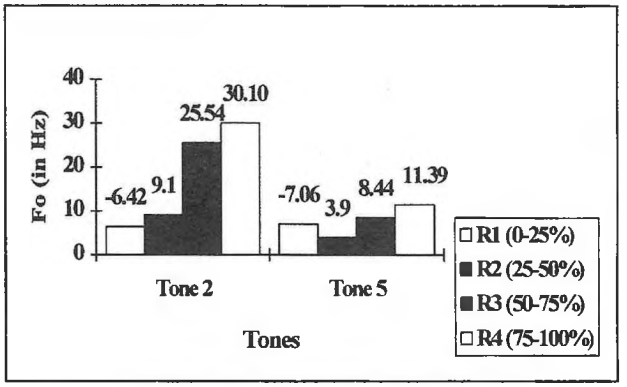

Figure 2. Average Changed Fos of Tone 2 and Tone 5 in the NC.

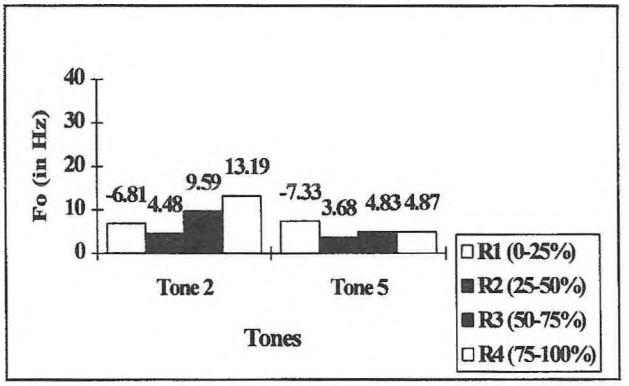

Figure 3. Average Changed Fos of Tone 2 and Tone 5 in the CRC.

The Perception of Spoken Language by Elderly Listeners: Contribution of Auditory Temporal Processes

Natalie Haubert and Kathleen Pichora-Fuller
University of British Columbia, 5804 Fairview Avenue, Vancouver, BC, V6T 1Z3

I INTRODUCTION

Older adults, even those with normal pure-tone hearing thresholds, commonly report difficulties understanding spoken language, particularly as the listening task becomes more challenging (CHABA, 1988). Fast speaking rate and background noise both make listening more challenging.

Numerous studies have established that older normal-hearing adults show decrements in the perception of spoken language presented in a background of competing noise (e.g. Gordon-Salant & Fitzgibbons, 1995; Stuart & Phillips, 1996). Age-related decrements in comprehension for fast speech rates have also been found in numerous studies (e.g. Letowski & Poch. 1996; Schmitt & Carroll, 1985: Wingfield, 1996). At the level of a single word, Price & Simon (1984) showed that rate can influence an elderly listener's ability to identify words where the distinguishing feature is a silent interval (e.g. 'rabid' vs. 'rapid').

A number of possible factors have been proposed to account for older adults' difficulties understanding spoken language. Some researchers believe that small changes in pure-tone high frequency sensitivity account for the poorer speech perception abilities of older adults (e.g., Humes, 1996). Others propose that changes in cognitive ability are responsible for these language processing deficits (e.g., Wingfield, 1996). Hypotheses based on auditory processing deficits, other than threshold hearing loss, constitute another plausible position.

One particular auditory processing ability of interest is temporal resolution. The ability of the auditory system to accurately analyze events that occur over time is critical to the understanding of spoken language. In fact, a large portion of sentence information is carried solely by temporal structure (e.g., Shannon, Zeng, Kamath, Wygonski, & Ekelid, 1995).

Gap detection thresholds provided one means of quantifying temporal resolution ability. In regards to older adults, many studies do indicate that they have reduced temporal resolution ability when examined in relation to young listeners and that this impaired gap detection ability is unrelated to audiometric thresholds (e.g., Strouse, Ashmead, Ohde, & Grantham, 1998; Schneider, Pichora-Fuller, Kowalchuk, & Lamb, 1994). Furthermore, an important relationship has been demonstrated between the duration of the markers surrounding a gap and gap detection thresholds, with age effects being significant when the marker duration is short (e.g. 2.5 ms) but not when it is long (e.g. 500 ms) (Hamstra & Schneider, 1999).

Decreased ability to detect gaps seems likely to interfere with some aspects of speech perception, especially at fast speaking rates. To date, however, no clear relationship has been found between gap detection ability and speech perception in old age (e.g. Strouse, Ashmead, Ohde, & Grantham, 1998). It may be that some relationship does exist, but that the particular stimuli used in these studies did not allow for this potential connection to be observed.

The purpose of the present study is to examine gap detection thresholds and speech perception abilities for stimuli selected to be representative of the challenging listening conditions in question. We assume that there is a correspondence between the marker-gap-marker sequence in a gap detection experiment and the VCV sequence in speech where C is a stop consonant. Therefore, a clearer relationship between measures of gap detection ability and speech perception should be observed in challenging conditions when the marker duration is short and the speech rate is fast compared to less challenging conditions when the marker duration is long and the speech rate is slow.

II METHOD

A. SUBJECTS

Eight young listeners (20-30 years old) and eight older listeners (68-74 years old) were tested. All listeners had pure-tone audiometric thresholds equal to or better than 25 dB HL from .25 to 3 kHz. All listeners were native speakers of English.

B. PROCEDURES

Each listener completed three tasks in the following order: word identification in quiet, gap detection, and word identification in noise. All testing took place in a double-walled, sound-attenuating IAC booth with stimuli presented monaurally over TDH-39 headphones.

Word Identification in Quiet

Four word pair continuums consisting of 14 tokens each were tested in quiet: 'cash'-'catch', 'dish'-'ditch', 'slit'-'split', and 'soon'-'spoon'. The slow speech rate continuums were based on naturally-spoken tokens of 'cash', 'dish', 'slit', and 'soon', respectively. To create the other members of each continuum a silent interval was inserted into the words and systematically adjusted in length to progress from short (5-10 ms) to long (75-120 ms). As the length of the inserted silent interval increased, the other member of the stimulus continuum, e.g. 'catch', was approximated. A fast speech rate continuum was also created for each word pair based on the originally spoken token. The original tokens were compressed to about two thirds of their original duration by deleting portions from the steady-state portions of the signal. All deletions were made at the zero-crossings in the signal to avoid any waveform discontinuities. Using these edited original tokens, silent intervals were inserted into the words and the length of the interval adjusted to construct the remaining 13 members of each continuum.

Subjects were presented with these tokens in a single-interval two-alternative forced-choice paradigm. The listeners first heard the ordered continuum presented twice. This served to familiarize the listeners to the materials. The tokens were then presented ten times each in random order. This sequence of events was then repeated allowing for the collection of 20 responses to each member of each stimulus continuum by each subject. The order of presentation of the stimulus continuums was counterbalanced across listeners with each listener first listening to the slow speaking rate continuums and then the fast speaking rate continuums. The stimuli were all presented at 40 dB SL referenced to the listener's SRT.

Gap Detection

Following Schneider and Hamstra (1999), the materials consisted of 2-kHz tonal gap and non-gap stimuli created by summing a number of temporally distributed Gaussian envelopes. Five gap marker durations were assessed: 0.83, 5, 10, 80, and 400 ms. The rise and fall times of the stimuli was held constant with stimulus duration specified from the peak of the first Gaussian envelope to the peak of the final Gaussian envelope. In order to prevent off-frequency cues resulting from spectral splatter, the gap detection stimuli were all presented in an amplitude-modulated broadband noise constructed to simulate a 6-person babble (ICRA, 1997). The gap detection stimuli were presented monaurally at 90 dB SPL and the noise was presented at 85 dB SPL to the same ear.

The gap detection stimuli were presented in a two-interval forced-choice paradigm. The gap size was either increased or decreased according to a 3 down 1 up rule to determine the 79.7% point on the psychometric function (Levitt, 1971). The duration of the gap markers changed after each run in the same irregular order for each participant. This order was cycled through four times, with the gap detection threshold being established as the mean of the final three runs.

Word Identification in Noise

The testing of word identification in noise was based on each listener's word identification performance in quiet. Only two stimulus tokens from each stimulus continuum were selected for further testing in noise, one for which one member of the pair was identified correctly at least 80% of the time and one for which the other member of the pair was identified correctly at least 80% of the time. In the few cases where a listener did not reach this criterion level of performance in quiet, testing was not completed in noise for that particular stimulus continuum. Testing was conducted at three signal to noise levels: 10, -5, and –15 dB, presented in order from most to least favorable and with the signal level held constant at 40 dB SL referenced to the listener's SRT. The same noise that was used in the gap detection task was used for the word identification test in noise. Following a period of familiarization at each noise level, the

selected tokens were presented 20 times each. The selected tokens were presented in the same order as the corresponding continuums had been presented in quiet. As in quiet, word identification performance was assessed using a single-interval two-alternative forced-choice design.

III RESULTS

A. WORD IDENTIFICATION IN QUIET

All young subjects were able to distinguish the word pairs in quiet at both rates; however, some old subjects were unable to distinguish the 'slit'-'split', 'soon'-'spoon', and 'dish'-'ditch' contrasts even in quiet, and especially for the fast rate. For both slow and fast speech rates, the word boundary for the old listeners occurred at longer gap durations than for the younger listeners. For both age groups the word boundary occurred at longer gap durations for the slow rate than for the fast rate. Significant age by gap duration effects on word identification were found for 'cash'-'catch' at the slow rate (Figure 1) and for all of the other pairs at the fast rate. These findings were confirmed by analyses of variance (ANOVA) conducted for each word pair at each rate.

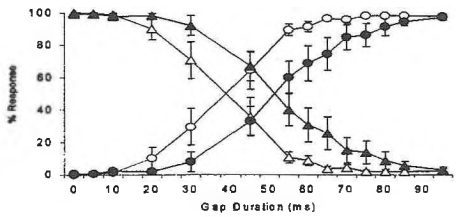

Figure 1: Word identification scores and standard error bars as a function of gap duration for 'cash'-'catch', slow rate. Unfilled triangles: young 'cash'; filled triangles: old 'cash'; unfilled circles: young 'catch'; filled circles: old 'catch'.

B. GAP DETECTION

As shown in Figure 2, the results of this study replicate prior findings by Schneider and his colleagues (Schneider & Hamstra, 1999; Schneider et al., 1994). At the two shortest marker durations (0.83 and 5 ms), the mean gap detection thresholds of the older listeners (mean = 7.399 ms and 6.073 ms, respectively) differed significantly from those of the younger listeners (mean = 2.938 ms and 2.227 ms respectively), as confirmed by an ANOVA [$F(1,4) = 2.987$, $p<.05$] and a Student-Newman-Keuls test ($p<0.01$).

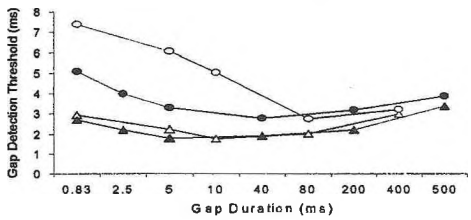

Figure 3: Gap detection thresholds as a function of marker duration for younger and older adults. Unfilled triangles: young adults, present study; filled triangles: young adults, Schneider and Hamstra (1999); unfilled circles: young adults, present study; filled circles: Schneider and Hamstra (1999).

C. WORD IDENTIFICATION IN NOISE

For all word pair contrasts, the addition of noise had a more adverse effect on word identification in the fast speech conditions than in the slow speech conditions. Specifically, word identification declined more for the member of the pair with the stop consonant. Age effects were not apparent for the 'cash'-'catch' and 'dish'-'ditch' pairs, but the old subjects performed more poorly than young subjects on the 'slit'-'split' and 'soon'-'spoon' pairs, especially at the fast rate (Figure 3).

D. CORRELATIONS

Overall, there was no clear pattern of correlations between audiometric thresholds and gap thresholds, consistent with the results of Schneider and his colleagues (Schneider & Hamstra, 1999; Schneider et al., 1994). Neither was there any clear pattern of correlations between the audiometric thresholds or the gap thresholds and word identification measures. The absence of clear patterns of significant correlations is not suprising given the small number of subjects in each age group.

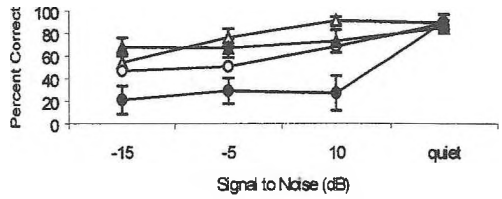

Figure 3: Word identification as a function of signal to noise ratio for 'slit' and 'split' fast speech rate. Unfilled triangles: 'slit' young adults; filled triangles 'slit' old adults; unfilled circles: 'split' young adults; filled circles: 'split' old adults.

IV DISCUSSION

The data from this study indicate that older adults are poorer than younger adults at detecting gaps embedded in non-speech stimuli (2 kHz markers) when the surrounding material is short. Correspondingly, older adults were also shown to have greater difficulty identifying speech when a gap served to differentiate two words, particularly for fast speech. Common to both these cases is the poorer performance evidenced by old listeners in the context of fast rates/ short duration stimuli. This pattern of findings is consistent with a hypothesis that proposes that recovery from neural adaptation occurs more slowly in the old compared to the young auditory system (Schneider & Hamstra, 1999). As the duration of the material surrounding the gap is shortened, less time is available for neural recovery and therefore fewer neurons are available to mark the onset of the material trailing the gap. With the response to the trailing material weakening, detection of the gap will become more difficult. If recovery from neural adaptation occurs more slowly in older adults, then it follows that they will be particularly disadvantaged when required to detect a gap in short duration non-speech stimuli. They would also face greater challenges with fast speech where the detection of a silent interval can influence stop gap detection and subsequent word identification.

V REFERENCES

CHABA. (1988). Speech understanding and aging. J of the Acoustical society of America, 83, 859-895.

Gordon-Salant, S., & Fitzgibbons, P.J. (1995). Recognition of multiply degraded speech by young and elderly listeners. J of Speech and Hearing Research, 38, 1150-1156.

Humes, L.E. (1996). Speech Understanding in the Elderly. J of the American Academy of Audiology, 7, 161-167.

ICRA. (1997). Noise Signals, Version 0.3. International Collegium of Rehabilitative Audiology, Hearing Aid Clinical Test Environment Standardization Work Group.

Letowski, T., & Poch, N. (1996). Comprehension of Time-Compressed Speech: Effects of Age and Speech Complexity. J of the American Academy of Audiology, 7, 447-457.

Levitt, H. (1971). Transformed Up-Down Methods in Psychoacoustics. J of the Acoustical Society of America, 49(2), 467-476.

Schmitt, J.F., & Carroll, M.R. (1985). Older listeners' ability to comprehend speaker-generated rate alteration of passages. J of Speech and Hearing Research,28, 309-312

Schneider, B.A., & Hamstra, S.J. (1999). Gap detection as a function of tonal marker duartion for younger and older listeners. J of the Acoustical Society of America, 106 (1), 371-380.

Schneider, B.A., Pichora-Fuller, M.K., Kowalchuk, D., & Lamb, M. (1994). Gap detection and the precedence effect in young and old adults. J of the Acoustical Society of America, 95(2), 980-991.

Shannon, R.V., Zeng, F-G., Kamath, V., Wygonski, J., & Ekelid, M. (1995). Speech recognition with primarily temporal cues. Science, 270, 303-304.

Strouse, A., Ashmead, D.H., Ohde, R.N., & Grantham, D.W. (1998). Temporal processing in the aging auditory system. J of the Acoustical Society of America, 104(4), 2385-2399).

Stuart, A., & Phillips, D.P. (1996). Word Recogntion in Continuous and Interrupted Broadband Noise by Young Normal-Hearing, Older Normal-Hearing, and Presbyacusic Listeners. Ear and Hearing, 17(6), 478-489.

Wingfield, A. (1996). Cognitive Factors in Auditory Performance: Context, Speed of Processing, and Constraints of Memory. J of the American Acedemy of Audiology, 7, 175-182).

Funded by NSERC, MRC, BCMSF.

Modality Specific Attentional Mechanisms Can Govern the Attentional Blink

Kim M. Goddard & Elzbieta B. Slawinski
Department of Psychology, University of Calgary, Calgary, AB., T2N 1N4

INTRODUCTION

The impairment in the ability to detect or identify a secondary target (T2) when it follows within approximately 500 ms of correct detection or identification of a primary target (T1) is a phenomenon known as the attentional blink (1), which may be related to informational masking (2). However, while the Attentional Blink (AB) has been repeatedly demonstrated in the visual domain and more recently, cross-modally (3, 4), pure auditory AB investigations are few. Further, most cross-modal studies have found evidence of auditory ABs with the use of compressed speech (e.g., 4). These types of studies can be problematic for two reasons. First, because it is possible to form visual representations from spoken words or letters, cross-modal studies may make it difficult to unambiguously attribute these effects to the auditory modality. Second, and relatedly, when attentional effects cannot be definitively attributed to a specific modality, it also becomes difficult to determine whether attentional mechanisms operate within or across modalities, or possibly both. To address this issue, this study employed pure tones, for which, no visual representations exist, in a rapid auditory presentation paradigm (11 tones/second). A visual rapid presentation paradigm, consisting of simple visual stimuli (11 lines/second) was also employed to compare visual AB effects with auditory AB effects in a within-subjects design.

METHODS

Participants 20 young adults (Mean = 21.2 yrs) participated in the study for course credit. All participants reported normal hearing and normal or corrected-to-normal vision.

Auditory Stimuli Rapid Auditory Presentation (RAP) stream stimuli consisted of 25 randomly presented tones comprising the range of 1000 Hz to 2490 Hz in 10 Hz multiples. Properties of these tones allowed the processing of the stream as a unit. Tones of 1500 Hz (low), 2000 Hz (medium) and 2500 Hz (high) were not stream items, being reserved for T1 and T2. All tones were equally loud (approximately 50 dB SPL) except for T1 and T2 which were increased in intensity by approximately 10 dB SPL over and above the level of the stream items. All tones, including T1, T2, and stream items were 85 ms in duration, separated by a silent 5 ms Interstimulus Interval (ISI).

Visual Stimuli Rapid Serial Visual Presentation (RSVP) stream stimuli consisted of 25 randomly presented lines in orientations of 30, 60, 120, and 180 degrees. Lines of orientations 45, 90, and 145 degrees were not stream items, being reserved for T1 and T2. All lines were 3 cm long and stream lines were of identical thickness. T1 and T2 were thicker lines, clearly discriminable from stream lines. At a viewing distance of 30 cm, all line stimuli subtended .95 X .76 degrees visual angle, and all were displayed for 15 ms, separated by a blank 75 ms ISI.

Design After receiving training on a frequency identification task and a lines orientation task, all participants performed both the auditory and the visual task. In the experimental condition (Exptl), T1 was presented equally often at positions 5, 9, or 13 in the stream on independent random halves of the trials. T2 was presented on all trials, equally often at all T1-T2 intervals. Participants were asked to report the first loud tone according to pitch (low, medium or high), and then, if a second loud tone was heard, it was also to be reported according to pitch. In the control condition (Ctrl), participants performed only the T2 task, where T2 was present on independent random halves of the trials. The experimenter recorded the number of loud tones reported in both conditions. The control condition was identical to the experimental condition except that in the T1-present trials, T1 was not louder. Procedures were identical for the visual task, where participants reported the thicker lines (targets and probes) according to orientation (45, 90, or 135 degrees). Condition (Exptl, Ctrl) and Task (auditory, visual) was counterbalanced across participants.

RESULTS

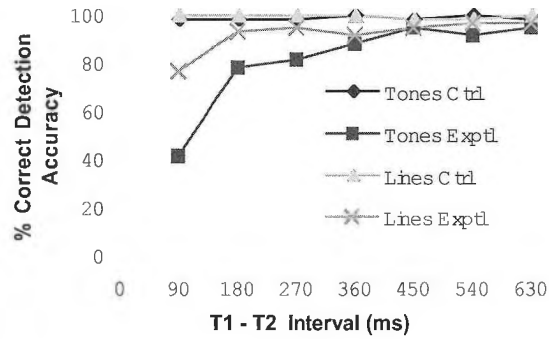

Figure 1. Detection accuracy as a function of T1-T2 Intervals for visual and auditory tasks

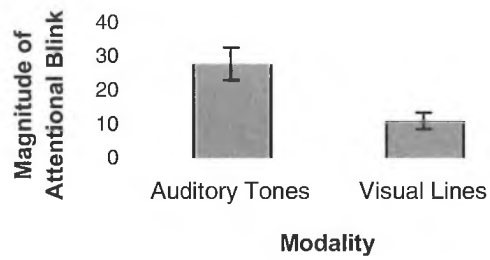

Figure 2. Magnitude of the Attentional Blink as a function of modality.

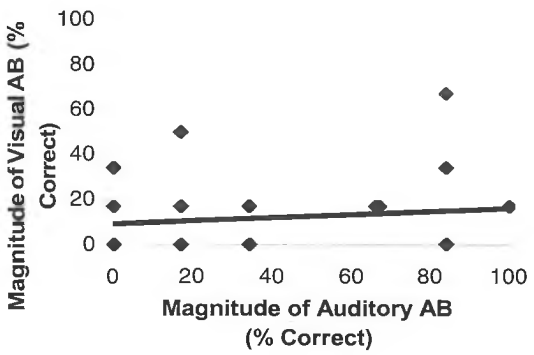

Figure 3. Scatterplot of individual AB magnitudes as a function of modality with trendline (some data points represent more than one individual).

The mean percentage of trials in which T2 was correctly detected is plotted as a function of the T1-T2- interval in the experimental and control conditions for both tasks. These results are presented in Figure 1. In the control condition, participants correctly detected T2 on 97% or better of trials for all T1-T2 intervals in both tasks. However, for the experimental condition, percent correct T2 detection for the range of 90 ms to 360 ms averaged only 72.5% for the auditory task and 89.2% for the visual task. T2 detection accuracy for the interval range of 360 to 630 ms averaged 93.9% for the auditory task and 96.1% for the visual task; T2 detection accuracy at these ranges however, was not significantly different than overall T2 detection accuracy in the control condition for either task. False alarm rates averaged less than 3% across conditions on both tasks.

Multiple paired comparisons revealed that T2 detection accuracy in the experimental condition for both tasks was significantly lower (p's $<.05$) when T2 was presented at T1-T2 intervals of 90, 180, 270 and 360 ms than the corresponding interval in the control condition; this indicated a significant AB-like T2 detection impairment for those intervals. Furthermore, when collapsed across these intervals, the magnitude of the Attentional Blink for the auditory task was greater than the magnitude of the visual task by a factor of almost 2.5, and this difference was statistically significant ($p<.025$; see Figure 2). Finally, correlational analyses revealed no significant correlations between individual task performance; that is, the magnitude of the auditory AB did not predict the magnitude of the visual AB. These results are shown in Figure 3.

DISCUSSION

Our results indicate the presence of an Attentional Blink for both the visual and the auditory task. More importantly, because of the nature of the stimuli employed in this study, we may be confident that these ABs are uncontaminated by cross-modal effects. That is, if we assume that no auditory representations exist for visual lines and no visual representations exist for auditory tones, then these ABs would appear to reflect modality-pure attentional effects.

Two interesting findings have emerged from this study. The first is the greater auditory AB magnitude when compared to the visual AB magnitude. This is notable given the less favorable conditions for auditory target detection. That is, it is typically more difficult to detect an auditory target in a stream of auditory stimuli than it is to detect a visual target in a stream of visual stimuli (5), and this was consistent with our participants subjective reports. Nevertheless, Control Condition performance did not differ across tasks, and thus, while differential task difficulty make possibly contribute to magnitude differences between the modalities, it is unlikely to be the major cause.

We have previously argued that the auditory AB reflects an inhibitory mechanism (6), putatively designed to protect the processing of the target (7) during selective attention tasks. Banks, Roberts, and Ciranni (8) note that auditory selective attention is not aided by any structural analogue similar to that of visual fixation that can choose to place important targets within foveal vision and less important targets in peripheral vision. They further suggest that because audition does not have these external capabilities, attentional inhibition must operate solely by internal auditory processes. Consequently, attentional inhibition should be more pronounced in audition than in vision. Our magnitude differences, where magnitude is an indication of the strength and/or extent of attentional inhibition, agree with Bank et al's interpretation.

A second interesting finding is that there was a lack of correlation between individual performance on the auditory task versus the visual task. To the extent that a central, amodal attentional system governs incoming sensory information, then individual performance should be, at least, modestly correlated across visual and auditory tasks. Our lack of a significant correlation, together with pure, modality specific stimuli and magnitude differences between the tasks, suggests that attentional mechanisms can, and do operate in a modality specific fashion.

REFERENCES

1. Raymond, J.E., Shapiro, K.L. & Arnell, K.M. (1992a). Temporary suppression of visual processing in an RSVP task: An attentional blink? Journal of Experimental Psychology: Human Perception and Performance, 18, 849-860.
2. Pollock, I. (1975). Auditory informational masking. Journal of the Acoustical Society of American, 57, S5.
3. Jolicouer, P. (1999). Restricted attentional capacity between sensory modalities. Psychonomic Bulletin & Review, 6, 87-92.
4. Potter, M.C., Chun, M., Banks, B.S. & Muckenhoupt, M. (1998). Two attentional deficits in serial target search: The visual attentional blink and an amodal task-switch. Journal of Experimental Psychology: Learning, Memory & Cognition, 24, 979-992.
5. Leek, M.R., Brown, M.E., & Dorman, M.F. (1991). Informational masking and auditory attention. Perception & Psychophysics, 50, 205-214.
6. Goddard, K.M., Isaak, M.I., & Slawinski, E.B. (1998). The Auditory Attentional Blink in a Congenitally Blind Population. Journal of the Acoustical Society of America, 103, 3018.
7. McDowd, J.M. & Filion, D.L. (1992). Aging, selective attention and inhibitory processes: A psychophysiological approach. Psychology and Aging, 7, 65-71.
8. Banks, W.P., Roberts, D., & Ciranni, M. (1995). Negative priming in auditory attention. Journal of Experimental. Psychology: Human Perception & Performance, 21, 1354-1361.

Subjective Evaluation Of Different Error Correction Schemes For Application With A 900 Mhz Frequency Hopper Communication System

Kimberly Braaten (1), Dean Foster (2), Bruno Korst-Fagundes (2) and Haoye Shen (2)
(1) Faculty of Engineering, University of Regina, Regina, SK, S4S 0A2
(2) Acoustics Group - ENC Nortel, 3705 35th St. N.E., Calgary, AB, T1Y 6C2

1. INTRODUCTION

Wireless communication systems are required to communicate over selected frequency ranges. Each channel has a limited bandwidth or frequency range in which it must operate and the frequency spectrum is becoming increasingly more congested.

Spread spectrum is a modulation scheme that uses the spectrum efficiently and operates with a minimum amount of interference. In a spread spectrum system, the signals are spread over a wide range of frequencies by using a variety of broadband or frequency hopping techniques. Interference is present and subjectively noticeable in some circumstances with the use of frequency hoppers. The effect of having many users utilizing the same frequency bandwidth promotes a special problem since it becomes possible for one user to jam the signal of another. This creates noise or other user perceived anomalies that considerably degrade the audio quality. Errors, caused by jamming and other sources, can be introduced into the signal from anomalies inherent in the transmit and receive modes of a wireless communication unit transporting digital information. These errors are quantified through the bit error rate (BER). An error can occur in transmission from the receiver to transmitter, from transmitter to receiver or from transmitter to transmitter. The bit error rate (BER) is the probability of an error occurring in a bit, or a change in the transmitted information.

Subjective testing was performed on two types of interference associated with such a frequency hopping system. In this article we analyzed two of the simplest techniques used to correct corrupted data. The first correction method studied, called 'repeating', used the previously sent block of data picked up by the receiver and then repeated it. A second correction method used, called 'muting', simply muted any erroneous data that was picked up by the receiver.

2. EXPERIMENT

Digital speech transmission systems can generate degradation's that involve difficulty in the listening path. These degradation's can be perceived to the end user as clicks, pops, distortion, fuzziness, etc. in the receive listening audio path. Since the listening transmission path is involved. we created a test for subjective listener's. Each test person would listen to the same audio file each time creating a consistent test base. The results from this series of tests helped the designer's choose the best error correction scheme that was available to them. To assist the designers in making the correct decision from the results, a method of assessing the subjective listener's opinions on the various audio samples was used. This technique is called the Mean Opinion Score or MOS method [3]. The speech samples used in the listening tests contained audible errors created by software that simulated conditions where jamming and various levels of BER had occurred.

Test 1 determined the type of correction scheme and the threshold of correction for errors preferred by listeners for corrected jammed signals. The threshold determines the level of correction for errors the software is using. Test 2 threshold levels were based on the results from Test 1. For Test 2, since jamming was of more concern for audio quality, the threshold parameters of Test 1 for jamming were incorporated into several selected BER's. Test 3 is based on the chosen threshold and error correction schemes determined from Tests 1 and 2. Test 3 determined when the audio quality would degrade for jamming as the numbers of users increased. It compared two different scenarios that might occur in a jamming situation. The listeners evaluated the audio quality when the jams occurred as users interfered with each other at the same time or when the interference occurred at different times.

3. RESULTS AND DISCUSSIONS

3.1 Test 1

In this project, jamming contributes to the quality of the audio signal to a greater degree than does BER, meaning, if a signal is jammed, it is much more noticeable to a listener than the BER factor. Therefore, Test 1 was performed to find out whether jamming using a correction scheme called muting or using the repeating method of a previous block was preferable. The listeners would find which threshold level was most acceptable using the DCR MOS subjective test method. From Test 1 it appears from Figure 4 (shown on the next page) that Thresholds 1, 2 and 3 have the highest DCR MOS scoring.

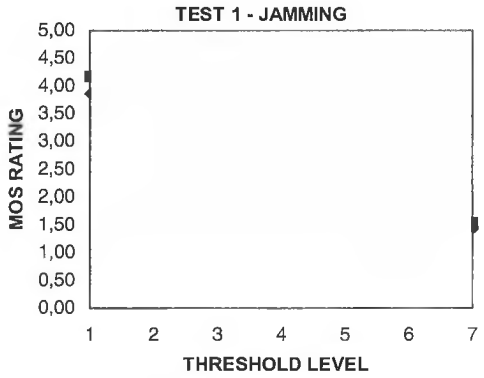

Figure 4 Test 1. Jamming from Threshold's 1 to 7.

3.2 Test 2

Test 2 will use the chosen threshold value and error correction scheme from Test 1 with the selected bit error rates. Since jamming and the BER can only be corrected with one chosen threshold, the need to see how the parameters chosen from Test 1 for jamming compared to the selected BER's became apparent. This became the testing performed for Test 2.

Testing was accomplished by comparing a speech sample that was corrected to the original uncorrected speech sample. All of the samples were corrected using the muting correction method at Threshold's 1, 2 and 3 chosen from Test 1. The threshold test values were so close in Test 1, you cannot really say that a threshold of 2 is completely superior, so 3 threshold's were chosen.

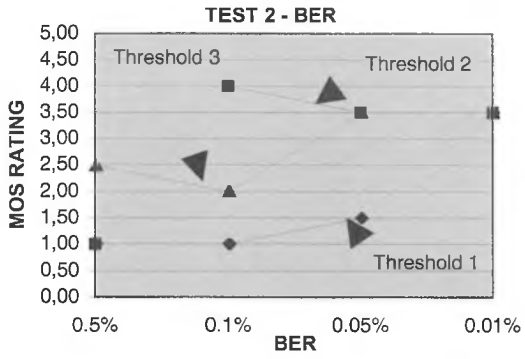

Figure 6 Test 2 for a chosen threshold of 2 with threshold's 1 and 3 using the muting correction scheme and the selected BER's.

3.3 Test 3

Test 3 used an absolute rating schedule was used for each trial based on a single speech sample that was heard one at a time by the listener.

The two graphs shown are for close together jams (to simulate jamming at the same time) and jams far apart to simulate dispersed jams.

From the data in Figure 9, it appears that when the jams are dispersed (highlighted as Far in the figure), most ratings were below fair (MOS < 2.5). The best scenario for dispersed jams is 4 jams since there is a drop off in quality after that. For close together jams, the ratings are fair - up to 9 jams, with an anomaly at 3 jams/s.

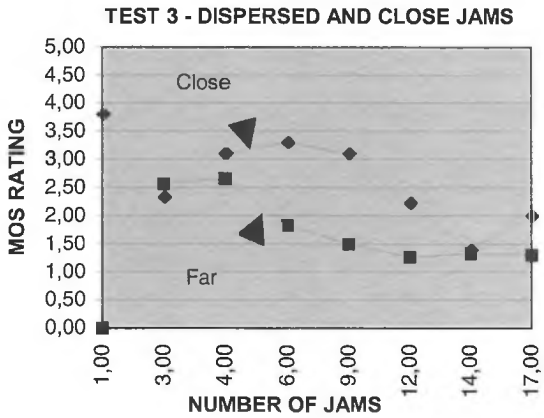

Figure 9 Test 3 for far apart and close Jams from 1 to 17 Jams with a muting error correction scheme at threshold 2.

4. CONCLUSIONS

A 32 kbits/s ADPCM coding scheme gave the best audio quality for the lowest number of bits. For Test 1, the threshold chosen was number 2. This means that the error correction scheme was invoked only after two consecutive errors were detected. From looking at the graph (Figure 4), you can see that these threshold levels received the highest ratings from the listeners. The correction scheme chosen was muting since the speech samples that were corrected using this scheme received higher ratings than the samples corrected with the repeating "previous block" method. See Figure 4 for more information on Test 1. The DCR MOS test rating was used since the basis of the test was to compare a reference sample to a corrected sample.

Test 2 concentrated on finding the BER with the best audio quality for the chosen threshold and error correction scheme from Test 1. To give more variety during testing, the chosen threshold from Test 1 along with the upper and lower threshold were chosen for Test 2, therefore, the threshold's used for Test 2 were 1, 2 and 3. The level chosen from Test 2 that had the best audio quality for BER was threshold 2, which was the same as the threshold chosen for Test 1. Test 2 was conducted for a BER of 0.5%, 0.1%, 0.05% and 0.01%. Any BER meeting or exceeding 0.01% would have an acceptable level of audio quality according to our preliminary tests. Once again, the DCR MOS test for comparison ratings was used. For more information on Test 2, please see Figure 6.

Test 3 incorporated parameters found from Test 1 and Test 2, which are a threshold of 2 with a muting correction scheme, to do a density evaluation for jamming. From reviewing the data, it is evident that using more than 4 dispersed jams does not have an acceptable audio quality. Between 1and occurring at the same time, or close jams, has a fair quality (except at 3 jams), but there is a drop off on either side of these values. Test 3 used the ACR MOS test method that asks for the overall opinion of each sample on its own. For more information on Test 3, please refer to Figures 8 and 9.

5. REFERENCES

[1] Paul G. Flikkema, "Spread-Spectrum Techniques for Wireless Communications", IEEE Signal Processing Magazine, 14:3, May 1997, p.26.

[2] J.D. Laster and J.H. Reed, "Interference Rejection in Digital Wireless Communications", IEEE Signal Processing Magazine, 14:3, May 1997, p. 37.

[3] B.S. Atal, V.Cuperman, and A. Gersho, Speech and Audio Coding for Wireless and Network Applications, (Norwell, MA: Kluwer, 1993), p. 43.

[4] Simon Haykin, Digital Communications (Singapore: John Wiley & Sons, 1988), pg. 210.

[5] Haoye Shen, ENC Nortel, Calgary, Alberta. Memo to Ashfaq A. Choudhury, S.G.S. Thomson Microelectronics, Nepean, Ontario, March 3, 1997.

[6] Leigh L.A. Thorpe, AT30-I BNR, Ottawa, Ontario. Memo to Dean Foster, ENC Nortel, Calgary, Alberta, April 25, 1997.

[7] John Chan, ENC Nortel, Calgary, Alberta. Letter to Kim Braaten, ENC Nortel, Calgary, Alberta.

[8] Leigh L.A. Thorpe, AT30-I BNR, Ottawa, Ontario, in conversation with Kim Braaten, ENC Nortel, Calgary, Alberta, July 16, 1997.

[9] Martin S. Rodin, Analog and Digital Communication Systems, (New Jersey: Prentice-Hall, Inc., 1996), pg.18.

L'UTILISATION DE PLANS D'EXPÉRIENCE POUR CHOISIR LA MODÉLISATION ACOUSTIQUE D'UN TÉLÉPHONE MAINS-LIBRES

Joris Brun-Berthet, Frédéric Laville et Stéphane Dedieu*
Ecole de Technologie Supérieure, Génie Mécanique, 1100, rue Notre Dame Ouest, Montréal (Québec) H3C 1K3
*Adresse actuelle : Mitel Corporation, 350 Legget Drive, Kanata (Ontario) K2K 1X3

1. Introduction

Le développement de téléphones mains-libres « Full Duplex » où le haut-parleur et le microphone fonctionnent en même temps a posé des problèmes de couplage acoustique entre les deux transducteurs. Ces problèmes sont actuellement résolus en partie grâce au développement d'algorithmes de traitement du signal [1]. Pour compléter la résolution de ces problèmes, il est nécessaire d'améliorer la conception physique du boîtier téléphonique, ce qui implique de développer un outil de simulation informatique de l'acoustique de ce boîtier.

La réalisation d'une telle simulation est rendue difficile à cause des nombreux phénomènes à prendre en compte, de la complexité de la géométrie du téléphone et de la largeur de la bande de fréquence utilisée (300 Hz à 3400 Hz en téléphonie classique et 150 Hz à 7000 Hz en téléphonie large bande). Plusieurs types de modélisation peuvent être élaborés. Le principal modèle est un modèle numérique mais celui ci a des limites (bande de fréquence, complexité de la géométrie) et nécessite le développement de modèles complémentaires. Il s'agit donc de déterminer quels sont les éléments importants à modéliser afin de choisir les modèles les plus appropriés. Ce choix sera fait grâce à la méthode des plans d'expérience. Cette méthode a été utilisée fréquemment en génie industriel [2] mais plus rarement en acoustique ([3] par exemple) et ne l'a pas encore été, à notre connaissance, pour le choix des modèles.

2. Plan d'expérience

Dans ce projet, la méthode des plans d'expérience va permettre à l'aide d'un nombre précis d'expérience de déterminer l'importance de divers facteurs ainsi que la bande de fréquence dans laquelle ces facteurs sont importants.

2.1. Principe

Cette théorie repose sur l'utilisation des outils d'analyse statistique de données et permet de planifier une série d'expériences utiles pour déterminer l'influence d'un ou de plusieurs facteurs sur les variables dépendantes. Dans ce projet, la variable dépendante sera, soit la réponse du haut-parleur du téléphone, soit la réponse du microphone du téléphone, ou alors le rapport du signal reçu par le microphone sur le signal émis par le haut-parleur (évaluation du retour ou bien du bouclage). La méthode consiste à définir une série d'expériences à partir de tables orthogonales. L'utilisation de ces tables orthogonales va permettre de séparer l'effet des facteurs de façon très simple.

L'intérêt des plans d'expérience vient du fait que toutes les informations sur les facteurs proviennent de l'ensemble des expériences faites, d'où la possibilité de réduire le nombre d'expérience par rapport à une méthode où chaque facteur est testé séparément. De plus, des informations supplémentaires sur les interactions entre les effets des facteurs sont disponibles. Les effets des facteurs sont calculés à partir de la table orthogonale qui a servi à faire les mesures, ensuite les effets calculés vont être normalisés puis comparés à l'aide d'un test statistique : le test de Fisher (F), à partir duquel l'effet du facteur va être évalué.

2.2. Expérience

Afin de bien comprendre les différents phénomènes présents dans l'acoustique du téléphone mains-libres, c'est à dire les différents chemins de transmission acoustique (représentés dans la figure 1 par les numéros 1, 2, 3, 4, 5 et 6), des prototypes à géométrie simplifiée ont été réalisés (Figure 1). Ceux ci ont servi aussi à valider les premiers modèles numériques.

La méthode est illustrée avec un plan d'expérience limité à quatre facteurs et une seule des trois variables dépendantes, la réponse du haut-parleur. Il s'agit d'un plan d'expérience factoriel fractionnaire 2^{4-1}, ce qui signifie que les effets de 4 facteurs vont être testés avec un plan réduit à seulement 8 expériences au lieu des 2^4, soit 16 expériences attendues pour le plan factoriel complet. Dans ce cas le plan fractionnaire ne permettra pas de connaître les interactions aux niveaux les plus élevés. Le nombre de niveau par facteur est de 2 car le but de ce plan d'expérience est de déterminer l'influence du facteur donc seulement 2 niveaux suffisent, par exemple présence ou absence du facteur.

Pour chaque expérience une répétition sera faite afin de pouvoir évaluer les interactions doubles avec un niveau de confiance suffisant.

Les 4 facteurs définis ici sont :

- A : Plaque : composants placés à l'intérieur du boîtier.
- B : Grille : grille de protection placée devant le haut-parleur.
- C : Epais : 2 épaisseurs de boîtier, 3 mm et 6 mm.
- D : Mousse : mousse ajoutée à l'intérieur du boîtier afin d'augmenter l'absorption interne.

Le déroulement des expériences (16 mesures) est décrit dans le tableau 1.

Tableau 1 : table orthogonale du plan d'expérience 2^{4-1} avec une répétition.

A (Plaque)	B (Grille)	C (Epais)	D (Mousse)	Mesures
Oui	Oui	6 mm	Non	1, 9
Non	Oui	6 mm	Oui	2, 10
Oui	Non	6 mm	Oui	3, 11
Non	Non	6 mm	Non	4, 12
Oui	Oui	3 mm	Oui	5, 13
Non	Oui	3 mm	Non	6, 14
Oui	Non	3 mm	Non	7, 15
Non	Non	3 mm	Oui	8, 16

Pour chaque expérience une mesure en bande fine est faite jusqu'à 10 kHz pour couvrir les bandes de fréquence de la téléphonie classique et de la téléphonie large bande

3. Résultats

Les résultats d'un plan d'expérience permettent de visualiser le niveau des effets normalisés par rapport au seuil correspondant au test statistique (Fisher). Ici, la conservation d'une grandeur physique est importante, la représentation des résultats proposée pour l'acoustique est donc une représentation des effets en décibel, c'est à dire sans normalisation. Le test statistique va donc être transposé en décibel pour apparaître sur les courbes de résultats.

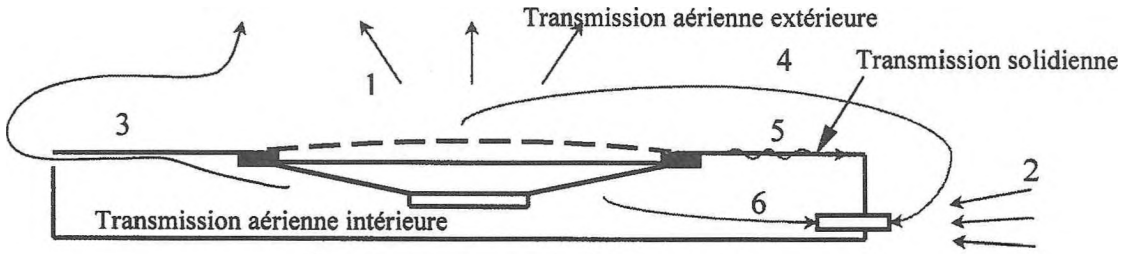

Figure 1 : Prototype et chemins de transmission

Les calculs du plan d'expérience sont faits sur chacun des 1602 points du spectre. Le résultat est donc un spectre des effets en fonction de la fréquence. Les effets des 4 facteurs ainsi que des interactions doubles sont analysés. La résolution du plan d'expérience 2^{4-1} avec une répétition impose que les interactions doubles soient couplées deux à deux. Les effets des facteurs et interactions suivants sont disponibles : A, B, C, D, AB = CD, AC = BD, AD = BC.

Deux sorties typiques des résultats sont représentées sur la figure 2, c'est à dire le spectre des effets (trait fort) pour les facteurs Plaque (A) et Grille (B) ainsi que les limites de signification du test de Fisher (traits fins).

Les résultats montrent :

- Plaque (figure 2) et Mousse ont des effets peu importants et très localisés en fréquence sur les modes de cavité (premier mode acoustique selon l'axe vertical vers 4 kHz).
- Pour la grille (figure 2) un effet intéressant semblable à une résonance très amortie apparaît (entre 2 kHz et 6 kHz). Cet effet pourra donc être probablement modélisé analytiquement et rajouté au modèle numérique, d'où l'économie de le modéliser numériquement.
- L'épaisseur a un effet sur toute la bande de fréquence.

Les effets des interactions permettent de clarifier les interprétations des effets des facteurs. L'interaction AD=BC est importante sur pratiquement toute la gamme de fréquence, ce qui peut s'expliquer par le fait que les facteurs Mousse et Plaque agissent sur les modes de la cavité et interagissent ensemble. Les interactions AB=CD et AC=BD sont faibles sur pratiquement toute la gamme de fréquence, ce qui peut s'expliquer par le fait que les facteurs Grille et Epaisseur n'ont pas beaucoup d'influence sur les facteurs qui agissent sur la cavité. Cela suggère une possible économie au point de vue du calcul numérique car il serait envisageable de modéliser boîtier et cavité en ignorant leur couplage.

4. Conclusion

Le plan d'expérience est une méthode couramment utilisée en génie industriel. Afin de l'appliquer comme aide à la décision pour la conception d'un modèle acoustique, elle a du être repensée en fonction des besoins propre à l'acoustique, en particulier le grand nombre de variable de sortie (1602 points) qui impose une représentation spectrale.

Le plan d'expérience présenté ici permet à l'aide d'un nombre réduit d'expérience de trouver les effets des facteurs choisis dans la gamme de fréquence désirée. Il permet aussi de faire des interprétations physiques et, en plus des mesures classiques, d'avoir des informations sur les interactions entre différents facteurs d'un système physique. Enfin, le plan d'expérience permet de faire des choix sur le type de modèle à utiliser comme pour le cas de la grille où un modèle plus approprié peut être développé.

5. Remerciements

Cette étude a été possible grâce au financement de MITEL Corp. et du CRSNG.

6. Bibliographie

[1]. Hänsler, Eberhard, 1994, *The hands-free telephone problem - An annotated bibliography update*, Ann. Télécommun., 49, n° 7-8, pp 360-367.

[2]. Montgomery, Douglas C., *Design and analysis of experiments Fourth edition*, John Wiley & Sons, 1996,

[3]. Thomas, M., Laville, F. Beauchamp, Y. et Simard, F., 1997, *An experimental design for reducing riveting noise*, présenté au 22nd International Conference on Computers and Industrial Engineering au Caire, Égypte, 20-22 décembre.

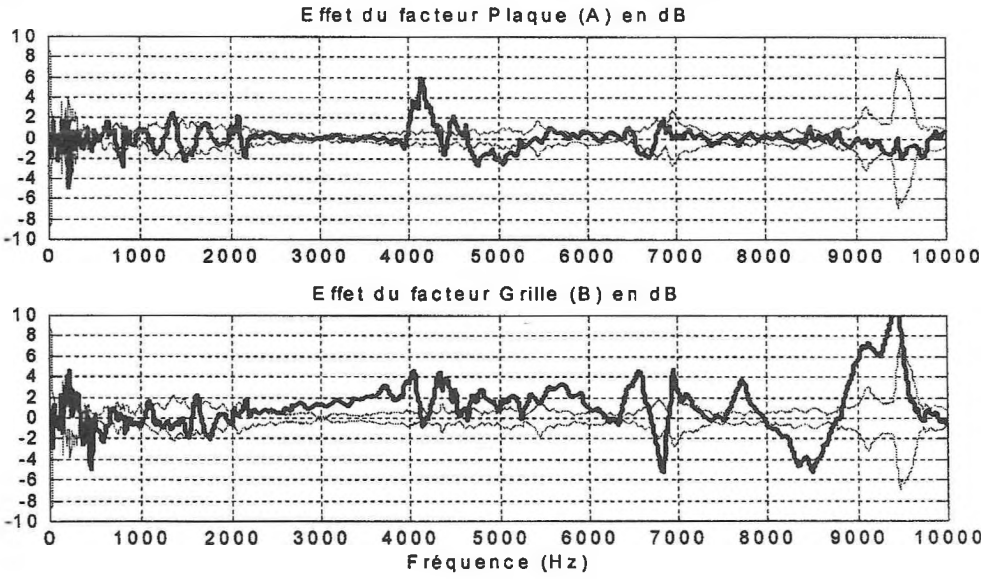

International Comparisons On Acoustical Calibrations And Measurements

George S. K. Wong
Institute for National Measurement Standards, National Research Council of Canada, Ottawa (ON), K1A 0R6

1.0 INTRODUCTION

The mutual acceptance of acoustical calibrations and measurements between industrial countries is essential for international trade and will also remove non-tariff trade barriers. In order to gain international acceptance of Canadian calibrations and measurements, INMS participates in international comparisons in acoustical calibrations and measurements. The Comité international des poids et mesures (CIPM), under the general umbrella of the Bureau International des Poids et Mesures (BIPM), has formed a Consultative Committee on Acoustics, Ultrasound and Vibration (CCAUV) to formalise international comparisons on Acoustics (primary calibrations of laboratory standard microphones), Ultrasound (ultrasound power measurements and hydrophone calibrations) and Vibration (accelerometer calibrations).

2.0 NORTH AND SOUTH AMERICA

In North America, under the North American Cooperation in Metrology (NORAMET), NRC (Canada), NIST (USA) and CENAM (Mexico) have completed comparisons of microphone and accelerometer calibrations. With the inclusion of countries from South America, such as Brazil and Argentina, comparisons with five countries, are under the supervision of SIM (Sistema Interamericano de Metrologia). The SIM comparison for accelerometers has been completed, and it is expected that the comparison for microphones will be completed by the end of 1999.

3.0 INTERNATIONAL COMPARISONS

The current CCAUV international comparisons involve more than twelve countries. The participants are responsible for hand carrying of the artefacts and returning them to the pilot laboratories: NPL, UK for the microphone comparisons, and PTB, Germany for the comparisons of ultrasound power measurements and accelerometer calibrations. For hydrophone comparisons, both NIST, USA and PTB, Germany will act as pilot laboratories. It is hoped to complete these comparisons by the year 2002.

3.1 PARTICIPATION IN INTERNATIONAL COMPARISONS

The participants in Consultative Committee (CC) comparisons are restricted to members. However, there are three major requirements in order to become a full member of a CC: (a) to be a national laboratory charged with establishing national standards in the field, (b) to be active in research and have a record of publications in research journals of international repute, and (c) to have demonstrated competence by a record of participation on international comparisons organised either by the Consultative Committee, the BIPM or a regional metrology organization. Requirements (b) above, will most likely restrict some national laboratories to observer status.

4.0 MEASUREMENT TRACEABILITY

For international trade, it is essential to have mutual recognition of measurements made by both the exporting and the importing country. For example, the noise level emitted by a machine measured at the factory with certified instruments and methods in accordance to international standards, should be acceptable to the importing country without the requirement to duplicate the measurements. To achieve this mutual recognition, it is necessary for the exporting country to have proven capabilities in international comparisons and an unbroken chain of traceability from the respective national laboratories to the machine shop level.

5.0 BENEFICIARY OF INTERNATIONAL COMPARISONS

"Who benefits from International comparisons?" This question is often asked by many organizations and governments. From the above, one may conclude that it is the consumer that reaps the benefits. Apart from mutual recognition to avoid non-tarriff trade barriers, there are other aspects that benefit the consumers. For example, in connection to being active in research and development pertaining to acoustical calibrations, INMS developed an economically attractive interchange microphone method for microphone calibrations by comparison [1, 2]. The method enables the users of microphones to have their microphones calibrated at regular intervals without the relatively higher cost of an absolute calibration by the reciprocity technique. The above interchange microphone method of microphone calibrations by comparison has been accepted by the International Electrotechnical Commission (IEC) as an international standard IEC/61904-5 in the stage of a second committee draft.

6.0 SOME RELATED CURRENT ACOUSTICAL RESEARCH AT INMS

6.1 MICROPHONE CALIBRATIONS

The sensitivity of condenser microphones is affected by a change in barometric pressure. As an example, when the barometric pressure changes from 94 to 106 kPa, the sensitivity of a Brüel and Kjær 4160 laboratory standard microphone changes by approximately 0.2 dB and 0.35 dB at 1 kHz and 10 kHz, respectively [3]. A pressure coefficient curve has been obtained for this microphone so that users can correct their results to reduce their measurement uncertainties. All that is necessary is to measure the barometric pressure during the acoustical measurements.

To obtain the above pressure coefficient data, the Acoustical Standards Program at INMS designed and developed a calibration chamber with a controlled environment such that the pressure coefficients of microphones can be measured accurately. The chamber is currently being used for the SIM microphone calibration comparison for which INMS is the pilot laboratory, and will be used for

participation in the coming CCAUV comparison.

6.2 ULTRASOUND POWER MEASUREMENTS

At the request of Health Canada, INMS has developed a high-power ultrasound standard. A large absorbing or reflecting target submerged in a water tank is suspended with thin wires from a small hook at the bottom of an electronic balance. The test transducer with its active surface submerged in water is positioned coaxially above the target. The radiation force generated by the transducer and impinged on the target is measured by the electronic balance. Within a range of approximately 0.1 to 10 watts, and depending on the frequency of measurement, the uncertainty of the measured ultrasound power is between 5 and 10 percent at a confidence level of approximately 95%.

6.3 ACCELEROMETER CALIBRATIONS

To satisfy industrial needs, and possible future low frequency calibration requirements, a test rig has been built to enable accelerometer calibrations by comparison to frequencies as low as 2 Hz. A thin beam is excited with a shaker. One end of the beam is clamped with the shaker located at a short distance from the clamp. A reference accelerometer is mounted back-to-back with the test accelerometer at the far end of the beam. Under excitation, a sinusoidal motion is generated at the free end of the beam. The uncertainty of the comparison is estimated to be 3% at a confidence level of approximately 95%.

7.0 CONCLUSIONS

International comparisons on acoustical calibrations and measurements are essential for international trade. The research and development that support the international comparisons benefit the consumers

REFERENCES

[1] G. S. K. Wong, L. Wu, Interchange microphone method for calibration by comparison, Congress on Noise Control Engineering, Christchurch, New Zealand, paper #15, (1998)

[2] G. S. K Wong, Comparison methods for microphone calibration, Chapter 13, AIP Handbook of Condenser Microphones. Theory, Calibration, and Measurements, edited by George S. K. Wong and Tony F. W. Embleton (American Institute of Physics, New York, 1995).

[3] G. S. K. Wong and L. Wu, Controlled environment for reciprocity calibration of laboratory standard microphone and measurement of sensitivity pressure correction. (Accepted for publication in Metrologia).

HEARING PROTECTORS STANDARDS ACTIVITIES

Alberto Behar, P.Eng., C.I.H. Noise Control.
45 Meadowcliffe Dr., Scarborough, ON, M1M 2X8

1. INTRODUCTION

Despite increasing efforts toward hearing conservation, occupational hearing loss is still the most prevalent work-related illnesses in the industrialized world. Because of this fact, every effort should be made to reduce the sound energy entering the ear and damaging the delicate hear cells, damage, that has no cure. Engineering noise controls are accepted to be the best way of reducing the sound levels. However, because of the high cost involved in implementing noise control measures, the use of hearing protectors is still the most popular mean of defence against potentially damaging noise levels. This is why normalization of their testing and applications is such an important activity.

Out of the two main characteristics: sound attenuation and comfort, only the first one has gained wide acceptance up to the point that there is a consistent uniformity among standards produced in different countries. There are, however, some outstanding issues that had to be addressed, and that are, at present, being dealt at national and at the international scene. They are, among others:

- testing method that will produce attenuation figures similar to those observed in the field
- an easy way of using the results from the measurement to assess the noise level of the protected ear.
- methods for measuring the attenuation of nonlinear protectors in continuous and impulsive noise.

In this presentation, we will review the hearing protectors normalization activities performed by the Canadian Standard Association (CSA), the American National Standard Institute (ANSI) and the International Organization for Standardization (ISO). We will describe the writing groups and discuss the standards already produced, those in revision and those that are in the process of writing.

2. CANADA

The Canadian Standard Association (CSA) Technical Committee on Hearing Protection Z94.2, under the jurisdiction of the Standards Steering Committee on Occupational Health and Safety, has the task of preparing and updating the CSA Standard Z94.2 "Hearing Protectors". As with all other standards, the Z94.2 has to be revised/updated every five years. Presently, the Technical Committee is revising the 1994 issue of the Standard. (Originally published in 1974 it was updated in 1979, 1984 and 1994).

For this purpose, the Committee was split into two groups. The first is looking into development of Testing and Classification Criteria, taking into account new developments as well as the experience accrued with the existing standard. The second group will develop a comprehensive Selection, Care and Use Guideline using as a basis the existing Appendix. The result of the work of the second group will also be included in the main body of the Standard. At the present time, both groups are working on their respective texts, aiming at having drafts ready for the general meeting scheduled for October 1999.

3. USA

The American National Standards Institute (ANSI) is the official organization responsible for preparing and issuing standards in the USA. The Acoustical Society of America (ASA) provides the Secretariat for several Accredited Standards Committees. The Accredited Standards Committee S12, Noise, has prepared the latest issue of the American Standard Method for Measuring the Real-Ear Attenuation of Hearing Protectors, ANSI S12.6 -1997, (revision of the ANSI S12.6 -1984).

The Standard contains two testing methods. The first one (Method "A") introduces minor revisions to the 1984 issue of the standard. It is intended to measure the highest attenuation that can be achieved by the protector under test.

The second, Method "B", is the result of a research that lasted for 10 years, thus constituting a unique effort in the field of normalization of hearing protectors testing. Its objective is to obtain attenuations similar to those found in workplaces that have efficient hearing conservation programs in place. The physical environment, test signals and the audiometric procedures are essentially the same for both methods. The main difference between them consists of how the subjects are selected and how the protectors are fitted.

At present, the Standard Committee is working in the forthcoming revision of the Standard, due in the year 2002.

4. ISO

Standard activities at the International Organization for Standardization (ISO), are carried out by Technical Committees (TS), that in turn are divided in Subcommittees (SC). The actual work of writing is done by Working Groups (WG) attached either to a SC or to a TC.

The WG 17 "Methods for the measurement of sound attenuation of hearing protectors" is a part of the TC 43 "Acoustics", SC 1 "Noise". It is responsible for the ISO 4869 Standard "Acoustics-Hearing Protectors". Members of the WG come from Australia, Canada, Czech Republic, Finland, France, Germany, New Zealand, Norway, Sweden, Switzerland, United Kingdom and USA. The Convener is from Denmark.

The Standard has several parts, some of them already finished (and issued), while other are either in revision, in the process or writing, or just intended to be written.

Following is the list of the parts:

Part 1: Subjective method for the measurement of sound attenuation, 1990 (Presently under ordinary revision)

Part 2: Estimation of effective A-weighted sound pressure levels when hearing protectors are worn, 1994

Part 3: Simplified method for the measurement of insertion loss of ear-muff type protectors for quality inspection purposes, 1989. This is a Technical Report and not a full Standard

Part 4: Method for the measurement of effective sound pressure levels for level dependent sound restoration earmuffs, 1998. This is a Technical Report and not a full Standard

Part 5: Measurement of performance characteristics for hearing protectors impulsive noise (under preparation).

Part 6: Active noise reduction of hearing protectors (under consideration)

Part 7: Subjective method for the measurement of sound attenuation.

Right now, the WG is at the task of performing the periodic review of the Part 1. After lengthy discussions, it was decided that there will be also a Part 7 in the Standard, that essentially will be following the Method "B" of the ANSI S12.6-1997.

Development Of Bona-Fide Occupational Requirements For Hearing In Canadian Coast Guard Operations

Laurel Ritmiller
BC Research Inc.
3650 Wesbrook Mall
Vancouver, BC V6S 2L2

Stanley Forshaw
3958 Sherwood Rd.
Victoria, BC V8N 4E6

Murray Hodgson
Occupational Hygiene Program
Dept. of Mechanical Engg.
University of British Columbia
Vancouver, BC V6T 1Z3

Chantal Laroche
Audiology and Speech Pathology
Faculty of Health Sciences
University of Ottawa
Ottawa, ON K1N 6N5

1. INTRODUCTION

The Canadian Coast Guard (CCG), a division of the Department of Fisheries and Oceans (DFO), provides continuous support for a number of essential services in Canadian waters, including: ice-breaking and ice escort; maintenance of navigational aids; conservation and protection; environmental response; fisheries research; hydrography; and search and rescue. These services are often performed under hostile meteorological conditions, in remote locations and for extended periods of time. It is essential that Ships' Officers and Ships' Crew meet appropriate minimum medical requirements to ensure safety and performance in a range of operating conditions.

To address fitness-for-work requirements, CCG has a mandate to review its medical standards to better define relevant components of medical fitness essential to safe and effective seagoing operations. The Canadian Human Rights Commission (CHRC) requires that *bona-fide* occupational requirements (BFORs) must be based on the requirements for tasks performed on the job, rather than historical precedent and expert opinion. The CHRC requires that medical standards and subsequent testing procedures be based on:

- identification of essential tasks that are the requirements of the job;
- identification of relevant skills and capabilities required to perform the essential tasks of the job;
- methods that evaluate the ability of the individual to perform essential tasks of the job with regard to reasonable accommodation; and
- standards that do not exceed the minimum requirements of the job (CHRRS, 1982, TR/82-3).

The objective of this project was to support the CCG in the development of defensible, task-oriented, performance-based hearing standards relevant to CCG seagoing occupations. Hearing standards have been developed for this occupational setting for the following three reasons:

- to ensure the safety of the individual;
- to ensure the safety of others and of the vessel; and
- to ensure that an individual can perform the required tasks to complete the vessel's operational program.

2. METHODS

To address the needs of CCG, a project team was assembled with expertise in relevant subject areas, including: acoustics; audiology; signal processing; task analysis; and development of occupational standards. The project was completed in five phases.

- Phases 1 and 2 involved the application of a comprehensive task analysis methodology that identified the CCG seagoing occupations and operational tasks most important to safety and program completion and the critical aspects of hearing required to perform these tasks.
- In Phase 3, acoustic characteristics of the critical tasks identified in Phases 1 and 2 were collected with a representative sample of CCG vessels, regions and operations.
- Phase 4 involved analysis of the acoustic data based on the latest available technology and standards (Forshaw *et al.*, 1999; Hodgson *et al.*, 1999; Laroche *et al.*, 1999). The analysis methods used during the project also included the newly established *Speech Intelligibility Index* (SII) (ANSI S3.5-1997). Data were collected and analyzed to evaluate both speech discrimination and signal and alarm detection under a variety of operational conditions.
- In Phase 5, issues relative to the use of hearing aids in a marine environment were reviewed, specifically the impact of hearing aid reliability on safety and performance.

3. RESULTS AND DISCUSSION

Based on empirical study of the hearing requirements of the CCG seagoing environment, recommendations were provided for a minimum hearing requirement for three CCG departments: Deck, Engineering, and Logistics. The data on which these recommendations are based include the specific tasks identified for each department, as well as the common tasks identified as a requirement for all departments (i.e., Marine Emergency Duties). Minimum hearing threshold loss (HTL) profiles to meet the hearing requirements in each of the three departments were calculated. A limiting *Speech Intelligibility Index* criteria of 0.50 (on a scale of 0 to 1) was selected based on other international military standards and cornerstone research (Forshaw et al., 1999).

The results indicated that the speech discrimination tasks required a more sensitive level of hearing than did the signal detection tasks. Therefore, the recommended overall minimum hearing requirement was based on the speech discrimination limits, which encompassed the hearing requirement to detect signals and alarms on board the vessels in CCG operations.

It must be emphasized that the HTL profiles recommended by this research are intended to represent the *minimum* HTL profile required to pass a first round of audiological testing. Those individuals whose pure-tone audiograms meet this minimum profile require no additional testing and should be considered to meet the medical requirement for hearing. However, those individuals who do not meet this requirement should be directed to additional otological/audiological assessment. The clinical assessment should include speech discrimination, signal detection, and localization evaluations.

The data collection and analysis methodology used for the current project was an adaptation of the latest research and standards that are relevant to the development of hearing standards, considering the issues and environments experienced in CCG seagoing operations. The interpretations within the project are subject to a number of limitations, including some related to data collection conducted in the field. Other limitations are related to the unique, groundbreaking research that was completed to develop BFORs in this type of environment. These limitations include the following:

- issues related to field data collection on board CCG vessels; including vessel and region scheduling availability, meteorological conditions, and the logistical and safe use of electronic equipment in a marine environment;
- the data were based on engineering analysis methodologies; consequently psychoacoustic normative data is required for further validation and development of the testing methodology; and
- the information available on the reliability of hearing aids in marine environments was limited and may require simulation testing and/or field evaluation as a further investigation.

Notwithstanding the project limitations and requirements for future research, the project methodology that was developed met the requirements of the CHRC to develop a task-oriented minimum medical standard that is focused on safety, performance and fairness.

4. ACKNOWLEDGEMENT

This work was supported by Transport Canada - Transportation Development Centre (TDC) and Canadian Coast Guard (CCG) under contract T8200-5-5567/A. The views, opinions and/or findings contained in this report are those of the authors and should not be construed as an official TDC or CCG policy or decision unless so designated by other documentation.

5. REFERENCES

ANSI (1997). *American National Standard methods for the calculation of the Speech Intelligibility Index.* (ANSI S3.5-1997) (Revision of ANSI S3.5-1969). New York.

CHRRS (Canadian Human Rights Reporter Supplement) (1982-3). *Federal Canadian Human Rights Act. Bona Fide Occupational Requirements Guidelines.*

Forshaw, S., Ritmiller, L., Hodgson, M., and Laroche, C. (1999). Estimates of speech intelligibility based on equivalent speech- and noise-spectrum levels and hearing thresholds.. Canadian Acoustics, 27(3).

Hodgson, M., Forshaw, S., Ritmiller, L., and Laroche, C. (1999). Characterizing ship acoustical environments for speech communication. Canadian Acoustics, 27(3).

CHARACTERIZING SHIP ACOUSTICAL ENVIRONMENTS FOR SPEECH COMMUNICATION

Murray Hodgson
Occupational Hygiene Program
Dept. of Mechanical Engg.
University of British Columbia
Vancouver, BC V6T 1Z3

Stanley Forshaw
3958 Sherwood Rd.
Victoria, BC V8N 4E6

Laurel Ritmiller
BC Research Inc.
3650 Wesbrook Mall
Vancouver, BC V6S 2L2

Chantal Laroche
Audiology and Speech Pathology
Faculty of Health Sciences
University of Ottawa
Ottawa, ON K1N 6N5

1. INTRODUCTION

This paper describes one phase of research aimed at developing improved hearing criteria for the Canadian Coast Guard (CCG) [1]. The overall objective was to propose reliable criteria specifying whether or not CCG ship personnel have adequate hearing ability to carry out their jobs proficiently. The main concerns here were speech communication and warning-signal recognition. The required abilities depend on the tasks at hand and on the acoustical environments in which the personnel are working. Thus, it was necessary to include the effects of those attributes of the work environments with the potential to affect speech understanding and warning-signal detection. These attributes include the background noise, reverberation and communications equipment. A detailed task analysis was performed [1]. Typical work environments on board Coast Guard vessels, relevant to these tasks, were characterized – this was the objective of the work reported here. The results were used to calculate SII values for ship personnel with different hearing-loss profiles, to determine the maximum hearing loss that would result in the specified minimum SII [2] and warning-signal and alarm audibility [3].

2. METHODOLOGY

Three CCG departments – Deck, Engineering, and Logistics – and the specific tasks identified for each department, as well as the common tasks identified as a requirement for all departments (i.e., Marine Emergency Duties), were considered. Ship environments in which tests were carried out included the bridge, engine room, deck and galley.

ANSI Standard S3.5-1997: Methods for Calculating Speech Intelligibility Index [4] was used as the basic reference for the work. It contains details of all calculations involved in the data analysis. Acoustical environments for speech were characterized by the Speech Transmission Index (STI) and background-noise levels.

In the present context, the background noise used to calculate SII is the total effective background noise due to the three influencing factors. As discussed in the Standard, their effects were quantified by means of STI measurements made using a speech source (SSARAH), either a regular or dummy-head (KUNOV) microphone, and the Maximum Length Sequence System Analyzer (MLSSA).

STI measurements were done in a way simulating typical ship-communication situations, using a speech source with four output levels (corresponding to four standard speech levels [4]). Ship personnel communicate verbally, both without and with the aid of communications equipment. When communications equipment was involved (non-linear system, involving coupling of a head-set with the listener's ear), a dummy-head microphone was used as the receiver; measurements were made using relevant speech levels (i.e., the source output setting appropriate to the task associated with the test) and in realistic background-noise levels. The effect of the acoustical response of the dummy-head microphone on measured results was taken into account mathematically during subsequent data reduction. When no communications equipment was involved (linear system), measurements were made with unrealistically high signal-to-noise ratios (i.e., quiet ship-operating conditions and using the highest source output setting) to improve accuracy. Background-noise levels in the more realistic operating conditions relevant to the task being considered were measured separately. Final results corresponding to more realistic speech-signal levels, background-noise levels and, thus, signal-to-noise ratios were determined mathematically.

2.1 Background-Noise and Warning-Signal Measurement

The MLSSA system was used to measure, in octave and third-octave bands and under realistic operating conditions, the spectra of the ship background noises at the positions at which STI measurements were made. In addition, the spectra of typical ship warning signals and alarms were measured at appropriate positions.

2.2 STI Measurement

Following are details of the procedures used in the cases of both direct communication and electroacoustical-device communication.

Pre-Calibration

Calibration of the measurement system was required to characterize it for use in correcting measurement data for potential system imperfections. This involved measuring the impulse response of the system in a "perfect' environment (anechoic chamber, microphone close to the source, negligible noise). STI_0 values were calculated from the impulse responses. These were converted to effective signal-to-noise ratios SN_0 and then to effective modulation-transfer-functions MTF_0.

Ship Measurement

In each test environment, source and receiver positions were chosen which were typical of the tasks carried out in those

environments. For each source/receiver combination, the MLSSA system was used to measure the associated impulse response. The MLSSA system was subsequently used to determine combined speech and noise-spectrum levels (S_m) and speech-transmission indices STI_m. These were converted to effective signal-to-noise ratios SN_m, which were converted to effective modulation transfer functions MTF_m. Corrected modulation transfer functions MTF_c, accounting for measurement system imperfection, were calculated using the calibration data MTF_0. The resulting MTF_c's were then converted to corrected effective signal-to-noise ratios SN_c. These and the measured combined speech and noise-spectrum levels S_m were used to calculate the corresponding equivalent speech-spectrum levels E' and equivalent noise-spectrum levels N'. These noise spectrum levels were added logarithmically to the background-noise levels measured under realistic operating conditions. The final E' and N' values were direct inputs to the SII and warning-signal-detection calculations.

4. ACKNOWLEDGEMENT

This work was supported by Transport Canada - Transportation Development Centre (TDC) and Canadian Coast Guard (CCG) under contract T8200-5-5567/A. The views, opinions and/or findings contained in this report are those of the authors and should not be construed as an official TDC or CCG policy or decision unless so designated by other documentation.

REFERENCES

[1] Ritmiller, L., Forshaw, S., Hodgson, M., and Laroche, C. (1999). Development of *bona fide* occupational requirements for hearing in Canadian Coast Guard operations. *Canadian Acoustics* 27(3).

[2] Forshaw, S., Ritmiller, L., Hodgson, M., and Laroche, C. (1999). Estimates of speech intelligibility based on equivalent speech- and noise-spectrum levels and hearing thresholds, *Canadian Acoustics* 27(3).

[3] Laroche, C., Hodgson, M., Ritmiller, L., and Forshaw, S. (1999). Audibility of signals and alarms in a Coast Guard environment, *Canadian Acoustics* 27(3).

[4] ANSI (1997). *American National Standard methods for the calculation of the Speech Intelligibility Index.* (ANSI S3.5-1997) (Revision of ANSI S3.5-1969). New York.

NATIONAL CENTRE FOR AUDIOLOGY

Canadian Audiology received a boost with the recent announcement that a National Centre for Audiology (NCA) is to be created at the University of Western Ontario. This initiative will create a national resource at the front ranks of the discipline, internationally.

"The National Centre for Audiology will provide an interdisciplinary environment within which to expand knowledge of hearing function and hearing problems, the needs of people with hearing impairment, and behavioural and technological methods to assist persons with hearing loss. The Centre will assume a national leadership role in the education of Audiologists, Audio Engineers, and other highly-qualified personnel, in the communication of knowledge about human hearing, in the development of public policy relating to hearing health, and in the delivery of hearing health care services to Canadians."

The NCA is being built on the strengths of Western's present program in Audiology. Over the next few years, faculty will be added in key areas of the discipline, educational programs will be revised and expanded, existing research programs will be expanded, and new research programs added. Links between the educational, research and clinical elements of the program are being strengthened.

Funding for the National Centre will come from a variety of public and private sources. One important component -- the enhancement of the research infrastructure of the Centre -- was recently approved by the Canadian Foundation for Innovation and the Ontario Research Development Challenge Fund: together with private contributions, these agencies will contribute more than $3 million towards the purchase of equipment and space for the Centre.

Support for the development of the other components of the NCA is continuing to be sought. Erin Lawson, Community Relations Officer at Western's Faculty of Health Sciences, says that the community response to the NCA initiative has been extremely positive: "in planning Western's 125th anniversary fundraising campaign -- which is scheduled to begin shortly -- what we found was that the NCA initiative was the one that was immediately understood by everyone involved to be relevant and important. It's also been the one that has received the most encouragement from the community and the institution."

For more information on the NCA initiative, contact Lucy Kieffer, Administrative Officer, at (519) 661-3901 or by e-mail at kieffer@audio.hhcru.uwo.ca

ESTIMATES OF SPEECH INTELLIGIBILITY BASED ON EQUIVALENT SPEECH- AND NOISE-SPECTRUM LEVELS AND HEARING THRESHOLDS

Stanley Forshaw
3958 Sherwood Rd.
Victoria, BC V8N 4E6

Laurel Ritmiller
BC Research Inc.
3650 Wesbrook Mall
Vancouver, BC V6S 2L2

Murray Hodgson
Occupational Hygiene Program
Dept. of Mechanical Engg.
University of British Columbia
Vancouver, BC V6T 1Z3

Chantal Laroche
Audiology and Speech Pathology
Faculty of Health Sciences
University of Ottawa
Ottawa, ON K1N 6N5

1. INTRODUCTION

This paper describes the speech-reception phase of a multi-phase project to determine the hearing requirements of Canadian Coast Guard (CCG) seagoing operations. The aim of this phase was to obtain an estimate of the beginning of "hearing handicap" (low fence) for speech discrimination in the acoustical environments of CCG vessels.

The fence, defined in terms of hearing threshold levels (HTL), would represent the minimum hearing needed to meet the CCG medical entrance requirement. Individuals not meeting the HTL requirement would undergo otological examination and audiological evaluation, including speech discrimination testing in noise, to provide a suprathreshold assessment of their hearing capabilities (see companion paper, Ritmiller *et al.*, 1999).

An estimate of the fence was obtained using engineering and psychoacoustical procedures that were supported by experimental data. The procedures included Speech Transmission Index (STI) data processing for the determination of equivalent speech- and noise-spectrum levels (see companion paper, Hodgson *et al.*, 1999), and the Speech Intelligibility Index (ANSI S3.5-1997).

2. SPEECH INTELLIGIBILITY INDEX

The ANSI S3.5-1997 Standard is a updated version of the 1969 procedure (Articulation Index (AI)) for calculating a physical measure that is highly correlated with the intelligibility of speech under a variety of adverse listening conditions (e.g., noise, filtering and reverberation). To identify the revision, ANSI renamed the procedure *Speech Intelligibility Index (SII).*

The SII is calculated using octave or one-third octave-band noise and speech spectra and the hearing loss of a listener. Hearing loss is treated as a fictitious internal noise which, if it were an external masker, would result in the same masked threshold. The speech-to-noise ratio (S/N) in a given frequency band, within the range 0 to 30 dB, determines the degree to which the speech signal in the band contributes to intelligibility. Each band is weighted with an importance function representing the contribution to intelligibility of the band. The SII can be interpreted as a proportion of the total speech cues available to a listener. The maximum value of the SII is 1.0 and signifies that all speech cures are available to the listener. Its minimum value is 0.0 and signifies that no cues are available.

Although the AI/SII provides good predictions of speech intelligibility under various conditions of filtering, noise distortion, and low speech level, the studies of Pavlovic (1984) indicate that the procedure over estimates the speech-discrimination ability of individuals with severe sensorineural impairment. He concluded that if a correction factor were to be applied to the frequency importance functions, the resulting AI/SII predictions for sensorineural-impaired individuals would be improved (Pavlovic *et al.*, 1986). The corrected importance function is given by:

$$C_i = 1.19 - 0.0127L_i \qquad \text{for } 15 < L_i < 94,$$

where C_i is the importance function for the (i)th frequency band and L_i is the hearing loss (dB HTL) in the (i)th band. The SII determinations carried out in this study were corrected using the above equation and are designated as SII(C).

3. DEVELOPMENT OF HTL PROFILES

An array of hearing losses was prepared to encompass the range within which the low fence was likely to occur. Twenty profiles were defined, based on the epidemiological data published in ISO Standards 7029 (1982) and 1999 (1988), and represent typical manifestations of noise-induced and age-related hearing losses. The resulting HTLs at .5, 1, 2 and 4 kHz for five of the profiles are shown in Table 1, illustrating the extent to which hearing loss increases with profile number. These profiles were also used in the signal-detection phase of the project (see companion paper, Laroche *et al.*, 1999).

TABLE 1: Hearing thresholds in dB for five of the HTL Profiles at the four frequency bands that are most important for speech intelligibility.

PROFILE	.5 kHz	1 kHz	2 kHz	4 kHz
1	9	9	11	14
6	10	10	22	28
12	11	13	38	43
15	13	16	45	50
20	17	22	58	60

4. RESULTS AND DISCUSSION

Acoustical data files, comprised of equivalent speech- and noise-spectrum levels, were obtained for a number of ships' operating conditions and work areas in which speech-communication tasks had been identified as critically important (Ritmiller *et al.*, 1999). An array of SII(C) values was computed for each data file using the 20 HTL profiles. Table 2 shows a typical array. The SII(C) values descend from 0.79 (Profile 1) to 0.48 (Profile 20).

A number of investigators have produced estimates of the HTL at which persons begin to lose speech perception. Acton (1970) and Suter (1985) noted that the selection of a fence depends on the definition of hearing handicap and the conditions under which the handicap is assessed. Smoorenburg (1986) defined the onset of hearing handicap as the point at which an individual begins to notice a handicap in everyday noisy situations. Robinson *et al.*

(1984) concluded that a threshold of handicap is dependent on the difficulty of the listening task, and hence the selection of any one set of conditions for the definition of handicap is necessarily arbitrary. The estimates of the low fence determined by these investigators are summarized in Table 3.

TABLE 2: A typical array of SII(C) values.

HTL PROFILE	SII(C)	HTL PROFILE	SII(C)
1	0.79	11	0.64
2	0.78	12	0.63
3	0.76	13	0.61
4	0.75	14	0.59
5	0.74	15	0.58
6	0.72	16	0.56
7	0.70	17	0.55
8	0.68	18	0.54
9	0.67	19	0.52
10	0.65	20	0.48

TABLE 3: Estimates of the low fence for speech discrimination in terms of mean HTL, averaged across specified audiometric test frequencies.

AVERAGE HTL	FREQUENCY RANGE	SOURCE
19 dB	1, 2, 3 kHz	Acton (1970), Suter (1985)
27 - 34 dB	1, 2, 3 kHz	Robinson *et al.* (1984)
30 dB	2, 4 kHz	Smoorenburg (1992)

TABLE 4: US Army MIL-STD-1472 intelligibility requirements in terms of the Articulation Index (AI) (Anon, 1981).

COMMUNICATION REQUIREMENT	AI
Exceptionally high intelligibility (separate syllables understood)	0.7
Normally acceptable intelligibility (separate syllables understood, about 98% of sentences heard correctly, single digits understood)	0.5
Minimally acceptable intelligibility (limited standardized phrases understood, about 90 % of sentences heard correctly; not acceptable for operational equipment)	0.3

The implications of setting a low fence must be considered carefully. A fence that is unnecessarily restrictive will require a number of the candidates seeking employment to undergo otological and audiological assessment that would not otherwise be required. A fence that is too permissive may result in persons performing critical communication tasks who are not able to perceive speech in noise adequately. With reference to the communication requirements given in US Army MIL-STD-1472 (Table 4, Anon (1981)), it was concluded that a SII(C) cut-off in the range 0.50 and 0.60 would meet the CCG hearing requirements.

The HTL profiles occurring at SII(C) cut-off values equal to 0.50 and 0.55 were averaged across the critical speech-communication task results. The resulting mean HTL profiles and their corresponding hearing thresholds fell within the range of the low-fence estimates summarized in Table 3.

5. ACKNOWLEDGEMENT

This work was supported by Transport Canada - Transportation Development Centre (TDC) and Canadian Coast Guard (CCG) under contract T8200-5-5567/A. The views, opinions and/or findings contained in this report are those of the authors and should not be construed as an official TDC or CCG policy or decision unless so designated by other documentation.

6. REFERENCES

Acton, W.I. (1970). Speech intelligibility in background noise and noise-induced hearing loss. Ergonomics 13, 546-554.

Anon (1981). U.S. MIL-STD-1472. Summarized in *Human Engineering Design Data Digest.* Table XVII. Human Engineering Laboratory Detachment, Redstone Arsenal, Alabama.

ANSI (1997). *American National Standard methods for the calculation of the Speech Intelligibility Index.* (ANSI S3.5-1997) (Revision of ANSI S3.5-1969). New York.

Hodgson, M., Forshaw, S., Ritmiller, L., and Laroche, C. (1999). Characterizing ship acoustical environments for speech communication. Canadian Acoustics, 27(3).

ISO. (1982). *Threshold of Hearing by Air Conduction as a Function of Age and Sex for Otologically Normal Persons.* ISO Standard 7029. International Organization for Standardization.

ISO. (1988). *Determination of Occupational Noise Exposure and Estimation of Noise-Induced Impairment.* ISO Standard 1999. International Organization for Standardization.

Laroche, C., Hodgson, M., Ritmiller, L., and Forshaw, S. (1999). Audibility of signals and alarms in a Coast Guard environment. Canadian Acoustics, 27(3).

Pavlovic, C.V. (1984). Use of the Articulation Index for assessing residual auditory function in listeners with sensorineural impairment. J.Acoust.Soc.Am., 75, 1253-1258.

Pavlovic, C.V., Studebaker, R.L., and Sherbecoe, R.L. (1986). An Articulation Index based procedure for predicting the speech recognition performance of hearing-impaired individuals. J.Acoust.Soc.Am., 80(1), 50-57.

Ritmiller, L., Forshaw, S., Hodgson, M., and Laroche, C. (1999). Development of bona fide occupational requirements for hearing in Canadian Coast Guard operations. Canadian Acoustics, 27 (3).

Robinson, D.W., Wilkins, P.A., Thyer, N.J., and Lawes, J.F. 1984). *Auditory impairment and the onset of disability and handicap in noise-induced hearing loss.* ISVR Technical Report No. 126. Institute of Sound and Vibration Research, Southampton, England.

Smoorenburg, G.F. (1986). Speech perception in individuals with noise-induced hearing loss and its implications for hearing loss criteria. In *Basic and Applied Aspects of Noise-Induced Hearing Loss*, edited by R.J. Salvi, D.Henderson, and R.P. Hamernik. (Plenum, New York), pp. 335-344.

Suter, A.H. (1985). Speech recognition by individuals with mild hearing impairments. J.Acoust.Soc.Am., 78, 887-900.

AUDIBILITY OF SIGNALS AND ALARMS IN A COAST GUARD ENVIRONMENT

Chantal Laroche
Audiology and Speech Pathology
Faculty of Health Sciences
University of Ottawa
Ottawa, ON K1N 6N5

Murray Hodgson
Occupational Hygiene Program
Dept. of Mechanical Engg.
University of British Columbia
Vancouver, BC V6T 1Z3

Laurel Ritmiller
BC Research Inc.
3650 Wesbrook Mall
Vancouver, BC V6S 2L2

Stanley Forshaw
3958 Sherwood Rd.
Victoria, BC V8N 4E6

1. INTRODUCTION

This paper is a report on one phase of a research project aimed at developing occupational hearing criteria for the Canadian Coast Guard (CCG). The overall objective was to propose reliable criteria specifying whether or not CCG ship personnel have adequate hearing abilities to carry out their jobs proficiently. In three companion papers (Ritmiller *et al.*, 1999, Hodgson *et al.*, 1999, Forshaw *et al.*, 1999), details are given about the prediction of speech intelligibility in noise, one of the most important hearing abilities necessary to perform CCG duties safely. An additional concern addressed in this paper is the audibility of signals (e.g., sound of telephone ringing) and alarms (e.g., radar alarm). In CCG environments, the perception of auditory signals and alarms is crucial to ensure safety of people and equipment. The assessment of the different auditory signals and alarms collected on the CCG vessels (Ritmiller *et al.*, 1999) were performed with a computerized model, called DETECTSOUND™ (Laroche *et al.*, 1991). This model has been used previously in different environments (Laroche and Lefebvre, 1998; Proulx *et al.*, 1995).

2. DETECTSOUND™ MODEL

DETECTSOUND™ allows users to determine the characteristics of warning sounds to be used in a specific environment or to evaluate the effectiveness of the warning sounds currently used in an environment. The foundations of the model have been presented in a previous paper (Laroche *et al.*, 1991). DETECTSOUND™ considers the following information:

- the background noise at each workstation (1/3 octave band levels from 25 to 12,500 Hz);
- the hearing protectors worn by a standard individual or by specific individuals (attenuation in dB from 63 to 8,000 Hz);
- the audiogram of a standard individual or the actual individuals assigned to a workstation (hearing thresholds from 125 to 8,000 Hz);
- all warning sounds that can be heard at the station (1/3 octave band levels from 25 to 12,500 Hz).

The loss of frequency selectivity (i.e., the ability of the ear to extract a sound signal in a background noise) is also taken into account in the software. It is statistically related to the loss of sensitivity.

These factors are analyzed together and the results are displayed in a graphic or a table form. Figure 1 is an example of a graphic display. In Figure 1, the frequency content is presented on the x axis and the level of each 1/3 octave band of the noise or the warning sound is on the y axis. The full horizontal line corresponds to the background noise level at the workstation. The vertical lines correspond to the spectral content of the signal heard at this workstation. The dark zone represents the "hearing window" (i.e., the spectral and level region in which at least three spectral lines of a warning sound should be in order to attract attention and be recognized among different warning sounds). This zone is based on the masked threshold (i.e., hearing threshold in noise) computed for each third octave band to which 13 to 25 dB is added. These last values are extracted from the ISO 7731 standard (1986) and other publications (Patterson, 1982).

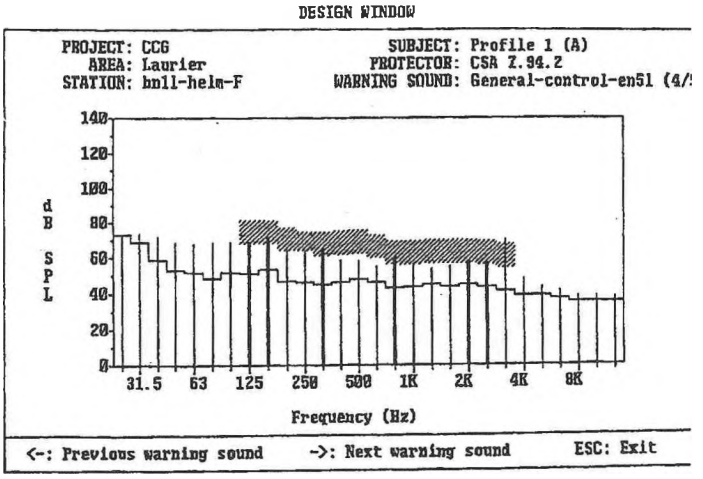

Figure 1: Graphical display of the "hearing window" for a particular workstation and a particular sound signal

According to the ISO standard (1986), at least one spectral component should reach the "hearing window". In order to address fluctuations in background noise common in work environments, many authors have suggested that more than one component must reach the "hearing window". This ensures that if one component is temporarily masked by the background noise other components would then be available. In Figure 1, the alarm should be well perceived and recognized by people with normal hearing because six spectral lines are inside or at the borders of the "hearing window". If all the spectral lines would have been below the design window, modifications would have been required. For example, the spectral content of the warning sound should have been changed, the signal level increased or the background noise reduced. If the lines would have been over the design window, the warning sound level would have been too high and could have caused hearing damage, interference with communication or a startle reaction. Based on these facts, a specific method of analysis was developed.

3. METHOD

The purpose of this phase of the project was to estimate the low fence for auditory signal-perception in terms of sensorineural hearing loss. Hence, an array of hearing losses was prepared to encompass the range within which the low fence was likely to occur. As explained in a companion paper (Forshaw *et al.*, 1999) twenty hearing threshold level (HTL) profiles were defined, based on the epidemiological data published in ISO Standards 7029 (1982) and 1999 (1988), and represent typical manifestations of noise-induced and age-related hearing losses. The resulting HTLs at .5, 1, 2 and 4 kHz are shown in Table 1 of the companion paper (Forshaw *et al.*, 1999) for five of the profiles.

In order to run DETECTSOUND^{TM}, the 1/3 octave-band levels of each signal or alarm and each background noise (for the same position in space) have to be entered. The data were collected using a Rion Type 1 sound level meter and a digital audiotape recorder at each workstation where an alarm or signal was used.

For the hearing protectors requirement of DETECTSOUND^{TM}, the attenuation values of a Type A protector (CSA Z94.2 Standard, 1994) were used. These values were used only for workstations where hearing protectors were normally worn. The CSA Z94.2 Standard was used because of the variability in the type of hearing protectors used on CCG vessels. By using Type A values, we were confident that the predictions would be conservative.

To determine the low fence for signal perception, each alarm or signal was analysed according to the following decision matrix (Table 1).

Table 1: Decision matrix for signal and alarm perception using the DETECTSOUND^{TM} model

(++)	3 or more components in the "hearing window"
(+)	1 or 2 components in the "hearing window" and some under, but above noise level
(+-)	1 or 2 components in the "hearing window"
(-)	All components under the "hearing window" but above noise level
(--)	All components under noise level

The low fence was set at the lowest HTL profile for which the (+-) label was met, for each alarm and signal. This decision represents a compromise and was motivated by the ISO 7731 standard (1986) which states that one component should at least be well over the background noise, and the fact that the (++) label would be the ideal situation. In fact, in this project, the (++) label was not achieved in many situations, mainly due to high background noises, low levels of signal or a limited number of spectral components in the signal. In certain background noises, DETECTSOUND^{TM} predicted that it was even impossible for people with HTL Profile 1 (best hearing profile) to perceive the signal.

4. RESULTS AND DISCUSSION

Figure 1 showed an example of a (++) label for a specific alarm on a specific vessel. Figure 2 shows an example of (+-) label, which would represent the low fence HTL profile for this specific alarm.

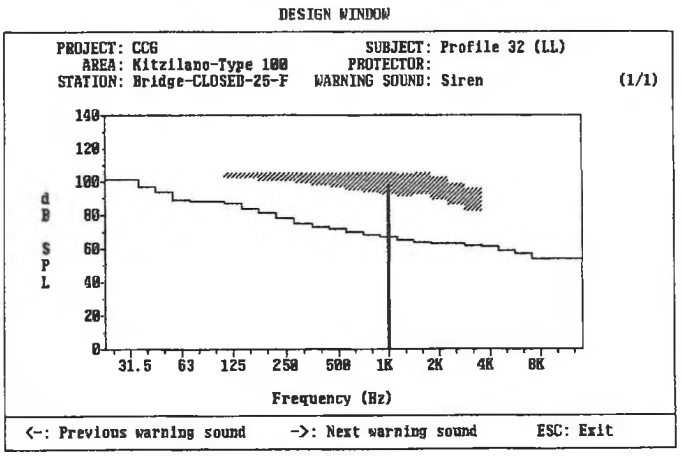

Overall, the minimum signal perception HTL profile was less than the minimum speech perception profile. This finding is not surprising as speech perception in noise refers to much more complex auditory abilities than signal perception. This phase of the project has nevertheless shown that many alarms or signals have not been designed or chosen as a function of the background noise, worker hearing loss and the wearing of hearing protectors. It is important to mention that all these results are based on prediction models and would have to be validated on human subjects in order to propose hiring criteria which takes into account more than just hearing sensitivity.

5. ACKNOWLEDGEMENT

This work was supported by Transport Canada-Transportation Development Centre (TDC) and the Canadian Coast Guard (CCG) under contract T8200-5-5567/A. The views, opinions and/or findings contained in this report are those of the authors and should not be construed as an official TDC or CCG policy or decision unless so designated by other documentation.

6. REFERENCES

C.S.A. (1994) *Hearing Protectors*. Canadian Standards Association, Standard Z94.2.

Forshaw, S., Ritmiller, L., Hodgson, M., Laroche, C. (1999). Estimates of speech intelligibility based on equivalent speech- and noise-spectrum levels and hearing thresholds. *Canadian Acoustics*, 27(3).

Hodgson, M., Forshaw, S., Ritmiller, L., Laroche, C. (1999). Characterizing ship acoustical environments for speech communication. *Canadian Acoustics*, 27(3).

ISO (1982). *Acoustics-Threshold of Hearing by Air Conduction as a Function of Age, Sex for Otologically Normal Persons*. International Organisation for Standardization, Standard 7029.

ISO (1986). *Danger signals for workplaces-Auditory danger signals*. International Organisation for Standardization, Standard 7731.

ISO (1988). *Acoustics-Determination of Occupational Noise Exposure and Estimation of Noise-Induced Hearing Impairment*. International Organisation for Standardization, Standard 1999.

Laroche, C., Lefebvre, L. (1998). Determination of optimal acoustic features for reverse alarms. *Ergonomics*, 41, 1203-1221.

Laroche, C., TranQuoc, H., Hétu, R., McDuff, S. (1991). "Detectsound": A computerized model for predicting the detectability of warning signals in noisy workplaces. *Applied Acoustics*, 32, 193-214.

Patterson, R. (1982). Guidelines for auditory warning systems on civil aircraft. *CAA Paper 82017*, Civil Aviation Authority, London.

Proulx, G., Laroche, C., Latour, J.C. (1995). Auditory problems with fire alarms in apartment buildings. *Proceedings of the Human Factors and Ergonomics Society*, 39th Annual Meeting, San Diego, 2, 989-993.

Ritmiller, L., Forshaw, S., Hodgson, M., and Laroche, C. (1999). Development of bona fide occupational requirements for hearing in Canadian Coast Guard operations. *Canadian Acoustics*, 27 (3).

CONTROL OF LOW-FREQUENCY FOOTSTEP SOUND & VIBRATION TRANSMISSION THROUGH A WOOD-FRAMED, CONCRETE-TOPPED FLOOR

Clair W. Wakefield
Wakefield Acoustics Ltd., 1818 Belmont Avenue, Victoria, BC V8W 3Z2

NATURE OF THE PROBLEM

The owners of certain units within a new wood-frame condominium building in Victoria were experiencing excessive low-frequency noise and vibration due to the footsteps of the occupants of the units above. This problem was occurring even though the floor system (which consisted of a 38mm concrete topping layer over 16mm plywood sheathing on 38 x 235mm wooden joists, R28 Batt insulation in the joist cavities and a ceiling of 16mm GWB suspended on 22mm resilient channels) had been field tested at FSTC 56 and FIIC 77 to 80 (carpeted areas) and met the maximum deflection (stiffness) requirements of the 1992 B.C. Building Code. It was, however, concluded that the problem (which included very low-frequency thudding noise and the perception of vibration in objects as well as in the floors of the units below) was due to the insufficient stiffness of the basic floor section, particularly in the living room/dining room areas where joist spans were longest.

PROPOSED SOLUTION

After consideration by the building's structural engineer of the options available to stiffen the floor section, it was decided to remove the existing GWB ceiling and "glue and screw" 38 x 89mm wood studs to the bottoms of the wood joists to form "I-beam"-like structures. The 16 mm GWB ceiling would then be reapplied on resilient channels with a second layer of 13mm GWB attached and foam spacer strips inserted between the edges of the suspended ceiling and the walls to minimize "flanking transmission" between wall and ceiling GWB surfaces.

TEST OF EFFECTIVENESS OF STIFFENING

To test the effectiveness of the proposed stiffening measures, before-and-after noise transmission tests were planned for one living room/dining room area. Since the floor section had proved acceptable under the standard FIIC test and since the problem was primarily at frequencies below the 100 Hz. lower limit of the standard test, it was decided to employ a "controlled walker" test instead, so as to better simulate the real source of the disturbance.

One-third octave band average sound spectra were recorded (using a Larson-Davis Model 2800 Real Time Analyzer) at two positions in the lower unit while a "standard person" (an approximatley 75 kg male) walked diagonally back and forth across the length of the carpeted living room/dining room of the upper unit. This test was then repeated after the corrective work was completed using the same walker wearing the same street shoes and walking in nominally the same fashion.

FOOTSTEP NOISE REDUCTION DUE TO STIFFENING

The results of the before and after tests of footstep noise levels in the lower condominium unit are summarized in the table below. When analyzed in one-third octave bands, it is seen that the noise reductions achieved varied widely, from as much as 15 to 18 dB in the 8, 50, and 63 Hz. bands, to as little as 2 to 3 dB in the 16 and 20 Hz. bands. It is of interest to note that, unfortunately, the smallest improvement occurred in the frequency band (16 Hz.) containing the highest unweighted noise level. This variation in effectiveness is to be expected since the primary result of the stiffening treatment would have been to alter the natural modes of vibration of the floor and therefore redistribute their natural, resonant frequencies. Since the force created by footsteps is by nature impulsive, the spectrum of the force input into the floor will be quite broad band. Energy will then be available to excite natural modes of vibration even though they may have generally been shifted upwards in frequency by the stiffening of the floor section. The non-resonant response of the floor (at frequencies away from its natural modes), however, will tend to be reduced due to the overall increased stiffness of the section.

In terms of the perception of the noise situation within the lower unit, the A-weighted footstep noise levels were reduced by 6.9 and 8.4 dBA at microphone positions 1 and 2 respectively. Subjectively, there was a marked improvement in the overall impression of very low-frequency sound being radiated from the ceiling. In particular, during the "before" tests, sub-audible sound radiated from the ceiling overhead was distinctly "feelable" as a "pressure wave". During the "after" tests, this sensation was no longer evident. The unit's owner now perceived much less vibration and his CD player no longer skipped when his neighbour walked across the floor above

Microphone Position	Test Condition	Footstep Noise Levels (dB) in One-Third Octave Frequency Bands (Hz.)											
		8	10	12.5	16	20	25	31.5	40	50	63	80	100
1	Before	49.8	56.7	69.2	76.1	71.2	64.2	58.2	57.6	61.1	52.5	42.9	37.0
	After	39.4	49.6	60.6	72.5	64.7	57.7	47.4	47.6	46.8	37.2	35.7	31.3
	Reduction	10.4	7.1	8.6	3.6	6.5	6.5	10.7	9.9	14.3	15.3	7.2	5.6
2	Before	51.6	60.3	68.1	71.1	67.8	63.3	63.6	62.1	59.9	58.0	44.7	35.4
	After	33.8	48.1	54.8	69.3	64.4	57.9	53.8	54.4	44.9	41.7	38.6	29.5
	Reduction	17.8	12.1	13.3	1.8	3.4	5.3	9.8	7.7	15.0	16.4	6.1	5.9

PRECISION MICROPHONES and MICROPHONE SYSTEMS

ACO Pacific, Inc.

2604 Read Ave.
Belmont, CA 94002 U.S.A.
Tel:650-595-8588 FAX:650-591-2891
e-mail: acopac@acopacific.com

Established in 1978 ACO Pacific, Inc. is chartered to serve the needs of both End-users and Equipment Manufacturers. Headquartered in the San Francisco Bay Area, ACO Pacific, Inc. has manufacturing facilities and suppliers both in California and internationally.

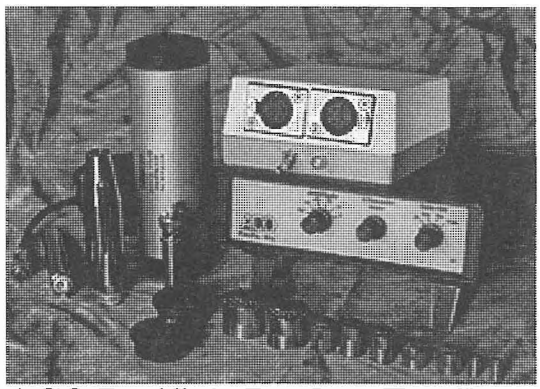

Our OEM relationships include Hewlett Packard, Audio Precision, SPS, DRA Labs and many other large and small instrumentation and process control manufacturers. Our End-user customers include: manufacturers of loudspeakers; computers and peripherals; heavy equipment; automobiles and automotive parts - tires, brakes, engines; universities; aerospace; and an alphabet soup of government agencies US and foreign.

ACO Pacific's Product Family

Measurement Microphones
Microphone Preamplifiers
Microphone Power Supplies
SPL Calibrators
Simple Intensity™ Sound Intensity Systems
Very Random™ Noise Generators

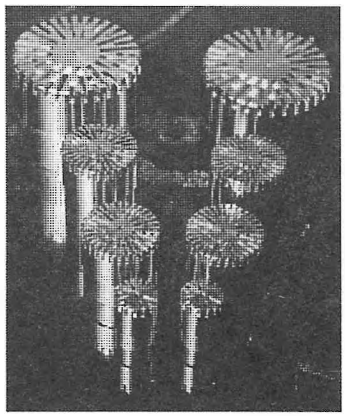

The "Alternative"

Type 1 Measurement Microphones
1, 1/2 and 1/4 Inch Models
Stainless Steel
and
Titanium Diaphragms
Quartz Insulators
Frequency Responses to 120 kHz
Noise Floors below 10 dBA
Meets or Exceeds IEC and ANSI Standards

Model 3024

Very Random™Noise Generator

Pink and White Noise, 1kHz Sine Outputs
1.6 Hz to 39 kHz (-3dB)
Portable - Battery and AC Power

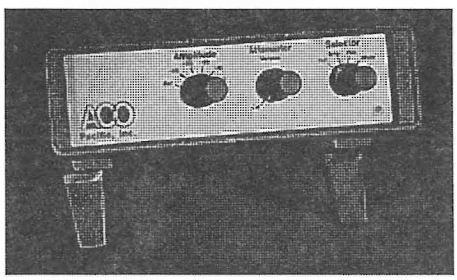

ACOustical Interface™

Precision Microphone Power Supplies
2 and 4 Channels - Gain Available
XLR and Lemo™ Connectors

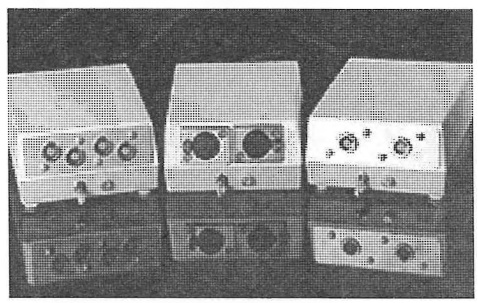

PS9200KIT

Includes: PS9200 (XLR) Power Supply
AC Adaptor
4012 Preamplifier w/CA4012-5 Cable
Selection of 1/2 Inch Type 1 Microphone
WS1 - 3 inch Windscreen
SC1 Die Cut Storage Case (SC2 optional)
Options: 511E SPL Calibrator (shown)
"G" Gain Stage

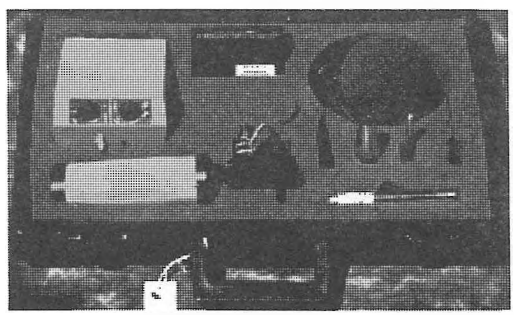

ACOustics Begins With ACO™

AGGREGATE SUBJECTIVE RATINGS OF AIRBORNE SOUND INSULATION

J.S. Bradley
Institute for Research in Construction, National Research Council, Montreal Rd. Ottawa, K1A 0R6

Introduction

This paper reports the results of a survey of sound insulation between homes in multi-family dwellings. The survey included interviews of 600 subjects and airborne sound insulation measurements of their 300 party walls. The subjects lived in both row housing and multi-floor apartment buildings in three different Canadian cities. The questionnaire first asked about general issues concerning the subjects building followed by more specific questions rating the sound insulation and the audibility of various noises. Sound transmission loss measurements were made in 1/3-octave bands from 100 to 4000 Hz. In addition to the standard ISO and ASTM single number ratings, 20 other single number sound isolation measures were calculated.

Acoustical Data

Figure 1 summarises the results of the sound transmission loss measurements of the 300 walls. This figure shows the average, ± 1 standard deviation and the complete range of transmission loss values in each frequency band. Measured effective STC values varied from 38 to 60 with an average of 49.7 and a standard deviation of ± 4.7 dB. (In this paper responses are primarily related to the standard The effective Sound transmission Class value which is referred to as STC1 to discriminate from other non-standard versions.).

The average noise levels recorded in the 600 homes and their standard deviations were LeqD 47.5 ±8.9 dBA, LeqN 39.8 ±8.4 dBA, Leq24 46.2 ±7.9 dBA. A summary of the acoustical measurements was published some time ago [1].

Principal Survey Results

Subjects were first approached by letter and asked to participate in a neighbourhood satisfaction survey. They were subsequently interviewed in their homes. Initial questions were to obtain spontaneous responses without any mention of sound insulation or noise. These included responses concerning satisfaction with their building, whether they would like to move and how considerate their neighbours were. Subsequent questions obtained directly elicited responses concerning whether they heard various sounds and how annoying they were. For most survey questions, responses were obtained using 7-point response scales. For convenience this paper concentrates on 3 principal responses: the single question response giving a subjective evaluation of the residents' sound insulation and composite response scales concerning sounds that they heard (HEAR) and the resulting annoyance (ANOY).

A number of spontaneous responses were significantly related to STC1 values. (STC1 is the ASTM standard STC rating including the 8-dB rule). Residents with party walls having lower sound insulation were more likely to want to move and less likely to be satisfied with their building. There was also a statistically significant relationship between STC1 values and how considerate neighbours were rated. That is, people with poor sound insulation tended to blame the resulting disturbance on inconsiderate neighbours rather than on poor sound insulation.

The principal elicited responses were also significantly related to measured sound insulation. Figure 2 plots aggregate subjective ratings of sound insulation as a function of measured STC1 values. For the 2nd order polynomial fit shown in this figure the associated R^2 value was 0.939 and there is clearly a strong relationship between objective and subjective ratings of sound insulation. On average, people can accurately evaluate the amount of sound insulation between them and their neighbours. Composite ANOY responses were similarly related to measured STC1 values. (R^2 = 0.960). Annoyance decreased with increasing values of STC1 and appeared to approach a rating of 1 (Not at all annoyed) at approximately STC1 = 65 dB.

Figure 3 shows the relationship between the composite HEAR responses. Again there is a very strong relationship with STC1 values but the form of the relationship is quite different than for the previous two cases. Above about STC1 = 50, residents report hearing the sounds from their neighbours less often as STC1 values increase. That is, when there is better sound insulation they hear their neighbours less often. Extrapolating this trend would suggest that between an STC1 60 and 65 they would not hear their neighbours at all. However, below about STC1 = 50 this HEAR response does not vary with STC1. This is because how often they hear their neighbours depends not only on sound insulation but also on how often neighbours typically make audible sounds. It appears that below an STC1 of about 50 responses are not influenced by sound insulation but only by how frequently neighbours make audible sounds. For a party wall to minimize this disturbance it must have an STC1 of greater than 50 and a party-wall sound insulation of STC1 = 55 or more is required to significantly reduce the disturbance that neighbours hear. Other responses led to similar relationships and support this trend.

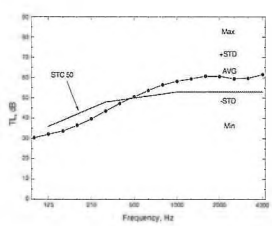

Figure 1. Transmission loss values of the 300 walls and STC rating contour of the average wall

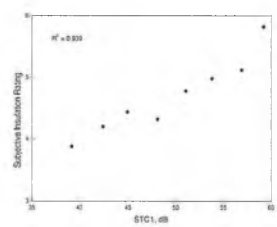

Figure 2. Mean subjective ratings of sound insulation versus aggregate STC1 values.

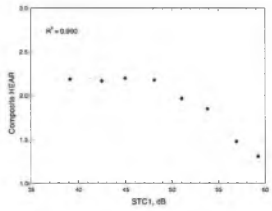

Figure 3. Figure 3. Mean subjective ratings of the composite HEAR scale versus aggregate STC1 values.

Other Measures of Sound Insulation

The ASTM STC and the ISO R_W are now the most commonly used single number measures of sound insulation. These and a number of other measures were tested using second order polynomial fits to the principal responses. The R^2 values from these relationships are given in Figure 4. The standard STC1 measure was best correlated with all three responses. Correlations with STC2 (excluding the 8 dB rule) and variations of the ISO R_W measure were slightly less successful although the differences were not statistically significant. Various average TL values [2] were less successful. It was concluded that these results give no reason to change the standard STC measure (including the 8 dB).

Conclusions

In this study the average party wall corresponded to STC 50. This may suggests that 50% of party walls in Canada provide less insulation than the current recommendations of the National Building Code.

There is considerable evidence that residents in multi-unit buildings are disturbed by noises from there neighbours and that this disturbance decreases with increasing sound insulation between the homes. Residents even mistakenly blame neighbours for being inconsiderate when poor sound insulation is the cause of the disturbance.

Many responses do not decrease unless party-wall sound insulation exceeds STC 50 and significant reductions in these responses require party-wall sound insulation of STC 55 or more.

STC 55 is therefore recommended as a realistic goal for better sound insulation to reduce annoyance and disturbance.

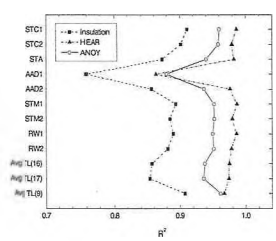

Figure 4. R^2 values associated with 2nd order polynomial fits of 3 principal survey responses with single number sound insulation measures.

STC 60 is identified as a more ideal goal for party-wall sound insulation that would essentially eliminate disturbance by noise from neighbours.

References

Bradley J.S., "Acoustical Measurements in Some Canadian Homes", Canadian Acoustics, Vol. 14, No. 4, 1986, 19-21, 24-25, (1986).

Tachibana, H., Yano, H., Hamada, Y., and Koyasu, M., "Relationships among Various Single-Number Indices for Sound Insulation of Building Walls", Proceed. Inter Noise 96, pp. 1801-1806, Liverpool, (1996).

Acknowledgements

Field measurements were made by Valcoustics Canada Ltd, Harford Kennedy Ltd and SNC Inc.

Acoustic Ecology: Concept And Case Study

M. Kathleen Pichora-Fuller
University of British Columbia, 5804 Fairview Ave., Vancouver, BC, V6T 1Z3

INTRODUCTION

Communications researchers have studied 'soundscapes' by recording and analyzing the sounds found in specific environments. Such studies emphasize the person-environment relation or how the sound environment is perceived and understood by individuals or society (Truax, 1978, 1994; Schafer, 1977). Acoustic ecology is the study of systematic relationships between humans and soundscapes. Furthermore, inter-personal communication by spoken language modulate and are modulated by soundscapes. Soundscapes can be created, improved or modeled. Given the recent recognition that environments can affect social participation (WHO, 1998), this study explores the acoustic ecology of older adults in terms of the influences of sound on their feelings of personhood and connectedness to the physical world and to others.

METHOD

Participant. An elderly woman living in a care facility was recruited for the study by the audiologist working at the facility. The resident had worn binaural in-the-ear hearing aids daily for one year . Her cognitive and physical abilities were good. Mental health issues were the main reason she lived in residential care. She was well-educated and artistically inclined, with writing, painting and music filling her time.

Conditions. An student (P. Kooner) enrolled in Barry Truax's soundscape course at SFU accompanied the author for a half-day visit with the participant and recorded about four hours of the participants' soundscape in her normal activities from breakfast until her mid-afternoon rest.

Measures. As well as recording the soundscape, the participant's spontaneous comments about her soundscape, and her responses to the questions of the researchers were also audiorecorded. Her comments and responses were transcribed, analyzed, and with the researchers' observations, they were used to describe the meanings of sounds to the participant.

RESULTS

Soundscape Elements. Six different scenes were evaluated: 1. breakfast in the dining hall; 2. morning announcements; 3. elevator ride; 4. getting pills at the nursing station; 5. the resident's private room; 6. a walk on the seawall.

Common sounds in the dining hall included talking by residents and staff, dishes during serving and eating, music, and traffic. The morning announcements were made in the dining hall using a good quality soundfield system. Many residents rode the elevator to go to their rooms after breakfast and there was lively discussion about who was getting off at which floor. The nursing station scene featured residents waiting to talk to a nurse behind a counter in the hallway on the floor where the resident had her room. Sounds recorded in her private room included talking with the researchers and on the phone, her breathing, news and classical music on the radio. Sounds heard on the walk outside, included buses, footsteps, birds, bicycles, children playing, and a leaf blower in the distance.

Meanings of the Soundscape. Sound served three primary purposes for the participant: 1. overcoming loneliness; 2. providing supportive structure; 3. providing stimulation.

Loneliness. In her spontaneous comments, the participant spoke of feelings of social isolation. She said, "I'm finding that, that 100-year-old lady -- she lives in the next room -- she's been here for three months. I was terribly lonely until she came. But she and I've just clicked. And so I do things to ease her life a little.... I've been terribly lonely." However, at the same time that she had few opportunities for intimate social interaction, sound enabled remote social connections that took on the significance of friendships for her. About the radio, she said, "I live by the CBC. The CBC is my daily routine. You know, I'm a friend of the CBC. I support them... I listen to the news... These are my friends, the announcers."

Structure. Routines provide supportive structure for the participant as they do for many elderly persons. She organized her day by routines: "I don't usually go to any of the programs. I go walking about 11 o'clock. Lunch is at 12:30." Sound played a significant role as a kind of familiar structure: "I have season tickets to the symphony... Music is highly important to me.. . I learn music by repeating it... when I hear it again, I'm alerted to it. Now, last night they played Beethoven's violin concerto. And I went through a period of really loving that, playing it and playing it.. I haven't heard it for a long time. It was an old friend last night."

Stimulation. Her daily walks to and along the seawall provide the participant with opportunities to observe and explore a wider environment and to remain connected to society in general. About the sound of children at play, she said, "I really enjoy living on the creek, the way the kids talk to their mothers and fathers -- it's comforting to know that things are all rights." Sounds also trigger an awareness and curiosity about what others are doing. Whereas the sound of the leafblower was backgrounded for the researchers, it was an interesting foregrounded sound for the participant; she said, "That's a leafblower... there's another noise over here, the same kind of engine but I think that's for carpet cleaning.. yesterday, that kind of noise was there... I thought that sounds like a lawnmower, but I thought surely it isn't time for lawnmowers yet, so I really had to look for it."

DISCUSSION

It was striking that connection by sound to the physical environment and to remote social partners seemed to compensate, at least partially, for the participant's impoverished intimate social connectedness. The social, psychological, and aesthetic importance of sound to listeners and the appreciation of what they foreground and background has yet to be adequately appreciated in hearing rehabilitation.

REFERENCES

Schafer, R.M. (1977). The soundscape, Destiny Books: Rochester, Vermont.

Truax, B.(1994). Acoustic communication, Ablex: Norwood.

Truax, B. (1978). Handbook for acoustic ecology. ARC Publications, Simon Fraser University: Burnaby, BC, Canada.

WHO. (1998). Towards a common language for functioning and disablement: ICIHD-2 -- The international classification of impairments, activities, and participation. Geneva: WHO.

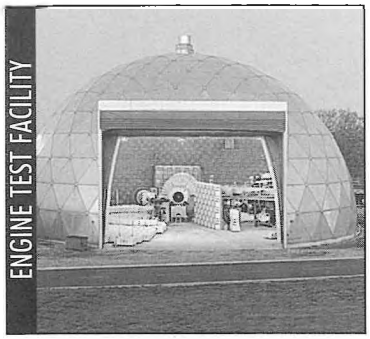

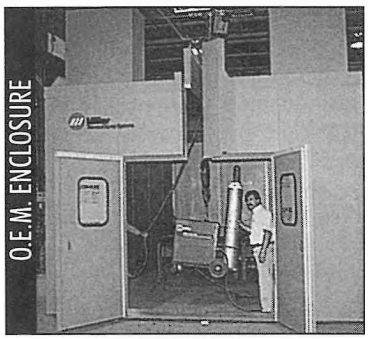

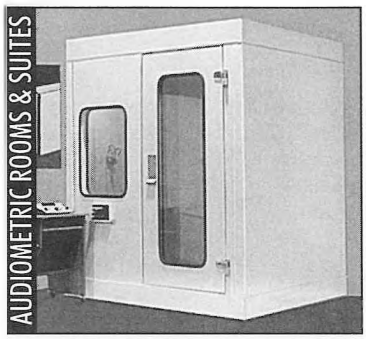

SOUND SOLUTIONS FOR THE FUTURE

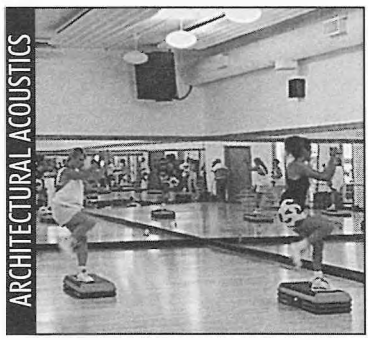

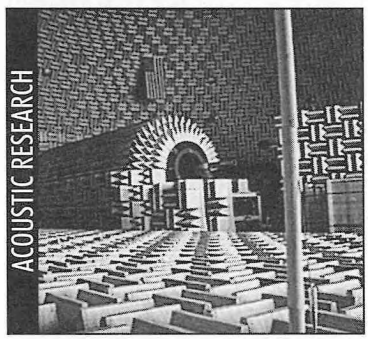

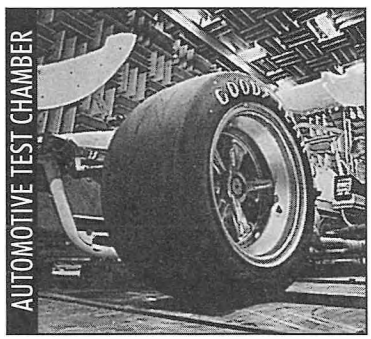

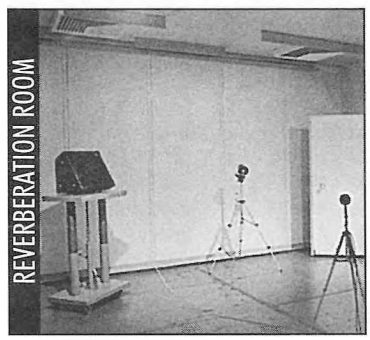

ECKEL

NOISE CONTROL TECHNOLOGIES

CANADIAN OFFICE
Box 776 100 Allison Avenue Morrisburg ON K0C 1X0
Tel: 613-543-2967 800-563-3574 Fax: 613-543-4173
Web site: www.eckel.ca/eckel e-mail: eckel@eckel.ca

NOISE CONTROL TECHNOLOGIES

IDENTIFICATION OF GATED ENVIRONMENTAL SOUNDS

Christiane Spanik and Kathleen Pichora-Fuller
University of British Columbia, 5804 Fairview Ave., Vancouver, BC, V6T 1Z3

INTRODUCTION

Environmental sounds are constantly present in our everyday lives, yet relatively little is known about how humans perceive such sounds and ascribe meaning to them (McAdams, 1993). Better understanding of how humans identify environmental sounds may have important implications for the design of machines that recognize and respond to specific auditory objects in complex scenes.

The gating paradigm has been very useful in research concerning the time course of word recognition (Grosjean, 1980, 1996). A meaningful sound sample is truncated into *gates*, or sub-samples, of varying duration. The first gate, or shortest sample, is presented and the listener attempts to identify the sound. Responses to each gate are recorded. The gate size is incremented until the sound is accurately and confidently identified. Misidentification errors for shorter gates are analyzed to determine the nature of the confusions that arose when the sample was insufficient for the listener to resolve perceptual ambiguities. By using this paradigm, the on-line auditory processing of environmental sounds could be compared to previous work on language processing.

METHOD

Participants. Sixteen normal-hearing listeners aged 20 to 35 years were paid to participate in the study. All had lived in the Greater Vancouver Region for at least two years.

Materials. The stimuli were eight recordings of natural environmental sounds selected from the Vancouver Soundscape Project library at Simon Fraser University (Truax, 1996). Four of the soundfiles consisted of high-context sequences of discrete or rapidly changing sound; for example, one soundfile consisted of the sound of the bus approaching and decelerating, braking, door opening, person stepping on steps, putting change in farebox, bus doors closing and engine revving as the bus drives away. The other four soundfiles consisted of low-context slowly changing or repetitive sounds; for example, one soundfile consisted of fizzling, crackling, and rumbling as the fire begins to burn with a slow increase in intensity as the fire burns more strongly. An auditory object occurring mid-soundfile was selected as the target to be identified (roughly analogous to a target word being selected from the middle of a sentence; e.g. Wingfield, 1996). For the four high-context files, the targets were: 1. change dropping into the bus farebox, 2. skytrain warning chimes, 3. computer drive booting up, 4. dot matrix printer printing. For the four low-context files, the targets were: 1. revving of motor cycle (Harley Davidson) engine, 2. ducks taking off from water, 3. fire crackling, 4. waves on a gravel shore. Pilot tests confirmed that the target auditory objects were easily identified in the intact soundfiles. A soundfile of squeaking door hinges was used for practice.

The smallest gate was a 400 ms sample centered on the target auditory object. Gate size could be incremented in either the preceding and following direction by progressively adding another 400 ms of the soundfile from the respective portion of the intact soundfile. Once all of the preceding gates were added, gate size continued to be incremented by adding the following gates until the entire soundfile was presented. Similarly, once all of the following gates were added, gate size continued to be incremented by adding the preceding gates until the entire soundfile was presented. The total duration of the intact soundfiles ranged from 10 to 40 seconds, with the average duration for the high-context sounds being 33 seconds and the average for the low-context sounds being 21 seconds.

Stimuli were prepared using Soundworks on a NeXT computer and converted from a 44 to a 20 kHz sampling rate for presentation using CSRE 4.5 (1995) software on a TDT system.

Conditions. Listeners were tested individually. Each listener attended two sessions, each lasting one to two hours. Hearing screening and the practice condition were completed before test conditions were administered. At each session, four soundfiles were presented, two high-context and two low-context. For each context type, one soundfile per session was presented with gates incrementing in the preceding direction and the other with gates incrementing in the following direction. The order of presentation of the eight soundfiles and the direction of the gate increments was counter-balanced such that each soundfile in each gating direction (8 x 2) was heard at least once in each order by one of the 16 listeners.

Procedures. Stimuli were presented binaurally at an average level of 70 dB SPL over TDH 39P earphones in a double-walled IAC sound-attenuating booth. After the presentation of each gate, the listener described what they thought they had heard. Participants were encouraged to guess and to give as much detail as possible. They also rated their confidence in their response on a scale from 1 to 10. Responses were recorded in writing by the experimenter throughout the experiment. Testing for a soundfile continued until the entire intact soundfile had been presented or until the listener identified the target correctly on five consecutive trials with confidence rated as 7 or greater.

RESULTS

Accuracy of sound identification. Four listeners identified all 8 targets correctly; ten listeners identified 7 correctly; one identified 6 correctly; one identified 5 correctly. Accuracy of identification of the sounds varied depending on the soundfile and gating direction (Figure 1). All listeners correctly identified high-context soundfiles 2 and 4. High-context soundfile 1 and low-context soundfile 4 were correctly identified by all listeners who heard preceding gates first, and low-context soundfile 1 was identified correctly by all listeners who heard following gates first. Performance was worse for other soundfiles. Performance was generally better for high-context compared to low-context soundfiles and for following compared to preceding gating, but the exceptions to this pattern suggest the importance of considering the unique properties of each soundfile that might have contributed to its identification.

Number of gates for identification. Considering each soundfile and each direction of gating, the time course of identification was considered for those listeners who accomplished correct identification. The median number of gates for accurate and confident identification are shown in Figure 2.

Figure 1: Number of listeners who correctly identified each the 8 environmental sound targets including 4 high-context targets and 4 low-context targets. Bars indicate the direction relative to the target in which the gates were incremented, dark bars for the preceding direction and light bars for the following direction.

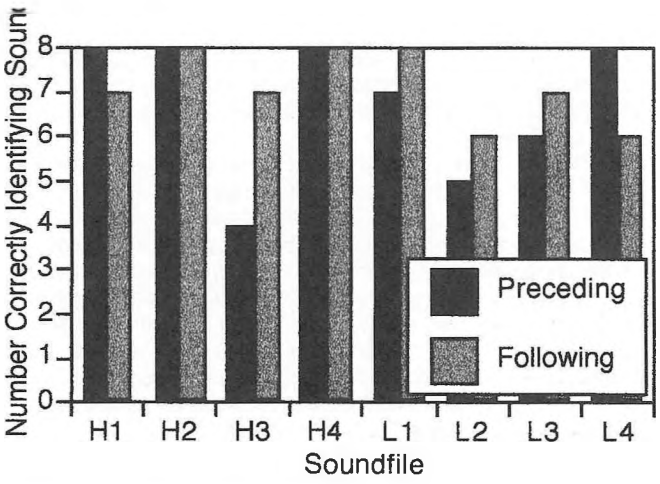

Figure 2: Median number of gates required for correct and confident target identification.

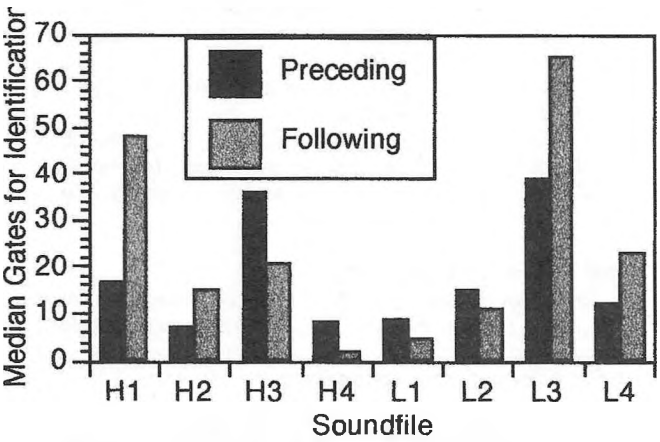

Overall, it is not surprising that few gates were required for listeners to identify the two high-context soundfiles that had been correctly identified by all listeners for both gating directions: 2 (skytrain chimes) and 4 (dot matrix printer). Likewise, few gates were required for listeners to identify the three soundfiles that were correctly identified by all listeners in one of the gating directions: high-context soundfile 1 (change in farebox) in the preceding direction, low-context soundfile 4 (waves on gravel) in the preceding direction, low-context soundfile 1 (motorcycle) in the following direction. However, few gates were also required for listeners to identify some of the files that were not correctly identified by all listeners: low-context soundfile 1 gated in the preceding direction, and low-context soundfile 2 (ducks) gated in both directions.

Error Analysis. The nature and frequencies of misidentifications were analyzed by listing all responses given for each target and counting the number of participants providing each response (Table 1). A large number of different responses were generated for each soundfile, with the majority of being idiosyncratic and with a much smaller set being generated by 3 or more listeners. The misidentifications were sometimes partially correct; for example, the listener identified ducks but did not specify the correct action of the ducks. Sometimes the misidentifications shared general semantic features with the target auditory object; for example, many subjects mentioned water for low-context soundfile 4 but did not mention waves on a beach. Sometimes misidentifications seemed to be acoustically rather than semantically based; for example, the most common misidentification for low-context soundfile 3 was 'rain' instead of 'fire'.

Table 1: Number of misidentifications for each soundfile.

Sound	Number of Different Incorrect Responses		
	> 3 Listeners	2-3 Listeners	1 Listener
H1	1	2	43
H2	3	8	21
H3	5	8	33
H4	2	7	17
L1	3	5	14
L2	5	9	17
L3	6	9	40
L4	5	13	18

DISCUSSION

The ability of listeners to identify environmental sounds increases as the number of gates are increased, but neither the amount nor the type of acoustical context surrounding the target sounds tested were related to identification of the target sound in a straightforward fashion. As suggested by Ballas (1993), performance seems likely to have been influenced by a variety of variables in different domains other than acoustics including the auditory objects' frequency, typicality, context independence, familiarity, and the availability of suitable linguistic labels. The pattern of misidentifications is reminiscent of the 'cohort' of words that listeners generate over the time course of word recognition (Marslen-Wilson & Tyler, 1980).

REFERENCES

Ballas, J.A. (1993). Common factors in the identification of an assortment of brief everyday sounds. Journal of Experimental Psychology: Human Perception and Performance, 19(2), 250-267.

CSRE (4.2) (1995). Computer Speech Research Environment. London, Ontario: AVAAZ Innovations Inc.

Grosjean, F. (1980). Spoken word recognition processes and the gating paradigm. Perception & Psychophysics, 28(4), 267-83.

Grosjean, F. (1996). Gating. Language and Cognitive Processes, 11(6), 597-604.

Marslen-Wilson, W.D., & Tyler, L.K. (1980). The temporal structure of spoken language understanding. Cognition, 8, 1-71.

McAdams (1993). Recognition of sound sources and events. In S. McAdams & E. Bigand (Eds.), Thinking in sound: The cognitive psychology of human audition, (pp. 146-198). Oxford: Clarendon Press.

Truax, B. (1996). Soundscape, acoustic communication and environmental sound composition. Contemporary Music Review, 15(1), 49-65.

Wingfield, A. (1996). Cognitive factors in auditory performance: Context, speed of processing, and constraints of memory. Journal of the American Academy of Audiology, 7, 175-182.

Machine Recognition of Sound Sources

Carol P. Jaeger and Charles A. Laszlo
Department of Electrical and Computer Engineering
University of British Columbia, 2356 Main Mall, Vancouver, B.C., V6T 1Z4

Introduction

In this paper an approach for machine-based classification of various types of sounds that may be present in an "everyday" acoustic environment is described. The classification process is part of a larger project that includes the identification of the presence of a sound source, classification of the source, and localization of the sound source relative to the microphone(s) with which it was measured. We have called the classification system the "Sound Class Framework" (SCF). The SCF and examples of signal processing techniques developed based on the SCF will be the focus of this paper.

Background

Understanding speech in noise is a common problem for the hard of hearing listener. A common method for improving the speech to noise ratio is to filter the signal acquired by a microphone to emphasize the bandwidth associated with speech. While this can result in an improvement in many cases, it is still a common occurrence that the spectral properties of the speech and noise sources present in a given situation overlap. This overlap limits the amount of noise reduction that can occur using spectral filtering alone. The approach we are taking in this project is to use spatial filtering to isolate a sound source of interest before transmitting it to the listener. In an earlier project [1], we found that spatial filtering was an effective way to isolate a sound source, and that with relatively simple signal processing techniques speech sources could be located and acquired in about 1.5 seconds. However, we also found that with the signal processing used, which was designed around the spectral and temporal qualities of speech only, the system was easily confused by multiple speech and noise sources. In order to achieve good spatial filtering, it is first necessary to identify the nature and position of all sound sources in a given environment relative to the recording microphone(s). It is only then that an informed decision can be made as to which sound to focus on.

The Sound Class Framework

The Sound Class Framework is a system that we have devised for the purpose of grouping sounds by their spectral and temporal characteristics. The SCF was developed to serve as an aid to the development of efficient signal processing techniques for the automatic identification and localization of sound sources. In this section we will first describe the basic structure of the SCF, and will then explain how it is used in the development of the signal processing techniques in this project.

There are four major categories in the SCF. They are: stationary-continuous (SC), stationary-intermittent (SI), nonstationary-continuous (NC), and nonstationary-intermittent (NI). Figure 1 shows the basic structure of the SCF. In the definition of these four categories, the distinction between stationary and nonstationary refers to the spectral properties of a sound and the distinction between continuous and intermittent refers to the temporal properties of a sound. Within these four categories, there is a further subdivision of sounds into more familiar groups (eg. speech, music, alarms, mechanical noise, etc.). In the SCF, speech and music would be classified as NI because the spectral distribution and signal intensity both change with time. Alarm noises such as a telephone ringer would be classified as SI because the spectral content is fixed for the duration of the ring but the ringing sound is heard for only short-lived intervals. It should be emphasized that in this project we have restricted the groups in the SCF to sounds likely found in an "everyday" acoustic environment such as the average home or office.

The goal of using the SCF as a basis for the signal processing in this project is to find just enough information about a particular sound source to be able to localize it and assign a priority to it in as short amount of time as possible. The way in which different types of sounds are grouped in the SCF allows the categorization of the sounds, such as "this is speech" or "this is an alarm", without the need to determine the exact details of the acoustical signal. We won't know what is being said, and won't be able to tell the difference between a telephone ringer and a microwave oven beeper, but it is our contention that we can successfully prioritize sound sources without knowing this level of detail. The priorities assigned to each type of sound source might vary from user to user, but a logical protocol being used as our default is as follows:

- under normal circumstances speech would be ranked as the highest priority sound source taking precedence over music and noise from machinery
- in the absence of a speech-only source the priority would shift to music or music and speech combinations (such as might come from a television)
- alarm and warning signals would take precedence over all other sources, speech or otherwise.

With the SCF in place, the next step in the project is the development of signal processing techniques that quickly and successfully identify sounds and automatically assign them to the correct group in the SCF.

Signal Processing Techniques

The signal processing for this project is divided into four parts. The first part is the identification and characterization of the sound sources present. The second part is the localization of the identified sounds relative to the recording microphone(s). The third is to create

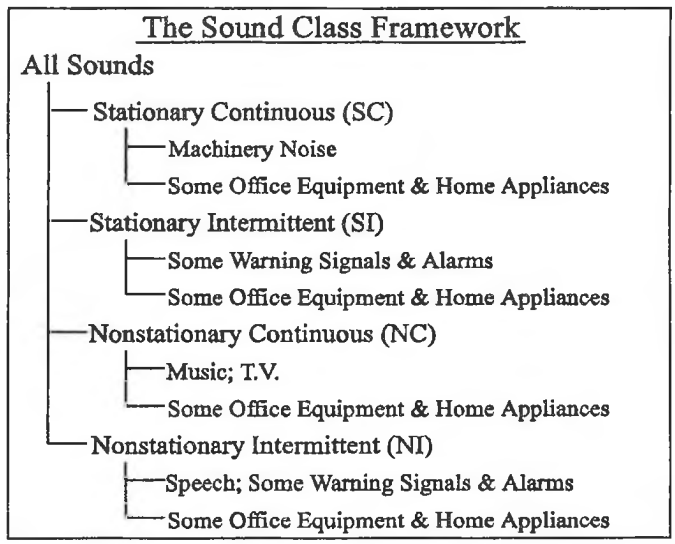

Figure 1: Structure of the Sound Class Framework. Note that some groups fit under more than one main category.

and/or update our "acoustic map" of the room and select a sound for amplification. The fourth is the control of an adaptive directional amplification system (eg. a mechanically controlled directional microphone, a phased array of microphones, or a series of fixed directional microphones arranged to accommodate all possible directions). In this paper we will describe the methodology of the first part of the signal processing, the identification and characterization of sounds, and give some examples.

We have taken an approach to signal processing that we are calling a "mixed transform technique". In essence, this means that we are using a variety of signal processing tools to achieve the desired goal of efficient localization and classification of sound sources. Sounds are identified based on unique "features" that they exhibit in the results of the algorithms applied. A library of features for different sounds has been developed and is being expanded on an ongoing basis.

The signal processing is structured in an iterative fashion, where initially fast and simple algorithms are used to get preliminary information about the acoustic environment. This is called the overview stage, and pending the results of the overview further algorithms are executed as necessary -- the detail stage. This iterative process is designed to speed up processing so that only as many algorithms as necessary are executed in order to isolate sound features.

Sound samples are recorded at a sampling rate of 16 kHz, and are divided into segments of 8192 samples long. There are three algorithms used in the overview stage: amplitude thresholding, a Discrete Wavelet Transform (DWT) on the full segment, and a Fast Fourier transform (FFT) on a 512 point subset of the segment extracted from the region of peak signal intensity. Amplitude thresholding is performed on each segment, and if no portion of the segment exceeds a predetermined threshold, it is assumed that there are no sound sources present and no further algorithms are applied to that segment. For segments that exceed the amplitude threshold, the DWT and FFT are computed.

The wavelet transform has recently become very popular in 1- and 2-dimensional signal analysis (many good texts and review articles are available on the subject, eg. [2]), and we have found a number of cases where they provide a new insight into our work.

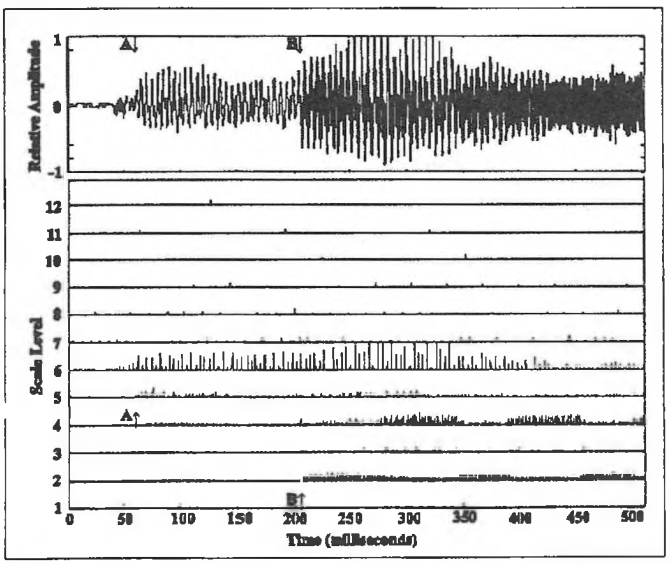

Figure 2: Time series (top) and DWT scalogram (bottom) for three overlapping sounds: the word 'test' (starting at **A**), a phone ringer (starting at **B**), and a fan (for the duration). In the scalogram the highest frequencies are represented in scale level 1.

Because the elemental building block in wavelet decomposition is localized in space and time, it seemed an obvious choice for use in sound source localization. However, we have found that the scalogram – the wavelet equivalent of a spectrogram – is also an efficient way to map a variety of different sound groups into different parts of a 2-dimensional mapping. The DWT of an 8192 point array gives 12 scale levels, each representing a different range of frequencies. The 3 or 4 levels representing the highest frequencies tend to contain information from alarm and warning signals and from music. The 5 levels representing the lowest frequencies tend to contain information from mechanical sources such as fans. The remaining levels in the mid-range of the spectrum tend to contain information from speech sources. Warning signals such as telephone ringers, alarm clocks, and other such devices have a distinctive pattern in the DWT. They generally have uniform amplitudes and repeatable patterns. Speech also has a distinctive pattern, though it is not as simple as that seen with the alarms. The low frequency noises from mechanical sources do not have a distinctive pattern that can be seen in the DWT scalogram. However, the presence of coefficients of significant magnitude in these low frequency scale levels suggests that further processing be done to identify their source. Figure 2 shows an example of both the time series and the scalogram for three overlapping sounds: a speech sample, a telephone ringer, and a fan. In figure 2 the start of the speech sample is marked with an 'A'. The distribution of the DWT coefficients in levels 5 and 6 are characteristic of speech. The start of the telephone ringer is marked with a 'B'. The alternating pattern of coefficients in levels 2 and 4 is characteristic of the two-tone electronic ringers used in many new telephones. The fan does not have a unique pattern in the scalogram, but the presence of coefficients in levels 8 through 12 suggest that a noise with a low frequency component such as a fan is present. It is easier to see the onset and duration of the different sounds in the scalogram than it is in the time series.

The FFT performed on the 512 point sample allows evaluation for a variety of features. The peaks in the FFT are isolated and from them the following features may be obtained: significant energy in the low frequency range, with few or no outstanding peaks, extending down to DC, suggests a mechanical noise source such as a fan or other equipment with either rotating parts or forced air; equally spaced peaks under 1 kHz with fundamental in range 80 to 200 Hz suggests a speech source; multiple peaks over 1kHz matching the frequencies of musical notes suggests music source. Different algorithms are executed on the results of the FFT based on the preliminary findings in the DWT.

Signal processing continues on each 8192 point segment in this fashion of fast overview analysis followed up by detailed analysis until it is appears that all sources present have been identified. In some cases the results of several 8192 point segments are concatenated together in order to identify patterns that extend beyond the 0.5 second duration of a single segment.

Summary

The method presented is an efficient and effective way of classifying sound sources. Further development is underway to automate the application of the source identification, as some user intervention is still required. Following completion of this task, algorithms for the localization of the sources and control of a directional amplification method will be implemented.

References

[1]. Harris, C.P, A Device to Localize Sound Sources, M.A.Sc. Thesis, University of British Columbia, Vancouver, BC, Canada, 1995.

[2]. Chan, Y.T., Wavelet Basics, Kluwer Academic Publishers, Norwell, Massachusetts, 1995.

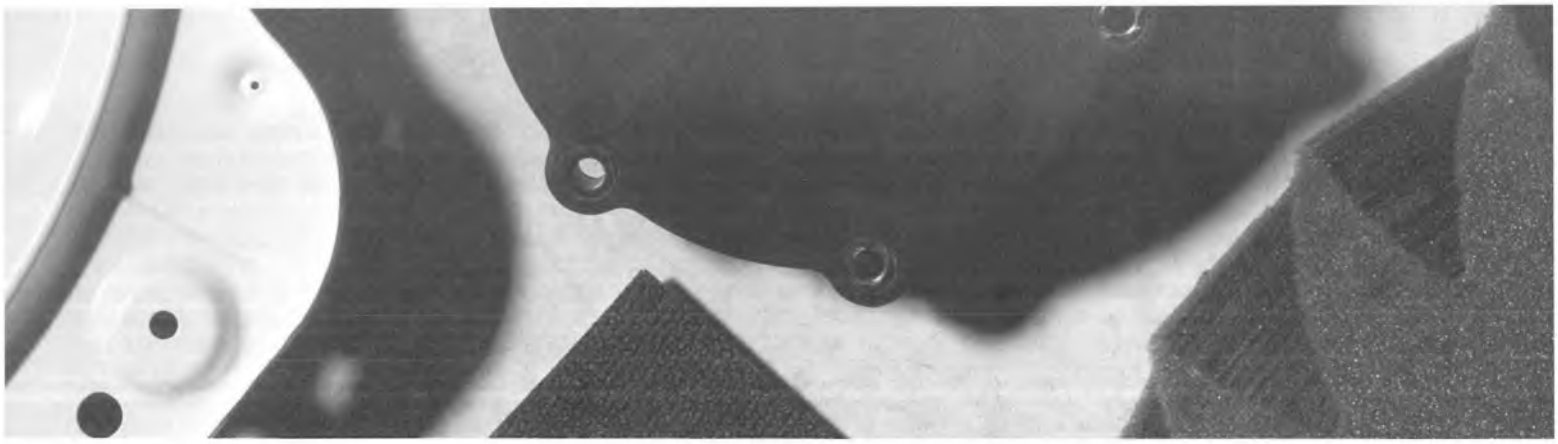

The ABC's of Noise Control

Comprehensive Noise Control Solutions

H.L. Blachford Ltd.'s Comprehensive Material Choices Noise treatments can be categorized into three basic elements: Vibration Dampers, Sound Absorbers and Sound Barriers.

Vibration Dampers

It is well known that noise is emitted from vibrating structures or substrates. The amount of noise can be drastically reduced by the application of a layer of a vibration damping compound to the surface. The damping compound causes the vibrational energy to be converted into heat energy. Blachford's superior damping material is called ANTIVIBE and is available in either a liquid or a sheet form.

Antivibe® DL is a liquid damping material that can be applied with conventional spray equipment or troweled for smaller or thicker applications.

It is water-based, non-toxic, and provides economical and highly effective noise reduction from vibration.

Antivibe DS is an effective form of damping material provided in sheet form with a pressure sensitive adhesive for direct application to your product.

Sound Barriers

Sound barriers are uniquely designed for insulating and blocking airborne noise. The reduction in the transmission of sound (transmission loss or "TL") is accomplished by the use of a material possessing such characteristics as high mass, limpness, and impermeability to air flow. Sound barrier can be a very effective and economical method of noise reduction.

Barymat® is a sound barrier that is limp, has high specific gravity, and comes in plastic sheets or die cut parts. It can be layered with other materials such as acoustical foam, protective and decorative facings or pressure sensitive adhesives to achieve the desired TL for individual applications.

Sound Absorbers

Blachford's **Conasorb®** materials provide a maximum reduction of airborne noise through absorption in the frequency ranges associated with most products that produce objectionable noise. Examples: Engine compartments, computer and printer casings, construction, forestry and agriculture equipment, buses and locomotives.

Available with a wide variety of surface treatments for protection or esthetics. Materials are available in sheets, rolls and die-cut parts – designed to meet your specific application.

Suggest Specific Materials or Design

Working with data supplied by you, H.L. Blachford Ltd. will recommend treatment methods which may include specific material proposals, design ideas, or modifications to components.

ISO 9001 REGISTERED A Quality Supplier

The complete integration of:

- Experience of over forty years
- Quality-oriented manufacturing
- Extensive research and development
- Problem solving approach to noise control

MISSISSAUGA
(905) 823-3200

MONTREAL
(514) 938-9775

VANCOUVER
(604) 263-1561

Blachford

www.blachford.ca

ABSOLUTE FIDELITY

At your beck and call

2238 MEDIATOR

No, it's not just another sound level meter!

2238 Mediator™ is much more. It's an entire range of cost-effective measurement systems with the ability to adapt to your specific needs. Mediator is the key link in a complete measurement chain, with Brüel & Kjær supporting your demands right from supplying transducers to final reporting and data management.

Product noise, environmental noise, and noise at work – they are all within the versatile Mediator's reach.

INDUSTRI SOLUTIO

- *Predefine setup and get a perfe result every tim*
- *Use 1/1- and 1/ octave spectra f noise rating analysis*
- *Store your field measurements the large memo*

EN VIRONMEN SOLUTION

- *Get it all in one shot, every time*
- *Time histories a statistics*
- *Log your choice parameters to a file or via the interface*

OCCUPATIO HEALT SOLUTIO

- *All you need fo full assessment*
- *Dose based on and 5 dB exchan rates*
- *Power and versatility for troubleshootin*

HEADQUARTERS: DK-2850 Nærum · Denmark · Telephone: +4545800500 · Fax: +4545801405 · http://www.bk.dk · e-mail: info@bk.dk
USA: 2815 Colonnades Court · Norcross, GA 30071 · Toll free: (888) 788-1138 · Fax: (770) 447-2327
http://www.BKhome.com · e-mail: BKInfo@SpectrisTech.com

Australia (02)9450-2066 · Austria 0043-1-8657400 · Brazil (011)5182-8166 · Canada (514)695-8225 · China (86)1068029906 · Czech Republic 02-67021100
Finland (0)9-755 950 · France (01)69906900 · Germany 06103/908-5 6 · Hong Kong 25487486 · Hungary (1)2158305 · Ireland (01)4504922 · Italy (02)57604141
Japan 03-3779-8671 · Republic of Korea (02)3473-0605 · Netherlands (0)318 559290 · Norway 66771155 · Poland (22)858 9392 · Portugal (1)4711453
Singapore (65) 377-4512 · Slovak Republic 421754430701 · Spain (91)3681000 · Sweden (08)4498600 · Switzerland 01/9436070 · Taiwan (02)7139303
United Kingdom (0181)954-2366
Local representatives and service organisations worldwide

Brüel & Kjær

NEWS / INFORMATIONS

CONFERENCES

The following list of conferences was mainly provided by the Acoustical Society of America. If you have any news to share with us, send them by mail or fax to the News Editor (see address on the inside cover), or via electronic mail to desharnais@drea.dnd.ca

1999

1-4 September: 15th International Symposium on Nonlinear Acoustics (ISNA-15), Gottingen, Germany. Contact: W. Lauterborn, Drittes Physikalisches Institut, Universitat Gottingen, Burgerstr. 42-44, 37073 Gottingen, Germany; Fax: +49 551 39 7720; Email: lb@physik3.gwdg.de

15-17 September: British Society of Audiology Annual Conference, Buxton, UK. Contact: BSA, 80 Brighton Road, Reading RG6 1PS, UK; Fax: +44 0118 935 1915; Email: bsa@b-s-a.demon.co.uk; Web: www.b-s-a.demon.co.uk

7-10 October: Symposium on Occupational Hearing Loss, Philadelphia, PA. Contact: American Institute for Voice and Ear Research, Attn: Barbara-Ruth Roberts, 1721 Pine St., Philadelphia, PA 19103, Tel: 215-545-2068; Fax: 215-735-2725.

18-19 October: 1999 Acoustics Week in Canada, Victoria, BC, Canada. Contact: Stan Dosso, School of Earth & Ocean Sciences, University of Victoria, Victoria, BC, Canada, V8W 3P6; Fax: (250) 721-6200; Email: sdosso@uvic.ca

20-22 October: Iberian Meeting of the Spanish Acoustical Society and the Portuguese Acoustical Society, Avila, Spain. Contact: Spanish Acoustical Society, c/Serrano 144, 28006 Madrid, Spain; Fax: +34 91 411 7651; email: ssantiago @fresno.csic.es

28-29 October: Swiss Acoustical Society Fall Meeting, Biel, Switzerland. Contact: Swiss Acoustical Society, P.O. Box 251, 8600 Dübendorf, Switzerland; Fax: +41 1 823 4793; email: beat.hohmann@compuserve.com

1-5 November: 138th meeting of the Acoustical Society of America, Columbus, OH. Contact: Acoustical Society of America, 500 Sunnyside Blvd., Woodbury, NY 11797; Tel.: 516-576-2360; Fax: 516-576-2377; email: asa@aip.org; WWW: asa.aip.org

24-26 November: Australian Acoustical Society Conference, Melbourne, Australia. Contact: G. Barnes, Acoustical Design Pty. Ltd., 2/72 Bayfield Road, Bayswater VIC, Australia 3153; Fax: +61 3 9720 6952; email: acousticdes@bigpond.com

6-8 December: Inter-Noise 99, Fort Lauderdale, FL. Contact: Institute of Noise Control Engineering, P.O. Box 3206 Arlington Branch, Poughkeepsie, NY 12603, Tel: 914-462-4006; Email: INCEUSA@aol.com

CONFÉRENCES

La liste de conférences ci-jointe a été offerte en majeure partie par l'Acoustical Society of America. Si vous avez des nouvelles à nous communiquer, envoyez-les par courrier ou fax (coordonnées incluses à l'envers de la page couverture), ou par courrier électronique à desharnais@drea.dnd.ca

1999

1-4 septembre: 15e Symposium international sur l'acoustique non-linéaire (ISNA-15), Gottingen, Allemagne. Info: W. Lauterborn, Drittes Physikalisches Institut, Universitat Gottingen, Burgerstr. 42-44, 37073 Gottingen, Germany; Fax: +49 551 39 7720; Email: lb@physik3 .gwdg.de

15-17 septembre: Conférence annuelle de la Société britannique d'audiologie, Buxton, Royaume-Uni. Info: BSA, 80 Brighton Road, Reading RG6 IPS, UK; Fax: +44 0118 935 1915; Email: bsa@b-s-a.demon.co.uk; Web: www.b-s-a.demon.co.uk

7-10 octobre: Symposium sur la perte d'audition occupationnelle, Philadelphie, PA. Info: American Institute for Voice and Ear Research, Attn: Barbara-Ruth Roberts, 1721 Pine St., Philadelphia, PA 19103, Tél: 215-545-2068; Fax: 215-735-2725.

18-19 octobre: Semaine canadienne d'acoustique 1999, Victoria, BC, Canada. Info: Stan Dosso, School of Earth & Ocean Sciences, University of Victoria, Victoria, BC, Canada, V8W 3P6; Fax: (250) 721-6200; Email: sdosso@uvic.ca

20-22 octobre: Rencontre ibérique de la Société d'acoustique espagnole et de la Société d'acoustique portuguaise, Avila, Espagne. Info: Spanish Acoustical Society, c/Serrano 144, 28006 Madrid, Spain; Fax: +34 91 411 7651; email: ssantiago@fresno.csic.es

28-29 octobre: Rencontre d'automne de la Société d'acoustique suisse, Biel, Suisse. Info: Swiss Acoustical Society, P.O. Box 251, 8600 Dübendorf, Switzerland; Fax: +41 1 823 4793; email: beat.hohmann@compuserve.com

1-5 novembre: 138e rencontre de l'Acoustical Society of America, Columbus, OH. Info: Acoustical Society of America, 500 Sunnyside Blvd., Woodbury, NY 11797; Tél.: 516-576-2360; Fax: 516-576-2377; email: asa@aip.org; WWW: asa.aip.org

24-26 novembre: Conférence de la Société d'acoustique australienne, Melbourne, Australie. Info: G. Barnes, Acoustical Design Pty. Ltd., 2/72 Bayfield Road, Bayswater VIC, Australia 3153; Fax: +61 3 9720 6952; email: acousticdes@bigpond.com

6-8 décembre: Inter-Noise 99, Fort Lauderdale, FL. Info: Institute of Noise Control Engineering, P.O. Box 3206 Arlington Branch, Poughkeepsie, NY 12603, Tél: 914-462-4006; Email: INCEUSA@aol.com

2000

20-24 March: Meeting of the German Acoustical Society (DAGA), Oldenburg, Germany. Contact: DEGA, FB Physik, Universität Oldenburg, 26111 Oldenburg, Germany; Fax: +49 441 798 3698; Email: dega@aku.physik.uni-oldenburg.de

17-19 May: 9th International Meeting on Low Frequency Noise and Vibration, Aalborg, Denmark. Contact: W. Tempest, Multi-Science Publishing Co. Ltd., 5 Wates Way, Brentwood, Essex CM15 9TB, UK; Fax: +44 1277 223453.

5-9 June: International Conference on Acoustics, Speech and Signal Processing (ICASSP-2000), Istanbul, Turkey. Contact: T. Adali, EE and Computer Science Department, University of Maryland Baltimore County, 1000 Hilltop Circle, Baltimore, MD 21250; Fax: +1 410 455 3639; Web: icassp2000.sdsu.edu

6-9 June: 5th International Symposium on Transport Noise and Vibration, St. Petersburg, Russia. Contact: East-European Acoustical Association, Moskovskoe Shosse 44, 196158 St. Petersburg, Russia; Fax: +7 812 1279323; Email: noise@mail.rcom.ru

4-7 July: 7th International Congress on Sound and Vibration, Garmisch-Partenkirchen, Germany. Contact: H. Heller, DLR, Postfach 3267, 38022 Braunschweig, Germany; Fax: +49 531 295 2320; email: hanno.heller@dlr.de; WWW: www.iiav.org/icsv7.html

28-30 August: Inter-Noise 2000, Nice, France. Contact: SFA, 23 avenue Brunetière, 75017 Paris, France; Fax: +33 1 47 88 90 60; Web: www.inrets.fr/services/manif

31 August - 2 September: International Conference on Noise and Vibration Pre-Design and Characterization Using Energy Methods (NOVEM), Lyon, France. Contact: LVA, INSA de Lyon, Bldg. 303, 20 avenue Albert Einstein, 69621 Villeurbane, France; Fax: +33 4 7243 8712; Web: www.insa-lyon.fr/Laboratoires/lva.html

3-6 September: 5th French Congress on Acoustics - Joint meeting of the Swiss and French Acoustical Societies, Lausanne, Switzerland. Contact: M.-N. Rossi, Ecole Polytechnique Fédérale, 1015 Lausanne, Switzerland; Fax: +41 21693 26 73.

3-5 October: WESPRAC VII, Kumamoto, Japan. Contact: Computer Science Dept., Kumamoto Univ., 2-39-1 Kurokami, Kumamoto, Japan 860-0862; Fax: +81 96 342 3630; Email: wesprac7@cogni.eecs.kumamoto-u.ac.jp

16-18 October: 2nd Iberoamerican Congress on Acoustics, 31st National Meeting of the Spanish Acoustical Society, and EAA Symposium, Madrid, Spain. Contact: Spanish Acoustical Society, c/Serrano 144, 28006 Madrid, Spain; Fax: +34 91 411 7651; email: ssantiago@fresno.csic.es

16-20 October: 6th International Conference on Spoken Language Processing, Beijing, China. Contact: ICSLP 2000 Secretariat, Institute of Acoustics, PO Box 2712, 17 Zhong Guan Cun Road, 100 080 Beijing, China; Fax: +86 10 6256 9079; Email: mchu@plum.ioa.ac.cn

2000

20-24 mars: Rencontre de la Société allemande d'acoustique (DAGA), Oldenburg, Allemagne. Info: DEGA, FB Physik, Universität Oldenburg, 26111 Oldenburg, Germany; Fax: +49 441 798 3698; Email: dega@aku.physik.uni-oldenburg.de

17-19 mai: 9e rencontre internationale sur le bruit et les vibrations de basse fréquence, Aalborg, Danemark. Info: W. Tempest, Multi-Science Publishing Co. Ltd., 5 Wates Way, Brentwood, Essex CM15 9TB, UK; Fax: +44 1277 223453.

5-9 juin: Conférence internationale sur l'acoustique, la parole et le traitement de signal (ICASSP-2000), Istanboul, Turquie. Info: T. Adali, EE and Computer Science Department, University of Maryland Baltimore County, 1000 Hilltop Circle, Baltimore, MD 21250; Fax: +1 410 455 3639; Web: icassp2000.sdsu.edu

6-9 juin: 5e symposium international sur le bruit et vibrations du transport, St Petersbourg, Russie. Info: East-European Acoustical Association, Moskovskoe Shosse 44, 196158 St. Petersburg, Russia; Fax: +7 812 1279323; Email: noise@mail.rcom.ru

4-7 juillet: 7e Congrès international sur le son et les vibrations, Garmisch-Partenkirchen, Allemagne. Info: H. Heller, DLR, Postfach 3267, 38022 Braunschweig, Germany; Fax: +49 531 295 2320; email: hanno.heller@dlr.de; Web: www.iiav.org/icsv7.html

28-30 août: Inter-Noise 2000, Nice, France. Info: SFA, 23 avenue Brunetière, 75017 Paris, France; Fax: +33 1 47 88 90 60; Web: www.inrets.fr/services/manif

31 août - 2 septembre: Conférence internationale sur l'utilisation des méthodes d'énergie pour la prévision vibroacoustique (NOVEM), Lyon, France. Info: LVA, INSA de Lyon, Bldg. 303, 20 avenue Albert Einstein, 69621 Villeurbane, France; Fax: +33 4 7243 8712; Web: www.insa-lyon.fr/Laboratoires/lva.html

3-6 septembre: 5e Congrès français d'acoustique - Rencontre conjointe des Sociétés suisse et française d'acoustique, Lausanne, Suisse. Info: M.-N. Rossi, Ecole Polytechnique Fédérale, 1015 Lausanne, Suisse; Fax: +41 21693 26 73.

3-5 octobre: WESPRAC VII, Kumamoto, Japon. Info: Computer Science Dept., Kumamoto Univ., 2-39-1 Kurokami, Kumamoto, Japan 860-0862; Fax: +81 96 342 3630; Email: wesprac7@cogni.eecs.kumamoto-u.ac.jp

16-18 octobre: 2e congrès ibéro-américain sur l'acoustique, 31e Rencontre nationale de la Société d'acoustique espagnole, et Symposium de l'EAA, Madrid, Espagne. Info: Spanish Acoustical Society, c/Serrano 144, 28006 Madrid, Spain; Fax: +34 91 411 7651; email: ssantiago@fresno .csic.es

16-20 octobre: 6e conférence internationale sur le traitement de la langue parlée, Beijing, Chine. Info: ICSLP 2000 Secretariat, Institute of Acoustics, PO Box 2712, 17 Zhong Guan Cun Road, 100 080 Beijing, China; Fax: +86 10 6256 9079; Email: mchu@plum.ioa.ac.cn

Gunnar Rasmussen Acoustic Solutions:

Precision Acoustic Measurement Instrumentation

Condenser Microphones and Preamplifiers
Intensity Probes
Outdoor Microphones / Hydrophones
Calibration Instrumentation and Accessories

G.R.A.S.
Sound & Vibration

Represented in Canada by

NOVEL DYNAMICS INC.
Dynamic Test and Analysis Systems

Integrated Solutions from World Leaders

Novel Dynamics Inc.
Phone 519-853-4495 Fax 519-853-3366
Email: metelka@aztec-net.com
Ottawa Office 613-599-6275 Fax 613-599-6274

INSTRUCTIONS TO AUTHORS FOR THE PREPARATION OF MANUSCRIPTS

Submissions: The original manuscript and two copies should be sent to the Editor-in-Chief.

General Presentation: Papers should be submitted in camera-ready format. Paper size 8.5" x 11". If you have access to a word processor, copy as closely as possible the format of the articles in Canadian Acoustics 18(4) 1990. All text in Times-Roman 10 pt font, with single (12 pt) spacing. Main body of text in two columns separated by 0.25". One line space between paragraphs.

Margins: Top - title page: 1.25"; other pages, 0.75"; bottom, 1" minimum; sides, 0.75".

Title: Bold, 14 pt with 14 pt spacing, upper case, centered.

Authors/addresses: Names and full mailing addresses, 10 pt with single (12 pt) spacing, upper and lower case, centered. Names in bold text.

Abstracts: English and French versions. Headings, 12 pt bold, upper case, centered. Indent text 0.5" on both sides.

Headings: Headings to be in 12 pt bold, Times-Roman font. Number at the left margin and indent text 0.5". Main headings, numbered as 1, 2, 3, ... to be in upper case. Sub-headings numbered as 1.1, 1.2, 1.3, ... in upper and lower case. Sub-sub-headings not numbered, in upper and lower case, underlined.

Equations: Minimize. Place in text if short. Numbered.

Figures/Tables: Keep small. Insert in text at top or bottom of page. Name as "Figure 1, 2, ..." Caption in 9 pt with single (12 pt) spacing. Leave 0.5" between text.

Photographs: Submit original glossy, black and white photograph.

References: Cite in text and list at end in any consistent format, 9 pt with single (12 pt) spacing.

Page numbers: In light pencil at the bottom of each page.

Reprints: Can be ordered at time of acceptance of paper.

DIRECTIVES A L'INTENTION DES AUTEURS PREPARATION DES MANUSCRITS

Soumissions: Le manuscrit original ainsi que deux copies doivent être soumis au rédacteur-en-chef.

Présentation générale: Le manuscript doit comprendre le collage. Dimensions des pages, 8.5" x 11". Si vous avez accès à un système de traitement de texte, dans la mesure du possible, suivre le format des articles dans l'Acoustique Canadienne 18(4) 1990. Tout le texte doit être en caractères Times-Roman, 10 pt et à simple (12 pt) interligne. Le texte principal doit être en deux colonnes séparées d'un espace de 0.25". Les paragraphes sont séparés d'un espace d'une ligne.

Marges: Dans le haut - page titre, 1.25"; autres pages, 0.75"; dans le bas, 1" minimum; latérales, 0.75".

Titre du manuscrit: 14 pt à 14 pt interligne, lettres majuscules, caractères gras. Centré.

Auteurs/adresses: Noms et adresses postales. Lettres majuscules et minuscules, 10 pt à simple (12 pt) interligne. Centré. Les noms doivent être en caractères gras.

Sommaire: En versions anglaise et française. Titre en 12 pt, lettres majuscules, caractères gras, centré. Paragraphe 0.5" en alinéa de la marge, des 2 cotés.

Titres des sections: Tous en caractères gras, 12 pt, Times-Roman. Premiers titres: numéroter 1, 2, 3, ..., en lettres majuscules; sous-titres: numéroter 1.1, 1.2, 1.3, ..., en lettres majuscules et minuscules; sous-sous-titres: ne pas numéroter, en lettres majuscules et minuscules et soulignés.

Equations: Les minimiser. Les insérer dans le texte si elles sont courtes. Les numéroter.

Figures/Tableaux: De petites tailles. Les insérer dans le texte dans le haut ou dans le bas de la page. Les nommer "Figure 1, 2, 3,..." Légende en 9 pt à simple (12 pt) interligne. Laisser un espace de 0.5" entre le texte.

Photographies: Soumettre la photographie originale sur papier glacé, noir et blanc.

Références: Les citer dans le texte et en faire la liste à la fin du document, en format uniforme, 9 pt à simple (12 pt) interligne.

Pagination: Au crayon pâle, au bas de chaque page.

Tirés-à-part: Ils peuvent être commandés au moment de l'acceptation du manuscrit.

The Canadian Acoustical Association

l'Association Canadienne d'Acoustique

SUBSCRIPTION INVOICE

Subscription for the current calendar year is due January 31. New subscriptions received before July 1 will be applied to the current year and include that year's back issues of Canadian Acoustics, if available. Subscriptions received from July 1 will be applied to the next year.

FACTURE D'ABONNEMENT

L'abonnement pour la présente année est dû le 31 janvier. Les nouveaux abonnements reçus avant le 1 juillet s'appliquent à l'année courante et incluent les anciens numéros (non-épuisés) de l'Acoustique Canadienne de cette année. Les abonnements reçus après le 1 juillet s'appliquent à l'année suivante.

Check ONE Item Only:

Cocher la case appropriée:

CAA Membership	_____	$50	_____	Membre individuel
CAA Student membership	_____	$10	_____	Membre étudiant(e)
Institutional Subscription	_____	$50	_____	Membre institutionnel
Sustaining Subscription	_____	$150	_____	Abonnement de soutien
	Total Remitted	$_____		Versement total

INFORMATION FOR MEMBERSHIP DIRECTORY

Check areas of interest (max 3):

RENSEIGNEMENT POUR L'ANNUAIRE DES MEMBRES

Cocher vos champs d'intérêt (max. 3):

Architectural Acoustics	1.	_____	1. Acoustique architecturale
Engineering Acoustics / Noise Control	2.	_____	2. Génie acoustique / Contrôle du bruit
Physical Acoustics / Ultrasound	3.	_____	3. Acoustique physique / Ultrasons
Musical Acoustics / Electroacoustics	4.	_____	4. Acoustique musicale / Electroacoustique
Psychological / Physiological Acoustics	5.	_____	5. Physio/psycho-acoustique
Shock and Vibration	6.	_____	6. Chocs et vibrations
Hearing Sciences	7.	_____	7. Audition
Speech Sciences	8.	_____	8. Parole
Underwater Acoustics	9.	_____	9. Acoustique sous-marine
Signal Processing / Numerical Methods	10.	_____	10. Traitement des signaux / Méthodes numériques
Other	11.	_____	11. Autre

Business telephone number (_____) _____ Numéro de téléphone au bureau

Business facsimile number (_____) _____ Numéro de télécopieur au bureau

Business E-Mail number _____ Numéro de courier électronique au bureau

PLEASE TYPE NAME AND ADDRESS BELOW:

VEUILLEZ ECRIRE VOTRE NOM ET VOTRE ADRESSE CI-DESSOUS:

Faites parvenir ce formulaire à l'adresse suivante en prenant soin d'y joindre un chèque fait au nom de L'ASSOCIATION CANADIENNE D'ACOUSTIQUE:

Make cheques payable to THE CANADIAN ACOUSTICAL ASSOCIATION. Mail this form with payment to:

Trevor Nightingale
Secretary, Canadian Acoustical Association
P. O. Box 74068
Ottawa, Ontario K1M 2H9

The Canadian Acoustical Association
l'Association Canadienne d'Acoustique

SUSTAINING SUBSCRIBERS / ABONNES DE SOUTIEN

The Canadian Acoustical Association gratefully acknowledges the financial assistance of the Sustaining Subscribers listed below. Annual donations (of $150.00 or more) enable the journal to be distributed to all at a reasonable cost. Sustaining Subscribers receive the journal free of charge. Please address donation (made payable to the Canadian Acoustical Association) to the Secretary of the Association.

L'Association Canadienne d'Acoustique tient à témoigner sa reconnaissance à l'égard de ses Abonnés de Soutien en publiant ci-dessous leur nom et leur adresse. En amortissant les coûts de publication et de distribution, les dons annuels (de $150.00 et plus) rendent le journal accessible à tous nos membres. Les Abonnés de Soutien reçoivent le journal gratuitement. Pour devenir un Abonné de Soutien, faites parvenir vos dons (chèque ou mandat-poste fait au nom de l'Association Canadienne d'Acoustique) au secrétaire de l'Association.

ACO Pacific
2604 Read Ave.
Belmont, CA, USA 94002
(650) 595-8588 FAX: (650) 591-2891

Acoustec Inc.
Attn: Dr. J.G. Migneron
1381 rue Galilée, Suite 103
Québec, Québec G1P 4G4
(418) 682-2331 FAX: (418) 682-1472

Aercoustics Engineering Limited
Barman & Associates
50 Ronson Drive, Suite 127
Rexdale, Ontario M9W 1B3
(416) 249-3361 FAX: (416) 249-3613

Atlantic Acoustical Associates
P.O. Box 96, Station M
Halifax, Nova Scotia B3J 2L4
(902) 425-3096

H. L. Blachford Ltd.
Attn: Mr. D.E. Watson
2323 Royal Windsor Dr.
Mississauga, Ontario L5J 1K5
(905) 823-3200 FAX: (905) 823-9290

Bruel & Kjaer Canada Ltd.
90 Leacock Road
Pointe Claire, Québec H9R 1H1
(514) 695-8225 FAX: (514) 695-4808

J. E. Coulter Associates Ltd.
Suite 507
1200 Sheppard Ave. E
Willowdale, Ontario M2K 2S5
(416) 502-8598 FAX: (416) 502-3473

Dalimar Instruments Inc.
193, Joseph Carrier
Vaudreuil-Dorion, Québec J7V 5V5
(514) 424-0033 FAX: (514) 424-0030

Eckel Industries of Canada Ltd.
Attn: Mr. Blake Noon
P.O. Box 776
Morrisburg, Ontario K0C 1X0
(613) 543-2967 FAX: (613) 543-4173

Environmental Acoustics Inc.
Attn: Mr. H.J. Doedens
#13 - 5155 Spectrum Way
Mississauga, Ontario L4W 5A1
(905) 238-1077 FAX: (905) 238-9079

Hatch Associates Ltd.
Attn: Tim Kelsall
2800 Speakman Dr.
Mississauga, Ontario L5K 2R7
(905) 855-7600 FAX: (905) 855-8270

HGC Engineering
Plaza One, Suite 203
2000 Argentia Road
Mississauga, Ontario L5N 1P7
(905) 826-4044 FAX: (905) 826-4940

Hydro-Quebec
Vice-presidence Environnement
75 Rene Levesque ouest, 16e etage
Montreal, Québec H2Z 1A4

Industrial metal Fabricators (Chatham) Ltd.
Industrial Noise Control
Attn: Mr. Frank Van Oirschot
P.O. Box 834, 288 Inshes Ave.
Chatham, Ontario N7M 5L1
(519) 354-4270 FAX: (519) 354-4193

Integral DX Engineering Ltd.
907 Admiral Ave.
Ottawa, Ontario K1Z 6L6
(613) 761-1565 FAX: (613) 729-4337

Jade Acoustics Inc.
545 North Rivermede Road, Suite 203
Concord, Ontario L4K 4H1
(905) 660-2444 FAX: (905) 660-4110

John Swallow Associates
Attn: John C. Swallow
250 Galaxy Boulevard
Etobicoke, Ontario M9W 5R8
(416) 798-0522

Larson Davis Laboratories
1681 West 820 North
Provo, Utah, USA 84601
(801) 375-0177

MJM Conseillers en Acoustique Inc.
Attn: M. Michel Morin
6555 Cote des Neiges, Suite 400
Montréal, Québec H3S 2A6
(514) 737-9811 FAX: (514) 737-9816

Nelson Industries Inc.
Corporate Research Dept.
P.O. Box 600
Stoughton, WI, USA 53589-0600
(608) 873-4370

OZA Inspections Ltd.
P.O. Box 271
Grimsby, Ontario L3M 4G5
(416) 945-5471 FAX: (416) 945-3942

Peutz & Associés
Attn: Marc Asselineau
34 rue de Paradis
F-75010 Paris, France
+33 1 45230500 FAX: +33 1 45230504

J. L. Richards & Assoc. Ltd.
Attn: Fernando Ribas
864 Lady Ellen Place
Ottawa, Ontario K1Z 5M2
(613) 728-3571 FAX: (613) 728-6012

Scantek Inc.
916 Gist Ave.
Silver Spring, MD, USA 20910
(301) 495-7738 FAX: (301) 495-7739

SNC/Lavalin Environment Inc.
2 Felix Martin Place
Montréal, Québec H2Z 1Z3
(514) 393-1000

Spaarg Engineering Limited
Noise and Vibration Analysis
822 Lounsborough St.
Windsor, Ontario N9G 1G3
(519) 972-0677 FAX: (519) 972-0677

State of the Art Acoustik Inc.
Attn. Dr. C. Fortier
Unit 43, 1010 Polytek St.
Ottawa, Ontario, K1J 9J3

Tacet Engineering Ltd.
Attn: Dr. M.P. Sacks
111 Ava Road
Toronto, Ontario M6C 1W2
(416) 782-0298 FAX: (416) 785-9880

University of Alberta
MEANU, Dept. of Mech. Eng.
6720 - 30 St.
Edmonton, Alberta T6P 1J6
(403) 466-6465 FAX: (403) 466-6465

Valcoustics Canada Ltd.
30 Wertheim Court, Unit 25
Richmond Hill, Ontario L4B 1B9
(905) 764-5223 FAX: (905) 764-6813

Wilrep Ltd.
1515 Matheson Blvd. E, Unit C 10
Mississauga, Ontario L4W 2P5
(905) 625-8944 FAX: (905) 625-7142